Fall 2020

Investigation on nanoparticle based combination therapy for targeted cancer treatment

Muhammad Raisul Abedin

Department: Chemical and Biochemical Engineering

INVESTIGATION ON NANOPARTICLE BASED COMBINATION THERAPY FOR TARGETED CANCER TREATMENT

by

MUHAMMAD RAISUL ABEDIN

A DISSERTATION

Presented to the Faculty of the Graduate School of the

MISSOURI UNIVERSITY OF SCIENCE AND TECHNOLOGY

In Partial Fulfillment of the Requirements for the Degree

DOCTOR OF PHILOSOPHY

in

CHEMICAL ENGINEERING

2020

Approved by:

Sutapa Barua, Advisor
Daniel Forciniti
Yongjian Liu
Jee Ching Wang
Hu Yang

PUBLICATION DISSERTATION OPTION

This dissertation consists of the following five articles, formatted in the style used by the Missouri University of Science and Technology:

Paper I, found on pages 25-67, is currently under review in Scientific Reports.

Paper II, found on pages 68-123, is currently under review in Nano LIFE journal.

Paper III, found on pages 124-162, is ready for submission to a peer reviewed journal.

Paper IV, found on pages 163-194, was published in the Journal of Nanobiotechnology.

Paper V, found on pages 195-230, is currently in press (Scientific Reports).

ABSTRACT

The current treatment methods in cancer are associated with toxicity in healthy tissues, partial therapeutic response, drug resistance and finally recurrence of the disease. The cancer drugs are challenged by non-specific binding, undesired toxicity in healthy cells, low therapeutic index and finally poor therapeutic outcome. In this work, a targeted nanoscale therapeutic system Antibody Drug Nanoparticle (ADN) was engineered to selectively inhibit the breast cancer cell growth with reduced toxicity in healthy cells. The ADNs were designed by synthesizing rod shaped nanoparticles using pure chemotherapeutic drug and covalently conjugating a therapeutic monoclonal antibody (mAb) on the surface of the drug nanorods. The rod shaped nanosized formulation of ADNs significantly enhanced the aqueous phase stability and therapeutic payload of the system while the conjugated mAb was utilized for specific targeting of breast cancer cells. The designed ADN was effective for active targeting and synergistic inhibition of breast cancer cells. The mechanisms of actions of ADN was investigated at the cellular, molecular and genetic levels in cancer cells. The engineered ADN synergistically inhibited the growth of >80% of the human epidermal growth factor receptor 2 (HER2) - positive breast cancer cells *in vitro*. The cell cycle and protein expression analysis showed that ADN arrested the cellular growth for a prolonged time and induced a programmed cell death mechanism in HER2-positive breast cancer cells *in vitro*. Finally, the gene regulatory analysis showed the genetic mechanisms of programmed cell death regulation induced by ADN in breast cancer cell lines.

ACKNOWLEDGMENTS

I would like to express my gratitude to my advisor Dr. Sutapa Barua for her kind guidance throughout this uneven journey. Dr. Barua has been mentoring me from the very beginning till this date. All these years, Dr. Barua has been kind enough to keep her belief on me. The learnings from Dr. Barua will be the most valuable asset that I will take from this experience.

I am also thankful to my other Ph.D. committee members, Dr. Daniel Forciniti, Dr. Yongjian Liu, Dr. Jee-Ching Wang and Dr. Hu Yang for agreeing to serve on my committee, investing their valuable time and providing valuable feedback.

I would like to thank extremely talented fellow researchers in my lab, Dr. Sidharth Razdan, Kaitlyne Powers, Rachel Aiardo, Jawahar Khetan, Dr. Md Shahinuzzaman, Dr. Mohammad Aminul Islam. I appreciate their support during my hard times. My gratitude extends to all the faculty members of the Department of Chemical and Biochemical Engineering at Missouri S&T.

Finally, I would like to thank my family: my parents, grandparents and my sister for their endless encouragement from nine thousand miles away in Bangladesh. My banker father and my loving homemaker mother sacrificed their whole lives for our better future. Today, this Ph.D. is their achievement more than mine.

TABLE OF CONTENTS

PAPER

LIST OF ILLUSTRATIONS

PAPER V

LIST OF TABLES

NOMENCLATURE

Symbol	Description
μm	micrometer
nm	nanometer
nM	nanomolar
δ	chemical shift
λ	wavelength

1. INTRODUCTION

1.1. NANOTECHNOLOGY IN CANCER

In 2020, cancer is still the second leading cause of death in the United States. It was estimated that in 2019, close to 1.8 million new cases of cancer were expected to be diagnosed in the U.S. and over 0.6 million people would die from the disease[1]. The conventional treatment methods in cancer are still associated with poor diagnostics, toxicity to the normal cells and drug resistance. The limitations in conventional therapeutic methods promoted the use of nanoparticles as cancer therapeutics for safer and more efficacious treatment [2]. The term "Nanotechnology" is defined as the "intentional design, characterization, production, and applications of materials, structures, devices, and systems by controlling their size and shape in the nanoscale range" [3,4]. The concept of nanotechnology in cancer has shifted the paradigm of developing cancer drugs. The cancer nanomedicine field aims to utilize the multifunctional novel physical characteristics of nanosized materials for the diagnostic and therapeutic application at the molecular level [5]. In cancer treatment, nanomaterials are being engineered to enhance the transport property of therapeutic agents and diagnostic tools through the complex biological barriers and to aid the interaction with biomolecules. The unique characteristics of nanomaterials, for example, high surface area to volume ratio, surface physical and chemical characteristics depending on variable sizes or shapes, tunable optical, magnetic and electronic properties have made the use of nanomedicine more appealing in cancer treatment than the contemporary atomic or macroscale materials [6,7]. These characteristics of nanomaterials are potentially being applied in drug delivery,

diagnosis of early-stage cancer, imaging and tracking the progression of tumor formation, development of anti-cancer nano-vaccine therapeutics. The current Food and Drug Administration (FDA) approved and clinically used nanomaterials with size ranging from 1-100 nm for cancer treatment shown in Figure 1.1 can be categorized into inorganic and organic nanoparticle platforms [5,8,9].

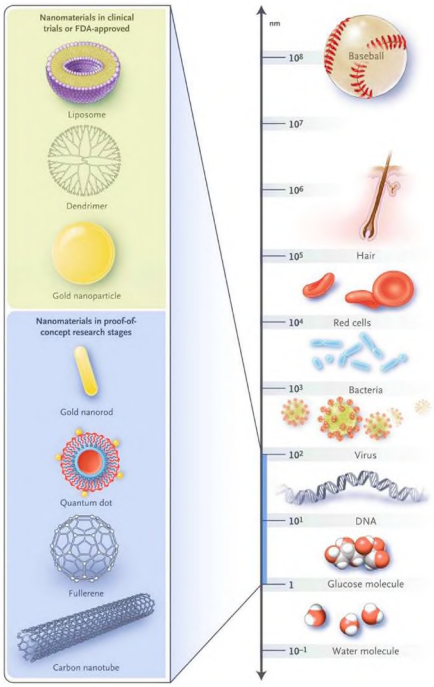

Figure 1.1. Inorganic and organic nanomaterials used in cancer therapy [5]

The inorganic nanoparticles comprises mostly carbon nanotubes, fullerenes, quantum dots and multifunctional metal nanoparticles [5]. A combination of materials integrating a wide range of physical and chemical properties into a single system has enabled the design of novel inorganic materials for cancer treatment. The organic nanomaterials include polymers, lipids, micelles, dendrimers, small protein molecules

and nucleic acid based nano assemblies [8]. The hydrophilic surface and biocompatibility of organic nanomaterials have made them highly potential therapeutics for cancer treatment.

1.2. CURRENT TREATMENT METHODS IN CANCER

1.2.1. Surgery. Surgery is conducted to diagnose, characterize and treat cancer. A revolution in cancer surgery arose in 1957 marking the beginning of cancer surgery based on laboratory research and clinical trial outcomes [10]. The studies showed that the bloodstream plays a major role in the dissemination of cancer and regional surgical therapies are not enough for improving the survival of patients [11]. A scientific basis of cancer surgery was established and the studies justified less radical surgery and systemic therapy after surgery [10]. Currently, surgeries are conducted in cancer treatment in combination with other treatment strategies *e.g.,* radiation therapy, chemotherapy at different stages of cancer treatment. Initially, surgical biopsies are performed by taking out a tissue sample from the possibly affected organ and checking the sample under a microscope or by performing necessary pathological tests on the sample. After an initial positive diagnosis of cancer, staging surgery may be performed to investigate the extent of cancer cell dissemination in the primary organ or to the distant secondary sites (known as metastasis). Curative surgeries are operated in order to remove the tumor that has spread in a confined area. If the cancer has spread covering a lot of areas and is very close to sensitive organs then surgery is conducted to debulk a portion of the affected site known as debulking surgery. The rest of the cancer cells are treated by radiation or chemotherapy. In ovarian cancer and some lymphoma, debulking is a common surgical

procedure. Palliative surgery helps the patients get rid of any form of side effects of cancer treatment and to continue with the ongoing treatment.

1.2.2. Radiation Therapy. Radiation therapy involves high energy particles or waves to damage or destroy the cancer cells. The therapy might involve delivery of radioactive particles or substances, engineered nanomaterials accumulating in the tumor site and consequent ablation of substances by radiation to exert therapeutic effect [10,12-15]. In the U.S. about 60% of the cancer patients receive radiation treatment at some point of the systemic cancer treatment [16]. Radiation damages the DNA of the cancer cells and inhibit the growth [16-18]. The therapy also affects the normal cells but most of the slow growing normal cells are able to fix the damage and go back to their normal functioning. As the cancer cells are rapidly dividing cells and replicate their DNA more often than the normal cells, the toxic effect is more dominant on the cancer cells upon DNA damage. The radiation therapy is conducted in a confined tumor area. The objective of the radiation therapy in cancer treatment is to eradicate maximally possible cancer cells while minimal killing of normal cells [19]. The precise removal of tumor cells with minimally affecting the normal tissues is achieved by the advancements in the radiation treatment technologies such as intensity modulated radiation therapy (IMRT)[20], image guided radiation therapy (IGRT) [21], stereotactic body radiation therapy (SBRT)[22] and Delta4 Discoverer[16]. These technologies offer precise and controlled damage of tumor site leaving a large portion of normal cells. Moreover, advancement in imaging technologies such as positron emission tomography-computed tomography (PET-CT)[23,24], MRI [25,26] and pretreatment CT enhanced the efficacy of radiation therapy [27]. Radiation therapy is used in combination with surgery or chemotherapy to treat cancer patients.

1.2.3. Chemotherapy. While surgery and radiation therapy can treat localized tumors spreading over a smaller area and are unable to treat metastasized tumors, chemotherapy can reach to every organ in the body in an effort to cure cancer. Chemotherapy is the major form of treatment method for both the localized and metastasized cancer across all cancer types[28]. Conventional chemotherapeutic drugs are associated with poor aqueous phase solubility, non-specificity and multi drug resistance. Because of the lack of solubility the chemotherapeutics are required to administer with solvents causing severe toxicity. The non-selective chemo drugs affect the fast growing healthy cells in the body and cause poor survival rate following the treatment. Moreover, multi drug resistance mechanism causes transport of the drug molecules out of the cancer cells through enhanced activity of efflux pump molecules such as P-glycoproteins in cancer cell membrane which causes partial therapeutic response or cancer recurrence. Despite the therapeutic limitations and severe toxicity chemotherapeutic drugs are being used ubiquitously in cancer treatment as a first line of defense and in some cancers non targeted chemo drugs are the only treatment option because of lacking of any targetable surface biomarker. For example, in triple negative breast cancer non targeted chemotherapy is still the sole option for treatment [29]. Several chemotherapeutic drugs have been approved by FDA and are being used clinically either alone or in combination with another chemotherapeutic drug. Chemotherapeutic drugs have wide range of mechanisms of action. The alkylating agent drug class impair cancer cell growth by alkylating specific sites on protein molecules, DNA and RNA[30]. Their activity mostly depends on the relatively fast duplication rate of the cancer cells. The common clinically used alkylating agent drugs include nitrogen mustards, platinum complexes (Cisplatin,

Carboplatin), nitrosoureas and many others [31]. Hyperactive DNA repair mechanism and efficient glutathione conjugation in cancer cells cause resistance to alkylating agent drugs[32]. The antimetabolites, for example, 5- fluorouracil interfere with the DNA synthesis and inhibit the cancer cell growth [33]. Bleomycin, a member of antitumor antibiotics drug class intercalates DNA, forms free oxygen radicals causing DNA breaks and cell growth inhibition[34,35]. The anthracycline antibiotics such as Doxorubicin cause intercalation between the base pairs of DNA and specifically inhibit the DNA topoisomerases I and II resulting in cell growth arrest [36]. The epipodophyllotoxin drugs inhibit the cell growth by stabilizing the DNA topoisomerase II complex[37]. Vinca alkaloid chemo drugs dissemble the microtubule assembly and block the polymerization of microtubules resulting in cell growth inhibition[38]. In contrast to the mechanisms of vinca alkaloids which cause microtubule disassembly, Taxanes such as Paclitaxel and Docetaxel promote microtubule assembly and stabilization resulting in cell growth arrest in mitosis phase [39,40]. Alkaloid camptothecin semi-synthetic analogs such as Irinotecan and Topotecan cause interruption in DNA replication elongation phase and inhibit topoisomerase I resulting in cell growth inhibition [41,42].

1.2.4. Cancer Immunotherapy. Cancer immunotherapy is a relatively recent therapeutic strategy that involves activating, boosting or engineering the immune cells to recognize malignant tumor cells and fight them[43]. Immune cells are programmed to kill any malignant cells or foreign they encounter. However, as the cancer cells evolve from normal cell phenotype of our own body, the immune system cannot see them as foreign or malignant. Sometimes the cancer cells impose a brake on the activity of these immune cells. Moreover, the aggressive form of cancer tissue surpasses the capability of immune

cells to fight them. Several strategies have been adopted over the years to stimulate the activity of immune cells to fight against cancer. The checkpoint inhibitor immunotherapeutic drugs (*e.g.,* anti-PD1/PDL1, anti-CTLA4) take the brakes off the immune cells and help them recognize and attack the cancer cells[44-47]. In chimeric antigen receptor (CAR)-T cell therapy, cytotoxic T cells from patients' blood are drawn, modified in the laboratory condition to recognize specific marker on the malignant cell surface and reintroduced into the individual again. The modified T cells now attack only the malignant cells that they were trained to attack[43]. However, the CAR-T therapy is currently not therapeutically effective in treatment of solid tumors and limited to refractory hematological malignancies[48]. There are drugs that boost the immune cells to fight against cancers known as immunomodulatory drugs, are widely used in cancer treatment. Targeted therapeutic mAb *e.g.,* Trastuzumab recognize a specific antigen or biomarker and inhibit the growth of cancer cells[49]. Therapeutics involving cancer vaccines, oncolytic viruses, and cytokine delivery are also novel immunotherapeutic strategies to fight cancer[50].

1.3. NANOPARTICLE BASED THERAPEUTICS IN CANCER TREATMENT

Therapeutic molecules including small molecule drugs, chemotherapeutic drugs, RNA interference molecules are being integrated with nanosized drug delivery vehicle systems and utilized for cancer treatment. The drug encapsulated nanocarriers facilitate the entry of therapeutics into the tumor tissue by providing with improved solubility in physiological conditions inside the blood vessel, enhanced bio-availability and bio-distribution. The selective targeting of cancer tissue with minimal effect on the healthy

cells can be achieved by utilizing the concepts of "passive" and "active" targeting principles of cancer therapeutics (Figure 1.2).

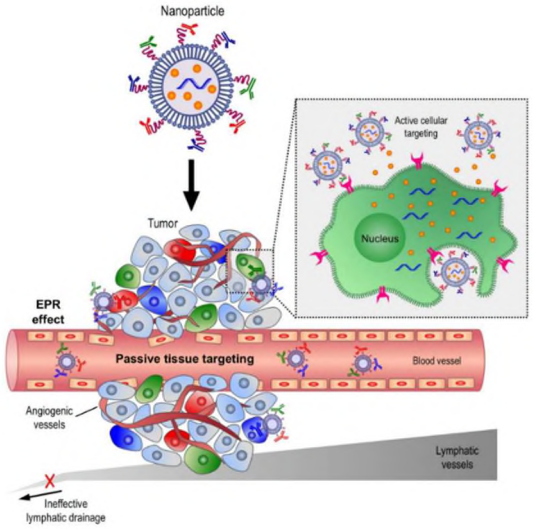

Figure 1.2. A representation of passive and active targeting of nanoparticle based cancer therapeutics [51]

- **Passive targeting and EPR effect:** In passive targeting approach, nanocarriers utilize the defective "leaky" tumor blood vessels and poor lymphatic drainage system in the vicinity of solid tumor. These characteristics of the tumor microenvironment allow the preferential accumulation of nanoparticles in the tumor site, a phenomenon known as enhanced permeability and retention (EPR) effect [52].
- **Advantages and limitations of passive targeting:** The nanocarriers used in drug formulation provide the system with a better pharmacokinetics profile, enhanced solubility of drugs, improved toxicological profile. For example, the polymeric nanoparticle formulations used in clinically approved drugs showed the characteristics of water solubility, non-toxicity and biodegradability. Moreover, the EPR mechanism

allowed the formulation to selectively accumulate in the cancer site. Polymeric micelles have been proven to be a suitable carrier of the water insoluble drug. The self-assembling system is easy to modify, biocompatible, biodegradable and has a good targeting potential. Liposomes are another class of cancer drug nanocarrier having a self-assembling colloidal structure composed of lipid bilayers. The drug nanocarrier system is biocompatible, easier for surface modification and has good potential for selective targeting of tumor cells. Dendrimers nanocarriers can provide high ligand density, tunable pharmacokinetics and bio-distribution profile. The system is convenient to functionalize and has high structural and chemical homogeneity. Taken together, integration of nanotechnology in the drug delivery system has shifted the paradigm of cancer drug design and development. However, only 15 passively targeted nanoparticle based drugs were in clinical practice till 2018. Instability in circulation, premature drug release, toxicity to normal cells, poor oral bioavailability, insufficient accumulation of drugs at the cancer site have caused hindrances in clinical translation of nanoparticle based cancer therapeutics. Moreover, the understanding is limited by the poorly known mechanisms of complex nano-bio interactions in the tumor microenvironment. The other potential causes limiting the therapeutic efficacy of nanoparticle based drugs can largely be attributed to the heterogeneity in permeability in tumor blood vessels, poor tumor penetration, hypoxia and angiogenesis, and poor intracellular endosomal escape capability of the drug. In addition to that, a major portion of the nanoparticle therapeutics are cleared by the phagocytic systems, hepatocytes, kupffer cells while some physically cannot get through the sinusoids of the liver.

- **Current passively targeted nanoparticle based therapeutics:** Till November, 2018, only 15 passively targeted drugs got approval for cancer treatment [53]. Doxil (PEGylated liposomal doxorubicin, liposomal system), approved in 1995 by FDA is the first clinically used passively targeted nanoparticle based drug for cancer treatment [54]. The promising characteristics of the drug formulation include prolonged blood circulation time, avoidance of reticuloendothelial system (RES) or phagocytic elimination and high doxorubicin loading [54]. Other examples of clinically approved passively targeted nanoparticle based drugs include Abraxane [55,56](albumin-taxol, polymer drug conjugate system), Marqibo [57](vincristine sulfate, liposomal system), DaunoXome [58](liposomal daunorubicin, liposomal system), Onivyde [59,60](irinotecan, liposomal system), Vyxeos [61](cytarabinee-daunorubicin combination, liposomal system), Myocet [62,63](Non, PEGylated liposomal doxorubicin, liposomal system), Mepact [64,65](mifamurtide, liposomal system) , Genexol-PM [66](PEG-PLA-taxol, polymeric micelles system), and SMANCS [67,68](neocarzinostatin, polymer drug conjugate system). While most of the formulations mainly focus on improving the drug pharmacokinetics, drug solubility and toxicological profile, some nanoparticle based cancer drug formulations have enhanced therapeutic response in patients and improved the overall survival percentage compared to the standard non-formulated chemo drugs. For example, Abraxane (albumin-Paclitaxel) polymer drug conjugate formulation significantly enhanced the therapeutic response in metastatic breast cancer patients in phase III clinical trial compared to the standard Paclitaxel treatment [55,69].
- **Active targeting:** The "active" targeting involves binding of affinity ligands functionalized on the nanocarrier surface to the specific overexpressed biomarkers or

receptors on the target cells improving selective tissue homing and enhanced retention at the tumor vicinity [70]. The targeted biomarker enhances the internalization of nanoparticles upon binding with nanoparticle surface functionalized ligands.

- **Advantages and limitations of active targeting:** Actively targeted nanoparticle based drugs showed greater potential in cancer treatment by utilizing the enhanced tumor localization and most crucially by the selective inhibition of cancer cells minimizing the side effects in cancer treatment [71,72]. In fact, integration of actively targeting mechanism with optimization in nanocarrier design will allow for the design of a more efficacious nanotherapeutic platform for cancer treatment [73]. Ligands employed on the actively targeted nanocarrier surface enhance the nanoparticle accumulation in the intravascular tumor cells or endothelial cells of tumor blood vessels[70,74]. Moreover, the internalization of ligand functionalized targeted drug nanoparticle can be mediated through a specific pathway by a specific antigen overexpressing tumor cells and the intracellular accumulation can be increased [75]. However, the greater potential is associated with more complex challenges. The first barrier comes with the transport process of the nano-drug delivery systems. The protein coating formed around the surface of the nanoparticles, known as the "protein corona" limits the blood circulation time of the particles by altering the stability and surface architecture of the particle[76-79] though longer blood circulation time for nanoparticles might not be so crucial considering a high pressure blood flow in the tumor microenvironment blood vessels[53]. The protein coating alters the pharmacokinetics and helps elimination by immune systems of the delivery system [80]. The protein corona also hinders the receptor targeting, intracellular uptake, intracellular trafficking of the actively targeted nanoparticle based drugs[77]. The challenge also remains

in predicting the correlations between nanoparticle size and the binding affinity or tissue specific accumulation of drugs. Such a mechanistic model predicts that the nanoparticle size ≥50 nm does not enhance the accumulation of drugs at the malignant tumor site when compared to the non-targeted nanotherapeutic system[81]. Endosomal escape into the cytosol is one of the major barriers of the actively targeted nanoparticle based drug delivery systems. Nanoparticles internalized or uptaken by the tumor cells in clatherin mediated endocytic pathway enter the endosomes and are subsequently degraded in lysosomes by a intracellular degradative mechanism often driven by the pH of these subcellular compartments[82]. One of the ingenious mechanisms to enhance endosomal escape efficiency is "proton sponge effect" that utilizes the pH buffering substances for endosomal escape[83]. Exocytosis, the cellular recycling process is another major limitation for actively targeted nanoparticle based drugs. It has been demonstrated that 70% of the uptaken endosomal siRNA encapsulated lipid nanoparticle were rejected by the tumor cells through exocytosis[84]. The current drug delivery vehicles targeting a single biomarker or mechanism of action often develop tumor resistance and promotes tumor relapse because of the partial and non-sustainable therapeutic outcome[85]. Moreover, the choice of specific biomarker ligands, conjugation of ligands with nanoparticle and complex manufacturing process impose great hindrance on the efficacy of actively targeted nanoparticle based therapeutic drug delivery vehicles [2].

- **Current actively targeted nanoparticle based cancer therapeutics:** None of the actively targeted therapeutics have been approved for clinical use in cancer treatment till November, 2018 [53]. However, a number of drugs have entered in clinical trials. Table

1.1 summarizes the all intravenous actively targeted nanoparticle based cancer therapeutics that are in different stages of clinical trials as of August 2019 [86].

Table 1.1. Current intravenous nanoparticle based actively targeted therapeutics in clinical trials [86]

Generic/ Propriety Name	Formulation	Ligand/Target	Payload	Cancer Type	Phase (As of August,19)
BIND-014	Poly(lactide)-poly(ethylene glycol)	PSMA substrate analog inhibitor	Docetaxel	Metastatic castration resistant PC	Phase I/II completed
REXIN-G	Retroviral expression vector	SIG-binding peptide	Cytocidal cyclin G1 gene	PanC, osteosarcoma, mBC, soft tissue sarcoma	Phase I/II completed
2B3-101	PEGylated liposome	Glutathione/Blood brain barrier	Doxorubicin	Advanced solid tumor, brain metastasis, LC,BC, melanoma, malignant glioma	Phase I/II completed
SGT 53	Cationic liposome	Anti-transferrin scFv/transferrin receptor	WT p53 gene (plasmid DNA) and chemo drug combination	Glioblastoma, solid tumors, mBC, mPanC, childhood CNS tumors	Phase I/II recruiting
ANTI-EGFR-IL-DOX	PEGylated immunoliposome	Antigen binding fragments (Fab') of cetuximab	Doxorubicin	TNBC	Phase I/II recruiting
CORNELL DOTS	PEGylated silica nanoparticles	cRGDY targeting peptide	NIR dye and 89Zr/124I	Imaging of melanoma and brain tumor	Phase I/II recruiting
MBP-426	Liposome	Transferrin /transferrin receptor	Oxaliplatin	Metastatic solid tumor,	Phase I/II
SGT-94	Cationic liposome	Anti-transferrin scFv/transferrin receptor	RB94 plasmid of the WT Rb tumor suppressor protein	Rb negative minors	Phase I completed
MESOMIR 1	Nonliving bacterial minicells	Anto-EGFR bispecific antibody/EGFR	miR-16 based microRNA	Mesothelioma, NCLC	Phase I completed
LIPOVAXIN-MM	Liposome	V_H domain antibody (dAb) fragment /DC-SIGN	Vaccine for inducing antitumor T cells	Metastatic melanoma	Phase I completed
MM-302	Liposome	Anti HER2-scFv/HER2	Doxorubicin	mBC (HER2 positive)	Phase II terminated
MCC-465	PEGylated immunoliposome	F(ab")2 fragment of human mAb GAH	Doxorubicin	Metastatic stomach cancer	Phase I/II terminated
CALAA-01	PEGylated cyclodextrin	Transferrin /transferrin receptor	C05C siRNA	Solid tumors	Phase I terminated

WT, Wild Type; Rb, Retinoblastoma; mBC, metastatic breast cancer; TNBC, triple negative breast cancer; PC, prostate cancer; LC,lung cancer; NCLC, non-small lung cancer; PanC, pancreatic cancer; mPanC, metastatic pancreatic cancer,siRNA; small interfering RNA

MCC-465 being the first actively targeted nanoparticle based drug showed selective accumulation in stomach cancer tissues over the normal cells [87]. SGT-53, a transferrin receptor targeted and p53 plasmid DNA encapsulating cationic liposome nanocarrier has been shown to sensitize cancer cells to the subsequent treatment with radiation therapy and systemic chemotherapy[88,89]. The first polymer based targeted nanotherapeutic drug to enter the clinical trial is CALAA-01 which encapsulates small interfering RNA molecule (siRNA), has shown RNA interfering mechanisms in patients and also showed enhanced accumulation in tumor cells intracellularly [75]. These examples show promising insights towards future clinical success of actively targeted nanoparticle based cancer drugs.

1.4. COMBINATION THERAPY TO OVERCOME THE THERAPEUTIC RESISTANCE IN CANCER TREATMENT

Treatment with a single drug often causes partial response in cancer treatment. The cancer cells often acquire resistance to the treatment and hence cause disease recurrence. Old age chemotherapeutic drugs, mAb-based targeted drugs, small molecule kinase inhibitors have been proven to improve the therapeutic response in cancer patients when used in combination with other suitable drugs[90,91]. In fact, the combination therapy is the key treatment strategy for most cancer treatments now [92]. For example, Trastuzumab is used to treat early stage HER2- positive breast cancer as a first line of treatment. However, the complete response of the treatment is not achieved in 20-60% cases of the HER2- positive and HER2-enriched breast cancer patients[93]. The treatment is also associated with the risk of therapeutic resistance and tumor recurrence after a certain period of the treatment. The lower risk of tumor recurrence and better outcome can be

expected when Trastuzumab is administered with another chemotherapeutic drug in combination[94,95]. Till 2013, four phase III clinical trials involving more than 8,000 patients showed that the risk of recurrence was decreased by 50% in when Trastuzumab was administered with or after chemotherapy in combination[91,96-99]. The American Society of Clinical Oncology (ASCO) guideline updated in 2018, recommended anti HER2 therapy in combination with chemotherapy or a taxane (Paclitaxel and Docetaxel are most common in practice) as a first line of treatment for metastatic HER2-positive breast cancer. Trastuzumab treatment has been shown to sensitize the breast cancer cells to the microtubulin polymerization agent especially to the taxols and the drugs synergize improving the therapeutic outcome *in vivo* [100-102]. Combination therapy with Paclitaxel and Trastuzumab for adjuvant HER2- positive breast showed promising long term clinical outcome in recent years. In 2015, after a median follow up period of 4 yr, adjuvant Paclitaxel and Trastuzumab combination treatment trial involving 406 node negative HER2-positive breast cancer patients reported the 3 yr disease free survival rate (DFS) to be 98.7%[103]. In 2019, after 7 yr follow up period, the DFS was 93% with an overall survival rate (OS) of 95% [104].

1.5. ANTIBODY DRUG CONJUGATES

Antibody Drug Conjugates (ADCs) are the combination therapeutic system consisting small molecule cytotoxic drugs covalently bound to the mAb via a stable linker (Figure 1.3).

The coupled antibody directs towards a specific antigen that is highly expressed on the cancer cell surface.

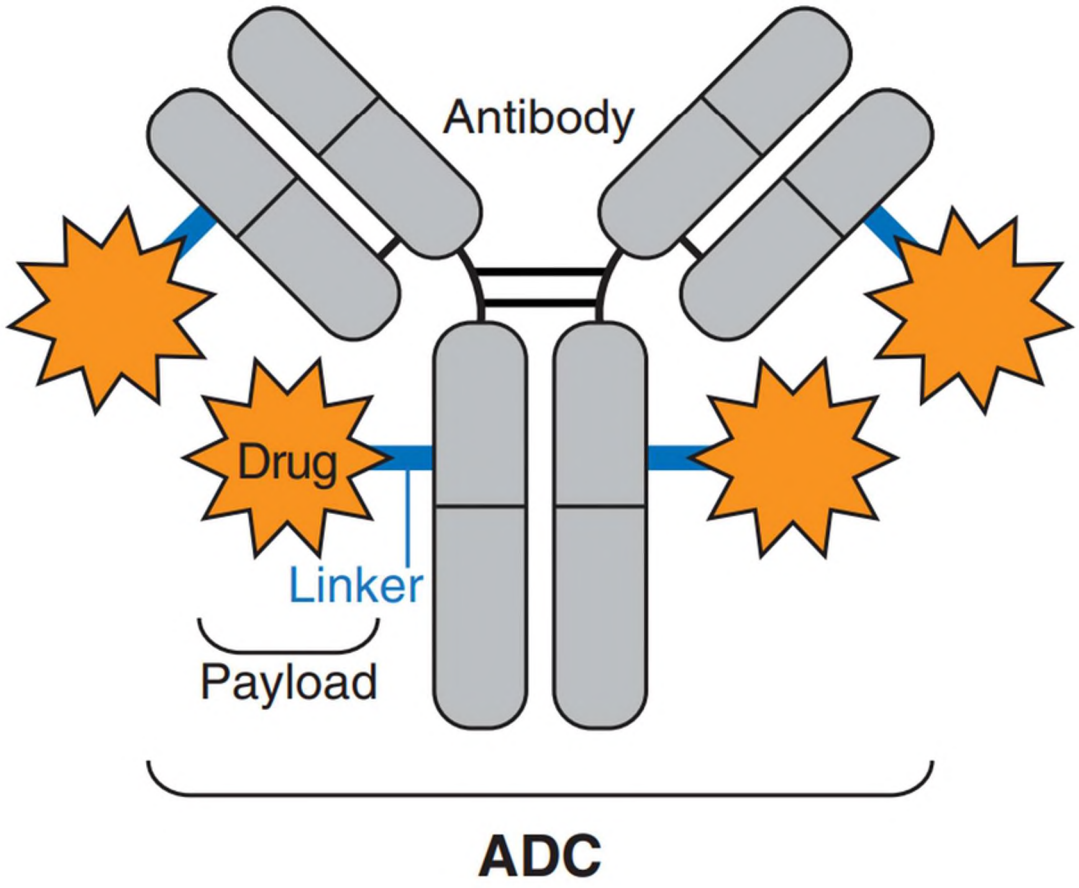

Figure 1.3. Schematic structure of ADC [105]

Antigen binding initiates downstream signaling pathways to inhibit the cancer cell growth. Eventually, the antibody is internalized in the intracellular endosomes with the conjugated therapeutic drug molecule through a clathrin or caveolae mediated endocytosis [106] and pinocytosis pathway [107] . The endosomes containing the ADC subsequently mature into lysosomes [108,109]. In the lysosome, the linker is cleaved and the drug molecule released in the cytosol exerts the therapeutic effect following reaching to its target either binding with cytosolic microtubules or nuclear DNA [110] (Figure 1.4).

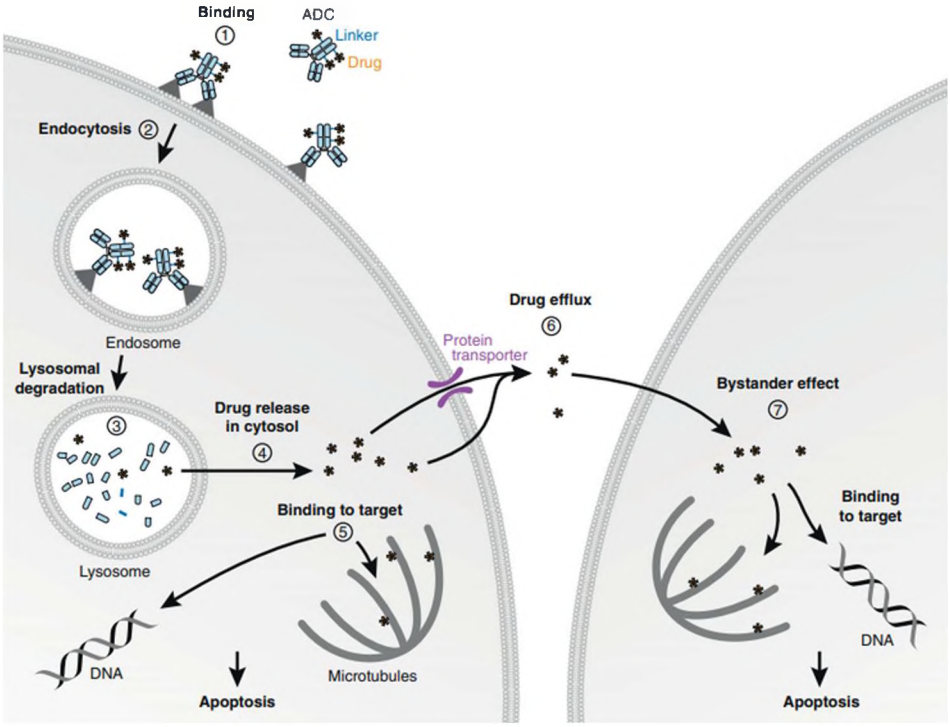

Figure 1.4. Antigen binding and intracellular trafficking of ADC [105]

1.5.1. Advantages and Challenges Associated with ADCs. ADCs have the novel advantages of utilizing mAb to specifically target cancer tissue site while also delivering cytotoxic potential anti-cancer drug molecule. The system can potentially enhance the tumor site specific accumulation of drugs with low or no cytotoxic effects on the normal cells[111,112]. There are major limitations involved along with the ingenuity of the ADC combination therapeutic system. Selection of target antigens, drug hydrophobicity, insufficiently low therapeutic payload, off target toxicity due to unstable linker conjugation in physiological system, drug efflux and multidrug resistance constitute the major limitations of ADC therapeutic system[113-118]. Till 2017, the two third of the cytotoxic small molecule drugs in the ADC systems that were on clinical trials came from only auristatins and maytansinoids family which inhibit the tubulin

assembly[119]. This suggests that there still lies limitations keeping from using diversified drug molecules in ADC system. High susceptibility to multi drug resistance is a common barrier in successful formulation of ADCs. Cancer cells often become resistant to multiple drugs through enhanced drug efflux mechanism. The upregulation of multidrug resistance protein encoding genes including MDR1, MRP1 and MRP3 promote the efflux transporter activity in cancer cells and result in drug resistance [120]. *In vitro* therapeutic efficacy of Mylotarg drug on acute myeloid leukemia (AML) cell lines showed that P-glycoprotein expression significantly altered the therapeutic potency of the drug molecule and treatment with efflux transporter inhibitor restored the potency of the payload [121]. An ADC system AVE9633 comprising the anti CD33 linked with a cytotoxic maytansine analog molecule DM4 has also been shown to be dependent on P-glycoprotein expression level for its therapeutic efficacy *in vitro* [122]. Hydrophobic nature of ADC reduces the pharmacokinetics and therapeutic index of the system. Hydrophobicity also induce antibody aggregation causing small shelf life and clearance by immune cells [112]. Moreover, the conventional drug to antibody ratio (DAR) in ADC system is 3.5-4.0 [106,113]. The *in vitro* therapeutic efficacy of ADC system increases with increasing DAR value[113]. Site specific highly loaded ADC system showed enhanced *in vivo* therapeutic efficacy in a system with low antigen expression at the target site [123]. In the same system, no or low therapeutic effect was observed when treated with similarly loaded conventional molecule or with the similar ADC having low payload. This suggests that a conventional therapeutic payload might not be sufficient for achieving satisfactory outcome while targeting cancer cells with lower abundance in antigen expression [124]. However, high DAR value has been showed to positively correlate with

enhanced ADC plasma clearance resulting in reduced *in vivo* efficacy [125]. So, balancing between the enhanced payload and best achievable therapeutic index in the conventional ADC platform is both a dilemma and a compromise [126]. Again, lower abundance of target antigens on the tumor cell surface results in further therapeutic inefficacy, often causing treatment resistance. These limitations have hindered the clinical success of methotrexate, doxorubicin and alkaloid based ADCs[119,127]. Optimization in linker conjugation and stability is another challenge in developing ADCs. Premature release of drug molecule in the blood circulation cause toxicity to normal tissue and poor therapeutic index. Hydrophobic linker molecule has been showed to promote enhanced efflux transporter activity in cancer cells resulting in drug resistance. Non polar linker molecule in maytansinoid-based ADC system showed low potency in MDR1 overexpressed cancer cells *in vitro* due to enhanced transport of hydrophobic molecule by MDR1 activity [113]. Moreover, majority of the ADCs have maleimide type conjugation chemistry and often undergo deconjugation, causing off target toxicity [113].

1.5.2. Strategies for Developing Efficacious ADCs. Diversification in the drug selection, linking chemistry and alternative form of mAbs are brought into the development of ADCs.

- **Selection of drugs:** For designing efficacious ADC system, the selected drug molecule must possess good aqueous phase solubility, potent toxicity, specified site for linker conjugation and maintenance of potency after conjugation[110,128,129] . In selection of potent cytotoxic drugs, lowering the minimum effective dose of cytotoxic drugs should be considered to reduce off target toxicity and improve the therapeutic index of ADCs. In case of malignant tissue selectivity, the therapeutic index can be improved by focusing on

increasing the maximum tolerated dose. The drugs must retain the efficacy and have aqueous phase stability after modification by linker chemistry. The drugs should be synthetically available and the manufacturing process should be cost effective [129]. Moreover, a better understanding of the toxicity profile of ADCs as a combination drug system should be addressed in the development of next generation ADCs.

- **Bystander effect:** The target antigen expression in solid tumor tissue is heterogeneous in nature. The designed ADC selective for a specific antigen might not affect a large cell population with low or no antigen expression. This might cause partial therapeutic response in cancer treatment. The design consideration or characterization of ADCs that allow the system to affect the neighboring malignant cells with low or no antigen expression is called bystander effect. For example, the FDA approved ADC brentuximab vedotin contains neutral monomethyl auristatin E (MMAE) drug molecule. Upon protease mediated cleavage of ADC, MMAE is released, crosses the bio membranes and kills the neighboring epithelial cancer cells[130-134]. Other example of ADCs that have been reported to possess bystander effect include trastuzumab duocarmazine (kills HER2- negative cells though targeted against HER2+ breast cancer population *in vitro*)[135] , coltuximab ravtansine (targets CD19, phase II clinical trial, 2017)[136] , anetumab ravtansine (targets mesothelin, phase I clinical trial , 2017) [137].
- **Selection of linkers and conjugation chemistry:** The mechanisms of drug release is an important consideration for developing ADCs. This is mostly achieved by the appropriate selection of linkers. The physiological stimuli such as pH, glutathione concentration, and proteolytic degradation are responsible degradation of cleavable linkers while the non-cleavable linkers rely on mAb degradation in the lysosomal

compartment to release the drug after internalization. ADCs comprising the both type of linkers were approved by FDA or are currently in clinical trials. For example, The ADC brentuximab vedotin (marketed as Adcetres) which was approved in 2011 by FDA for anaplastic large cell lymphoma, utilizes the degradation of cleavable linker valine-citrulline (vc) by lysosomal proteases such as cathepsin B [138]. Another FDA approved (in 2013) ADC Ado-trastuzumab emtansine (marketed as Kadcyla, popularly known as T-DM1) for HER2-positive metastatic breast cancer treatment comprised a non-cleavable linker lysine-SMCC that utilized the proteolytic degradation of mAb to release the drug molecule [139]. Each strategy has their own merits and demerits and optimization is needed considering the comprising drug, antibody and targeted site. The conventional thiosuccinimide linkage involving the reaction of thiols and alkyl maleimides are being replaced by novel site specific conjugation chemistries including engineered cysteines , unnatural amino acid engineering, enzyme assisted ligation , glycan remodeling and glycoconjugation, amino terminal engineered serine , ligation to Fab nucleotide –binding sites, cysteine rebridging, among many others [112].

- **Selection of alternative forms of antibody:** Alternative configurations of full length mAbs are also being investigated in state of the art ADC systems. This include nanobodies, tumor tissue specific novel probodies, single chain variable fragments (scFvs), antigen binding fragments (Fabs), ADCs with biparatopic activity (binds two different epitopes on the same antigen) and other formats.

As discussed, the use of diverse clinically approved chemo therapeutic drugs such as methotrexate, taxoids, anthracyclins and alkaloids is still a challenging task to incorporate in the ADC platform due to hydrophobic nature, insufficient drug delivery to

the tumor tissue and off target toxicity in the normal tissue resulting in poor therapeutic index [113,129]. In this work, these limitations have been addressed by integrating the concepts of nanotechnology, actively targeted drug delivery and combination therapy in a single novel therapeutic platform. The conventional ADC system was remodeled into an actively targeting nanosized therapeutic platform ADN designed for combination treatment in HER2-positive breast cancer. Rod shaped nanoparticles were synthesized using pure chemotherapeutic drug. The drug nanoparticles were covalently conjugated with mAb to target an actively expressed biomarker on the cancer cell surface. The engineered ADN showed enhanced *in vitro* selectivity and a synergistic therapeutic efficacy on the HER2-positive breast cancer cells compared to the single drug treatments. The therapeutic efficacy of the ADN was also mechanistically determined at the protein expression level. In a following study, the deep genetic mechanism and transcriptional regulation determining the treatment response with engineered ADN were investigated. The objective of the study was to identify the novel genetic pathways that might cause enhanced treatment response or potential therapeutic resistance in breast cancer cell lines upon treatment with ADN. Taken together, the work presented the development and therapeutic efficacy of ADN system for targeted cancer treatment with synergistic efficacy. The work also investigated the mechanisms of ADN therapeutic efficacy at cellular, molecular and gene expression levels. Figure 1.5 shows the schematic diagram of the primary works presented in the dissertation.

In addition, the dissertation also presents a study on the design and therapeutic efficacy of a multifunctional polymer coated superparamagnetic NIR responsive

nanosized therapeutic platform harnessing both the integrity of diagnostics and therapeutics in a single platform for cancer treatment.

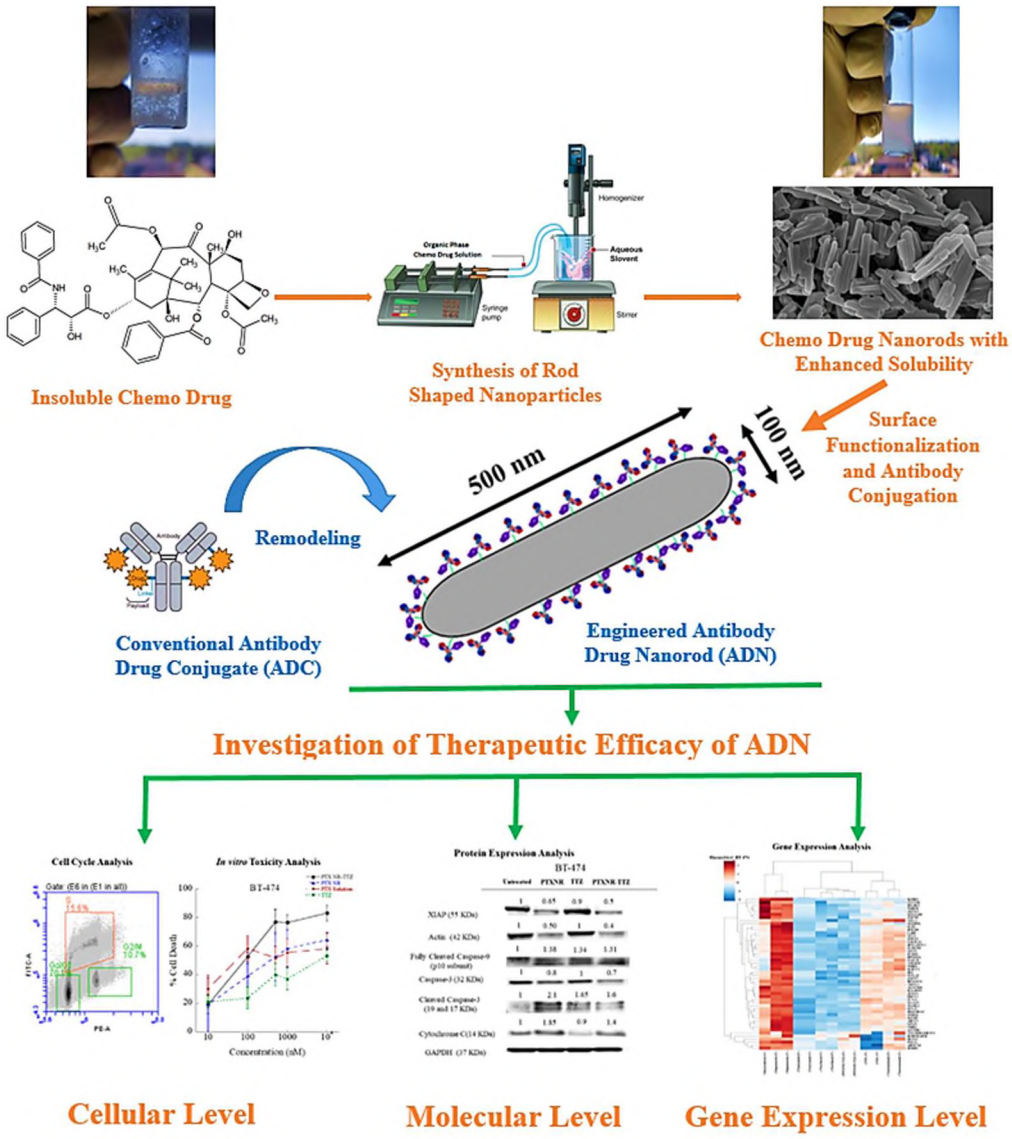

Figure 1.5. An overview of the primary works presented in the dissertation

Finally, the work presents a study on therapeutic efficacy of a natural cyanobacterial extract glycoglycerolipid molecule MGDG, that was investigated for

potential anti-cancer application. The sequential overview of the dissertation is shown in the following block diagram (Figure 1.6).

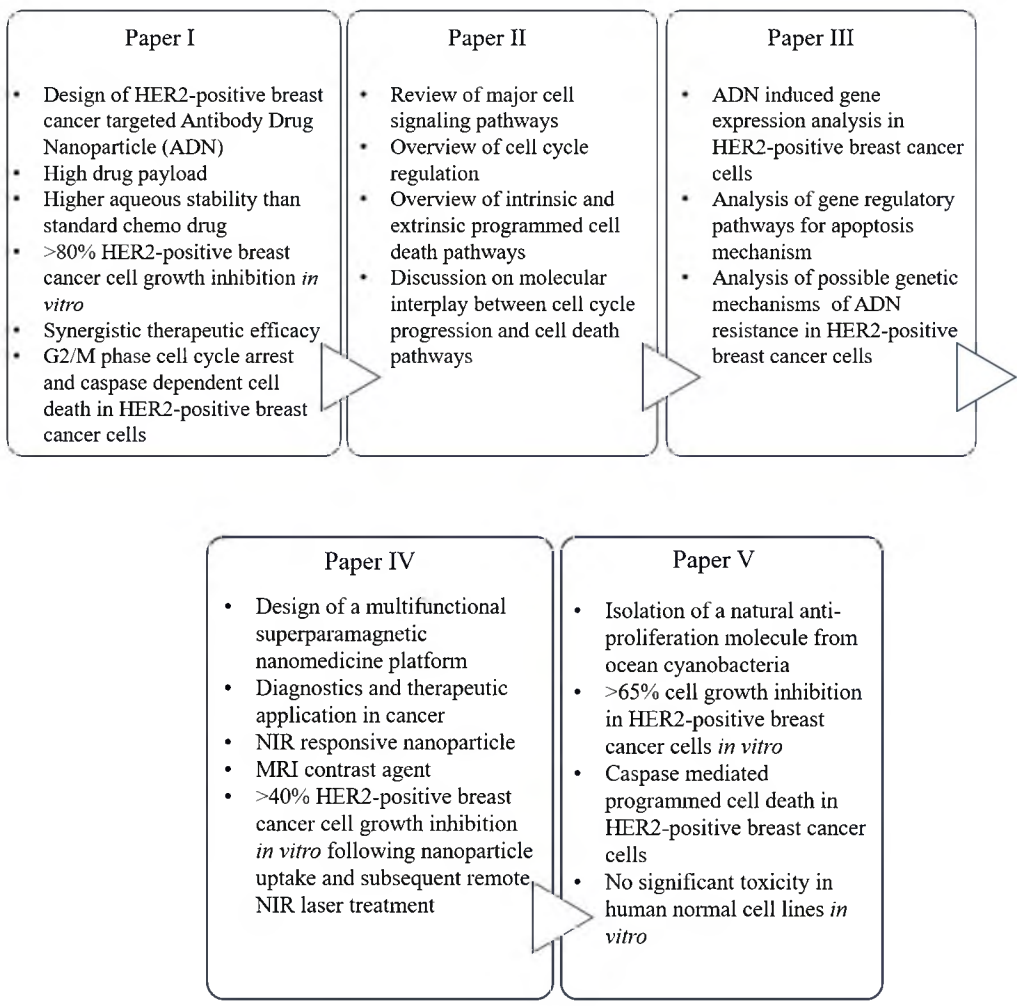

Figure 1.6. Overview of the dissertation

PAPER

I. ANTIBODY-DRUG NANOPARTICLES INDUCES SYNERGISTIC TREATMENT EFFICACIES IN BREAST CANCER CELLS

ABSTRACT

Chemotherapeutic drugs suffer from non-specific binding, undesired toxicity, and poor blood circulation which contribute to poor therapeutic efficacy. In this study, antibody-drug nanoparticles (ADNs) are engineered by synthesizing pure anti-cancer drug nanorods (NRs) in the core of nanoparticles with a therapeutic monoclonal antibody, Trastuzumab on the surface of the NRs for specific targeting and synergistic treatments of breast cancer cells. The ADNs were designed by first synthesizing ~95 nm diameter × ~500 nm long paclitaxel (PTX) NRs using the nanoprecipitation method. The surface of PTXNRs was functionalized at 2′ OH nucleophilic site using carbonyldiimidazole and conjugated to TTZ through the lysine residue interaction forming PTXNR-TTZ conjugates (ADNs). The size, shape, and surface charge of ADNs were characterized using scanning electron microscopy (SEM), SEM, and zeta potential, respectively. Using fluorophore labeling and response surface analysis, the percentage conjugation efficiency was found >95% with a PTX to TTZ mass ratio of 4 (molar ratio ≈ 682). *In vitro* therapeutic efficiency of PTXNR-TTZ was evaluated in human epidermal growth factor receptor 2 (HER2) positive BT-474 and HER2 negative MDA-MB-231 breast cancer cells using MTT assay. PTXNR-TTZ inhibited >80% of BT-474 cells at a higher

efficiency than individual PTX and TTZ treatments alone after 72 h. A combination index analysis indicated a synergistic combination of PTXNR-TTZ compared with the doses of single drug treatment. The molecular mechanisms of PTXNR-TTZ were investigated using cell cycle and Western blot analyses. The cell cycle analysis showed PTXNR-TTZ arrested >80% of BT-474 breast cancer cells in the G2/M phase, while >70% of untreated cells were found in the G0/G1 phase indicating that G2/M arrest induced apoptosis. A similar percentage of G2/M arrested cells were found to induce caspase-dependent apoptosis in PTXNR-TTZ treated BT-474 cells as revealed using Western blot analysis. PTXNR-TTZ treated BT-474 cells showed ~1.3, 1.4, and 1.6-fold higher expressions of cleaved caspase-9, cytochrome C, and cleaved caspase-3, respectively than untreated cells, indicating up-regulation of caspase-dependent activation of apoptotic pathways. The PTXNR-TTZ ADN represents a novel nanoparticle design that holds promise for targeted and efficient anti-cancer therapy by selective targeting and cancer cell death *via* apoptosis and mitotic cell cycle arrest.

1. INTRODUCTION

Engineering nanoscale drug delivery systems have been studied extensively because of several advantages including high drug payloads,[1-5] improved drug release,[6,7] enhanced bioavailability,[8,9] and increased multivalence effects through receptor-ligand interactions.[10-13] The use of a ligand allows direct delivery of the cytotoxic agent to target cells, however, the clinical success of targeted antibody-drug conjugates is limited due to poor bioavailability and low therapeutic efficacy.[14-16] Improvements in drug design in

combination with active targeting are shown to enhance cellular uptake, targeting, and higher therapeutic efficacy which have led to the design of antibody-drug nanoparticles (ADNs). ADNs are comprised of an anticancer drug core nanoparticle conjugated with a therapeutic monoclonal antibody on the nanoparticle surface for targeted delivery and enhanced therapeutic efficacy. Trastuzumab (TTZ) is used to treat early-stage human epidermal growth factor receptor 2 (HER2) positive breast cancer as the first line of treatment. However, the complete response of the treatment is not achieved in 20-60% cases of the HER2 positive and HER2 enriched breast cancer patients.[17] The TTZ treatment is associated with the risk of therapeutic resistance and tumor recurrence after a certain period of the treatment. The lower risk of tumor recurrence and the better outcome can be expected when TTZ is administered with another chemotherapeutic drug in combination.[18,19] Till 2013, four Phase III clinical trials involving more than 8,000 patients showed that the risk of recurrence was decreased by 50% when TTZ was administered with or after chemotherapy in combination.[20-24] The American Society of Clinical Oncology (ASCO) guideline updated in 2018, recommended anti-HER2 therapy in combination with taxane as the first line of treatment for metastatic HER2 positive breast cancer.[25]

Combination therapy using paclitaxel (PTX) and TTZ for adjuvant HER2 positive breast cancer showed promising long-term clinical outcomes in recent years. In 2015, after a median follow up period of 4 yr, adjuvant PTX and TTZ combination treatment trials reported that the 3 yr disease-free survival rate is 98.7% in HER2 positive breast cancer patients.[26] In 2019, after 7 yr follow up period, the disease-free survival rate was 93% with an overall survival rate (OS) of 95%.[27] While the combination therapy of PTX

and TTZ are promising, the following challenges still have to overcome in terms of synergy between the drugs, toxicity and therapeutic efficacy.[28] The current clinically used intratumoral concentration of PTX (1-9 μM) is shown to be insufficient for breast cancer treatment.[29] Moreover, PTX is poorly soluble in aqueous phase causing a great limitation and trade-off in terms of toxicity in intravenous administration. The high concentration of TTZ used in clinical trials have always been associated with the risk of severe cardiac arrest.[26-28]

To overcome the limitations of toxicity and off-site targeting, nanoparticles have been engineered with advanced chemical composition,[14-16,30] surface functionalization,[31-35] and geometric modification.[35-38] Nanoparticles made of human serum albumin (Abraxane™) have been used for the delivery of PTX to breast cancer cells.[39] Another example of a nanoparticle-based drug delivery system is liposome-based doxorubicin (Doxil) for the treatment of ovarian cancer[40,41] and breast cancer.[42] However, the efficiency of these nanoparticles is controversial due to the lack of active targeting and controlled drug delivery. Currently, a large number of nanoparticles such as liposomes,[43] polymers,[44] micelles,[45] solid lipid nanoparticles,[46] and other organic and inorganic nanoparticles have been explored to improve the therapeutic efficiency by active targeting of cancer cells through the design of nanoparticle size, shape and surface charge.

Nanoparticle size in the range of 50-500 nm size nanoparticles is desirable for enhanced blood circulation, tissue penetration, and cellular interaction.[36,47,48] Size less than 10 nm is cleared by renal excretion, while larger particles are cleared by phagocytosis.[11,12,49,50] Non-spherical nanoparticles have been reported to be less clearance

by macrophages than spherical nanoparticles as dictated by the contact angle of nanoparticles with the macrophage membrane.[51] Nanoparticle also leads to a dramatic increase in surface area for surface functionalization with targeting ligands such as monoclonal antibodies, affibodies, peptides, and aptamers. For example, binding of rod-shaped nanoparticles can be high if the particle aligns with its major axis parallel to the cell membrane increasing the multivalence effects of receptor-ligand interactions.[10-13]

In this study, we synthesized PTX nanorods (PTXNRs) of the size (96.8 ± 33) × (503.4 ± 210) nm using the nanoprecipitation method. TTZ was used as a HER2 targeting antibody for specific PTX delivery to HER2 positive breast cancer cells. The surface of PTXNRs was conjugated *via* carbonyldiimidazole (CDI), a highly reactive crosslinker to form an active N-acyl imidazole group capable of coupling with amine-containing TTZ and formed a stable amide linkage. Flow cytometry analysis of a fluorophore-labeled PTXNR-TTZ and response surface analysis confirmed the TTZ conjugation efficiency of >95%. A combination approach of PTXNR-TTZ ADNs was explored in exploiting the therapeutic efficacy of the ADNs towards HER2 positive breast cancer cells. It is hypothesized that a combination system using PTXNR-TTZ ADNs enhances therapeutic payloads and treatment efficiency by selective targeting of HER2 positive breast cancer cells.

2. MATERIALS AND METHODS

2.1. SYNTHESIS OF PTXNRs

PTXNRs were prepared using the nanoprecipitation method (SI Figure 1).[10,52,53] Briefly, PTX powder (>99.5%, Alfa Aesar) was dissolved in 5 ml of ethanol at a

concentration of 3 mg/ml. The solution was homogenized at 1000 rpm, sonicated, and injected to 20 mL deionized (DI) water at a flow rate of 2 ml/min to form PTXNRs. PTXNRs were washed three times using DI water by centrifuging at 18,000 rcf for 2 h, suspended, and lyophilized (Labconco) overnight to obtain the dried particles.

2.2. CHARACTERIZATION OF PTXNR

The size and shape of PTXNRs were analyzed using a scanning electron microscope (Hitachi S4700 FESEM). The images were obtained at 10.0 KV accelerating voltage with 4.5 mm working distance and 40,000X magnification. The size distribution of NRs was analyzed using Fiji image processing software(Image J; Win 64 Java 1.8.0). The surface charge of PTXNRs was measured in DI water and phosphate-buffered saline (PBS) using zeta potential (Nano series Zetasizer, Malvern).

2.3. ACTIVATION OF 2′ OH NUCLEOPHILIC SITE OF PTXNR

TTZ (Genentech) was conjugated with the 2′OH nucleophilic site group of PTX using the CDI activation reaction (SI Figure 2). Briefly, 1 mg of dry PTXNRs was suspended in 1 ml of PBS. 5 mg CDI was added directly to the NR suspension with a continuous stirring speed of 600 rpm. The reaction was carried out at 4°C for 20 min to form the amine-reactive PTX-carbamate (PTXNR-CDI). The PTXNRs-CDI were centrifuged at 16,000×g for 30 min and washed five times using DI water to remove the unreacted CDI or imidazole. The particles were lyophilized for subsequent TTZ conjugation reaction.

2.4. ^{1}H-NMR ANALYSIS OF ACTIVATED PTXNR

To confirm the linkage of the activated carbamate group at the 2′OH site of PTXNR, the ^{1}H-NMR experiment was carried out. In carrying out the experiment, 2 mg of each unmodified PTXNR and surface functionalized PTXNR particles were dissolved in 600 µl of chloroform-d solvent (Alfa Aesar). The solvent was used as the internal reference to determine chemical shifts (δ) in ppm. ^{1}H-NMR spectra were then recorded using Bruker advanced III 400 MHz Liquid-State NMR instrument at R.T.

2.5. CONJUGATION OF TTZ WITH ACTIVATED PTXNR THROUGH THE LYSINE RESIDUE INTERACTION

The CDI activated PTXNRs were subsequently reacted with the ε-amino group of lysine residues of TTZ (pKa 10.53) for subsequent conjugation.[54] 100 µg of TTZ powder was dissolved in 100 µl carbonate buffer at pH 9.3-9.5 and added to the CDI activated 100 µl of 1 mg PTXNR-CDI particle suspension. The reaction was allowed to proceed for 48 h at room temperature (~22°C). The resulting TTZ conjugated PTXNR (PTXNR-TTZ) particles were centrifuged at 16,000×g for 25 min and washed using carbonate buffer at pH 9.3-9.5 (3× 1 ml). The supernatant was collected after each washing for quantifying the unbound TTZ. The concentrate was collected by centrifuging the membrane filter at 1,000×g for 2 min. The concentrated PTXNR-TTZ particles were finally re-suspended in 300 µl of PBS (pH 7.5). The amount of PTXNR in PTXNR-TTZ was quantified by measuring absorbance at 230 nm (BioTek Synergy 2; BioTek, Winooski, VT, USA) using a PTX calibration curve (SI Figure 3). The amount of unbound antibody was quantified using a BCA protein Assay (Pierce Biotechnology, Rockford, IL, USA) and a TTZ calibration curve (SI Figure 4). The size and shape of

PTXNR-TTZ particles were investigated using SEM (10.0 kV; accelerating voltage with 5.6 mm working distance and 20,000X magnification). The surface charge of the PTXNR-TTZ was measured in DI water and PBS using a Nano series Zetasizer (Malvern).

2.6. FLUORESCENCE DATA ANALYSIS TO CONFIRM THE CONJUGATION OF TTZ WITH PTXNR

To confirm the successful conjugation of TTZ with PTXNR, TTZ was tagged with Alexa 594 red fluorescent dye molecule (Invitrogen) according to the manufacturer's protocol before conjugating with PTXNR. The fluorescence data of both unconjugated bare PTXNR and conjugated Alexa 594 tagged PTXNR-TTZ particles were obtained using a flow cytometer (BD Accuri C6 plus). The fluorescence signal of the particles was acquired using a 585/40 bandpass filter with 488 nm laser excitation.

2.7. OPTIMIZATION OF TTZ CONJUGATION USING RESPONSE SURFACE ANALYSIS

The optimum conditions for maximum TTZ conjugation efficiency were investigated by the response surface analysis method using JMP statistical modeling software. The design of the experiment involved two factors, initial PTXNR, and initial TTZ concentration. Three levels were assigned to each of the two factors. For initial PTXNR concentration the levels were 5, 10, 15 mg/ml and for initial TTZ concentrations the levels were 0.5, 1.0, 1.5 mg/ml. Each experimental design unit was replicated three times resulting in a total 27 experimental units. For each experimental unit, a random number was assigned using JMP. The experiments were performed according to a

complete randomized design in three days with nine randomly assigned experiments in a single day. Conjugation efficiency of TTZ was chosen to be the yield or response of the experimental design. TTZ conjugation efficiency was calculated using Equation (1):

$$\%\ \text{conjugation efficiency} = \frac{(\text{initial amount of TTZ}) - (\text{unbound amount of TTZ})}{(\text{initial amount of TTZ})} \times 100 \qquad (1)$$

2.8. *IN VITRO* THERAPEUTIC EFFICACY

BT-474 and MDA-MB-231 cells were cultured in hybricare medium and RPMI-1640, respectively supplemented with 10% fetal bovine serum (FBS) and 1% penicillin-streptomycin at 37°C and 5% CO_2. Approximately, 10,000 cells per well were plated in 96-well plates and treated with different doses of PTXNR-TTZ, PTXNRs, TTZ alone, and PTX solution alone. After 72 h of incubation, cell viability was assessed using MTT (3-(4, 5-dimethylthiazol-2-yl)-2, 5-diphenyltetrazolium bromide, MW 414) assay. MTT reagent was added to each well to convert into an insoluble formazan from water-soluble MTT. After 4 h, sodium dodecyl sulfate (SDS) solution prepared in 0.01 N HCl was added to each well to solubilize the formazan. The percentage of live cells relative to untreated control wells was quantified by measuring the absorbance at 570 nm (BioTek Synergy 2). Cell viability was calculated as a means of six wells containing BT-474 and MDA-MB-231 cells by subtracting the mean background level of wells containing medium only. Nonspecific formation of formazan due to the presence of medium was determined from triplicate wells. The number of viable cells was calculated as follows (Equation (2)):

$$\%\ cell\ viability = \frac{A_{570\ of\ sample} - A_{570\ of\ medium}}{A_{570\ of\ live\ cells} - A_{570\ of\ medium}} \times 100 \qquad (2)$$

2.9. QUANTITATIVE ANALYSIS OF SYNERGISTIC EFFECTS OF PTXNR-TTZ

We investigated the quantitative effects of PTXNR-TTZ using combination index analysis (CI) by the Chou-Talalay method [55,56]. The CI of PTXNR alone, TTZ alone, and conjugated PTXNR-TTZ were calculated using Equation (3) and plotted as CI *versus* the fraction of cells being affected.

$$CI = \frac{(\,Dosage\ of\ PTXNR\ in\ PTXNR-TTZ)}{(Dosage\ of\ PTXNR)} + \frac{(Dosage\ of\ TTZ\ in\ PTXNR-TTZ)}{(Dosage\ of\ TTZ)} \quad (3)$$

2.10. CELL CYCLE ANALYSIS

The effect of the PTXNR-TTZ on the cell cycle of BT-474 cells was investigated after 24, 48, and 72 h of treatments. BT-474 cells without any treatments, PTXNR alone treatment, and TTZ alone treatment were used as controls. The cell cycle analysis protocol was developed by modifying the previously reported method [57,58]. For each sample of the analysis, 2×10^6 cells were seeded in a T25 cell culture flask. After 12 h, PTXNR-TTZ, PTXNR alone, and TTZ alone were added and incubated for 24, 48, and 72 h. The untreated sample was incubated with 1 ml of PBS solution. Before harvesting the cells, 100 µl of 5′-Bromo-2′-deoxyuridine (BrdU) (Alfa Aesar) stock solution per 5 ml of media was added to an active concentration of 40 µM and incubated for 1 h at 37°C. The culture media was removed completely, and the cells were collected in 15 ml centrifuge tubes. The cells were centrifuged, and the cell pellets were fixed by adding 1 ml of 100% ice-cold ethanol. The cells were stored at 4°C at least for 30 min. Ethanol was removed after centrifugation at 500×g for 5 min and was resuspended in 1 ml of

0.5% Triton X-100 prepared in 2N HCl. After 30 min of incubation at room temperature, cells were pelleted down to mix with 1 ml of 0.1 M $Na_2B_4O_7.10\ H_2O$ (pH 8.5) solution and was incubated for at least 30 min at room temperature. The cells were pelleted down again and washed with PBS containing 1mg/ml Bovine Serum Albumin (BSA) and 0.1 % Tween-20 (PBST) solution. After washing, cells were resuspended in 50 µl prediluted mouse anti-BrdU monoclonal antibody (Novus Biologicals, Cat. NBP248373) stock solution. After 30 min of incubation in dark, 0.5 ml PBST stock solution was added and washed. A 50 µl prediluted FITC conjugated rabbit anti-mouse secondary antibody (Sothern Biotech, Cat. 617002) stock solution was added to cell pellets and were incubated for 30 min at room temperature in dark. After washing again with PBST solution, cells were resuspended in 100 µl of 1 mg/ml RNAse A (Alfa Aesar) stock solution and incubated for at least 20 min. Finally, 300-500 µl of 35 µg/ml propidium iodide (PI) (Alfa Aesar) was added to cell pellets and incubated in the dark at 37°C for 45 min. Before analyzing the cells in a flow cytometer (BD accuri C6 Plus), cells were passed through a 40-micron cell strainer (Thermo Scientific) to remove the cell aggregates. For flow cytometry analysis, cells were gated to sort out the singlet cells and only the singlets were gated for subsequent analysis. For acquiring the fluorescent data, 530/30 and 585/40 bandpass filters were used to acquire the BrdU positive and PI-positive cells, respectively with a 488 nm of laser excitation.

2.11. WESTERN BLOT ANALYSIS

BT-474 and MDA-MB-231 cells were treated with PTXNR-TTZ, PTXNR alone, and TTZ alone for 48 h at 10,000 nM each for Western blot analysis. The cells were

harvested and lysed at 4° C using 50 mM Tris-HCl, pH 8.0, 150 mM NaCl, and 0.1% Triton X-100, 0.5% sodium deoxycholate and 0.1% sodium dodecyl sulfate (SDS). The lysate protein was quantified using the BCA assay and the BSA calibration curve (SI Figure 5). For each experiment, 40 µg of each sample was taken and added to an equal volume of 2X Laemmli sample buffer. The cell lysate in the sample buffer was heated at 86°C for 5 min before running the SDS-PAGE electrophoresis process. Novex Tris-Glycine SDS gels (8-16% and 16%) (Invitrogen) were used for gel electrophoresis. The electrophoresis was performed for 45 min to 1h at 200 V. The separated proteins were transferred from gel to nitrocellulose membrane using a Power Blotter (ThermoFisher Scientific) according to the manufacturer's protocol. After the transfer process, the membrane was blocked for 5 h with moderate shaking using 3% BSA protein in TBST buffer (20 mM Tris (pH 7.5), 150 mM NaCl, and 0.1% Tween 20). The membrane was incubated with a primary monoclonal antibody overnight at 4°C. GAPDH (ThermoFisher, Cat. MA5-15738, 1: 5000) monoclonal antibody was used as a loading control. Actin (ThermoFisher Cat. MA5-11869, 1: 2000), Caspase -9 (ThermoFisher, Cat PA5-16358, 1:500), Caspase-3 (ThermoFisher, Cat. 43-7800, 1:500), cleaved caspase-3 (ThermoFisher Cat. PA5- 23921, 1:1000), XIAP (ThermoFisher, Cat. PA1-84846, 1:1000) and Cytochrome-C (ThermoFisher, Cat. MA5-11674, 1:400) primary monoclonal antibodies were used to observe the corresponding proteins of interest. After primary antibody incubation, the membrane was washed 3-5 times for 5 min each with TBST buffer. The membrane was incubated in Horseradish peroxidase (HRP) enzyme-conjugated secondary anti-mouse (ThermoFisher Cat.A27025, 1:10000 or anti-rabbit monoclonal antibody (Cell Signaling Technology, Cat.7074P2, 1:10000) depending on

the primary antibody host species for 1 h followed by washing with TBST washing buffer. The electro-chemiluminescent substrate (Super Signal West Dura, ThermoFisher, and Cat. 34075) was added on the membrane and incubated for 5 min. The electro-chemiluminescent signal was captured using a Bio-Rad gel imager. The signals were analyzed by image processing using Fiji (Image J) software.

2.12. STATISTICAL ANALYSIS

To observe the statistically significant differences in protein expressions compared to controls, we performed the one-tailed (either overregulation or downregulation) t-test with a 95% confidence level. All other hypothesis testing was performed using a two-tailed t-test. The TTZ conjugation efficiency analysis was performed using a complete randomized (CR) model. The final conjugation efficiency data was predicted using a response surface analysis using JMP statistical software. $P<0.05$ was considered statistically significant.

3. RESULTS

3.1. SYNTHESIS OF PTXNRs

The SEM images of PTXNRs as shown in Figure 1(a) confirms the elongated rod shape PTX drug NRs. The average diameter and length of PTXNRs were (96.87 ± 33.08) and (503.42 ± 210) nm, respectively (Figure 1 (b)). The size distribution plots (Figure 1 (c), Figure 1 (d)) confirm the moderately narrow dispersity of the particle diameter and length. The polydispersity index (pDI) of the particles was measured as 0.20 ± 0.02.

PTXNRs showed high colloidal stability in DI water having a zeta potential value of (-32.60 ± 4.82) mV (Figure 1(e), SI Table 1). In 0.15 M PBS solution, the zeta potential value was measured (-13.40 ± 2.81) mV, indicating the stability of nanoparticles even in high salt concentrations (SI Table 1).

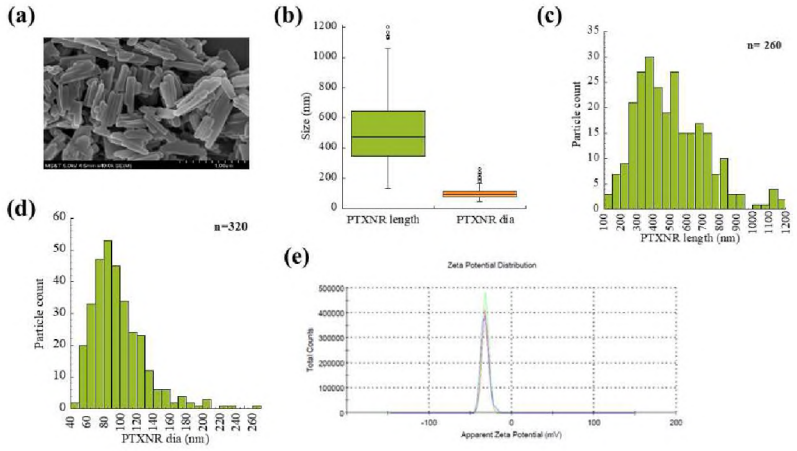

Figure 1. Characterization of PTXNRs. (a) Scanning electron microscopy (SEM) image of PTXNRs; (b) Particle size percentile plot of the PTXNR-TTZ particle length and diameter; (c) Size distribution of PTXNR particle length; (d) Size distribution of PTXNR particle diameter as calculated analyzing SEM images. The number 'n' denotes the particle population count for the analysis; and (e) Zeta potential (ξ) of PTXNR is -32.6±4.8 mV in water. Three colors indicate three different experiments

3.2. CONFIRMATION OF LINKER CONJUGATION WITH PTXNRs USING ^{1}H NMR ANALYSIS

We activated the 2′OH site of PTXNR to form an imidazole carbamate intermediate for subsequent conjugation step with the ε- amino group in the lysine side chain of TTZ (SI Figure 2). In ^{1}H NMR analysis, imidazole carbamate intermediate linkage was confirmed by the peak of the imidazole ring proton in 'a' position (Ha) at 8.35 ppm (Figure 2).[59,60]

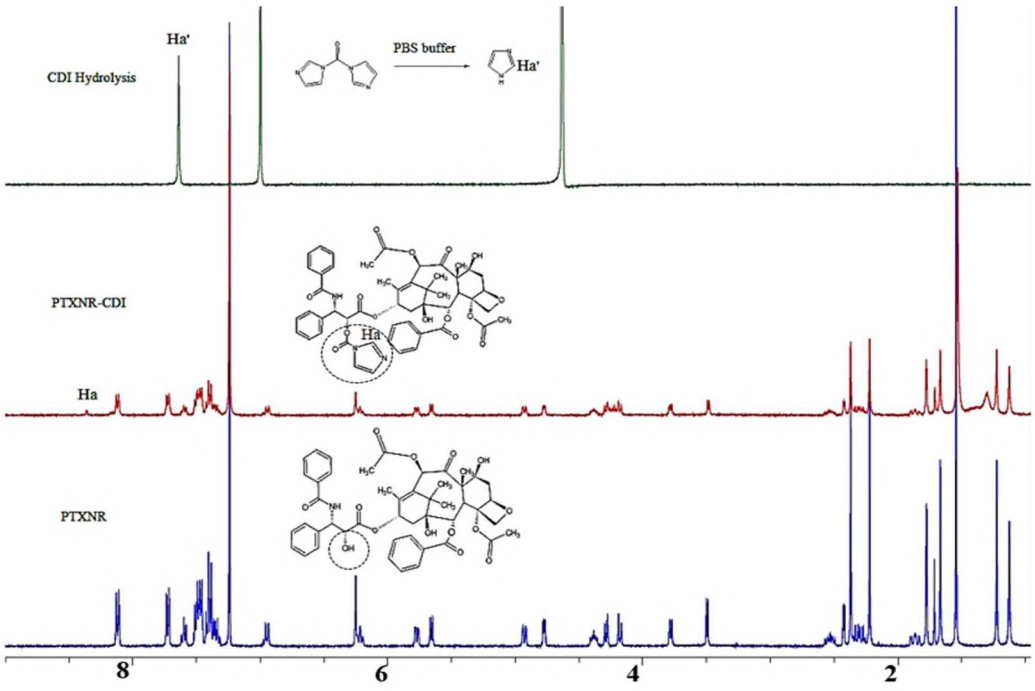

Figure 2. ^{1}H-NMR analysis to characterize PTX-imidazole carbamate formation. 1H-NMR spectra of hydrolyzed carbonyldiimidazole (CDI), PTX-imidazole carbamate (PTXNR-CDI), and PTXNR. The NMR spectra were acquired at room temperature. For characterization of PTXNR and PTXNR-CDI deuterated chloroform ($CDCl_3$, δ 7.24) and for hydrolyzed CDI deuterated oxide (D_2O, δ 4.65) were used as reference carrier solvents

In a parallel side reaction, CDI hydrolyzes in the aqueous phase of conjugation reaction with TTZ. Hydrolyzation of CDI produces free imidazole ring and might interfere in the NMR analysis as a free surface-bound residuals. To further confirm the linkage of the imidazole carbamate with the PTXNR, we performed the NMR analysis of hydrolyzed CDI residuals. Residual imidazole group was identified by the peak of the imidazole proton in "a′" position (Ha′) at 7.6 ppm.[59] So, the shift of NMR peak at 8.35 ppm represents only the Ha proton and hence confirms the successful linkage of

imidazole carbamate at 2′OH site of PTXNR particles forming the PTX-imidazole carbamate intermediate (PTXNR-CDI) particles.

3.3. CONFIRMATION OF TTZ CONJUGATION WITH PTXNR-CDI

The ε-amino group in lysine residue of TTZ acts as an active electrophile at the reaction pH and attacks the CDI activated site of PTXNR through nucleophilic substitution reaction. Attack by the electrophile amine group releases the imidazole ring but leaves the carbonyl group resulting in a one-carbon spacer forming a stable carbamate linkage. To confirm the TTZ conjugation, Alexa 594 fluorescent molecule was conjugated with TTZ. The bare unconjugated PTXNR showed a mean autofluorescence intensity of 42.60 a.u. (arbitrary unit). The Alexa 594 fluorophore bound PTXNR-TTZ, the mean fluorescence intensity was measured 13889.46 a.u. (Figure 3(a)) that is 326 fold higher than the mean fluorescence intensity of bare PTXNR confirming a successful conjugation of TTZ with PTXNRs (Figure 3(b)). PTXNR-TTZ showed good dispersibility in both water and PBS (SI Figure 6).

3.4. OPTIMIZATION OF TTZ CONJUGATION EFFICIENCY

The SEM image of the PTXNR-TTZ particles confirms the consistency in the size and shape of the particles after lyophilization (Figure 4(a)). The zeta potential of the PTXNR-TTZ in DI water was measured -17.1±3.83 mV (Figure 4(b), SI Table 1). In PBS, the zeta potential was measured -9.5± 0.02 mV (SI Table 1).

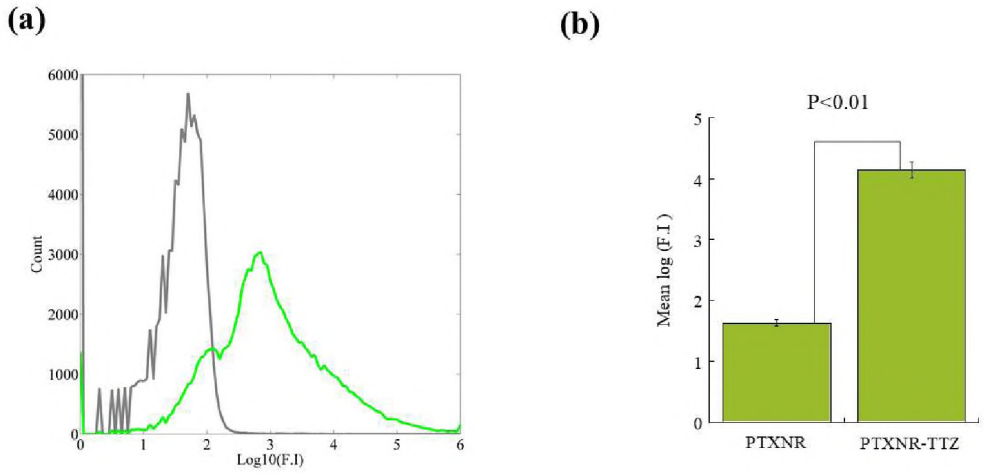

Figure 3. The fluorescence intensity of PTXNR-TTZ confirms the conjugation of TTZ on the surface of PTXNRs. (a) The F.I. of bare PTXNRs (grey) and Alexa 594 fluorophore bound TTZ conjugated PTXNR (PTXNR-TTZ) (green) shows a significant increase in emission spectra; (b) The quantitative mean F.I. of PTXNR-TTZ increases by ~14,000 fold (2.54 logarithmic fold) compared to bare PTXNRs indicating TTZ is effectively conjugated on the surface of PTXNRs using a CDI linker

The conjugated particles had a pDI of 0.21±0.11 showing significant homogeneity in size and shape. Optimization of TTZ conjugation efficiency was performed using response surface analysis (Figure 4(c)). The surface plot shows that the vicinity of lower concentrations of both initial PTXNR and TTZ result in 90-95% of conjugation efficiency, whereas the higher initial concentrations predict lower conjugation efficiency. The analysis suggests that the higher concentration of PTX results in precipitation of nanoparticles and less available surface for conjugation as well as several vacant reactive sites on the nanoparticle surface, whereas the higher concentration of TTZ produces excess unbound TTZ in the reaction medium. The maximum conjugation efficiency of TTZ to PTXNR was calculated 95.24 ± 1.40 % (SI Table 2), and hence, considered the optimum amount to use for subsequent experiments. The

optimum condition for the maximum conjugation efficiency was 5mg/ml and 0.5 mg/ml initial concentrations of PTXNR and TTZ, respectively. The drug to antibody ratio (DAR) of the conjugated particle was 4.0 ± 0.53 on a weight basis (molar ratio=681.67 ± 90.23) (SI Table 2).

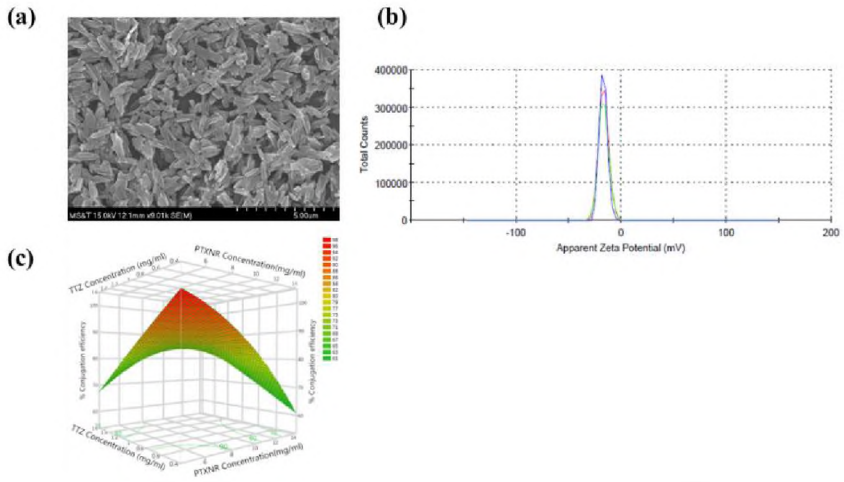

Figure 4. Characterization of PTXNR-TTZ ADNs. (a) SEM image of PTXNR-TTZ ADNs; (b) The zeta potential (ξ) of PTXNR-TTZ was observed -17.1±3.83 mV in DI water; (c) Contour plot of response surface analysis showing % conjugation efficiency of TTZ on the surface of PTXNRs. In response surface analysis, two factors PTXNR concentration and TTZ concentration were optimized for the highest conjugation efficiency. Each concentration factor had three levels. For PTXNR, the concentration levels were 5, 10, and 15 mg/ml and for TTZ the levels were 0.5, 1.0, and 1.5 mg/ml. Each level was replicated at least three times resulting in a total 27 experimental units. The maximum ~95% conjugation efficiency was obtained with PTXNR concentration 5 mg/ml and TTZ concentration 0.5 mg/ml. The experiment was designed according to a Complete Randomized (CR) model using JMP statistical software

3.5. *IN VITRO* ANTICANCER EFFICACY

To determine the anti-cancer efficacy *in vitro*, the dose-response cytotoxicity was measured using PTXNR-TTZ, PTX NR alone, TTZ alone, and PTX solution alone in BT-474 and MDA-MB-231 cells (Figure 5). PTXNR-TTZ was found to exert more

therapeutic efficiency in BT-474 cells than the individual effect of PTXNR, TTZ, and PTX solution treatments (Figure 5(a)) confirming the HER2 specificity of the ADNs. PTXNR-TTZ inhibited >83% and 51% of BT-474 (Figure 5(a)) and MDA-MB-231 (Figure 5(b)) cancer cells, respectively suggesting specific targeting and more therapeutic efficiency in HER2 positive BT-474 cells than MDA-MB-231 cells.

(a)

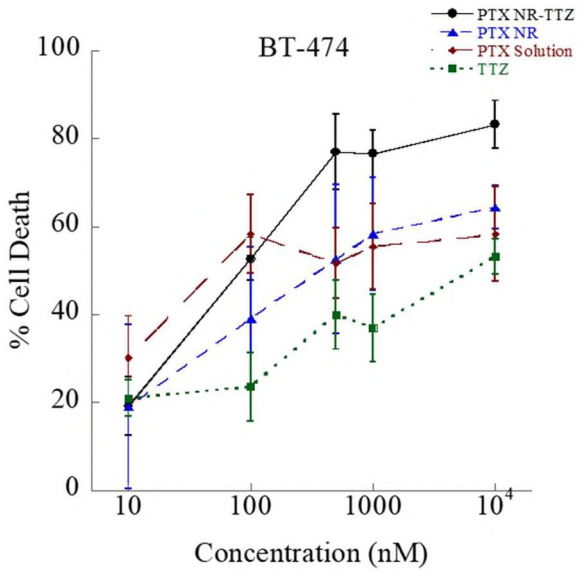

Figure 5. *In vitro* anti-cancer efficiency of PTXNR-TTZ ADNs. The cytotoxic effects of PTXNR-TTZ (closed circle), PTXNR (triangle), PTX Solution (diamond), and TTZ (square) on the growth of (a) BT-474, and (b) MDA-MB-231 cells. Each experiment was replicated at least n=6 times, and the average data is presented with mean ± standard deviation

(b)

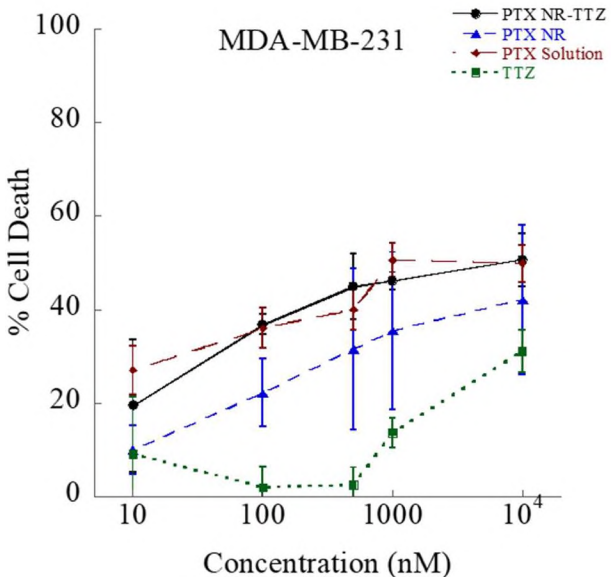

Figure 5. *In vitro* anti-cancer efficiency of PTXNR-TTZ ADNs.The cytotoxic effects of PTXNR-TTZ (closed circle), PTXNR (triangle), PTX Solution (diamond), and TTZ (square) on the growth of (a) BT-474, and (b) MDA-MB-231 cells. Each experiment was replicated at least n=6 times, and the average data is presented with mean ± standard deviation (cont.)

The half-maximal inhibitory concentration (IC_{50}), as defined as the concentration needed to kill 50% of cells, was found 106, 609 and 9000 nM for PTXNR-TTZ, PTX NR alone and TTZ alone, respectively in BT-474 cells indicating a synergistic therapeutic efficiency using ADNs compared to the individual treatments. MDA-MB-231 cells were resistant to PTXNR-TTZ exhibiting an IC_{50} >3,000 nM indicating intrinsic trastuzumab resistance *in vitro*. PTXNR alone and TTZ solution alone inhibited roughly 40% and 30% of the MDA-MB-231 cell growth, respectively. The cytotoxic effects of PTX solution were similar in both cell lines showing a dose-dependent cytotoxicity from 30-50%. PTXNR effectively killed more BT474 cells from 20-60% in a dose-dependent manner

than that in MDA-MB-231 cells from 10-30%. All these results suggest that PTXNR-TTZ exerts specific cytotoxicity in HER2 positive breast cancer cells.

3.6. THE EFFECTS OF PTXNR-TTZ IS SYNERGISTIC IN HER2 POSITIVE BREAST CANCER CELLS

The combination effects of PTXNR and TTZ were evaluated in BT-474 and MDA-MB-231 cells using the combination index (CI) analysis (Figure 6). The effects of the drugs were analyzed to determine whether a synergistic effect occurred in that cell line. On the plot, any point showing CI < 1 indicates a synergistic effect, and the values showing CI>1 is considered antagonistic. It is found that PTXNR-TTZ shows a synergistic effect in BT474 cells by decreasing CI values <1 with increasing fraction affected cells (Figure 6(a)). Very different CI *vs.* fraction affected line was observed in MDA-MB-231 cells showing increased CI values with increasing fraction affected cells up to 0.8 beyond which antagonistic effects were observed indicating a combination of PTX NR and TTZ is irrelevant in this cell line (Figure 6(b)).

3.7. PTXNR-TTZ ARRESTS HER2 POSITIVE BREAST CANCER CELLS IN THE G2/M PHASE

We quantified the population of BT-474 cells arrested in G0/G1, S, and G2/M cell cycle phases after treatment with PTXNR-TTZ, PTXNR alone, and TTZ alone (Figure 7 and SI Figures 7-9). PTXNR-TTZ arrested 39.90, 62.56, and 83.55% of BT-474 cells in the G2/M phase after 24, 48, and 72 h treatments, respectively. Conversely, it decreased the proportion of the G0/G1 phase from 43.70 to 30.6 to 15.39% at 24, 48, and 72 h, respectively.

(a)

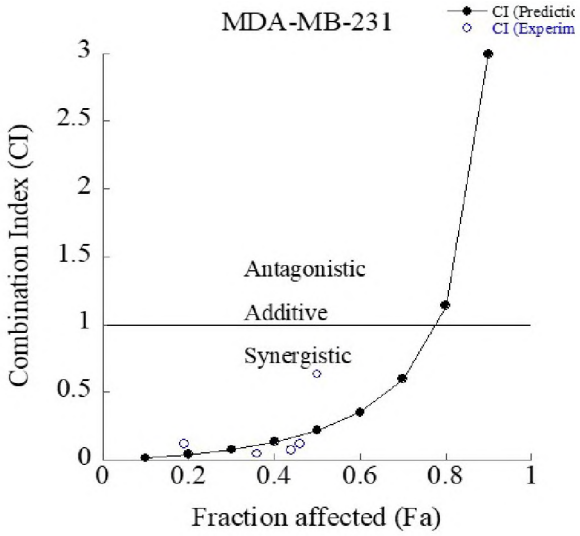

(b)

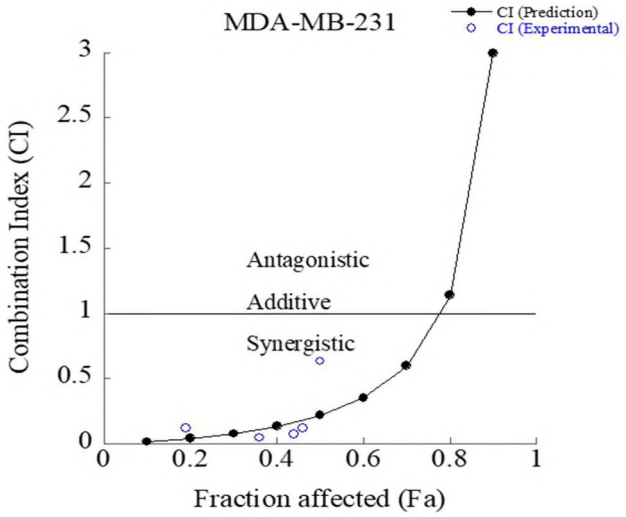

Figure 6. Combination Index (C.I.) analysis of PTXNR-TTZ ADNs. The C.I. plot as a function of each fraction of cells affected by PTXNR-TTZ particles in (a) BT-474, and (b) MDA-MB-231 cells. A C.I. value =1; additive effect, < 1; synergistic effect, > 1; antagonistic effect. The downward and upward curves in BT-474 and MDA-MB-231 cells indicate synergistic and antagonistic effects, respectively

PTXNR alone caused 39.76, 60.31, 76.18% arrest in the G2/M phase after 24, 48, and 72 h, respectively. TTZ alone treatment arrested 56.25, 53.39, 57.83% of BT-474 cells in the G1 phase after 24, 48, and 72 h, respectively. The cell cycle data confirms that PTXNR modulates the mitotic cell cycle arrest, or cell growth inhibition, and eventually apoptosis in BT-474 breast cancer cells.

(a)

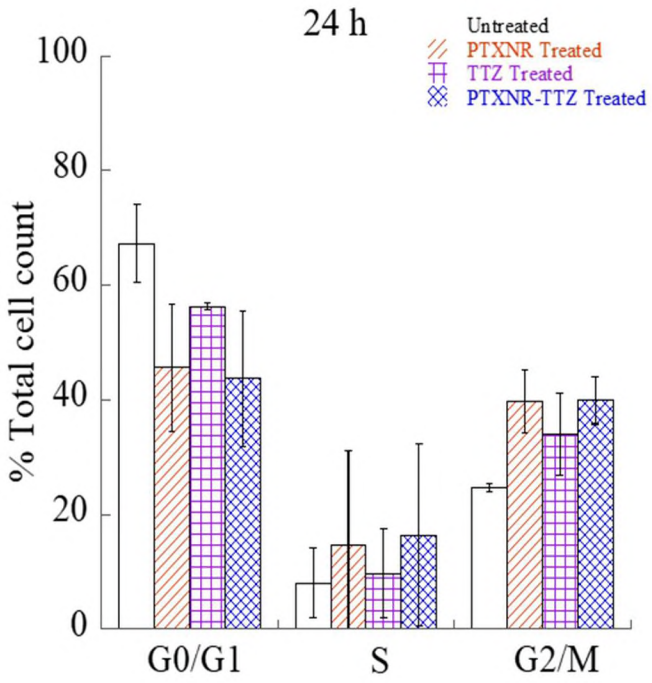

Figure 7. Cell cycle analysis. BT-474 cells were treated with PTXNR-TTZ, PTXNR alone, and TTZ alone. Cell cycle analysis was performed by flow cytometry after (a) 24 h, (b) 48 h, and (c) 72 h of treatment. Each experiment was replicated at least n=2 times and the average cell count data are presented as mean ± standard deviation

(b)

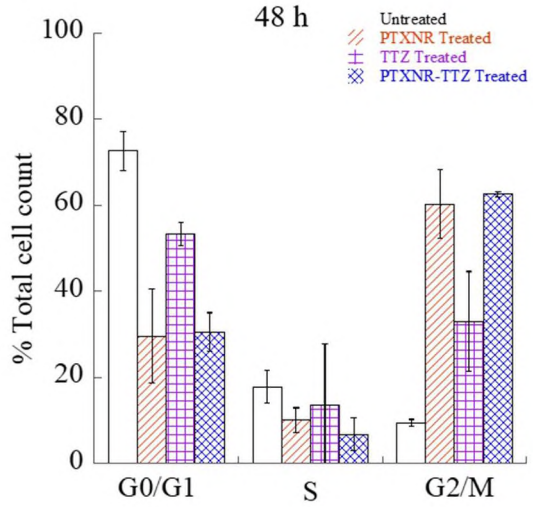

(c)

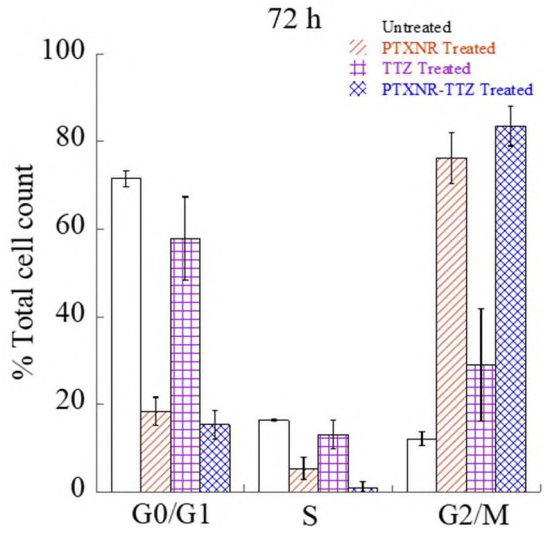

Figure 7. Cell cycle analysis.BT-474 cells were treated with PTXNR-TTZ, PTXNR alone, and TTZ alone. Cell cycle analysis was performed by flow cytometry after (a) 24 h, (b) 48 h, and (c) 72 h of treatment. Each experiment was replicated at least n=2 times and the average cell count data are presented as mean ± standard deviation (Cont.)

3.8. PTXNR-TTZ DOWNREGULATES ANTI-APOPTOTIC PROTEIN AND INDUCES APOPTOSIS IN A CASPASE-DEPENDENT INTRINSIC PATHWAY

We found that >80% of BT-474 cells were inhibited and arrested in the G2/M phase by PTXNR-TTZ ADN treatments. We investigated if the prolonged cell cycle arrest in the G2/M phase induced programmed cell death or apoptosis in cancer cells and the mechanisms of apoptotic induction by PTXNR-TTZ ADNs. PTXNR-TTZ induced apoptosis in HER2 positive BT-474 cells in an intrinsic cytochrome-C mediated pathway (Figure 8(a) and Figure 8(c)). In BT-474 cells, after 48 h of treatment using PTXNR-TTZ and PTX NR, we observed a significant release of cytochrome-C than that of untreated cells. We further observed a significantly higher expression of initiator apoptotic protein fully cleaved caspase-9. The lower expression of procaspase-3 was correlated with the upregulation of cleaved or active form of caspase-3. The observation is in agreement with the time-dependent expression study of caspase-3 on taxane treated HER2 positive SK-BR-3 cell line.[61] In BT-474 cells, the anti-apoptotic protein XIAP was significantly downregulated by PTXNR-TTZ treatment than the individual drug treatment. XIAP is a natural inhibitor of caspase-3 and caspase-9. [47,62-64] High XIAP activity may cause the inactivation of early apoptotic protein caspase-9 and inactivation of active caspase-3 at the later phase of apoptosis. The significant downregulation of XIAP by PTXNR-TTZ treatment facilitates the late apoptosis by overexpressing the effector caspase-3 apoptotic protein that attributes to the synergistic cytotoxic effect in BT-474 cells. The high concentration of PTXNR and PTXNR-TTZ significantly downregulated the actin production in BT-474 cells compared to MDA-MB-231 cells. In MDA-MB-231 cells, although cytochrome-C release was observed for both PTXNR-TTZ

and PTXNR treatments, there was no significant change in the expression of active caspase-9 suggesting that the apoptosome was not activated in the cytosolic area (Figure 8(b) and Figure 8(d)). The procaspase-3 expression in PTXNR-TTZ treated cells was not statistically different from that of untreated cells. Eventually, the cleaved form of the caspase-3 signal was not observed at all with the individual drug treatment and PTXNR-TTZ treatment. XIAP activity was observed in individually treated cells as well as in PTXNR-TTZ treated cells. XIAP activity in the drug-treated cells was found to be as high as that in untreated MDA-MB-231 cancer cells. XIAP is a potent anti-apoptotic protein and abnormal expression of XIAP can block the cell death pathways [47].

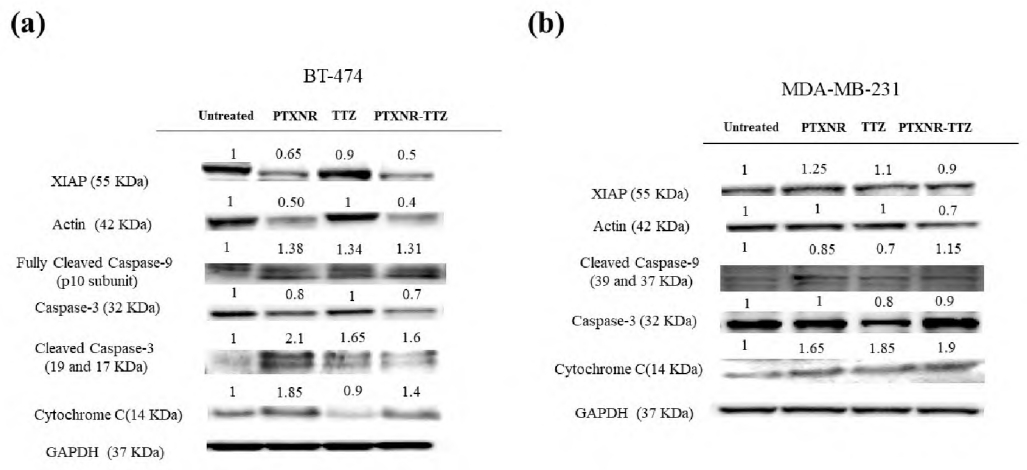

Figure 8. Western blot analysis. The cell signaling protein expressions of (a) BT-474 and (b) MDA-MB-231 cells using PBS, PTX alone, TTZ alone, and PTXNR-TTX treatments. The relative intensity of XIAP, actin, cleaved caspase-9, caspase 3, cleaved caspase 3 and cytochrome C is analyzed after 48 h of treatment in (c) BT-474 and (d) MDA-MB-231 cells. For each protein expression the experiment was replicated at least n=2-4 times and the average data is presented as mean ± standard deviation. The relative protein expressions are normalized to the untreated control cells and to the housekeeping GAPDH protein expression (hypothesized expression mean, $\mu=1$). The p-value for overexpression or downregulation of cytochrome-C, cleaved caspase-3 and XIAP in (d) BT-474 is 0.039, 0.003, and 0.000049, respectively. The p-value for the overexpression of cytochrome-C in MDA-MB-231 is 0.047

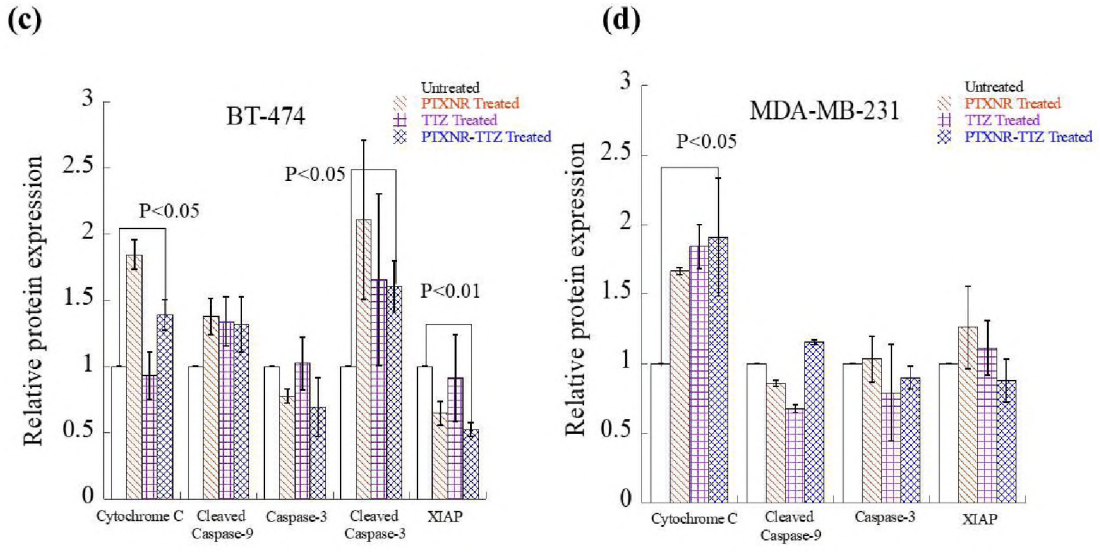

Figure 8. Western blot analysis. The cell signaling protein expressions of (a) BT-474 and (b) MDA-MB-231 cells using PBS, PTX alone, TTZ alone, and PTXNR-TTX treatments. The relative intensity of XIAP, actin, cleaved caspase-9, caspase 3, cleaved caspase 3 and cytochrome C is analyzed after 48 h of treatment in (c) BT-474 and (d) MDA-MB-231 cells. For each protein expression the experiment was replicated at least n=2-4 times and the average data is presented as mean ± standard deviation. The relative protein expressions are normalized to the untreated control cells and to the housekeeping GAPDH protein expression (hypothesized expression mean, μ=1). The p-value for overexpression or downregulation of cytochrome-C, cleaved caspase-3 and XIAP in (d) BT-474 is 0.039, 0.003, and 0.000049, respectively. The p-value for the overexpression of cytochrome-C in MDA-MB-231 is 0.047

4. DISCUSSION

Many chemotherapeutic drugs including PTX is a water-insoluble drug that results in low circulation time, poor bioavailability in the tumor tissue, and higher administrative dosage.[65-67] Nano-sized drug carriers, liposomes, polymeric nanoparticles, and micelles have been designed over the past decades to improve water dispersibility, stability and blood circulation half-life of chemotherapeutic drugs.[68-71] However, most nanoparticles suffer from poor specificity targeting only 1.6% of the administered dose of

the linked small molecule drug to be delivered in the targeted tumor vicinity.[72,73] In this study, we designed ADNs by conjugating TTZ monoclonal antibody on the surface of PTXNRs through a single carbonyl group spacing with >95% conjugation efficiency. PTXNR-TTZ was synthesized in two steps. First, PTX NRs were synthesized by phase separation of PTX drug solution from ethanol into water. This method is simple and scalable. Secondly, PTXNRs were reacted with CDI linker in water to form intermediate PTXNR-carbamate followed by coupling with the amine groups of TTZ using carbodiimide chemistry that forms PTXNR-TTZ ADN.[74,75] The reaction is chemically defined, efficient, and scalable with an overall yield of >80% and a high PTX: TTZ w/w ratio ≈ 4 (molar ratio ≈ 682). The cytotoxic payload in ADNs is 170-fold more than conventional antibody-drug conjugates (molar ratio ≈ 4) which improves the ability to deliver more active drugs at the target site and greater *in vitro* potency. The PTXNR-TTZ ADN showed greatly enhanced water dispersibility (>1 mg/ml) compared to PTX aqueous solution, indicating little aggregation in water.[52]

PTXNR-TTZ ADNs are designed to target HER2 receptors overexpressed in breast cancer cells so that the ADN binds to target cells, are internalized *via* endocytosis and exerts apoptosis mediated therapeutic effects.[10,48,50,76-90] The NRs, when coated with TTZ, exhibit high binding toward HER2-overexpressing breast cancer cells.[53,91] The adhesion strength of NRs has been shown high both experimentally and by theoretical modeling.[87,92-95] After targeting and internalization, PTXNR-TTZ ADNs activated intrinsic apoptosis pathways and inhibited >83% of HER2 positive BT-474 cells which was 43% more than the cytotoxicity in HER2 negative MDA-MB-231 cells. No difference in cytotoxicity was observed for PTXNR-TTZ, unconjugated PTXNR, PTX

solution alone, and TTZ alone treatments in MDA-MB-231 cells, indicating non-specific cell death. The IC_{50} of PTXNR-TTZ in BT-474 cells is lower than single drug treatments which is consistent with the previously published literature. The IC_{50}s of PTX vary between 2-200 nM in breast cancer cells due to differential basal level expressions of β-tubulin subunits of microtubules,[96-98] sensitivity of PTX toward binding with β-tubulin,[96] the expression of tau proteins involved in microtubule polymerization,[99] and HER2 expression levels.[100] PTXNR-TTZ inhibits tubulin polymerization and microtubule formation, blocks the cell cycle in G2/M, and induces apoptosis.

The CI analysis showed that PXNR-TTZ augments apoptosis in BT-474 cells synergistically indicating an induction in apoptosis through multiple pathways including intrinsic caspase-dependent pathway and cell cycle arrest. PTX and TTZ arrest cells in G2/M and G0/G1 phase, respectively by disrupting the microtubule dynamics and binding with HER2 extracellular domain.[101-105] In this study, individual treatment using PTXNR alone and TTZ alone arrested 76% and 57% of BT-474 cells in G2/M and G0/G1, respectively after 72 h of treatment. In contrast, PTXNR-TTZ arrested 83.5% of BT-474 cells in G2/M after 72 h of treatment indicating dominant effects of PTX in sensitizing and synchronizing cells in the G2/M phase which correlates with the percentage of apoptotic dead cells after PTXNR-TTZ treatment.[106-108] The cleaved caspase-3 and cytochrome C were significantly increased, while anti-apoptotic XIAP was decreased in BT-474 cells after 72 h of PTXNR and PTNR-TTZ treatments compared with untreated control. Cytochrome-C binds to apoptosis protease-activating factor-1 (APAF1), inducing its oligomerization to form apoptosome that recruits and activates an apoptosis initiator protein, caspase-9, cleaves caspase-9 into its active small subunits and

initiates the late apoptotic caspase cascade reactions.[47,64,109,110] The cleaved caspase-9 eventually activates the late apoptotic protein caspase-3.[111-113] The overexpression of cleaved or active form of caspase-3 ultimately confirms the late phase of apoptosis in BT-474 cells using PTXNR-TTZ treatment.[111,114-116] In the late phase, apoptosis is facilitated by two-fold downregulation of anti-apoptotic XIAP protein after PTXNR-TTZ treatment compared to that in the untreated control. In contrast, MDA-MB-231 cells did not show any sign of mid- or late phase apoptosis though having overexpression of the cytochrome-C protein. No changes in XIAP expression was observed in MDA-MB-231 cells treated with PTXNR-TTZ. XIAP, a key member of the inhibitor of apoptosis protein (IAP) family,[117] has been shown to be a direct inhibitor of caspase-3 and to interfere with the cytochrome-C pathway by inhibiting caspase-9 in lung cancer cells,[118-120] and leukemia cells.[121-124] In this study, the downregulation of XIAP and activation of caspase cascades in BT-474 cells by PTXNR-TTZ has proven to be an effective approach for the treatment of HER2 positive breast cancer cells.

5. CONCLUSION

The first synthesis of PTXNR-TTZ ADNs and its therapeutic efficiency *in vitro* are presented which induces higher apoptosis responses than single drug treatments in HER2 positive breast cancer cells. The use of PTXNR of ~95 nm in diameter and 500 nm in length remove the compromising need for toxic organic carrier solvent for intravenous administration of PTX alone. The particles are stable in the aqueous phase that makes it suitable for intravenous administration without any need for any organic solvent. The

surface of PTXNR was functionalized by CDI activation reaction in the aqueous phase and successfully conjugated TTZ without altering the size and shape of the nanoparticles. PTXNR-TTZ synergistically inhibited HER2 positive breast cancer cells. The IC_{50} of PTXNR-TTZ is 106 nM in BT-474 cancer cells which facilitates lower dose, and hence, fewer side effects than individual treatments. PTXNR-TTZ arrested >83% of the proliferating cells in the G2/M phase of the cell cycle after 72h of the treatment, which was well corroborated with cell cycle analysis. The higher number of cells (>80%) arrested in the G2/M phase after PTXNR-TTZ treatment than individual treatments using PTXNR and TTZ (arrests in the G0/G1 phase) confirms the synergistic crosstalk between PTX and TTZ. The Western blot analysis demonstrates that PTXNR-TTZ activates the effector caspase proteins in HER2 positive breast cancer cells, and downregulates the anti-apoptotic XIAP facilitating caspase-dependent apoptosis followed by the cell cycle arrest in G2/M phase. Taken together, it is envisaged that the results from this study will facilitate the rational design of combination therapy through a novel design of ADNs.

ACKNOWLEDGMENTS

This work was supported by the Center for Biomedical Research (CBR) at Missouri S&T. We would like to thank Kaitlyne Powers and Rachel Aiardo for their excellent technical assistance.

REFERENCES

(1) Vega-Vásquez, P.; Mosier, N. S.; Irudayaraj, J. Nanoscale Drug Delivery Systems: From Medicine to Agriculture. Frontiers in Bioengineering and Biotechnology 2020, 8.

(2) Patra, J. K.; Das, G.; Fraceto, L. F.; Campos, E. V. R.; Rodriguez-Torres, M. D. P.; Acosta-Torres, L. S.; Diaz-Torres, L. A.; Grillo, R.; Swamy, M. K.; Sharma, S.; Habtemariam, S.; Shin, H.-S. Nano based drug delivery systems: recent developments and future prospects. J Nanobiotechnology 2018, 16, 71-71.

(3) Scicluna, M. C.; Vella-Zarb, L. Evolution of Nanocarrier Drug-Delivery Systems and Recent Advancements in Covalent Organic Framework–Drug Systems. ACS Applied Nano Materials 2020, 3, 3097-3115.

(4) Hossen, S.; Hossain, M. K.; Basher, M. K.; Mia, M. N. H.; Rahman, M. T.; Uddin, M. J. Smart nanocarrier-based drug delivery systems for cancer therapy and toxicity studies: A review. Journal of Advanced Research 2019, 15, 1-18.

(5) Liechty, W. B.; Kryscio, D. R.; Slaughter, B. V.; Peppas, N. A. Polymers for Drug Delivery Systems. Annual Review of Chemical and Biomolecular Engineering 2010, 1, 149-173.

(6) Caldorera-Moore, M.; Guimard, N.; Shi, L.; Roy, K. Designer nanoparticles: incorporating size, shape and triggered release into nanoscale drug carriers. Expert Opin Drug Deliv 2010, 7, 479-495.

(7) Malam, Y.; Loizidou, M.; Seifalian, A. M. Liposomes and nanoparticles: nanosized vehicles for drug delivery in cancer. Trends in pharmacological sciences 2009, 30, 592-599.

(8) Lombardo, D.; Kiselev, M. A.; Caccamo, M. T. Smart Nanoparticles for Drug Delivery Application: Development of Versatile Nanocarrier Platforms in Biotechnology and Nanomedicine. Journal of Nanomaterials 2019, 2019, 3702518.

(9) Qin, S.-Y.; Zhang, A.-Q.; Cheng, S.-X.; Rong, L.; Zhang, X.-Z. Drug self-delivery systems for cancer therapy. Biomaterials 2017, 112, 234-247.

(10) Barua, S.; Yoo, J.-W.; Kolhar, P.; Wakankar, A.; Gokarn, Y. R.; Mitragotri, S. Particle shape enhances specificity of antibody-displaying nanoparticles. Proceedings of the National Academy of Sciences 2013, 110, 3270-3275.

(11) Bertrand, N.; Wu, J.; Xu, X.; Kamaly, N.; Farokhzad, O. C. Cancer nanotechnology: The impact of passive and active targeting in the era of modern cancer biology. Advanced Drug Delivery Reviews 2014, 66, 2-25.

(12) Larson, N.; Ghandehari, H. Polymeric Conjugates for Drug Delivery. Chemistry of Materials 2012, 24, 840-853.

(13) Srinivasarao, M.; Galliford, C. V.; Low, P. S. Principles in the design of ligand-targeted cancer therapeutics and imaging agents. Nature Reviews Drug Discovery 2015, 14, 203-219.

(14) Chari, R. V. J. Targeted delivery of chemotherapeutics: tumor-activated prodrug therapy. Advanced Drug Delivery Reviews 1998, 31, 89-104.

(15) Lin, K.; Tibbitts, J. Pharmacokinetic Considerations for Antibody Drug Conjugates. Pharmaceutical Research 2012, 29, 2354-2366.

(16) Mack, F.; Ritchie, M.; Sapra, P. The Next Generation of Antibody Drug Conjugates. Seminars in Oncology 2014, 41, 637-652.

(17) Brasó-Maristany, F.; Griguolo, G.; Pascual, T.; Paré, L.; Nuciforo, P.; Llombart-Cussac, A.; Bermejo, B.; Oliveira, M.; Morales, S.; Martínez, N.; Vidal, M.; Adamo, B.; Martínez, O.; Pernas, S.; López, R.; Muñoz, M.; Chic, N.; Galván, P.; Garau, I.; Manso, L.; Alarcón, J.; Martínez, E.; Gregorio, S.; Gomis, R. R.; Villagrasa, P.; Cortés, J.; Ciruelos, E.; Prat, A. Phenotypic changes of HER2-positive breast cancer during and after dual HER2 blockade. Nature communications 2020, 11, 385.

(18) Marty, M.; Cognetti, F.; Maraninchi, D.; Snyder, R.; Mauriac, L.; Tubiana-Hulin, M.; Chan, S.; Grimes, D.; Antón, A.; Lluch, A. Randomized phase II trial of the efficacy and safety of trastuzumab combined with docetaxel in patients with human epidermal growth factor receptor 2–positive metastatic breast cancer administered as first-line treatment: the M77001 study group. Journal of clinical oncology 2005, 23, 4265-4274.

(19) Von Minckwitz, G.; Procter, M.; De Azambuja, E.; Zardavas, D.; Benyunes, M.; Viale, G.; Suter, T.; Arahmani, A.; Rouchet, N.; Clark, E. Adjuvant pertuzumab and trastuzumab in early HER2-positive breast cancer. New England Journal of Medicine 2017, 377, 122-131.

(20) Goldhirsch, A.; Gelber, R. D.; Piccart-Gebhart, M. J.; De Azambuja, E.; Procter, M.; Suter, T. M.; Jackisch, C.; Cameron, D.; Weber, H. A.; Heinzmann, D. 2 years versus 1 year of adjuvant trastuzumab for HER2-positive breast cancer (HERA): an open-label, randomised controlled trial. The Lancet 2013, 382, 1021-1028.

(21) Piccart-Gebhart, M. J.; Procter, M.; Leyland-Jones, B.; Goldhirsch, A.; Untch, M.; Smith, I.; Gianni, L.; Baselga, J.; Bell, R.; Jackisch, C. Trastuzumab after adjuvant chemotherapy in HER2-positive breast cancer. New England Journal of Medicine 2005, 353, 1659-1672.

(22) Romond, E. H.; Perez, E. A.; Bryant, J.; Suman, V. J.; Geyer Jr, C. E.; Davidson, N. E.; Tan-Chiu, E.; Martino, S.; Paik, S.; Kaufman, P. A. Trastuzumab plus adjuvant chemotherapy for operable HER2-positive breast cancer. New England Journal of Medicine 2005, 353, 1673-1684.

(23) Slamon, D.; Eiermann, W.; Robert, N.; Pienkowski, T.; Martin, M.; Press, M.; Mackey, J.; Glaspy, J.; Chan, A.; Pawlicki, M. Adjuvant trastuzumab in HER2-positive breast cancer. New England Journal of Medicine 2011, 365, 1273-1283.

(24) Perez, E.; Romond, E.; Suman, V. Trastuzumab plus adjuvant chemotherapy for HER2-positive breast cancer: Final planned joint analysis of overall survival (OS) from NSABP B-31 and NCCTG N9831. Journal of clinical oncology : official journal of the American Society of Clinical Oncology 2014, 32, 3744-3752.

(25) Giordano, S. H.; Temin, S.; Chandarlapaty, S.; Crews, J. R.; Esteva, F. J.; Kirshner, J. J.; Krop, I. E.; Levinson, J.; Lin, N. U.; Modi, S.; Patt, D. A.; Perlmutter, J.; Ramakrishna, N.; Winer, E. P.; Davidson, N. E. Systemic Therapy for Patients With Advanced Human Epidermal Growth Factor Receptor 2-Positive Breast Cancer: ASCO Clinical Practice Guideline Update. Journal of clinical oncology : official journal of the American Society of Clinical Oncology 2018, 36, 2736-2740.

(26) Tolaney, S. M.; Barry, W. T.; Dang, C. T.; Yardley, D. A.; Moy, B.; Marcom, P. K.; Albain, K. S.; Rugo, H. S.; Ellis, M.; Shapira, I.; Wolff, A. C.; Carey, L. A.; Overmoyer, B. A.; Partridge, A. H.; Guo, H.; Hudis, C. A.; Krop, I. E.; Burstein, H. J.; Winer, E. P. Adjuvant Paclitaxel and Trastuzumab for Node-Negative, HER2-Positive Breast Cancer. New England Journal of Medicine 2015, 372, 134-141.

(27) Tolaney, S. M.; Guo, H.; Pernas, S.; Barry, W. T.; Dillon, D. A.; Ritterhouse, L.; Schneider, B. P.; Shen, F.; Fuhrman, K.; Baltay, M.; Dang, C. T.; Yardley, D. A.; Moy, B.; Marcom, P. K.; Albain, K. S.; Rugo, H. S.; Ellis, M. J.; Shapira, I.; Wolff, A. C.; Carey, L. A.; Overmoyer, B.; Partridge, A. H.; Hudis, C. A.; Krop, I. E.; Burstein, H. J.; Winer, E. P. Seven-Year Follow-Up Analysis of Adjuvant Paclitaxel and Trastuzumab Trial for Node-Negative, Human Epidermal Growth Factor Receptor 2-Positive Breast Cancer. Journal of clinical oncology : official journal of the American Society of Clinical Oncology 2019, 37, 1868-1875.

(28) Bullock, K.; Blackwell, K. Clinical efficacy of taxane–trastuzumab combination regimens for HER-2–positive metastatic breast cancer. The Oncologist 2008, 13, 515-525.

(29) Weaver, B. A. How Taxol/paclitaxel kills cancer cells. Molecular biology of the cell 2014, 25, 2677-2681.

(30) Muller, R. H.; Keck, C. M. Challenges and solutions for the delivery of biotech drugs – a review of drug nanocrystal technology and lipid nanoparticles. Journal of Biotechnology 2004, 113, 151-170.

(31) Schrama, D.; Reisfeld, R. A.; Becker, J. C. Antibody targeted drugs as cancer therapeutics. Nature Reviews Drug Discovery 2006, 5, 147-159.

(32) Beck, A.; Goetsch, L.; Dumontet, C.; Corvaïa, N. Strategies and challenges for the next generation of antibody–drug conjugates. Nature reviews Drug discovery 2017, 16, 315.

(33) Panowski, S.; Bhakta, S.; Raab, H.; Polakis, P.; Junutula, J. R. Site-specific antibody drug conjugates for cancer therapy. mAbs 2014, 6, 34-45.

(34) Tsuchikama, K.; An, Z. Antibody-drug conjugates: recent advances in conjugation and linker chemistries. Protein & Cell 2018, 9, 33-46.

(35) Flygare, J. A.; Pillow, T. H.; Aristoff, P. Antibody-Drug Conjugates for the Treatment of Cancer. Chemical Biology & Drug Design 2013, 81, 113-121.

(36) Simone, E. A.; Dziubla, T. D.; Muzykantov, V. R. Polymeric carriers: role of geometry in drug delivery. Expert Opin Drug Deliv 2008, 5, 1283-1300.

(37) Mitragotri, S.; Burke, P. A.; Langer, R. Overcoming the challenges in administering biopharmaceuticals: formulation and delivery strategies. Nature Reviews Drug Discovery 2014, 13, 655-672.

(38) Vicent, M. J.; Duncan, R. Polymer conjugates: nanosized medicines for treating cancer. Trends in Biotechnology 2006, 24, 39-47.

(39) Gradishar, W. J.; Tjulandin, S.; Davidson, N.; Shaw, H.; Desai, N.; Bhar, P.; Hawkins, M.; O'Shaughnessy, J. Phase III Trial of Nanoparticle Albumin-Bound Paclitaxel Compared With Polyethylated Castor Oil–Based Paclitaxel in Women With Breast Cancer. Journal of Clinical Oncology 2005, 23, 7794-7803.

(40) McGuire, W. P.; Hoskins, W. J.; Brady, M. F.; Kucera, P. R.; Partridge, E. E.; Look, K. Y.; Clarke-Pearson, D. L.; Davidson, M. Cyclophosphamide and Cisplatin Compared with Paclitaxel and Cisplatin in Patients with Stage III and Stage IV Ovarian Cancer. New England Journal of Medicine 1996, 334, 1-6.

(41) Campos, S. M.; Penson, R. T.; Mays, A. R.; Berkowitz, R. S.; Fuller, A. F.; Goodman, A.; Matulonis, U. A.; Muzikansky, A.; Seiden, M. V. The Clinical Utility of Liposomal Doxorubicin in Recurrent Ovarian Cancer. Gynecologic Oncology 2001, 81, 206-212.

(42) Ranson, M. R.; Carmichael, J.; O'Byrne, K.; Stewart, S.; Smith, D.; Howell, A. Treatment of advanced breast cancer with sterically stabilized liposomal doxorubicin: results of a multicenter phase II trial. Journal of Clinical Oncology 1997, 15, 3185-3191.

(43) Abu Lila, A.; Ishida, T.; Kiwada, H. Targeting Anticancer Drugs to Tumor Vasculature Using Cationic Liposomes. Pharmaceutical Research 2010, 27, 1171-1183.

(44) Muro, S.; Garnacho, C.; Champion, J. A.; Leferovich, J.; Gajewski, C.; Schuchman, E. H.; Mitragotri, S.; Muzykantov, V. R. Control of endothelial targeting and intracellular delivery of therapeutic enzymes by modulating the size and shape of ICAM-1-targeted carriers. Mol Ther 2008, 16, 1450-1458.

(45) Wang, Y.; Yang, T.; Wang, X.; Wang, J.; Zhang, X.; Zhang, Q. Targeted Polymeric Micelle System for Delivery of Combretastatin A4 to Tumor Vasculature <i>In Vitro</i&gt. Pharmaceutical Research 2010, 27, 1861-1868.

(46) Zih-rou, H.; Shu-chiou, H.; Yueh-lung, Y.; Jia-you, F. Development and evaluation of lipid nanoparticles for camptothecin delivery: a comparison of solid lipid nanoparticles, nanostructured lipid carriers, and lipid emulsion. Acta Pharmacologica Sinica 2008, 29, 1094-1102.

(47) Fulda, S.; Vucic, D. Targeting IAP proteins for therapeutic intervention in cancer. Nature Reviews Drug Discovery 2012, 11, 109-124.

(48) Gratton, S. E. A.; Ropp, P. A.; Pohlhaus, P. D.; Luft, J. C.; Madden, V. J.; Napier, M. E.; DeSimone, J. M. The effect of particle design on cellular internalization pathways. Proceedings of the National Academy of Sciences 2008, 105, 11613-11618.

(49) Alexis, F.; Pridgen, E.; Molnar, L. K.; Farokhzad, O. C. Factors Affecting the Clearance and Biodistribution of Polymeric Nanoparticles. Molecular Pharmaceutics 2008, 5, 505-515.

(50) Arnida; Janat-Amsbury, M. M.; Ray, A.; Peterson, C. M.; Ghandehari, H. Geometry and surface characteristics of gold nanoparticles influence their biodistribution and uptake by macrophages. European journal of pharmaceutics and biopharmaceutics : official journal of Arbeitsgemeinschaft fur Pharmazeutische Verfahrenstechnik e.V 2011, 77, 417-423.

(51) Champion, J. A.; Mitragotri, S. Role of target geometry in phagocytosis. Proceedings of the National Academy of Sciences of the United States of America 2006, 103, 4930-4934.

(52) Laemthong, T.; Kim, H. H.; Dunlap, K.; Brocker, C.; Barua, D.; Forciniti, D.; Huang, Y.-W.; Barua, S. Bioresponsive polymer coated drug nanorods for breast cancer treatment. Nanotechnology 2016, 28, 045601.

(53) Barua, S.; Mitragotri, S. Synergistic targeting of cell membrane, cytoplasm, and nucleus of cancer cells using rod-shaped nanoparticles. ACS nano 2013, 7, 9558-9570.

(54) Dennler, P.; Fischer, E.; Schibli, R. Antibody conjugates: from heterogeneous populations to defined reagents. Antibodies 2015, 4, 197-224.

(55) Chou, T. C. Drug combination studies and their synergy quantification using the Chou-Talalay method. Cancer Res 2010, 70, 440-446.

(56) Chou, T.-C.; Talalay, P. Quantitative analysis of dose-effect relationships: the combined effects of multiple drugs or enzyme inhibitors. Advances in enzyme regulation 1984, 22, 27-55.

(57) Cecchini, M. J.; Amiri, M.; Dick, F. A. Analysis of cell cycle position in mammalian cells. JoVE (Journal of Visualized Experiments) 2012, e3491.

(58) Sarsour, E. H.; Agarwal, M.; Pandita, T. K.; Oberley, L. W.; Goswami, P. C. Manganese superoxide dismutase protects the proliferative capacity of confluent normal human fibroblasts. Journal of Biological Chemistry 2005, 280, 18033-18041.

(59) Olsson, J. V.; Hult, D.; Cai, Y.; García-Gallego, S.; Malkoch, M. Reactive imidazole intermediates: simplified synthetic approach to functional aliphatic cyclic carbonates. Polymer Chemistry 2014, 5, 6651-6655.

(60) Hornig, S.; Liebert, T.; Heinze, T. Structure design of multifunctional furoate and pyroglutamate esters of dextran by polymer-analogous reactions. Macromolecular bioscience 2007, 7, 297-306.

(61) Jelínek, M.; Balušíková, K.; Schmiedlová, M.; Němcová-Fürstová, V.; Šrámek, J.; Stančíková, J.; Zanardi, I.; Ojima, I.; Kovář, J. The role of individual caspases in cell death induction by taxanes in breast cancer cells. Cancer cell international 2015, 15, 8.

(62) Allan, L. A.; Clarke, P. R. Apoptosis and autophagy: Regulation of caspase-9 by phosphorylation. The FEBS journal 2009, 276, 6063-6073.

(63) Galbán, S.; Duckett, C. S. XIAP as a ubiquitin ligase in cellular signaling. Cell death and differentiation 2010, 17, 54.

(64) Würstle, M. L.; Laussmann, M. A.; Rehm, M. The central role of initiator caspase-9 in apoptosis signal transduction and the regulation of its activation and activity on the apoptosome. Experimental cell research 2012, 318, 1213-1220.

(65) Kipp, J. The role of solid nanoparticle technology in the parenteral delivery of poorly water-soluble drugs. International journal of pharmaceutics 2004, 284, 109-122.

(66) Lukyanov, A. N.; Torchilin, V. P. Micelles from lipid derivatives of water-soluble polymers as delivery systems for poorly soluble drugs. Advanced drug delivery reviews 2004, 56, 1273-1289.

(67) Zhang, Z.; Mei, L.; Feng, S.-S. Paclitaxel drug delivery systems. Expert Opin Drug Deliv 2013, 10, 325-340.

(68) Senapati, S.; Mahanta, A. K.; Kumar, S.; Maiti, P. Controlled drug delivery vehicles for cancer treatment and their performance. Signal Transduction and Targeted Therapy 2018, 3, 7.

(69) Tong, R.; Cheng, J. Anticancer Polymeric Nanomedicines. Polymer Reviews 2007, 47, 345-381.

(70) Mishra, B.; Patel, B. B.; Tiwari, S. Colloidal nanocarriers: a review on formulation technology, types and applications toward targeted drug delivery. Nanomedicine: Nanotechnology, Biology and Medicine 2010, 6, 9-24.

(71) Naksuriya, O.; Okonogi, S.; Schiffelers, R. M.; Hennink, W. E. Curcumin nanoformulations: A review of pharmaceutical properties and preclinical studies and clinical data related to cancer treatment. Biomaterials 2014, 35, 3365-3383.

(72) Teicher, B. A.; Chari, R. V. J. Antibody Conjugate Therapeutics: Challenges and Potential. Clinical Cancer Research 2011, 17, 6389.

(73) Nejadmoghaddam, M.-R.; Minai-Tehrani, A.; Ghahremanzadeh, R.; Mahmoudi, M.; Dinarvand, R.; Zarnani, A.-H. Antibody-Drug Conjugates: Possibilities and Challenges. Avicenna J Med Biotechnol 2019, 11, 3-23.

(74) Ghosh, A. K.; Brindisi, M. Organic Carbamates in Drug Design and Medicinal Chemistry. Journal of Medicinal Chemistry 2015, 58, 2895-2940.

(75) Quiles, S.; Raisch, K. P.; Sanford, L. L.; Bonner, J. A.; Safavy, A. Synthesis and Preliminary Biological Evaluation of High-Drug-Load Paclitaxel-Antibody Conjugates for Tumor-Targeted Chemotherapy. Journal of Medicinal Chemistry 2010, 53, 586-594.

(76) Fahmy, T. M.; Samstein, R. M.; Harness, C. C.; Saltzman, W. M. Surface modification of biodegradable polyesters with fatty acid conjugates for improved drug targeting. Biomaterials 2005, 26, 5727-5736.

(77) Steenblock, E. R.; Fadel, T.; Labowsky, M.; Pober, J. S.; Fahmy, T. M. An artificial antigen-presenting cell with paracrine delivery of IL-2 impacts the magnitude and direction of the T cell response. Journal of Biological Chemistry 2011, 286, 34883-34892.

(78) Steenblock, E. R.; Fahmy, T. M. A Comprehensive Platform for Ex Vivo T-cell Expansion Based on Biodegradable Polymeric Artificial Antigen-presenting Cells. Molecular Therapy 2008, 16, 765-772.

(79) Ben-Akiva, E.; Meyer, R. A.; Wilson, D. R.; Green, J. J. Surface engineering for lymphocyte programming. Advanced Drug Delivery Reviews 2017, 114, 102-115.

(80) Munisvaradass, R.; Kumar, S.; Govindasamy, C.; Alnumair, K. S.; Mok, P. L. Human CD3+ T-Cells with the Anti-ERBB2 Chimeric Antigen Receptor Exhibit Efficient Targeting and Induce Apoptosis in ERBB2 Overexpressing Breast Cancer Cells. International Journal of Molecular Sciences 2017, 18, 1797.

(81) Sunshine, J. C.; Perica, K.; Schneck, J. P.; Green, J. J. Particle shape dependence of CD8+ T cell activation by artificial antigen presenting cells. Biomaterials 2014, 35, 269-277.

(82) Meyer, R. A.; Sunshine, J. C.; Perica, K.; Kosmides, A. K.; Aje, K.; Schneck, J. P.; Green, J. J. Biodegradable Nanoellipsoidal Artificial Antigen Presenting Cells for Antigen Specific T-Cell Activation. Small 2015, 11, 1519-1525.

(83) Schütz, C.; Fleck, M.; Mackensen, A.; Zoso, A.; Halbritter, D.; Schneck, J. P.; Oelke, M. Killer artificial antigen-presenting cells: A novel strategy to delete specific T cells. Blood 2008, 111, 3546-3552.

(84) Perica, K.; Tu, A.; Richter, A.; Bieler, J. G.; Edidin, M.; Schneck, J. P. Magnetic field-induced t cell receptor clustering by nanoparticles enhances t cell activation and stimulates antitumor activity. ACS Nano 2014, 8, 2252-2260.

(85) Champion, J.; Mitragotri, S. Shape Induced Inhibition of Phagocytosis of Polymer Particles. Pharmaceutical Research 2009, 26, 244-249.

(86) Champion, J. A.; Mitragotri, S. Role of target geometry in phagocytosis. Proceedings of the National Academy of Sciences of the United States of America 2006, 103, 4930-4934.

(87) Decuzzi, P.; Ferrari, M. The adhesive strength of non-spherical particles mediated by specific interactions. Biomaterials 2006, 27, 5307-5314.

(88) Decuzzi, P.; Ferrari, M. The receptor-mediated endocytosis of nonspherical particles. Biophysical journal 2008, 94, 3790-3797.

(89) Yan, G.; Paul, D.; Shenshen, C.; Richard, T.; Manorama, T.; Tamara, M.; Dennis, E. D. Shape effects of filaments versus spherical particles in flow and drug delivery. Nature Nanotechnology 2007, 2, 249-255.

(90) Huang, X.; Teng, X.; Chen, D.; Tang, F.; He, J. The effect of the shape of mesoporous silica nanoparticles on cellular uptake and cell function. Biomaterials 2010, 31, 438-448.

(91) Barua, S.; Yoo, J.-W.; Kolhar, P.; Wakankar, A.; Gokarn, Y. R.; Mitragotri, S. Particle shape enhances specificity of antibody-displaying nanoparticles. Proc. Natl. Acad. Sci. U.S.A. 2013.

(92) Gentile, F.; Chiappini, C.; Fine, D.; Bhavane, R. C.; Peluccio, M. S.; Cheng, M. M.-C.; Liu, X.; Ferrari, M.; Decuzzi, P. The effect of shape on the margination dynamics of non-neutrally buoyant particles in two-dimensional shear flows. Journal of Biomechanics 2008, 41, 2312-2318.

(93) Decuzzi, P.; Godin, B.; Tanaka, T.; Lee, S. Y.; Chiappini, C.; Liu, X.; Ferrari, M. Size and shape effects in the biodistribution of intravascularly injected particles. Journal of Controlled Release 2010, 141, 320-327.

(94) Adriani, G.; de Tullio, M. D.; Ferrari, M.; Hussain, F.; Pascazio, G.; Liu, X.; Decuzzi, P. The preferential targeting of the diseased microvasculature by disk-like particles. Biomaterials 2012, 33, 5504-5513.

(95) Godin, B.; Chiappini, C.; Srinivasan, S.; Alexander, J. F.; Yokoi, K.; Ferrari, M.; Decuzzi, P.; Liu, X. Drug Delivery: Discoidal Porous Silicon Particles: Fabrication and Biodistribution in Breast Cancer Bearing Mice (Adv. Funct. Mater. 20/2012). Advanced Functional Materials 2012, 22, 4186-4186.

(96) Tommasi, S.; Mangia, A.; Lacalamita, R.; Bellizzi, A.; Fedele, V.; Chiriatti, A.; Thomssen, C.; Kendzierski, N.; Latorre, A.; Lorusso, V.; Schittulli, F.; Zito, F.; Kavallaris, M.; Paradiso, A. Cytoskeleton and paclitaxel sensitivity in breast cancer: The role of β-tubulins. International Journal of Cancer 2007, 120, 2078-2085.

(97) Marc, S. G.; Ahmed, T. A.; Asok, B.; Cassandra, D. M. C.; Philip, W.; Mariusz, K.; Carol E., C.; Richard, F. L.; Jack A., T.; Sambasivarao, D.: IC₅₀ Values for Paclitaxel and Analogs in Cytotoxicity Assays with Breast Cancer Cell Lines, 2015.

(98) McCloskey, D. E.; Kaufmann, S. H.; Prestigiacomo, L. J.; Davidson, N. E. Paclitaxel induces programmed cell death in MDA-MB-468 human breast cancer cells. Clinical Cancer Research 1996, 2, 847-854.

(99) Rouzier, R.; Rajan, R.; Wagner, P.; Hess, K. R.; Gold, D. L.; Stec, J.; Ayers, M.; Ross, J. S.; Zhang, P.; Buchholz, T. A.; Kuerer, H.; Green, M.; Arun, B.; Hortobagyi, G. N.; Symmans, W. F.; Pusztai, L. Microtubule-associated protein tau: a marker of paclitaxel sensitivity in breast cancer. Proceedings of the National Academy of Sciences of the United States of America 2005, 102, 8315-8320.

(100) Haghnavaz, N.; Asghari, F.; Elieh Ali Komi, D.; Shanehbandi, D.; Baradaran, B.; Kazemi, T. HER2 positivity may confer resistance to therapy with paclitaxel in breast cancer cell lines. Artificial cells, nanomedicine, and biotechnology 2018, 46, 518-523.

(101) Fisi, V.; Kátai, E.; Bogner, P.; Miseta, A.; Nagy, T. Timed, sequential administration of paclitaxel improves its cytotoxic effectiveness in a cell culture model. Cell Cycle 2016, 15, 1227-1233.

(102) Sui, M.; Dziadyk, J. M.; Zhu, X.; Fan, W. Cell Cycle–Dependent Antagonistic Interactions between Paclitaxel and γ-Radiation in Combination Therapy. Clinical Cancer Research 2004, 10, 4848-4857.

(103) Weissenstein, U.; Kunz, M.; Urech, K.; Regueiro, U.; Baumgartner, S. Interaction of a standardized mistletoe (Viscum album) preparation with antitumor effects of Trastuzumab in vitro. BMC Complement Altern Med 2016, 16, 271-271.

(104) Rodríguez, C. E.; Reidel, S. I.; De Kier Joffé, E. D. B.; Jasnis, M. A.; Fiszman, G. L. Autophagy protects from trastuzumab-induced cytotoxicity in HER2 overexpressing breast tumor spheroids. PLoS ONE 2015, 10, e0137920.

(105) Wang, C.-X.; Koay, D. C.; Edwards, A.; Lu, Z.; Mor, G.; Ocal, I. T.; DiGiovanna, M. P. In vitro and in vivo Effects of Combination of Trastuzumab (Herceptin) and Tamoxifen in Breast Cancer. Breast Cancer Research and Treatment 2005, 92, 251-263.

(106) Foley, E. A.; Kapoor, T. M. Microtubule attachment and spindle assembly checkpoint signalling at the kinetochore. Nature reviews Molecular cell biology 2013, 14, 25.

(107) Kops, G. J.; Weaver, B. A.; Cleveland, D. W. On the road to cancer: aneuploidy and the mitotic checkpoint. Nature Reviews Cancer 2005, 5, 773.

(108) Lara-Gonzalez, P.; Westhorpe, F. G.; Taylor, S. S. The spindle assembly checkpoint. Current biology 2012, 22, R966-R980.

(109) Portt, L.; Norman, G.; Clapp, C.; Greenwood, M.; Greenwood, M. T. Anti-apoptosis and cell survival: a review. Biochimica et Biophysica Acta (BBA)-Molecular Cell Research 2011, 1813, 238-259.

(110) Twiddy, D.; Cain, K. Caspase-9 cleavage, do you need it? Biochem J 2007, 405, e1-e2.

(111) Gupta, S.; Kass, G. E. N.; Szegezdi, E.; Joseph, B. The mitochondrial death pathway: a promising therapeutic target in diseases. Journal of Cellular and Molecular Medicine 2009, 13, 1004-1033.

(112) Brunelle, J. K.; Letai, A. Control of mitochondrial apoptosis by the Bcl-2 family. Journal of Cell Science 2009, 122, 437-441.

(113) Galluzzi, L.; Morselli, E.; Kepp, O.; Vitale, I.; Rigoni, A.; Vacchelli, E.; Michaud, M.; Zischka, H.; Castedo, M.; Kroemer, G. Mitochondrial gateways to cancer. Molecular Aspects of Medicine 2010, 31, 1-20.

(114) Allan, L. A.; Clarke, P. R. Phosphorylation of Caspase-9 by CDK1/Cyclin B1 Protects Mitotic Cells against Apoptosis. Molecular Cell 2007, 26, 301-310.

(115) Andersen, J. L.; Johnson, C. E.; Freel, C. D.; Parrish, A. B.; Day, J. L.; Buchakjian, M. R.; Nutt, L. K.; Thompson, J. W.; Moseley, M. A.; Kornbluth, S. Restraint of apoptosis during mitosis through interdomain phosphorylation of caspase-2. The EMBO Journal 2009, 28, 3216-3227.

(116) Ola, M. S.; Nawaz, M.; Ahsan, H. Role of Bcl-2 family proteins and caspases in the regulation of apoptosis. Molecular and Cellular Biochemistry 2011, 351, 41-58.

(117) Deveraux, Q. L.; Reed, J. C. IAP family proteins - Suppressors of apoptosis. Genes and Development 1999, 13, 239-252.

(118) Pardo, O. E.; Lesay, A.; Arcaro, A.; Lopes, R.; Ng, B. L.; Warne, P. H.; McNeish, I. A.; Tetley, T. D.; Lemoine, N. R.; Mehmet, H.; Seckl, M. J.; Downward, J. Fibroblast growth factor 2-mediated translational control of IAPs blocks mitochondrial release of Smac/DIABLO and apoptosis in small cell lung cancer cells. Mol Cell Biol 2003, 23, 7600-7610.

(119) Ferreira, C. G.; van der Valk, P.; Span, S. W.; Jonker, J. M.; Postmus, P. E.; Kruyt, F. A. E.; Giaccone, G. Assessment of IAP (inhibitor of apoptosis) proteins as predictors of response to chemotherapy in advanced non-small-cell lung cancer patients. Annals of Oncology 2001, 12, 799-805.

(120) Dong, F.; Guo, W.; Zhang, L.; Wu, S.; Teraishi, F.; Davis, J. J.; Fang, B. Downregulation of XIAP and induction of apoptosis by the synthetic cyclin-dependent kinase inhibitor GW8510 in non-small cell lung cancer cells. Cancer Biology & Therapy 2006, 5, 165-170.

(121) Asselin, E.; Mills, G. B.; Tsang, B. K. XIAP Regulates Akt Activity and Caspase-3-dependent Cleavage during Cisplatin-induced Apoptosis in Human Ovarian Epithelial Cancer Cells. Cancer research 2001, 61, 1862-1868.

(122) Deveraux, Q. L.; Roy, N.; Stennicke, H. R.; Van Arsdale, T.; Zhou, Q.; Srinivasula, S. M.; Alnemri, E. S.; Salvesen, G. S.; Reed, J. C. IAPs block apoptotic events induced by caspase-8 and cytochrome c by direct inhibition of distinct caspases. EMBO J 1998, 17, 2215-2223.

(123) Almenara, J.; Rosato, R.; Grant, S. Synergistic induction of mitochondrial damage and apoptosis in human leukemia cells by flavopiridol and the histone deacetylase inhibitor suberoylanilide hydroxamic acid (SAHA). Leukemia 2002, 16, 1331-1343.

(124) Dai, Y.; Chen, S.; Wang, L.; Pei, X.-Y.; Kramer, L. B.; Dent, P.; Grant, S. Bortezomib interacts synergistically with belinostat in human acute myeloid leukaemia and acute lymphoblastic leukaemia cells in association with perturbations in NF-κB and Bim. British Journal of Haematology 2011, 153, 222-235.

II. THE ROLE OF INTRINSIC SIGNALING PATHWAYS IN CELL PROLIFERRATION

ABSTRACT

Programmed cell death, or apoptosis, and controlled cell division, or mitosis are two highly regulated processes in the cell cycle. A balance between apoptosis and mitosis is critical for multiple distinct states including embryonic development, immune cell activation, stem cell differentiation, tissue formation (wound healing), and tumor prevention, among others. A cell undergoing apoptosis shows a series of characteristic morphological changes similar to normal mitosis and an aberrant form of mitosis. During each of these processes, nuclear chromatin condenses, the nuclear lamina and cytoplasmic membranes disintegrate, and cells decrease in volume. The morphological resemblance among cells undergoing these processes suggests that the underlying intracellular signaling pathways influence the mitotic cell fate. In this review paper, the relationship of intracellular signaling pathways, cell cycle dynamics, and apoptotic cell signaling pathways are discussed. The MAPK/Ras/Raf/ERK, PI3K/Akt, JAK/STAT, Wnt, and TGF-β are major cell signaling pathways that transmit signals from multiple cell surface receptors to transcription factors in the nucleus. The pathways are stimulated by cytokines, growth factors, and external stimuli, *i.e.*, reactive oxygen species which induce signal transduction pathways and regulate complex processes such as cell cycle progression, cell proliferation, cellular growth, differentiation, and apoptosis. Aberrant mutations in particular genes and proteins of these pathways contribute to cancers usually

by inhibiting pro-apoptotic proteins and stimulating anti-apoptotic proteins. The cell cycle is regulated by intracellular signaling pathways such as the MAPK/Ras/Raf/ERK and PI3K pathways to synthesize cyclin D and other mitosis regulating proteins (Myc and Jun). Cyclin D1 binds to CDK4/6 to form an effective complex, activate several substrates, and initiate the cell cycle. The prominent molecules that regulate signaling pathways in normal and cancer cells are described.

1. INTRODUCTION

Cell death and cell proliferation are coordinated in the cell cycle to maintain tissue function and tissue homeostasis.[1-4] The mammalian cell cycle is a regulated process that monitors the replication of genetic information and the division of cells. This regulation involves growth – regulatory signals and protein signals that ensure the genetic sequence of the cell receives no damage.[5] The cell cycle consists of four phases including a G0 or quiescence phase, G1 or Gap 1, S or DNA synthesis phase, a G2 or Gap 2 phase with mitosis or M phase at the end (Figure 1 (a)). These cell cycle phases are tightly controlled by a series of cell cycle proteins cyclin/cyclin-dependent kinases (CDKs) and cyclin inhibitors.[6] There are four cyclin groups (cyclin D, E, A, and B) that once bound activate specific cyclin-dependent kinase (CDK) pathways. The CDK pathways act as checkpoints that regulate the structure and property of the cellular chromosomes to either allow or deny entry into the next phase. Once the cyclin/CDKs of cyclin D1 to CDK 4/CDK 6 are bound and activated, the complex phosphorylates the retinoblastoma (Rb)

proteins and releases the activated E2F. At E2F this protein family determines whether the cells will reenter the cell cycle or eliminate the cell completely.[7]

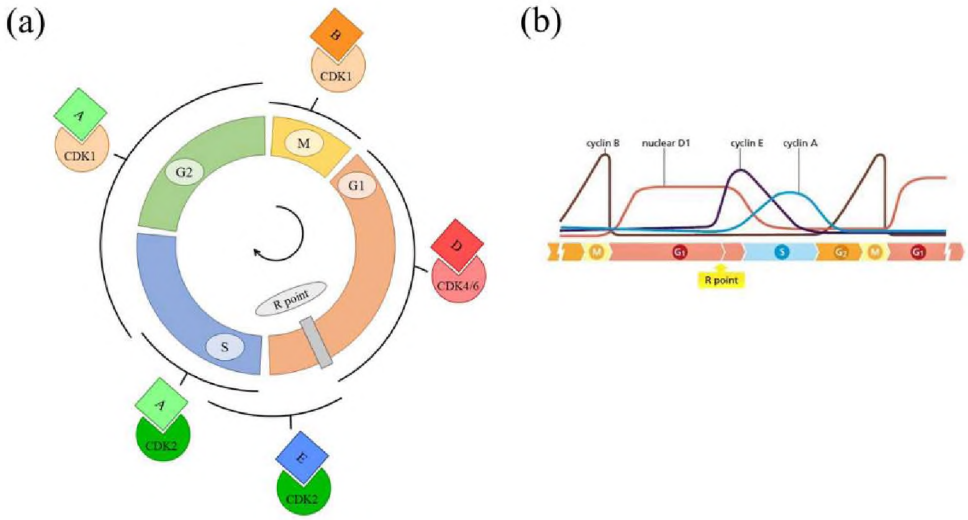

Figure 1. The cell cycle. (a) The cell cycle comprises four phases: G1, S, G2, and M. Extracellular signals received during the G1 phase lead to the production of D-type cyclins that interact with their dependent kinases. If the concentration of these cyclins is sufficient, the cell will pass the R phase, and E-, A-, and B-type cyclins will trigger DNA synthesis, a second gap phase to perform DNA repair, and mitosis. The cell is only responsive to extracellular signals in G1. (b) Cyclin levels during the cell cycle. The concentration of different types of cyclins varies with cell cycle progression. When a cell enters a new phase, a new type of cyclin associates with CDKs, ensuring the cycle only moves in the forward direction. The figure is reproduced with permission from Robert A. Weinberg (The Biology of Cancer, second edition) (2013)

Entry into the cell cycle is regulated by the mitogenic signaling pathways. The signaling pathways activate the downstream growth-promoting transcription factors including Myc, activator protein (AP1), β-catenin. Such transcription factors induce several cell cycle proteins such as cyclin D. D-type cyclins are typically present in the cell in extremely low concentrations. Unlike other cyclins, D-type cyclins are responsive to extracellular signals including mitogens. The E, A, and B-type cyclins are regulated in

a preprogrammed cyclic fashion to maintain the cell cycle in a unidirectional way (Figure 1 (b)). In response to the appropriate signals, the concentration of D-type cyclins increases in the cell. D-type cyclins bind to and activate CDK4 and CDK6.[8] Formation of active cyclin D-CDK4/6 complex is inhibited by the inhibitor of CDK-4 (INK4) family CDKIs (Figure 2 (a)). CDKIs act in response to growth factors, DNA damage, and other stressors. Two families of CDKIs exist p21 family members and INK4 proteins. p21, p27, and p57 belong to the p21 family and act by binding to cyclin-CDK complexes to block their active and binding sites.[8] Proteins of the INK4 family include p16, p15, p18, and p19 which bind to the catalytic subunit of CDK4/6 to bind D-type cyclins from activating them. The CDK inhibitors are activated in response to senescence inducing or growth-inhibitory signals including DNA damage, transforming growth factor-β (TGF-β), forkhead box protein O1/ O3 (FOXO1/ FOXO3) signaling pathways.

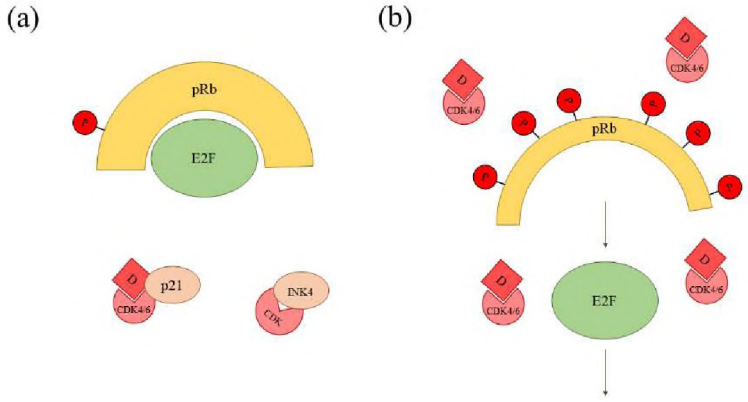

Figure 2. The pRb-E2F pathway. (a) pRb in a hypo- and hyperphosphorylated state. CDKIs act on CDKs and CDK-cyclin complexes to prevent pRb from becoming phosphorylated. (b) In the absence of CDKIs, CDK-cyclin complexes are free to phosphorylate pRb. This induces a conformational change that allows pRb to release E2F proteins

The retinoblastoma protein (pRb) normally exists in a hypophosphorylated state. Hypophosphorylated pRb binds E2F proteins. Upon the formation of active cyclin D-CDK4/6 complex and subsequent hyperphosphorylation of pRb, E2Fs are released which stimulate the transcription of several genes involved in cell cycle progression and cell division (Figure 2 (b)). D-type cyclin-CDK4/6 complexes begin the process of phosphorylating pRb. Among the many genes stimulated by E2Fs encode E-type cyclins. E-type cyclins form cyclin-CDK complexes with CDK2 and phosphorylate pRb. This positive feedback loop allows pRb to become hyperphosphorylated and allows the cell to progress from the G1 phase to the S phase.[8,9]

E2Fs activated the transcription of S phase promoting genes including CCNE1 and CCNE2, translating into cyclin E proteins. Cyclin E proteins pairs with CDK2 proteins. The cyclin E-CDK2 complexes remain in an inactivated state by the interactions with $p27^{KIP1}$ and $p21^{CIP1}$ cyclin-CDK complex inhibitor proteins. These inhibitor proteins are regulated by the p53 dependent DNA damage checkpoint protein molecules and growth-inhibitory signals. The sequestration of $p27^{KIP1}$ and $p21^{CIP1}$ inhibitory proteins by cyclin D-CDK4/6 complex and phosphorylation of $p27^{KIP1}$ by cyclin E-CDK2 complex activates the cyclin E-CDK2 complex. Upon activation of the cyclin E-CDK2 complex and further phosphorylation of pRb and other target proteins, the cells enter the S phase (Figure 3 (a)).

Entering the S phase, D type cyclins is exported to the cytoplasm from the nucleus where its level is no longer influenced by the extracellular growth factors. DNA replication occurs during the S phase while A-type cyclins replace E-type cyclins. The S phase is followed by G2, a second gap phase.

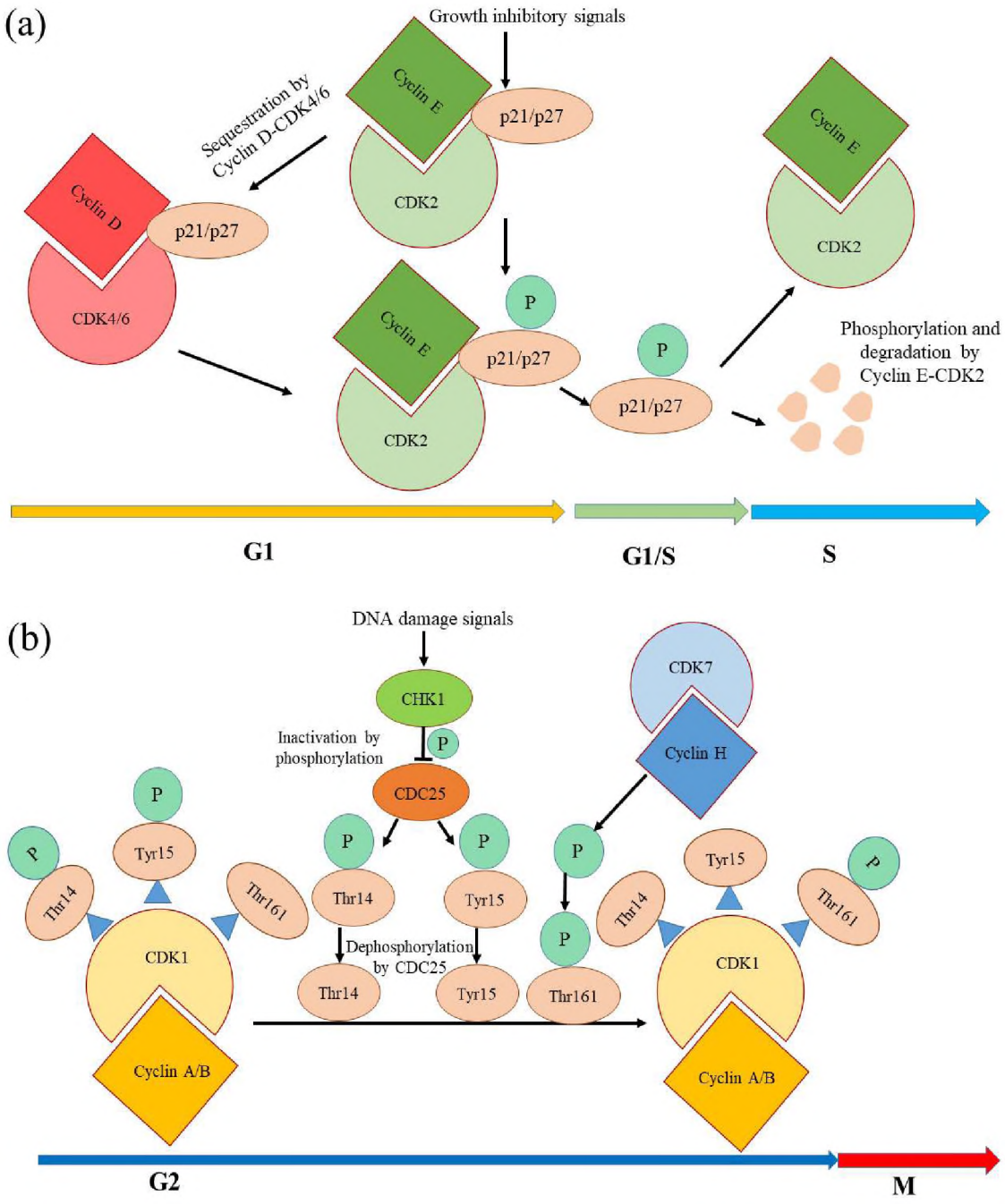

Figure 3. Representation of G1-S, G2-M cell cycle phase transition**.** The figure shows the regulation of (a) G1-S and (b) G2-M transition in the cell cycle. The cell cycle machinery is controlled by multiple proteins including cyclins, CDKs, CDKIs, and several transcription factors

This ensures that the cell has adequate time to complete DNA replication and repair any DNA damage that occurred during replication. During the late G2 phase, several G2 phase regulator proteins including B type cyclin proteins are translated replacing the A-type cyclins. The translation requires the association of multi-vulval class B protein (MUVB) complex with the forkhead box M1 (FOXM1) transcription factor. Together they bind with the cell cycle genes homology promoter region (CHR) and induce the transcription of G2 phase regulatory genes including cyclin B genes. Cyclin B pairs with CDK1 for cell cycle progression. The Cyclin B-CDK1 complex is activated in the following mechanism: CDK1 requires phosphorylation at threonine (Thr161) by the cyclin H-CDK7 protein complex and dephosphorylation at threonine 14 (Thr14) and tyrosine 15(Tyr15) kinase sites by cell division cycle 25 (CDC25) phosphatase enzyme. CDK7 is known as CDK activating kinase (CAK). The activation of the cyclin A/B-CDK2 complex promotes the cell cycle progression to the mitosis or M phase. This progression can be halted by checkpoint kinase-1 (CHK1) dependent G2 phase checkpoint upon DNA damage (Figure 3 (b)).

The events of mitosis include prophase, prometaphase, metaphase, anaphase, and telophase, resulting in two identical cells. After the M phase, the cell returns to G1 where it is once again receptive to internal and external signals and must divide whether to enter G0 or repeat the cell cycle. In this review, we will emphasize the major growth and anti-growth signals that stimulate the cells to take the exit from or retrieve to their quiescence phase. Aberrations in these signaling pathways can lead to two closely related hallmarks of cancer: evading growth suppressors and self-sufficiency in growth signals.[10] Pathways

of interest reviewed in this study are the MAPK, PI3K, Jak-STAT, Wnt, and TGFβ signaling pathways.

2. CELL SIGNALING PATHWAYS

2.1. MAPK/Ras/Raf/ERK SIGNALING PATHWAY

The MAPK pathway is a kinase cascade, also known as the extracellular signal-regulated kinase pathway (ERK). The first step in this pathway is Ras activation (or activation of other Ras family proteins). Ras activation begins when specific growth factors bind to transmembrane receptors, primarily receptor tyrosine kinases.[11] These receptors most commonly phosphorylate growth factor receptor-bound protein 2 (Grb2) or Shc. If Shc is phosphorylated, it will phosphorylate Grb2. Grb2 contains two functional domains: SH2 and SH3.[9] Upon phosphorylation, the SH2 domain binds to Shc or the receptor, and the SH3 domain is available for Sos binding.[9] This brings Sos into close proximity to Ras.[12]

Ras (and related Ras family proteins) are membrane-bound GTPases that function as G proteins. G proteins act as molecular switches that cycle between being GDP and GTP bound depending on extracellular signals such as growth factors and survival signals.[13] Sos can activate Ras by inducing it to convert GDP to GTP (Figure 4).

Ras binding and activation lead to Raf kinases including ARAF, BRAF, and CRAF, thus beginning the kinase cascade (Figure 5). Rafs are MAPKKKs which activate MAPKKs MEK1 and MEK2. MEK1/2 activates MAPKs ERK1 and ERK2.

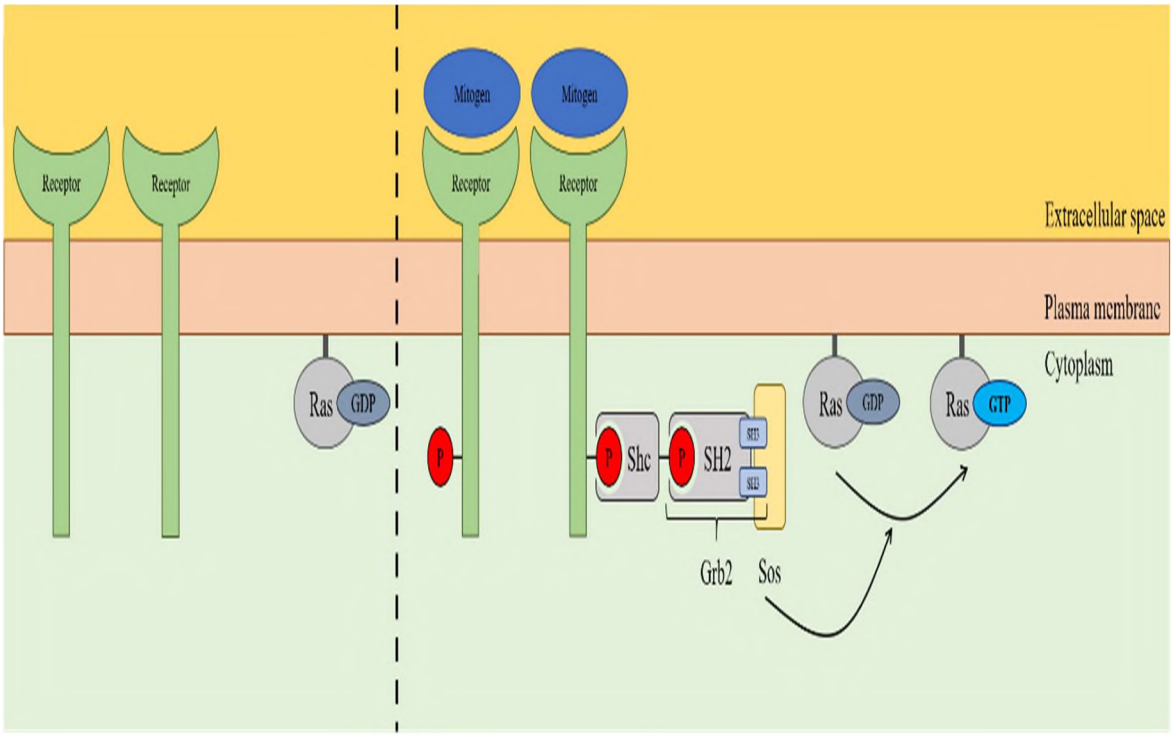

Figure 4. The Ras activation pathway. Growth factors bind to their respective receptors allowing them to bind Shc or Grb2. Grb2 binds Sos bringing it in proximity to Ras. This induces Ras to switch from an "off" to an "on" conformation, converting GDP to GTP

These MAPKs translocate to the nucleus and phosphorylate several proliferation promoting transcription factors including Myc.[14] Myc is a major regulator of cell cycle progression and pRb.[9] Myc is a transcription factor that elevates the expression of D-type cyclins, CDK4/6, and several E2F proteins. Myc also signals the expression of Cu11, a protein which phosphorylates the CDKI p27 for subsequent ubiquitination and degradation.[13] Myc is also capable of repressing p15 and p21 expression by associating with Myc-interacting zinc finger protein 1 (Miz-1).[9]

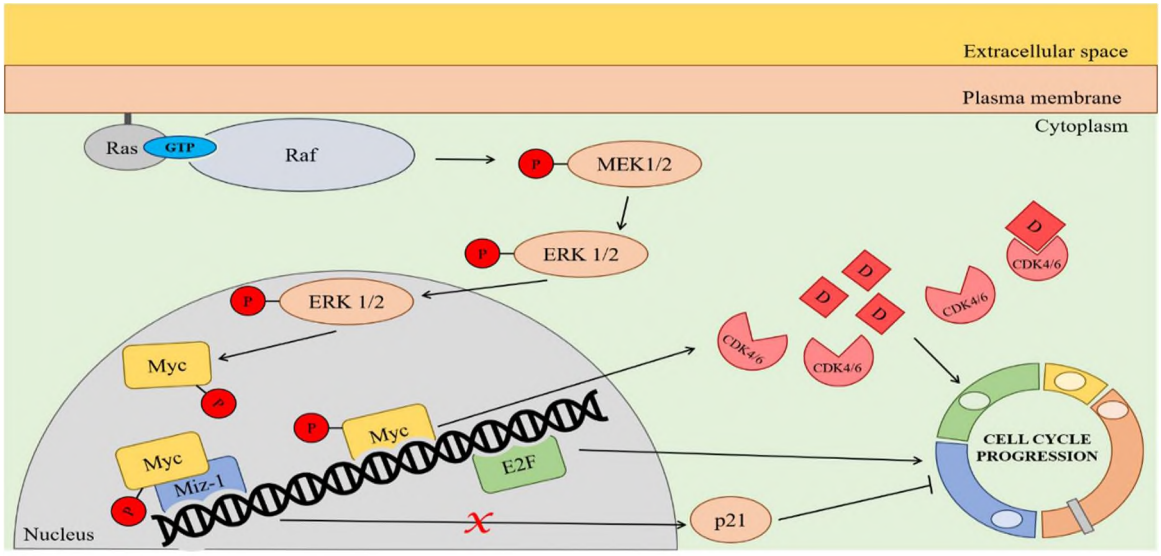

Figure 5. The MAPK signaling pathway. Ras activation initiates a kinase cascade. Eventually, MAPK proteins ERK1 and ERK2 enter the nucleus to phosphorylate and activate several pro-mitotic transcription factors including Myc

2.2. MAPK PATHWAY ASSOCIATED TARGETS FOR CANCER THERAPY

Extensive studies have been conducted targeting the Ras-Raf-MEK-ERK pathway alterations in cancer. The pathway is altered in almost 40% of all types of human cancers.[11,15] RAS point mutations are found in up to 30% of all human cancers and 90% of pancreatic adenocarcinomas.[11] These mutations often render Ras insensitive to inactivation leading them to remain activated in the absence of pro-mitotic factors.[11] BRAF mutation accounts for almost 10% of all human cancers.[16] In metastatic melanoma, BRAF mutation is altered in almost 50-60% of the cases and is considered to be the most prevalent acquired hallmark in melanoma.[15] Mutations resulting in hyperactive Raf proteins are also common among thyroid[17-19] and colon cancer,[20,21], among other types.[11] The prevalence of these mutations in cancer has led to considerable research into treatments and mechanisms of resistance targeting this pathway.[15]

One of the major strategies of targeting and blocking the MAPK signaling pathway includes the use of MEK inhibitors.[11] MEK inhibitors are small molecules that inhibit MEK1/2 either by inhibiting Raf phosphorylation activity or by allosterically blocking the conformational shift of MEK1/2 typically induced by phosphorylation.[22] Cobimetinib (brand name Cotellic) is an FDA approved MEK inhibitor which may be used in combination with Vemurafenib to treat melanoma. Vemurafenib (a Raf inhibitor) was previously approved for patients with a BRAF V600E mutation.[22] Dabrafenib and Encorafenib are also approved for advanced melanoma patients with BRAF V600E mutation. In combination, Cobimetinib has been shown to improve progression-free survival and response to the drug compared to Vemurafenib alone.[23] Two other MEK inhibitors, Trametinib (Mekinist) and Binimetinib (Mektovi) have been approved by the FDA to treat melanomas with mutations in the BRAF genes in combination with Raf inhibitors. The epidermal growth factor receptor (EGFR) inhibitors Gefitinib and Lapatinib are two approved drugs to inhibit the MAPK pathway in cancer treatment.

Though MEK inhibitors showed tremendous potency and high selectivity to inhibit this pathway, their success was limited by the acquired resistance upon treatment with single-arm MEK inhibitor.[24-26] Upon perturbation by the MEK inhibitor, a negative feedback loop mechanism inactivates the Raf protein in the pathway causing the drug to be ineffective on the MEK eventually. This negative feedback loop mechanism results in the restoration of the ERK signaling pathway. Hence, targeting the inhibition of both Raf and MEK is now a standard therapy in metastatic melanoma treatment. Inhibition of restoration of ERK pathway upon therapeutic intervention by Raf or MEK inhibitors is a major challenge in dealing with drug resistance.[27-29] The mechanisms of restoration often

impinge on the dimerization of Raf kinases,[30] though dimerization is a part of physiological Raf activation.[31] Raf kinases are frequently dimerized in tumors with mutated RAS. The dimerized Raf is drug-resistant can paradoxically reactivate the ERK pathways causing therapeutic resistance. Inhibitors targeting the inhibition Raf dimerization may overcome such resistance. Furthermore, the therapeutic resistance in this pathway is also attributed to the role of Jun N-terminal kinase (JNK) and p38 MAPK pathway mediated drug resistance.[31-35]

2.3. PI3K/Akt SIGNALING PATHWAY

The PI3K/Akt pathway influences cell proliferation (Figure 6). Extracellular cytokines bind to transmembrane receptors which activate PI3K via two mechanisms. Some receptors bind the regulatory subunit of PI3K (p85), recruiting the catalytic subunit (p110) of PI3K.[36] Ras can also activate the p110 subunit of PI3K in addition to its function in the MAPK signaling pathway.[14,36] Once activated, PI3K causes phosphatidylinositol-dependent kinase-1 (PDK1) to localize at the membrane.[36] PDK1 phosphorylates and activates Akt. Akt is known to phosphorylate a number of substrates, many of which have implications in controlling the cell cycle regulation.[9] Notably, it phosphorylates glycogen synthase kinase 3 beta (GSK-3β), tagging it for degradation.[9] GSK-3β, a major player in the Wnt signaling pathway described below, is responsible for phosphorylating β-catenin (an upstream regulator of Myc and cyclin D) for ubiquitination and degradation.[9,37] Akt also phosphorylates the CDK inhibitor p21.

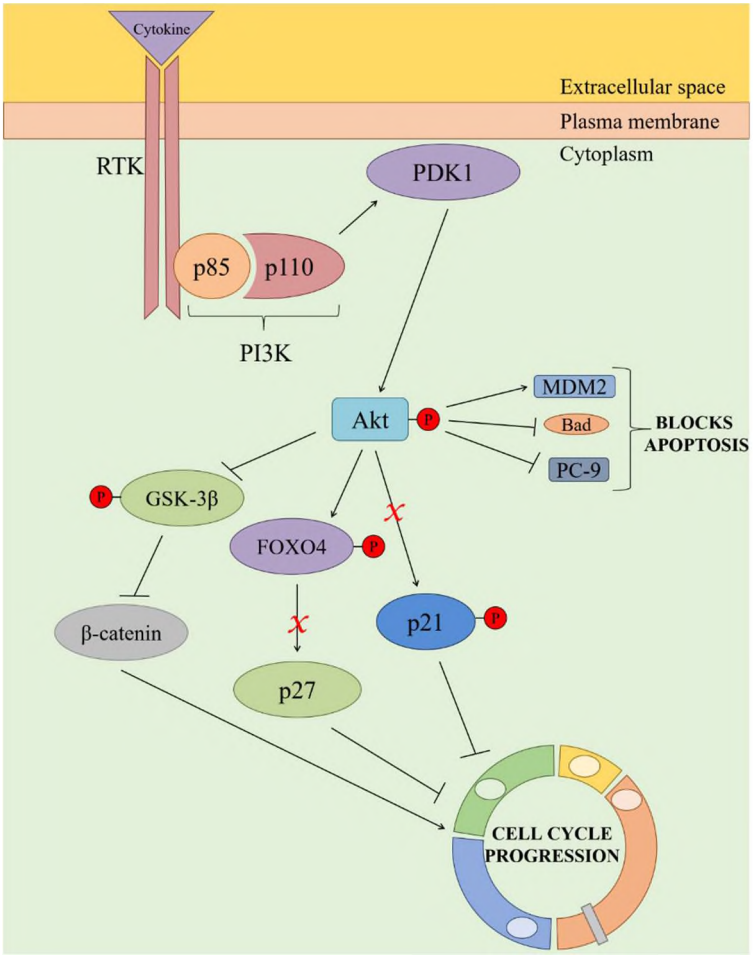

Figure 6. The PI3K signaling pathway. Ligand-receptor binding activates and associates p85 with p110 to form PI3K. PI3K activates PDK1 which phosphorylates Akt. Phosphorylated Akt can inhibit anti-mitotic proteins including GSK-3β or phosphorylate them for subsequent ubiquitination and degradation. Akt also has anti-apoptotic effects

Upon phosphorylation, p21 moves from the nucleus to the cytoplasm where it actually exhibits anti-apoptotic functions. The third substrate for Akt involved in proliferation is FOXO4. FOXO4 induces CDKI p27 expression; however, upon phosphorylation, FOXO4 is transported to the cytoplasm like p21.[9]

It is also interesting to note that Akt phosphorylates substrates directly related to the apoptotic machinery. Akt inhibits the pro-apoptotic proteins Bad and caspase 9 and

activates mouse-double minute 2 homolog (MDM2). Thus, Akt drives cell survival and proliferation by transmitting anti-apoptotic and pro-mitotic signals within the cell. Because of its role in regulating cell death and proliferation, it is perhaps unsurprising that aberrations in the PI3K pathway have been found in several cancers. Notably, a mutant p85 has been identified in Hodgkin's lymphoma cells and has been linked to breast cancer, lung cancer, melanomas, and leukemia.[36]

2.4. PI3K/Akt PATHWAY ASSOCIATED TARGETS FOR CANCER THERAPY

The PI3K/Akt pathway is an attractive therapy for chemotherapy due to its role in so many cancer types. PI3K inhibitors act *via* various mechanisms to inhibit members of the PI3K/Akt pathway, primarily PI3K or Akt.[36] Wortmannin was the first PI3K inhibitor to be approved by the FDA.[36] Wortmannin is not selective and binds to PI3K as well as several related proteins.[38] Wortmannin irreversibly inhibits PI3K by covalently binding to a lysine residue in the protein's catalytic subunit.[38] Wortmannin has good efficacy but is somewhat unstable; following its development other PI3K inhibitors have been developed.

Two more recently approved drugs include Aleplisib and Idelalisib. Alpelisib (Piqray) was approved by the FDA to treat HER2 negative breast cancer with mutant PI3K. Idelalisib (Zydelig) has been approved for solo or combination treatment of chronic lymphocytic leukemia and two types of Non-Hodgkin lymphomas. PIK3CA is a mediator of HER2 targeted treatment resistance. PIK3CA mutation accounts for almost 20% of HER2 positive breast cancer patients and imposes the insufficiency of HER2 blockade strategy to suppress the downstream PI3K signaling pathway. PI3K activation

pathway is most often accompanied by loss of tumor suppressor gene PTEN in breast cancer.

2.5. Jak-STAT SIGNALING PATHWAY

The Jak-STAT signaling pathway offers another method for cytokines and growth factors to directly influence cell proliferation (Figure 7).[39]

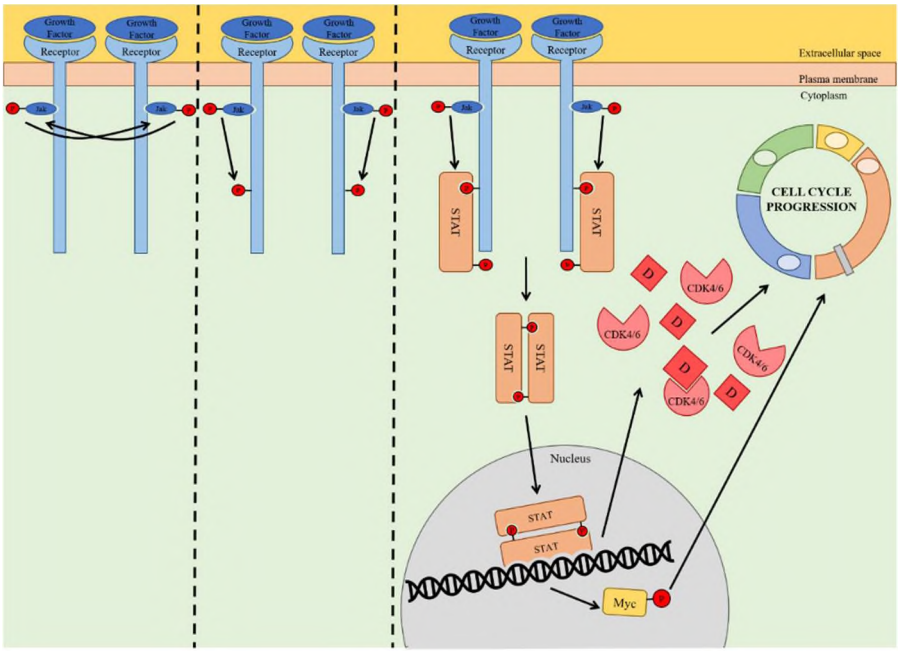

Figure 7. The Jak-STAT signaling pathway. Associated growth factors bind receptors to activate Jak family proteins. These proteins phosphorylate each other followed by their receptor. This leads to the binding and phosphorylation of STAT proteins. STAT proteins dimerize and translocate to the nucleus to activate pro-mitotic genes that encode for D-type cyclins, CDK4/6, and Myc

Upon the binding of their extracellular ligands, receptors in the Jak-STAT pathway dimerize and associated Janus kinases (Jaks) phosphorylate tyrosines on the opposing receptors. Activated Jaks can then phosphorylate STATs (signal transducers

and activators of transcription). Upon phosphorylation, STAT proteins dimerize and translocate from the cytoplasm to the nucleus. STATs activate several target genes involved in cell proliferation including those encoding for Myc and two D-type cyclins. This pathway offers a simple opportunity for signal transduction between extracellular signals and the cell cycle; however, this pathway also interacts with some of the more complex pathways described above. For example, Jaks are capable of phosphorylating tyrosines on receptors in the MAPK or PI3K pathway as well as their own pathway. This phosphorylation leads to the same activation of Ras (in MAPK signaling) and p85 (in PI3K), enabling those pathways to send proliferative signals to the nucleus as well.[39,40]

2.6. Jak-STAT PATHWAY ASSOCIATED TARGETS FOR CANCER THERAPY

In healthy cells, STAT proteins are only active upon phosphorylation by Jaks. In some cancers, constitutively active STAT proteins have been found, signaling for proliferation in the absence of cytokines and growth factors. Notably, STAT3 (a protein in the STAT family) has been found to be constitutively active in 40% of breast cancers and T-cell large granular lymphocytic leukemia cases, as well as many cases of prostate, glioblastoma, thyroid, and non-small cell lung cancer.[40] The Jak-STAT pathway also regulates components of the immune response; several mutations resulting in hyperactive Jak or STAT proteins are known to influence immune diseases.[40,41] Because of this, Jak and STAT inhibitors have been studied for many cancers and immune diseases.[42] Several Jak inhibitors have been approved to treat immune disorders such as psoriasis, myelofibrosis, and rheumatoid arthritis.[41,43] While many of these agents are also being investigated to treat different cancer types, none have yet passed clinical trials.[41,43]

2.7. Wnt SIGNALING PATHWAY

The Wnt signaling pathway can also influence cellular proliferation (Figure 8).[37]

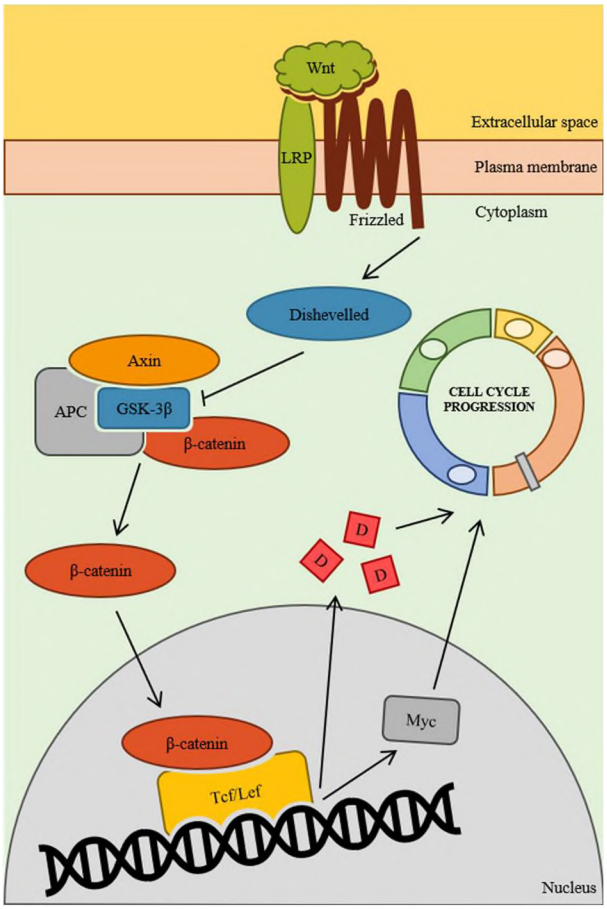

Figure 8. The Wnt signaling pathway. Wnt binds to the transmembrane receptor Frizzled to activate Disheveled. Disheveled inhibits GSK-3β preventing β-catenin degradation. Instead, B-catenin translocates to the nucleus, associates with Tcf/Lef, and induces the transcription of D-type cyclins and Myc

Wnts are secreted glycoproteins that interact with several signaling pathways that are not fully understood.[37,44] The most well-known is the canonical pathway which influences cell cycle progression.[9,37,44] β-catenin is normally present in the cell in very

low concentrations with a half-life of 20 minutes.[9] Cytoplasmic β-catenin forms a complex with axin, adenomatous polyposis coli protein (APC), and GSK-3β.[9] This multiprotein complex enables GSK-3β to phosphorylate β-catenin, tagging it for ubiquitination and subsequent degradation, thus maintaining its short half-life and low intracellular concentration.[9] However, the canonical Wnt signaling pathway prevents this degradation from occurring. Wnts associate with low-density lipoprotein receptor-related protein (LRP) 5 and 6, Wnt ligand co-receptors, and bind to transmembrane receptors of the Frizzled gene family.[44] This binding, in turn, inhibits GSK-3β.[44] With GSK-3β unable to phosphorylate β-catenin, it accumulates in the cytoplasm before translocating to the nucleus.[44] There it binds to and activates the T-cell factor/lymphoid enhancer factor (Tcf/Lef) transcription factors.[9] This complex is responsible for the transcription of many genes, including Myc and cyclin D1, both of which are involved in cell cycle progression.[44]

2.8. Wnt SIGNALING PATHWAY ASSOCIATED TARGETS FOR CANCER THERAPY

Colorectal cancers (CRC) are the most commonly affected cancers by the dysregulation in the Wnt signaling pathway. A sequencing study on 1134 CRC samples identified that almost 96% % of the human CRC was associated with Wnt oncogenic activity.[45] Loss of function mutation in APC is the most common in colorectal cancers,[46-50] followed by alterations causing inhibition of the proteasomal degradation or downregulation of β-catenin.[51-54] Due to the acquired resistance upon conventional therapeutic intervention, a few Wnt/β-catenin inhibitors have been identified as useful agents in treating any type of cancer with Wnt pathway dysregulation. Krishnamurthy

and Kurzrock summarized 35 therapeutic drugs that inhibit the Wnt signaling pathway.[55] Of those, three off label drugs were FDA approved: Niclosamide, a drug traditionally used to treat tapeworm infestations, thought to downregulate disheveled; Sulindac, a nonsteroidal anti-inflammatory drug, also thought to target disheveled; and Pyrvinium, an anthelmintic, thought to target the Wnt inhibitor CK1a.[55] The wide domain of Wnt signaling dysregulation across the cancer types has led to the identification of cancer-specific therapeutic targets in the Wnt signaling pathway. The list of Wnt/ β-catenin inhibitors in the past and present clinical trials and potential therapeutic target in this pathway beyond the β-catenin destruction pathways are well summarized in a recent review by Jung et. al.[56] In addition to the malignant progression caused by the aberrant Wnt signaling pathway emerging evidence suggests that Wnt pathway also alters the cancer-immune system surveillance and offers resistance to the immunotherapeutic drugs.[57-59]

2.9. TGF- β SIGNALING PATHWAY

The above-mentioned signaling pathways all rely on growth signals to stimulate proliferation. When those pathways acquire mutations resulting in constitutively active components, they fire and signal for cell cycle progression, whether or not growth signals are present. This is known as "self-sufficiency in growth signal," a hallmark of cancer.[10] However, cells do not rely solely on the presence of growth signals to stimulate proliferation. Anti-growth signals also regulate proliferation by commanding a cell not to progress through the cell cycle.

Transforming growth factor-beta (TGF-β) is the best studied growth-inhibitory signal (Figure 9).[5]

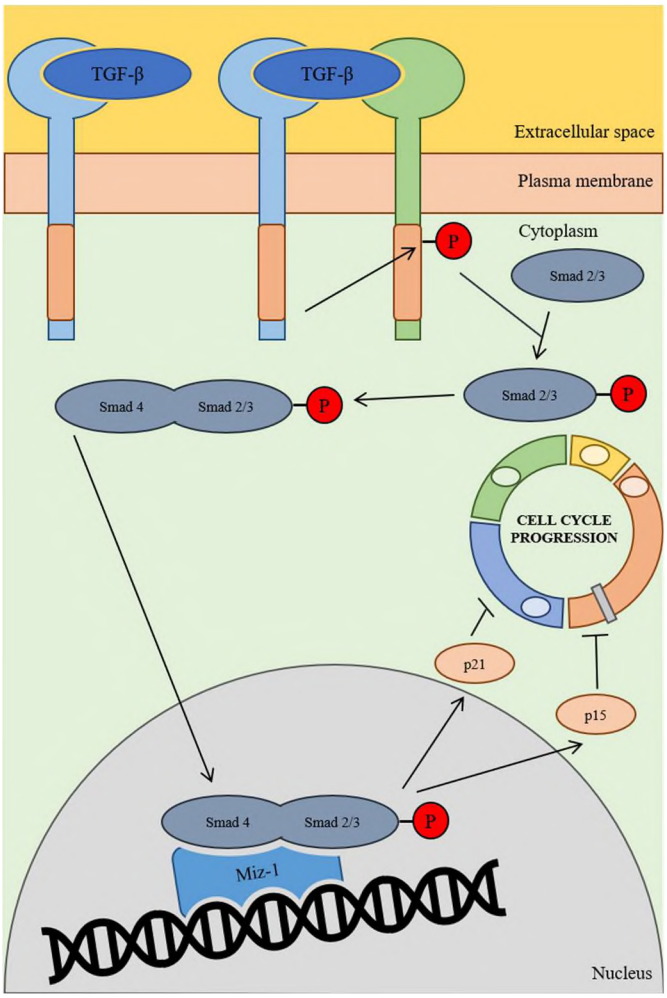

Figure 9. The TGF β signaling pathway. TGF β inhibits cell cycle progression by binding Type I (blue) and Type II (green) receptors. Binding induces Smad2/3 phosphorylation. Smad 2/3 then dimerizes with Smad 4 and translocates to the nucleus to associate with Miz-1. The Smad dimer-Miz-1 complex acts as a transcription factor for the CDKIs p21 and p15

When the TGF-β ligand binds receptors on the cell's surface, type I and II receptors associate leading to the phosphorylation of Smad2 and Smad3. Phosphorylated

Smad 2/3 is capable of dimerizing with Smad4.[9] These Smad dimers translocate to the nucleus where they associate with Miz-1.[9] Upon binding with Miz-1, Smad complexes act as transcription factors for CDKIs p15 and p21.[9]

In healthy cells, Smad complexes and Myc compete to bind with Miz-1 to control the expression or repression of these CDKIs.[9] To prevent proliferation, Smad3 is capable of binding to the promoter site of the MYC gene, blocking its expression and favoring binding between Miz-1 and Smads.[9] Many cancer cells develop strategies to avoid TGF-β's growth inhibitory effects, known as "insensitivity to antigrowth signals".[10]

Overexpression of Myc will favor Miz-1 binding to Myc rather than Smad dimers, preventing the expression of p21 and p15.[9] It is common among cancer cells for mutations in the MYC promoter site to prevent TGF-β induced repression.[5] In other cells, pRb is lost and the MAPK pathway is no longer the main pathway signaling to advance in the cell cycle.[9] Since TGF-β primarily inhibits Myc and the MAPK signaling pathway, this renders TGF-β ineffective as other signaling pathways continue to trigger activation.[13] In colon cancers, mutations in the TGFβ pathway are common. These take the form of mutations in the gene which encodes Smad2 or through the presence of Ski and Sno, proteins that bind to and inhibit Smad dimers.[9] Other colon cancers acquire mutations which inactivate the transmembrane receptors in the TGF-β pathway.[9]

2.10. TGF-β SIGNALING PATHWAY ASSOCIATED TARGETS FOR CANCER THERAPY

In premalignant state, TGF β maintains the tissue homeostasis by cytostasis, differentiation, induction of apoptosis, suppression of tumorigenic inflammation and stroma derived mitogens. The malignant cells can adulterate the suppressive pathway of

TGF β promoting tumor growth and invasion, deceiving the immune surveillance, and finally causing metastasis. There are two ways to do that. The first one is the upstream inactivation of the core component in the pathway, for example, mutations in the receptors. Secondly, the downstream alterations in the tumor-suppressive arm in the pathway such as defective cytostatic response in tumorigenesis. The consequence of the first type of malignancy in the cancer cells removes the chance for tumor suppression upon suppressive growth signals. The second type of malignancy is more aggressive as it allows the cancer cells to aberrantly use the TGF β regulatory functions, produce autocrine mitogens, release prometastatic cytokines and hence, create a pro-tumorigenic microenvironment along with deactivation of growth suppression capability. Additionally, TGF-β may contribute to invasion and metastasis.[60] Cancer cells TGF-β has been shown to induce Smad 2/3 dependent epithelial-mesenchymal transition (EMT).[60] EMT is a critical acquired ability in metastatic cancers. The therapeutic targets in this pathway include antisense oligonucleotides for TGF-β production inhibition, anti-TGF-β antibodies, and anti-receptor antibodies to inhibit the ligand-receptor interactions, small molecules targeting TGF-β receptor kinases and TGF-β trapping receptor codomain proteins.[61-64]

3. CELL CYCLE PROTEINS: CYCLINS, CDKs AND CDK INHIBITORS

In the following sections, the main molecules participating in the signaling pathways of the cell division and cell cycle are described.

3.1. CYCLINS

Cyclin Ds are important for the cell entry into the G1 phase of the cell cycle and the transition to the S phase. There are three members of the cyclin D family: D1, D2, and D3. Cyclin D1 plays an important role in cell cycle progression. Cyclin D1 conducts specific functions to regulate gene expression in the context of chromatin, cellular migration promotion, and chromosomal instability promotion.[65] Once the cyclin D family activates the kinases, CDK4 and CDK6, the cells can transition into the S phase. The cyclin E family plays an important checkpoint that allows the cells to transition from the G1 phase to the S phase. There are two members of the cyclin E family: E1 and E2. The cyclin E family limits the number of cells that enter the S phase and the G0 phase. Cyclin E also plays an important role in replication of DNA, the genomic stability, and the centrosome cycle. Once the cyclin E family activates the kinase CDK2, the cells can transition into the S phase. The cyclin A family regulates the cell proliferation through the S phase. The cyclin A family activates the kinase CDK2, during the S phase and will activate the kinase CDK2 at the checkpoint, to determine if the cell will transition to the G2 phase or remain in the S phase. Lastly, the cyclin B family regulates the last checkpoint that allows the cell to transition from the G2 phase to the M phase to complete division. The cyclin B family activates the kinase CDK1 to further allow entry of the cell into the M phase.

3.2. CYCLIN DEPENDENT KINASES

CDK4 and CDK6, activated by the cyclin D family, promote the cell transitioning by two major mechanisms; they sequester the CDK inhibitors p21 and p27, and they

phosphorylate the RB family to code for the p107 and p130 proteins.[5] The proteins p21 and p27 are responsible for the cell's progression through the G1 to the S phase by inhibiting the activity of CDK4/6. The proteins p107 and p130 are responsible for monitoring the activity of the E2F family by limiting the genetic material needed for the cell's transition through the cell cycle. Another way to describe the p107 and p130 proteins are as "pocket proteins".[66]

CDK2 can be activated by either cyclin E or cyclin A family. CDK2 is a serine/threonine protein kinase that is the key regulator in the cell phases of G1/S and S/G2.[67] In the transition from the G1/S phases, CDK4/6 phosphorylates the Rb proteins from the activation caused by cyclin D. CDK2, activated by cyclin E, further completes the phosphorylation of Rb to activate the E2F family. CDK2 is also required for mini chromosome maintenance proteins that are essential for the initiation of replication.[67] Overall CDK2 is responsible for the drive of the progression through the cell cycle.

CDK1 can be activated by either the cyclin A or cyclin B family. CDK1 is responsible for the successful completion of the M phase in the cell cycle. CDK1 activated by cyclin A, regulates the cell's entry into mitosis and proceeds until cyclin A eliminates the ubiquitin – proteasome system that starts in the early stages of prometaphase.[68] When CDK1 is activated by cyclin B, the cell is signaled to proceed onward through mitosis to complete the DNA replication to divide.

3.3. CYCLIN DEPENDENT KINASE INHIBITORS (CDKIs)

CDKIs are proteins that inhibit the activated CDKs of the cell cycle. Seven CDKI proteins can cause the cell's progression to be delayed including p15, p16, p18, p19, p21,

p27, and p57. p15 targets CDK4 by the CDKN2B gene to prevent the activation of the cyclin D family in the G0/G1 phase.[69] Thus, the p15 protein inhibits the cells progression in the early phase of the cell cycle. p16 delays the proliferation of the cell through the G1 and S phase by targeting CDK4/6 and is encoded by the gene CDKN2A. When CDKN2A is deleted, it can cause the p16 to be non-functional and result in an acceleration of the cell cycle.[70] p18 is encoded by the CDKN2C gene to target the activation of CDK4/6 in the early phase of cell progression. p19 also targets CDK4/6 in the early phase of cell progression by the CDKN2D gene. As mentioned in the cyclin - dependent kinase section, p21 and p27 can be sequestered by CDK4/6. p21 and p27 are encoded by the genes CDKN1A and CDKN1B to target CDK2 and CDK4. By inhibiting the activity of CDK4/6, p21 and p27 are responsible for the cell's progression through the cell cycle. Lastly, p57 is encoded by the gene CDKN1C to target CDK2 in the cells transition from the G1 phase to the S phase. Each CDKI protein acts as a tumor suppressor to delay the activity of the tumor formation.

3.4. THE ROLE OF p53 IN CELL CYCLE REGULATION

p53 is a nuclear transcription factor that targets genes involved in the induction of cell cycle arrest and/or apoptosis.[71] DNA damage usually involves the activation of p53 in response to damages to the DNA and stresses. Once p53 is activated, there are two pathways the cell can go. The first is cell cycle arrest and the second is apoptosis. The p53 pathway can signal to p21 that will mediate the binding to CDK2 and CDK1 to lead the arrest at specific stages in the cell cycle due to various stimuli.[72] On the other hand, p53 can activate either Bax or Puma for cell apoptosis. Bax is an apoptosis regulator that

is part of the Bcl-2 family of proteins that are the main regulators of cell death. BAX is the central mediator and contains BH1, BH2, and BH3 domains with a hydrophobic membrane.[72] Puma is a potent killer among the Bcl-2 homology 3 that transduces apoptosis signals primarily to the mitochondria.[73] PUMA indirectly responds with BAX to promote apoptosis of the cell.

3.5. THE ROLE OF Bax AND Puma IN p53 – MEDIATED THERAPY

Bax is one of two nuclear encoded proteins that mediate cell death. Bax was the first death inducing member of the Bcl-2 family due to studies that involved protein purification with Bcl-2. Bax is a globular protein that contains nine helices; Alpha 1 to Alpha 8 are the inhibitors of apoptosis.[74] Bax can be activated by cleavage of caspases, inhibition of protein kinases, activation of phosphates, and an increase in intracellular pH.[75] Specifically, to p53, under stress signals cytochrome c is released, inducing apoptosis. Puma is essential for apoptosis and is activated due to DNA damage on p53. Puma p53-mediated apoptosis includes the neuronal cell death induced by 6 - hydroxydopamine,[76] and cancer cell death induced by proteasome inhibitors.[77] Oncogenic stress can also activate Puma to function as a safeguard against neoplastic transformation.[73] Puma- induced apoptosis requires interactions with the Bcl-2 family proteins such as Bax and once triggered, mitochondrial dysfunction and caspase activation is induced. In cancer, Puma can be compromised due to p53 mutations caused by irradiation and chemotherapy drugs, overexpression of the Bcl-2 family proteins, and poor levels of Puma detection.[73] Even with the compromises, it is important to note that

Puma in p53-mediated therapies is still emerging and deciphering the different signaling pathways will contribute to targeting Puma p53-mediated therapies.

3.6. CYCLIN, CDK AND CDKI TARGETS FOR CANCER THERAPY

The CDK4/6-Rb pathway is frequently deregulated in cancer that influences the tumor cells to enter the restriction (R) point at the late G1 phase and complete the cell cycle.[5] The deregulations of major cell cycle proteins in this pathway in terms of deletions, amplifications and point mutations are summarized by Otto et.al.[5] In this pathway, the tumor suppressor CDK4/6 inhibitor $p16^{INK4A}$ protein is often silenced by promoter methylation or the $p16^{INK4A}$ encoding gene CDKN2A is frequently deleted across all human cancer types.[78] The frequent deletion of RB1, the pRb encoding gene also causes the proliferation of tumor cells irrespective of their cyclin D-CDK4/6 catalytic activity.[78]

The cyclin D1 gene (CCND1) is the second most frequently amplified gene in all cancer types.[5,78] The overexpression of cyclin D1 increases the catalytic activity of their binding partner CDK4/6 and hence increases the proliferation rate of tumor cells. In a transgenic mice model overexpression of cyclin D1 induced hyperplasia and carcinoma in mammary glands.[79] Carcinogen induced skin tumorigenesis was induced by the overexpression of cyclin D1 protein, cyclin D2 gene, and CDK4 protein overexpression.[16,80,81] Cyclin D1 protein is overexpressed in 50-70% of the breast cancer cases and is most frequent in Luminal B type and human epidermal growth factor receptor-2 (HER2) positive breast cancer.[82,83] Cyclin D1 promotes tumorigenesis in HER2 positive breast cancer.[84] The amplification in the CCND1 gene copy number is

present in only 9-30% of the cases suggesting underlying mechanisms of protein overexpression other than the copy number amplification.[83] An integrative study of CCND1 amplification in 2305 breast tumors found that CCND1 amplified tumors induced the co-expression of proliferative gene MKI67 across all of the PAM50 classified breast cancer subtypes including HER2 positive breast cancer.[83] The same study also suggests that CCND1 amplification is independent of CDK4/6 gene upregulation and could be a poor predictive biomarker for the prediction of response to CDK-4/6 inhibitors. CDK4 is constitutively amplified in glioblastomas.[85] CDK4 is most commonly mutated by an R24C point mutation in melanomas and becomes insensitive to the INK4 members of CDKIs promoting unhalted growth.[86] CDK4 promotes tumorigenesis in HER2 positive breast cancer cells.[87,88] An oncogenic $Kras^{G12V}$ driven lung cancer showed selective sensitivity to CDK4 inhibition indifferent to CDK2 or CDK6.[89] Altogether the data suggest that the CDK4/6-Rb pathway is a crucial target for cell cycle targeted therapeutic trials. The CDK 4/6 inhibitors Palbociclib, Ribociclib, and Abemaciclib have been approved for the treatment of Herceptin receptor-positive (HER2+) and Herceptin receptor-negative (HER2-) breast cancer treatment. Several other CDK 4/6 targeted therapeutic trials are ongoing for breast cancer,[90-92] and other solid tumors.[5,93]

Cyclin E1 encoding gene CCNE1 is commonly amplified in ovarian[94] and breast cancer.[95] CCNE1 copy number amplification or Cyclin E overexpression and corresponding CDK2 activity is associated with worse clinical benefit, poor progression-free survival with statistical significance. In a study on 395 breast cancer patients, Cyclin E expression was the most powerfully negatively correlated with patients overall and

disease-free survival.[96] CDK2 mutation is rare but the Cyclin E protein overexpression causes the hyper catalytic activity of Cyclin E-CDK2 complex.[5] CDK2 activity is normally kept inactivated by the association of CDK inhibitors $p21^{CIP1}$ and $p27^{KIP1}$ protein molecules. Degradation of these molecules has been shown to increase the activity of CDK2 and cyclin E-CDK2 complex and promote tumor formation.[97-99]

Cyclin A2/B-CDK1 catalytic activity is required for entry into the mitotic phase. CDK1 is rarely deregulated in cancer. But there is some evidence that CDK1 activity is required for tumorigenesis. For example, CDK1 inhibition induced apoptosis in Myc has driven mouse lymphomas, liver tumors,[100] and human triple-negative breast cancer cells.[101] In a KRas mutant colorectal cancer xenograft model, CDK inhibition blocked the tumor growth.[102] Despite of these evidence the inhibition of CDK1 is a tricky target as normal cells also require CDK1 for regular cell cycle progression.[5 103]

4. APOPTOTIC SIGNALING PATHWAYS

Apoptosis, programmed cell death, is used to regulate tissue development and homeostasis.[104] In healthy cells, this critical process is regulated by internal and external signals. The intrinsic pathway can be triggered by a myriad of events including severe DNA damage, anoxia, or other internal signaling imbalances. The extrinsic pathway is primarily triggered by death receptor ligands.

4.1. INTRINSIC PATHWAY

p53 is the primary regulator for triggering apoptosis in response to internal stress. p53 is always present in the cell at extremely low levels.[105] This is maintained by MDM2 which ubiquitinates p53 for degradation.[105] Stresses including but not limited to DNA damage, oncogene activation, anoxia, radiation, heat shock, oxidative stress, osmotic stress, and nutrient deprivation can increase the expression of p53 through various mechanisms.

For example, while small levels of DNA damage will trigger DNA repair pathways, extreme DNA damage will trigger apoptosis. The Mre11-Rad50-Nbs1(MRN) complex binds to double-stranded breaks in DNA.[106] MRN then recruits and activates ataxia telangiectasia protein (ATM). Similarly, ATR interacting protein (ATRIP) binds to single-stranded DNA exposed due to damage and recruits ATM-related protein (ATR).[106] ATM and ATR phosphorylate and activate p53.[107] Additionally, the ARF protein battles with MDM2 to regulate p53 levels in the cell. However, the insertion of an additional exon between the CDKIs INK4A and INK4B leads to the translation of an alternate reading frame (ARF).[108] The resulting protein, ARF, binds to MDM2 and prevents it from ubiquitinating p53.[108] Oxygen levels also influence p53 levels in the cell. Though not fully understood, the mechanism by which hypoxic conditions stabilize p53 in the cell involved hypoxia-inducible factor 1 alpha (HIF-1a) and von Hippel-Lindau tumor suppressor (VHL).[109] Under normal conditions, VHL interacts with and degrades HIF-1a. Under hypoxic or anoxic conditions, this interaction is disrupted. This allows HIF-1a to bind to p53, preventing ubiquitination by MDM2.[109]

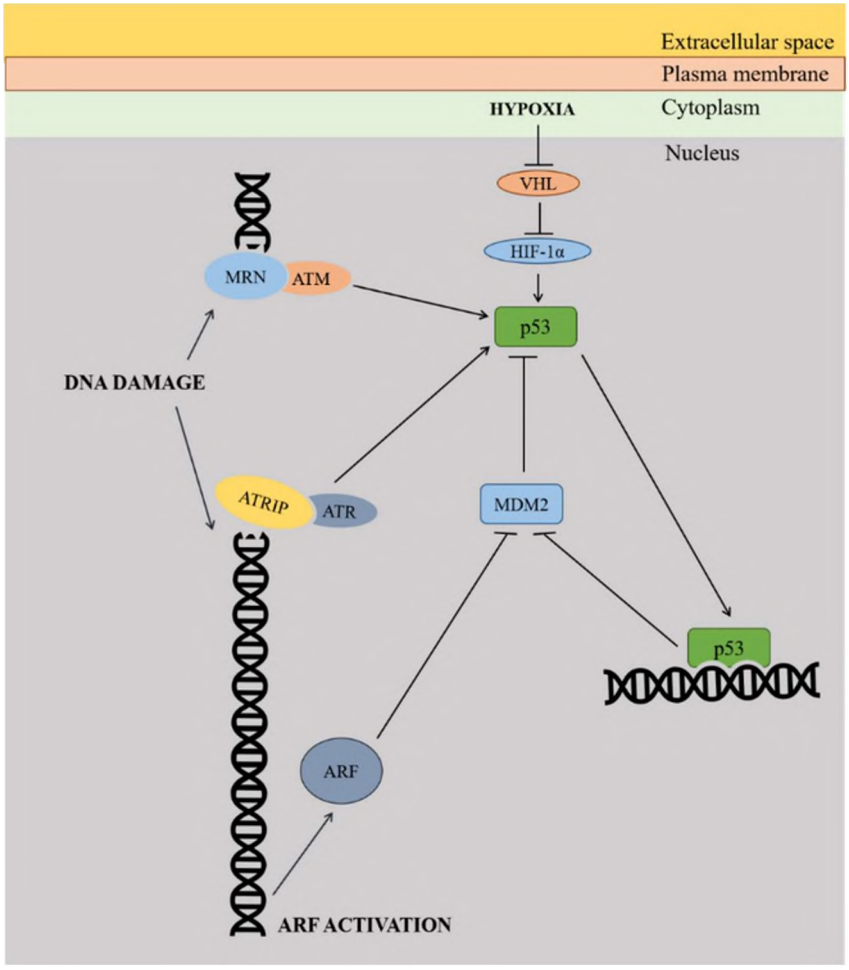

Figure 10. Examples of p53 activation via DNA damage, hypoxia, and ARF activation mechanisms,(1) MRN and ATRIP interact with exposed double-stranded and single-stranded DNA, respectively. Upon binding, MRN activates ATM and ATRIP activates ATR. ATM and ATR phosphorylate and activate p53. (2) Hypoxia disrupts the interaction between VHL and HIF-1α to prevent VHL from inhibiting HIF-1α. HIF-1α then phosphorylates and activates p53. (3) ARF interacts with MDM2 to prevent the ubiquitination and degradation of p53

Additionally, p53 is also capable of inhibiting MDM2, driving a positive feedback loop further stabilizing it in the cell. Through these and other pathways, p53 escapes degradation by MDM2 and triggers apoptosis (Figure 10). In this capacity, p53 primarily acts in the nucleus as a transcription factor for many apoptotic proteins (Figure 11).[109]

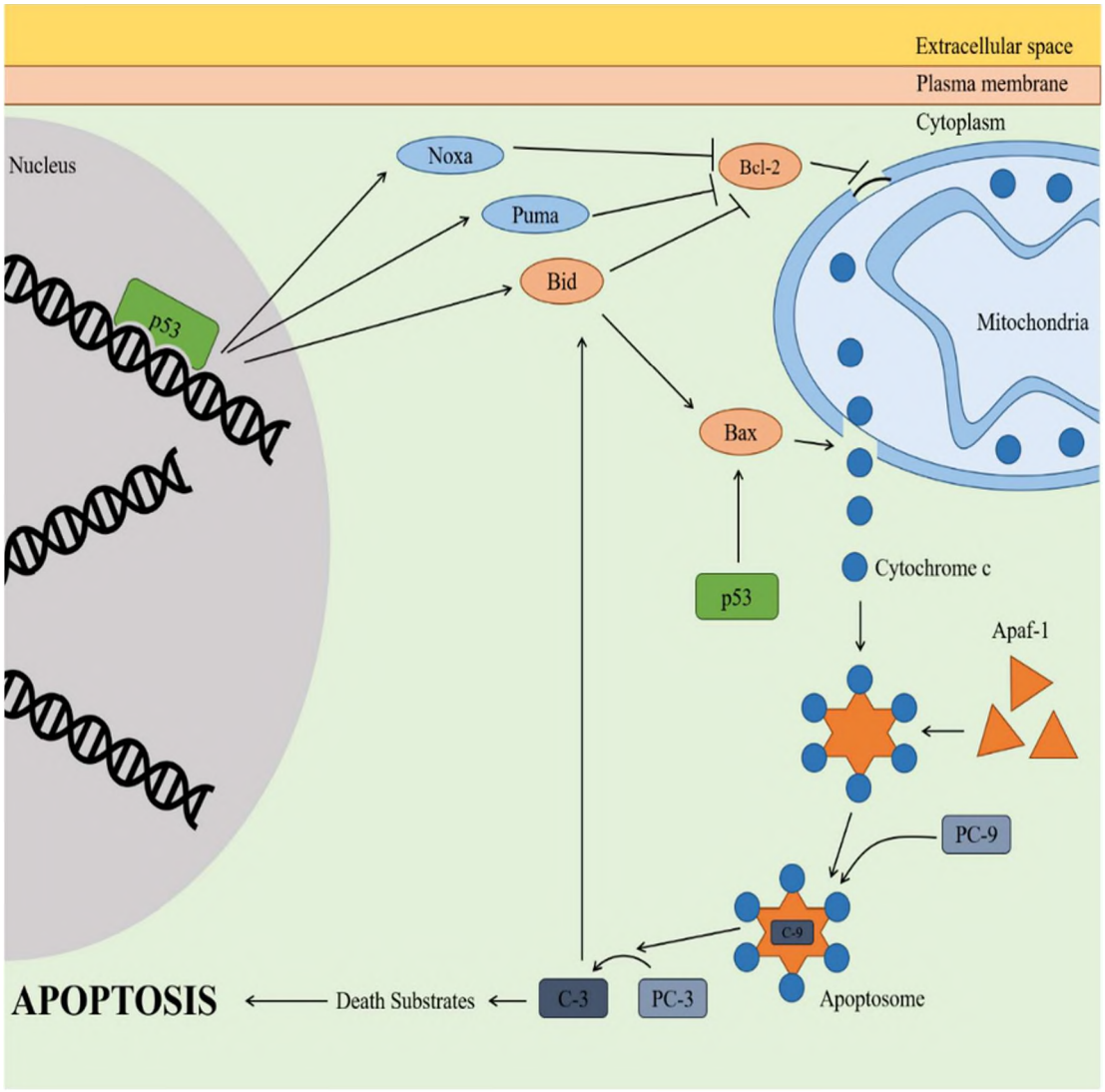

Figure 11. The Intrinsic apoptotic pathway. Upon activation, p53 acts as a transcription factor for several pro-apoptotic genes including those transcribing Noxa, Puma, and Bid. These proteins inhibit Bcl-2 from maintaining the mitochondrial membrane. Bid also acts with cytoplasmic p53 to activate Bax and related proteins to poke holes in the mitochondrial membrane. This releases cytochrome c to the cytoplasm where it interacts with Apaf-1 and caspase 9 to form the apoptosome. The apoptosome cleaves and activates caspase 3 to further stimulate bid and act on several death substrates to carry out apoptotic events

This begins with several members of the Bcl-2 family. Bcl-2 and related anti-apoptotic proteins keep the membrane of the mitochondria closed.[110] P53 acts as a

transcription factor for Puma and Noxa.[109] These two BH3 only proteins inhibit Bcl-2. Other transcriptional targets include Bax, Bid, and Bim. Bid acts like Puma and Noxa to inhibit Bcl-2 and other anti-apoptotic family members.[110] Bid and Bim also directly bind to and activate Bak and Bax which poke holes in the mitochondrial membrane.[110] p53 is capable of transporting to the cytoplasm to directly activate Bax, Puma, and Noxa.[73,111,112] As the mitochondrial membrane opens, cytochrome c is released.[110]

Cytochrome c is a member of the electron transport chain (ETC) and is normally involved in ATP production; however, when it is present in the cytosol it associates with Apaf-1. Together, they form the apoptosome, also known as the "wheel of death," which activates caspase 9. This is the first caspase activated in a caspase cascade. Caspases comprise a family of cysteine proteins which initiate apoptosis by activating downstream caspases or by directly carrying out apoptotic functions.[113]

Caspase 9, an initiator caspase, cleaves pro-caspase 3 to activate caspase 3, an execution phase caspase.[113] Caspase 3 activates downstream caspases by cleaving their respective pro-caspases, eventually triggering caspases which carry out functions to induce an apoptotic phenotype such as destruction of intracellular structures and organelles.[9,10,113]

4.2. MOLECULAR TARGETS OF THE DEFECTIVE INTRINSIC PATHWAY

Oxaliplatin (diaminocyclohexane) and other platinum-containing drugs also damage nuclear DNA.[114] Oxaliplatin binds to DNA to block replication and transcription, form lesions, and cause single-stranded breaks. These particular lesions are poorly recognized by DNA repair proteins in the cell so damage accumulates. An accumulation

of damaged DNA in the cell causes stress signals within the cell which activate the intrinsic apoptotic pathway.[114]

Oxaliplatin (brand name Eloxatin) has been approved by the FDA to treat colorectal and stage three colon cancer. Like most current small molecule cancer therapies, Oxaliplatin alone is not specific to cancer cells and has many undesirable side effects.[114,115] Shad *et. al.* investigated a strategy to encapsulate Oxaliplatin in folate conjugated hyaluronic acid-coated alginate nanogels.[115] In this system, folate is used for specific targeting to folate receptors which are overexpressed in many types of colorectal cancers and hyaluronic acid and alginate are natural, biocompatible polymers.[115] In this study, HT29 colorectal cancer cells were treated with encapsulated Oxaliplatin. Cells treated with encapsulated Oxaliplatin showed a higher ratio of apoptosis to necrosis, higher gene expression of Bax, and lower expression of Bcl-2 compared to untreated cells or cells treated with unencapsulated Oxaliplatin.[115] This suggests that novel drug delivery systems may improve treatment with Oxaliplatin and other platinum-based chemotherapeutics; however, further testing in animal models and clinical trials is required to determine if the encapsulation strategy employed here will improve efficacy and specificity and decrease negative side effects.

The function of p53 is lost in more than half of all human cancer cases.[71] Since cancer is typically the result of an accumulation of genetic mutations that occur over the years or decades, loss of the enzyme responsible for suicide in cells with damaged DNA greatly enables this process. A majority of p53 mutations occur in its reading frame and cause conformational changes.[71] Many mutations disable the catalytic site of p53 but allow it to still bind other p53 proteins and form the homotetramer required for its

activity. In this way, mutant p53 is an inhibitor to wild type p53 since the homotetramer requires four wild-type p53 proteins in order to function.[105] The use of small molecules and peptides to activate a p53-dependent process in cells with mutant forms of p53 are being investigated for clinical use.[116,117] However, p53 reactivation has proved difficult clinically.

While the loss of function of p53 is the most common mutation across human cancers, it is also common that p53 is still functional but its regulators such as MDM2 are overexpressed.[9,116-118] Nutlins, small molecule inhibitors that bind to MDM2, are currently being investigated as potential chemotherapeutics.[118] The first MDM2 inhibitor to undergo clinical trials was RG7112 which demonstrated high selectivity and efficacy in preclinical studies.[118] However, Clinical trials revealed that the necessary dose to activated p53 had severe side effects including death.[118] Now, second-generation MDM2 inhibitors such as Idasanutlin, which are thought to have more desirable toxicity profiles, are undergoing clinical trials.[118] These trials primarily investigate the use of MDM2 inhibitors in combination therapies or alongside radiation therapy.

4.3. EXTRINSIC PATHWAY

Apoptosis can also be triggered externally via the extrinsic or receptor-activated apoptotic pathway (Figure 12). The cell membrane contains several transmembrane proteins including death receptors which share a common "death domain". Members of the tumor necrosis factor (TNF) family known as "death receptor ligands" can bind to this domain.

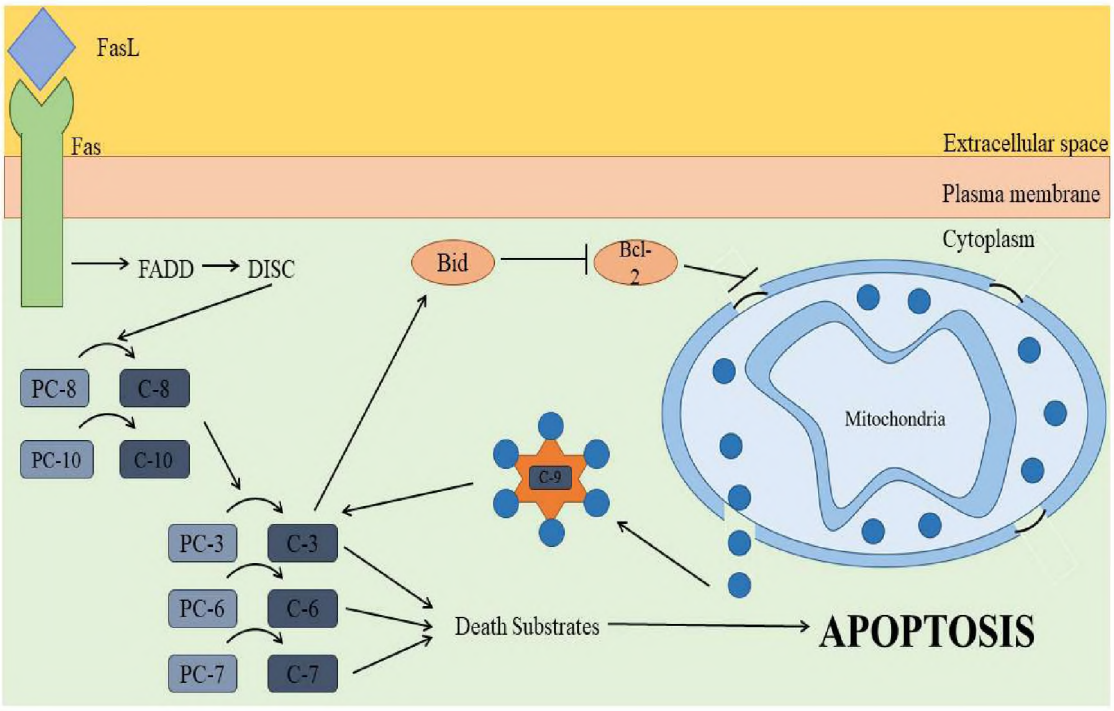

Figure 12. The extrinsic apoptotic pathway. Death receptor ligands such as FasL bind death receptors at the cell surface. Fas activates FADD, which in turn activates DISC. Disc cleaves and activates initiator caspases 8 and 10 which act on executioner caspases 3, 6, and 7. These caspases act on death substrates to achieve an apoptotic phenotype. Additionally, caspase 3 can activate Bid to activate the internal pathway

The most common death receptor ligand is the Fas ligand (FasL) which binds to the death receptor Fas (Apo-1 or CD95).[119] Ligand binding induces activation of the Fas-associated death domain (FADD) protein within the cytosol.[119] FADD triggers the death-inducing signaling complex (DISC) which in turn cleaves and triggers initiator caspases 8 and 10. At this point, the extrinsic pathway converges on the intrinsic pathway by activating the execution phase caspases 3, 6, and 7. Caspase 3 is also capable of cleaving and activating Bid to act on Bcl-2, amplifying pro-apoptotic signals and recruiting additional members of the intrinsic pathway.

4.4. MOLECULAR TARGETS OF THE DEFECTIVE EXTRINSIC PATHWAY

Several existing and potential cancer treatments attempt to kill cancer cells by taking advantage of apoptotic machinery in the cells. For example, all *trans* retinoic acid (ATRA) is a naturally occurring derivative of vitamin A that can be used to target apoptotic pathways in cancerous cells.[120] ATRA binds to the retinoic acid transmembrane receptors retinoic acid receptor (RAR) and retinoid x receptor (RXR), causing them to form a heterodimer.[121] This binding activates apoptosis through the external apoptotic pathway.[121] NB4 cells treated with ATRA showed decreased viability due to the activation of the apoptotic pathway.[113] ATRA has been shown to treat acute promyelocytic leukemia (APL).[122] Ades et al analyzed data from elderly patients at European centers who were treated for APL with ATRA in combination with chemotherapy[122]. Combination of ATRA with other chemotherapeutics improved the survival of elderly patients compared to traditional chemotherapy.[122]

ATRA is now also being investigated to treat other types of cancer. ATRA has a low solubility in water which makes delivery a challenge.[121] Ravichandran et al. encapsulated ATRA in liposome carriers to improve distribution.[9] The lipo-ATRA system reduced tumors in mice.[121] Another possible therapeutic agent is oxymatrine. Oxymatrine is derived from marine, an active in the Chinese herb *Sophora flavecens*.[123] Several laboratory studies have shown that oxymatrine inhibits cellular proliferation by inducing apoptosis.[123-125] Although the exact mechanism is not fully understood, Oxymatrine was shown to increase caspases associated with apoptosis in T24 cells (human bladder cancer) [123] and in A549 cells (human lung cancer).[125] It has also been shown to increase expression of p53 and Bax, and decrease expression of Bcl-2 in

DU145 cells (human prostate cancer), PC3 cells (human prostate cancer), and PNT1B cells (human prostate).[124] These effects on p53, Bax, and Bcl-2 were also seen in mice xenograft models.[124] Additionally, tumor weight stopped increasing in these mice, though the tumors did not shrink.[124]

5. DISCUSSION

Healthy cells depend on internal and external signals to decide whether to live or die, proliferate, or become quiescent entering the G0 phase. These signals are interpreted through signaling pathways within the cell to stimulate the production of proteins to carry out these actions. The cells get a license for the division at the late G1 phase or R point, and the later phases follow more or less the same mechanisms as normal cells unless there are major genetic and molecular alterations in cell cycle-associated genes or therapeutic intervention. So, the G0/G1 transition and early G1 phase are of much interest in cancer research. There is growing evidence that the R point deregulation is the determinant of abnormal cell growth and accompanies the tumorigenesis process in almost all the cancer types.[126-129]

For cell cycle targeted therapy, CDK4/6-Rb is one of the most critical pathways to target as it provides the cells license to enter the R point. In addition to the active targeting of molecules involved in the G1-S transition of the CDK4/6-Rb pathway, the cell cycle targeted therapy has already been shifted towards the inhibition of key players of the S and G2 checkpoints. Several chemo and radiotherapy target the alterations of the DNA as a mechanism of action against cancer progression. Cancer cells can manipulate

the cell cycle checkpoints to halt the progression allowing them time for DNA repair in response to the damage caused. The rationale for targeting the checkpoints is that inhibition of these regulatory proteins in cancer cells prevents cell cycle arrest in S and G2 phase allowing the cells to enter the mitosis phase with a defective genetic component and become susceptible to apoptosis or permanent arrest during mitosis, a mechanism known as a mitotic catastrophe.[130,131] Such indirect therapeutic strategy includes inhibition of ATM and ATR (inhibition of DNA damage response),[106,132-135] Aurora A and B kinases (inhibition of spindle machinery during mitosis),[136-141] PLK1 (inhibition of chromosome segregation, the permission of mitotic entry upon DNA damage),[142-145] BRCA1/2 (inhibition of homologous recombination), [146,147] MPS1,[148-151] CHK1 (induction of aberrant replication, chromosome fragmentation, mitotic death),[152-155] and WEE1 (induction of premature mitosis) molecules.[156-160] One of the major concerns in targeting the cell cycle targeted therapy is selectivity. To address the challenge, the cell cycle targeted therapeutic regimen can benefit to a great extent by incorporating the personalized treatment approach. The genomic signature tools can identify the subsets of patients who will get a maximum therapeutic response to the intervened cell cycle targeted treatment.

The role of major molecular circuitries responsible for cell proliferation, cell cycle, and apoptosis are interlinked and also share common molecular machinery.[2,161,162] There are evidence that apoptosis can be triggered by the genes that are involved in cell cycle progression. For example, Myc regulates several genes that control both cell cycle progression and apoptosis and metabolism in tumorigenesis.[163-171] Similarly, p53 is involved in molecular signaling circuitries for cell cycle arrest and cell death,[172,173] DNA

damage response,[174-176] and increasing evidence as a regulator of cell homeostasis and metabolism in cancer cells.[177] Cancer cells manipulate such interlinked cell signaling pathways for the acquisition of major hallmarks in cancer such as self-sufficiency in growth signals and suppressing or insensitivity to the death signals and tissue invasion and metastasis.[10,178] Thus, a comprehensive understanding of the linkage between the cell proliferation and apoptosis pathways will unveil the underlying causes of imbalanced tissue homeostasis and is critical to discover new therapeutic strategies to defeat cancer. Such elucidations help to behold cancer in a more logical way.

6. CONCLUSION

In this review, intracellular signaling pathways such as MAPK/Ras/Raf/ERK, PI3K/Akt, Jak-STAT, and Wnt regulating the cell proliferation and apoptosis are discussed. Growth factors activate the MAPK/Ras/Raf/ERK, PI3K, and Wnt pathways to synthesize cyclin Ds and other mitosis regulating proteins (Myc and Jun). Cyclin D1 binds to CDK4/6, forms CDK complexes, activates several substrates, and initiates the cell cycle. In contrast, TGFβ prevents the cells from initiating the cell cycle by expressing CDKIs and p53. p53 stops the cell cycle when DNA is not replicated correctly during the S phase, producing p21 proteins and promoting the transcription of apoptotic proteins. Alterations in the signaling pathways lead to diseases including cancer, cardiovascular diseases, immunological disorders, neurodegenerative diseases, and many other infectious diseases. As cancer therapy is becoming more and more personalized through precision medicine, understanding the intercorrelated cell signaling pathways and

identification of key regulatory molecules are so important to prescribe the effective individual molecular therapies.

REFERENCES

(1) Evan, G. I.; Vousden, K. H. Proliferation, cell cycle and apoptosis in cancer. Nature 2001, 411, 342-348.

(2) King, K. L.; Cidlowski, J. A. Cell cycle and apoptosis: common pathways to life and death. Journal of cellular biochemistry 1995, 58, 175-180.

(3) Vermeulen, K.; Berneman, Z. N.; Van Bockstaele, D. R. Cell cycle and apoptosis. Cell proliferation 2003, 36, 165-175.

(4) Pucci, B.; Kasten, M.; Giordano, A. Cell cycle and apoptosis. Neoplasia 2000, 2, 291-299.

(5) Otto, T.; Sicinski, P. Cell cycle proteins as promising targets in cancer therapy. Nature Reviews Cancer 2017, 17, 93-115.

(6) Xia, P.; Liu, Y.; Chen, J.; Cheng, Z. Cell Cycle Proteins as Key Regulators of Postmitotic Cell Death. Yale J Biol Med [Online early access]2019.

(7) Johnson, D. G.; Schneider-Broussard, R. Role of E2F in cell cycle control and cancer. Frontiers in bioscience : a journal and virtual library 1998, 3, d447-448.

(8) Duronio, R. J.; Xiong, Y. Signaling pathways that control cell proliferation. Cold Spring Harbor perspectives in biology 2013, 5, a008904.

(9) Weinberg, R. A.; Weinberg, R. A.: The biology of cancer; Garland science, 2013.

(10) Hanahan, D.; Weinberg, R. A. The hallmarks of cancer. cell 2000, 100, 57-70.

(11) Santarpia, L.; Lippman, S. M.; El-Naggar, A. K. Targeting the MAPK–RAS–RAF signaling pathway in cancer therapy. Expert opinion on therapeutic targets 2012, 16, 103-119.

(12) Margolis, B.; Skolnik, E. Y. Activation of Ras by receptor tyrosine kinases. Journal of the American Society of Nephrology 1994, 5, 1288-1299.

(13) Rhind, N.; Russell, P. Signaling pathways that regulate cell division. Cold Spring Harbor perspectives in biology 2012, 4, a005942.

(14) Zhang, W.; Liu, H. T. MAPK signal pathways in the regulation of cell proliferation in mammalian cells. Cell research 2002, 12, 9-18.

(15) Lee, S.; Rauch, J.; Kolch, W. Targeting MAPK signaling in cancer: Mechanisms of drug resistance and sensitivity. International journal of molecular sciences 2020, 21, 1102.

(16) Rojas, P.; Cadenas, M.; Lin, P.; Benavides, F.; Conti, C.; Rodriguez-Puebla, M. Cyclin D2 and cyclin D3 play opposite roles in mouse skin carcinogenesis. Oncogene 2007, 26, 1723-1730.

(17) Huang, Y.; Qu, S.; Zhu, G.; Wang, F.; Liu, R.; Shen, X.; Viola, D.; Elisei, R.; Puxeddu, E.; Fugazzola, L. BRAF V600E mutation-assisted risk stratification of solitary intrathyroidal papillary thyroid cancer for precision treatment. JNCI: Journal of the National Cancer Institute 2018, 110, 362-370.

(18) Kebebew, E.; Weng, J.; Bauer, J.; Ranvier, G.; Clark, O. H.; Duh, Q.-Y.; Shibru, D.; Bastian, B.; Griffin, A. The prevalence and prognostic value of BRAF mutation in thyroid cancer. Annals of surgery 2007, 246, 466.

(19) Xing, M. BRAF mutation in thyroid cancer. Endocrine-related cancer 2005, 12, 245-262.

(20) Gao, X. H.; Yu, G. Y.; Gong, H. F.; Liu, L. J.; Xu, Y.; Hao, L. Q.; Liu, P.; Liu, Z. H.; Bai, C. G.; Zhang, W. Differences of protein expression profiles, KRAS and BRAF mutation, and prognosis in right-sided colon, left-sided colon and rectal cancer. Scientific Reports 2017, 7, 1-12.

(21) Ogino, S.; Shima, K.; Meyerhardt, J. A.; McCleary, N. J.; Ng, K.; Hollis, D.; Saltz, L. B.; Mayer, R. J.; Schaefer, P.; Whittom, R. Predictive and prognostic roles of BRAF mutation in stage III colon cancer: results from intergroup trial CALGB 89803. Clinical Cancer Research 2012, 18, 890-900.

(22) Luke, J. J.; Ott, P. A.; Shapiro, G. I. The biology and clinical development of MEK inhibitors for cancer. Drugs 2014, 74, 2111-2128.

(23) Larkin, J.; Ascierto, P. A.; Dréno, B.; Atkinson, V.; Liszkay, G.; Maio, M.; Mandalà, M.; Demidov, L.; Stroyakovskiy, D.; Thomas, L. Combined vemurafenib and cobimetinib in BRAF-mutated melanoma. New England Journal of Medicine 2014, 371, 1867-1876.

(24) Hutchinson, K. E.; Lipson, D.; Stephens, P. J.; Otto, G.; Lehmann, B. D.; Lyle, P. L.; Vnencak-Jones, C. L.; Ross, J. S.; Pietenpol, J. A.; Sosman, J. A. BRAF fusions define a distinct molecular subset of melanomas with potential sensitivity to MEK inhibition. Clinical Cancer Research 2013, 19, 6696-6702.

(25) Mahapatra, D. K.; Asati, V.; Bharti, S. K. MEK inhibitors in oncology: A patent review (2015-Present). Expert Opinion on Therapeutic Patents 2017, 27, 887-906.

(26) Wu, P.-K.; Park, J.-I. In Tilte2015; Elsevier.

(27) Kakadia, S.; Yarlagadda, N.; Awad, R.; Kundranda, M.; Niu, J.; Naraev, B.; Mina, L.; Dragovich, T.; Gimbel, M.; Mahmoud, F. Mechanisms of resistance to BRAF and MEK inhibitors and clinical update of US Food and Drug Administration-approved targeted therapy in advanced melanoma. Onco Targets Ther 2018, 11, 7095.

(28) Luebker, S. A.; Koepsell, S. A. Diverse mechanisms of BRAF inhibitor resistance in melanoma identified in clinical and preclinical studies. Frontiers in oncology 2019, 9, 268.

(29) Sanchez, J. N.; Wang, T.; Cohen, M. S. BRAF and MEK inhibitors: use and resistance in BRAF-mutated cancers. Drugs 2018, 78, 549-566.

(30) Heidorn, S. J.; Milagre, C.; Whittaker, S.; Nourry, A.; Niculescu-Duvas, I.; Dhomen, N.; Hussain, J.; Reis-Filho, J. S.; Springer, C. J.; Pritchard, C. Kinase-dead BRAF and oncogenic RAS cooperate to drive tumor progression through CRAF. Cell 2010, 140, 209-221.

(31) Matallanas, D.; Birtwistle, M.; Romano, D.; Zebisch, A.; Rauch, J.; von Kriegsheim, A.; Kolch, W. Raf family kinases: old dogs have learned new tricks. Genes & cancer 2011, 2, 232-260.

(32) Gao, D.; Nong, S.; Huang, X.; Lu, Y.; Zhao, H.; Lin, Y.; Man, Y.; Wang, S.; Yang, J.; Li, J. The effects of palmitate on hepatic insulin resistance are mediated by NADPH Oxidase 3-derived reactive oxygen species through JNK and p38MAPK pathways. Journal of Biological Chemistry 2010, 285, 29965-29973.

(33) Kim, E. K.; Choi, E.-J. Compromised MAPK signaling in human diseases: an update. Archives of toxicology 2015, 89, 867-882.

(34) Sui, X.; Kong, N.; Ye, L.; Han, W.; Zhou, J.; Zhang, Q.; He, C.; Pan, H. p38 and JNK MAPK pathways control the balance of apoptosis and autophagy in response to chemotherapeutic agents. Cancer letters 2014, 344, 174-179.

(35) Xavier, C. P.; Lima, C. F.; Pedro, D. F.; Wilson, J. M.; Kristiansen, K.; Pereira-Wilson, C. Ursolic acid induces cell death and modulates autophagy through JNK pathway in apoptosis-resistant colorectal cancer cells. The Journal of nutritional biochemistry 2013, 24, 706-712.

(36) Chang, F.; Lee, J.; Navolanic, P.; Steelman, L.; Shelton, J.; Blalock, W.; Franklin, R.; McCubrey, J. Involvement of PI3K/Akt pathway in cell cycle progression, apoptosis, and neoplastic transformation: a target for cancer chemotherapy. Leukemia 2003, 17, 590-603.

(37) Huelsken, J.; Behrens, J. The Wnt signalling pathway. Journal of cell science 2002, 115, 3977-3978.

(38) Wipf, P.; Halter, R. J. Chemistry and biology of wortmannin. Organic & biomolecular chemistry 2005, 3, 2053-2061.

(39) Rawlings, J. S.; Rosler, K. M.; Harrison, D. A. The JAK/STAT signaling pathway. Journal of cell science 2004, 117, 1281-1283.

(40) Banerjee, K.; Resat, H. Constitutive activation of STAT 3 in breast cancer cells: A review. International journal of cancer 2016, 138, 2570-2578.

(41) Furqan, M.; Akinleye, A.; Mukhi, N.; Mittal, V.; Chen, Y.; Liu, D. STAT inhibitors for cancer therapy. J Hematol Oncol 2013, 6, 90-90.

(42) Thomas, SJ; Snowden, JA; Zeidler, MP; Danson, SJ. The role of JAK/STAT signalling in the pathogenesis, prognosis and treatment of solid tumours. British journal of cancer 2015, 113(3),365-371.

(43) Furumoto, Y.; Gadina, M. The arrival of JAK inhibitors: advancing the treatment of immune and hematologic disorders. BioDrugs 2013, 27, 431-438.

(44) Lustig, B.; Behrens, J. The Wnt signaling pathway and its role in tumor development. Journal of cancer research and clinical oncology 2003, 129, 199-221.

(45) Yaeger, R.; Chatila, W. K.; Lipsyc, M. D.; Hechtman, J. F.; Cercek, A.; Sanchez-Vega, F.; Jayakumaran, G.; Middha, S.; Zehir, A.; Donoghue, M. T. Clinical sequencing defines the genomic landscape of metastatic colorectal cancer. Cancer cell 2018, 33, 125-136. e123.

(46) Borowsky, J.; Dumenil, T.; Bettington, M.; Pearson, S.-A.; Bond, C.; Fennell, L.; Liu, C.; McKeone, D.; Rosty, C.; Brown, I.; Walker, N.; Leggett, B.; Whitehall, V. The role of APC in WNT pathway activation in serrated neoplasia. Modern Pathology 2018, 31, 495-504.

(47) Parker, T. W.; Neufeld, K. L. APC controls Wnt-induced β-catenin destruction complex recruitment in human colonocytes. Scientific Reports 2020, 10, 2957.

(48) Schneikert, J.; Behrens, J. The canonical Wnt signalling pathway and its APC partner in colon cancer development. Gut 2007, 56, 417-425.

(49) Dow, L. E.; O'Rourke, K. P.; Simon, J.; Tschaharganeh, D. F.; van Es, J. H.; Clevers, H.; Lowe, S. W. Apc restoration promotes cellular differentiation and reestablishes crypt homeostasis in colorectal cancer. Cell 2015, 161, 1539-1552.

(50) Luongo, C.; Moser, A. R.; Gledhill, S.; Dove, W. F. Loss of Apc+ in intestinal adenomas from Min mice. Cancer research 1994, 54, 5947-5952.

(51) Jiang, X.; Cao, Y.; Li, F.; Su, Y.; Li, Y.; Peng, Y.; Cheng, Y.; Zhang, C.; Wang, W.; Ning, G. Targeting β-catenin signaling for therapeutic intervention in MEN1-deficient pancreatic neuroendocrine tumours. Nature communications 2014, 5, 5809.

(52) Guezguez, B.; Almakadi, M.; Benoit, Y. D.; Shapovalova, Z.; Rahmig, S.; Fiebig-Comyn, A.; Casado, F. L.; Tanasijevic, B.; Bresolin, S.; Masetti, R. GSK3 deficiencies in hematopoietic stem cells initiate pre-neoplastic state that is predictive of clinical outcomes of human acute leukemia. Cancer cell 2016, 29, 61-74.

(53) Jiang, X.; Hao, H.-X.; Growney, J. D.; Woolfenden, S.; Bottiglio, C.; Ng, N.; Lu, B.; Hsieh, M. H.; Bagdasarian, L.; Meyer, R. Inactivating mutations of RNF43 confer Wnt dependency in pancreatic ductal adenocarcinoma. Proceedings of the National Academy of Sciences 2013, 110, 12649-12654.

(54) Steinhart, Z.; Pavlovic, Z.; Chandrashekhar, M.; Hart, T.; Wang, X.; Zhang, X.; Robitaille, M.; Brown, K. R.; Jaksani, S.; Overmeer, R. Genome-wide CRISPR screens reveal a Wnt–FZD5 signaling circuit as a druggable vulnerability of RNF43-mutant pancreatic tumors. Nature medicine 2017, 23, 60-68.

(55) Krishnamurthy, N.; Kurzrock, R. Targeting the Wnt/beta-catenin pathway in cancer: Update on effectors and inhibitors. Cancer treatment reviews 2018, 62, 50-60.

(56) Jung, Y.-S.; Park, J.-I. Wnt signaling in cancer: therapeutic targeting of Wnt signaling beyond β-catenin and the destruction complex. Experimental & Molecular Medicine 2020, 1-9.

(57) Galluzzi, L.; Spranger, S.; Fuchs, E.; López-Soto, A. WNT signaling in cancer immunosurveillance. Trends in cell biology 2019, 29, 44-65.

(58) Spranger, S. WNT Signaling in Cancer Immunosurveillance. 2019.

(59) Wang, B.; Tian, T.; Kalland, K.-H.; Ke, X.; Qu, Y. Targeting Wnt/β-catenin signaling for cancer immunotherapy. Trends in pharmacological sciences 2018, 39, 648-658.

(60) Witsch, E.; Sela, M.; Yarden, Y. Roles for growth factors in cancer progression. Physiology 2010.

(61) Akhurst, R. J.; Hata, A. Targeting the TGFβ signalling pathway in disease. Nature reviews Drug discovery 2012, 11, 790-811.

(62) Huynh, L. K.; Hipolito, C. J.; Ten Dijke, P. A Perspective on the Development of TGF-β Inhibitors for Cancer Treatment. Biomolecules 2019, 9.

(63) Massagué, J. TGFbeta in Cancer. Cell 2008, 134, 215-230.

(64) Smith, A. L.; Robin, T. P.; Ford, H. L. Molecular pathways: targeting the TGF-β pathway for cancer therapy. Clinical cancer research : an official journal of the American Association for Cancer Research 2012, 18, 4514-4521.

(65) Casimiro, M. C.; Crosariol, M.; Loro, E.; Li, Z.; Pestell, R. G. Cyclins and cell cycle control in cancer and disease. Genes & cancer 2012, 3, 649-657.

(66) Stengel, K. R.; Thangavel, C.; Solomon, D. A.; Angus, S. P.; Zheng, Y.; Knudsen, E. S. Retinoblastoma/p107/p130 Pocket Proteins PROTEIN DYNAMICS AND INTERACTIONS WITH TARGET GENE PROMOTERS. Journal of Biological Chemistry 2009, 284, 19265-19271.

(67) Peng, C.; Zeng, W.; Su, J.; Kuang, Y.; He, Y.; Zhao, S.; Zhang, J.; Ma, W.; Bode, A. M.; Dong, Z. Cyclin-dependent kinase 2 (CDK2) is a key mediator for EGF-induced cell transformation mediated through the ELK4/c-Fos signaling pathway. Oncogene 2016, 35, 1170-1179.

(68) Brown, N. R.; Korolchuk, S.; Martin, M. P.; Stanley, W. A.; Moukhametzianov, R.; Noble, M. E.; Endicott, J. A. CDK1 structures reveal conserved and unique features of the essential cell cycle CDK. Nature communications 2015, 6, 1-12.

(69) Hannon, G.; Beach, D. pI5INK4B is a potential effector ofTGF-) 3-induced cell cycle. Nature (Lond.), 371.

(70) Nobori, T.; Miura, K.; Wu, D. J.; Lois, A.; Takabayashi, K.; Carson, D. A. Deletions of the cyclin-dependent kinase-4 inhibitor gene in multiple human cancers. Nature 1994, 368, 753-756.

(71) Ozaki, T.; Nakagawara, A. Role of p53 in Cell Death and Human Cancers. Cancers 2011, 3, 994-1013.

(72) Abbas, T.; Dutta, A. p21 in cancer: intricate networks and multiple activities. Nature Reviews Cancer 2009, 9, 400-414.

(73) Yu, J.; Zhang, L. PUMA, a potent killer with or without p53. Oncogene 2008, 27, S71-S83.

(74) Yu, J.; Zhang, L. PUMA, a potent killer with or without p53. Oncogene 2008, 27 Suppl 1, S71-S83.

(75) Pawlowski, J.; Kraft, A. S. Bax-induced apoptotic cell death. Proceedings of the National Academy of Sciences 2000, 97, 529-531.

(76) Biswas, S. C.; Ryu, E.; Park, C.; Malagelada, C.; Greene, L. A. Puma and p53 Play Required Roles in Death Evoked in a Cellular Model of Parkinson Disease. Neurochemical Research 2005, 30, 839-845.

(77) Callus, B. A.; Ekert, P. G.; Heraud, J. E.; Jabbour, A. M.; Kotevski, A.; Vince, J. E.; Silke, J.; Vaux, D. L. Cytoplasmic p53 is not required for PUMA-induced apoptosis. Cell Death & Differentiation 2008, 15, 213-215.

(78) Beroukhim, R.; Mermel, C. H.; Porter, D.; Wei, G.; Raychaudhuri, S.; Donovan, J.; Barretina, J.; Boehm, J. S.; Dobson, J.; Urashima, M. The landscape of somatic copy-number alteration across human cancers. Nature 2010, 463, 899-905.

(79) Wang, T. C.; Cardiff, R. D.; Zukerberg, L.; Lees, E.; Arnold, A.; Schmidt, E. V. Mammary hyperplasia and carcinoma in MMTV-cyclin D1 transgenic mice. Nature 1994, 369, 669-671.

(80) Yamamoto, H.; Ochiya, T.; Takeshita, F.; Toriyama-Baba, H.; Hirai, K.; Sasaki, H.; Sasaki, H.; Sakamoto, H.; Yoshida, T.; Saito, I. Enhanced skin carcinogenesis in cyclin D1-conditional transgenic mice: cyclin D1 alters keratinocyte response to calcium-induced terminal differentiation. Cancer research 2002, 62, 1641-1647.

(81) de Marval, P. L. M.; Macias, E.; Conti, C. J.; Rodriguez-Puebla, M. L. Enhanced malignant tumorigenesis in Cdk4 transgenic mice. Oncogene 2004, 23, 1863-1873.

(82) Corona, S. P.; Ravelli, A.; Cretella, D.; Cappelletti, M. R.; Zanotti, L.; Dester, M.; Gobbi, A.; Petronini, P. G.; Generali, D. CDK4/6 inhibitors in HER2-positive breast cancer. Critical reviews in oncology/hematology 2017, 112, 208-214.

(83) Lundberg, A.; Lindström, L. S.; Li, J.; Harrell, J. C.; Darai-Ramqvist, E.; Sifakis, E. G.; Foukakis, T.; Perou, C. M.; Czene, K.; Bergh, J. The long-term prognostic and predictive capacity of cyclin D1 gene amplification in 2305 breast tumours. Breast Cancer Research 2019, 21, 34.

(84) Yu, Q.; Geng, Y.; Sicinski, P. Specific protection against breast cancers by cyclin D1 ablation. Nature 2001, 411, 1017-1021.

(85) Schmidt, E. E.; Ichimura, K.; Reifenberger, G.; Collins, V. P. CDKN2 (p16/MTS1) gene deletion or CDK4 amplification occurs in the majority of glioblastomas. Cancer research 1994, 54, 6321-6324.

(86) Wölfel, T.; Hauer, M.; Schneider, J.; Serrano, M.; Wolfel, C.; Klehmann-Hieb, E.; Plaen, E.; Hankeln, T. KHM z. Buschenfelde, D. Beach. 1995. A p16ink4a-insensitive CDK4 mutant targeted by cytolytic T lymphocytes in a human melanoma. Science, 269, 1281.

(87) Finn, R. S.; Dering, J.; Conklin, D.; Kalous, O.; Cohen, D. J.; Desai, A. J.; Ginther, C.; Atefi, M.; Chen, I.; Fowst, C. PD 0332991, a selective cyclin D kinase 4/6 inhibitor, preferentially inhibits proliferation of luminal estrogen receptor-positive human breast cancer cell lines in vitro. Breast Cancer Research 2009, 11, R77.

(88) Landis, M. W.; Pawlyk, B. S.; Li, T.; Sicinski, P.; Hinds, P. W. Cyclin D1-dependent kinase activity in murine development and mammary tumorigenesis. Cancer cell 2006, 9, 13-22.

(89) Puyol, M.; Martín, A.; Dubus, P.; Mulero, F.; Pizcueta, P.; Khan, G.; Guerra, C.; Santamaría, D.; Barbacid, M. A synthetic lethal interaction between K-Ras oncogenes and Cdk4 unveils a therapeutic strategy for non-small cell lung carcinoma. Cancer cell 2010, 18, 63-73.

(90) Chen, X.; Xu, D.; Li, X.; Zhang, J.; Xu, W.; Hou, J.; Zhang, W.; Tang, J. Latest Overview of the Cyclin-Dependent Kinases 4/6 Inhibitors in Breast Cancer: The Past, the Present and the Future. J Cancer 2019, 10, 6608-6617.

(91) Sobhani, N.; D'Angelo, A.; Pittacolo, M.; Roviello, G.; Miccoli, A.; Corona, S. P.; Bernocchi, O.; Generali, D.; Otto, T. Updates on the CDK4/6 Inhibitory Strategy and Combinations in Breast Cancer. Cells 2019, 8, 321.

(92) Goutsouliak, K.; Veeraraghavan, J.; Sethunath, V.; De Angelis, C.; Osborne, C. K.; Rimawi, M. F.; Schiff, R. Towards personalized treatment for early stage HER2-positive breast cancer. Nature Reviews Clinical Oncology 2020, 17, 233-250.

(93) Du, Q.; Guo, X.; Wang, M.; Li, Y.; Sun, X.; Li, Q. The application and prospect of CDK4/6 inhibitors in malignant solid tumors. J Hematol Oncol 2020, 13, 41.

(94) Etemadmoghadam, D.; Weir, B. A.; Au-Yeung, G.; Alsop, K.; Mitchell, G.; George, J.; Davis, S.; D'Andrea, A. D.; Simpson, K.; Hahn, W. C. Synthetic lethality between CCNE1 amplification and loss of BRCA1. Proceedings of the National Academy of Sciences 2013, 110, 19489-19494.

(95) Scaltriti, M.; Eichhorn, P. J.; Cortés, J.; Prudkin, L.; Aura, C.; Jiménez, J.; Chandarlapaty, S.; Serra, V.; Prat, A.; Ibrahim, Y. H. Cyclin E amplification/overexpression is a mechanism of trastuzumab resistance in HER2+ breast cancer patients. Proceedings of the National Academy of Sciences 2011, 108, 3761-3766.

(96) Keyomarsi, K.; Tucker, S. L.; Buchholz, T. A.; Callister, M.; Ding, Y.; Hortobagyi, G. N.; Bedrosian, I.; Knickerbocker, C.; Toyofuku, W.; Lowe, M. J. N. E. J. o. M. Cyclin E and survival in patients with breast cancer. 2002, 347, 1566-1575.

(97) Fero, M. L.; Randel, E.; Gurley, K. E.; Roberts, J. M.; Kemp, C. J. The murine gene p27 Kip1 is haplo-insufficient for tumour suppression. Nature 1998, 396, 177-180.

(98) Gstaiger, M.; Jordan, R.; Lim, M.; Catzavelos, C.; Mestan, J.; Slingerland, J.; Krek, W. Skp2 is oncogenic and overexpressed in human cancers. Proceedings of the National Academy of Sciences 2001, 98, 5043-5048.

(99) Martín-Caballero, J.; Flores, J. M.; García-Palencia, P.; Serrano, M. Tumor susceptibility of p21Waf1/Cip1-deficient mice. Cancer research 2001, 61, 6234-6238.

(100) Goga, A.; Yang, D.; Tward, A. D.; Morgan, D. O.; Bishop, J. M. Inhibition of CDK1 as a potential therapy for tumors over-expressing MYC. Nature medicine 2007, 13, 820-827.

(101) Horiuchi, D.; Kusdra, L.; Huskey, N. E.; Chandriani, S.; Lenburg, M. E.; Gonzalez-Angulo, A. M.; Creasman, K. J.; Bazarov, A. V.; Smyth, J. W.; Davis, S. E. MYC pathway activation in triple-negative breast cancer is synthetic lethal with CDK inhibition. Journal of Experimental Medicine 2012, 209, 679-696.

(102) Costa-Cabral, S.; Brough, R.; Konde, A.; Aarts, M.; Campbell, J.; Marinari, E.; Riffell, J.; Bardelli, A.; Torrance, C.; Lord, C. J. CDK1 is a synthetic lethal target for KRAS mutant tumours. PloS one 2016, 11, e0149099.

(103) Santamaría, D.; Barrière, C.; Cerqueira, A.; Hunt, S.; Tardy, C.; Newton, K.; Cáceres, J. F.; Dubus, P.; Malumbres, M.; Barbacid, M. Cdk1 is sufficient to drive the mammalian cell cycle. Nature 2007, 448, 811-815.

(104) Meynier, S.; Rieux-Laucat, F. FAS and RAS related Apoptosis defects: From autoimmunity to leukemia. Immunological reviews 2019, 287, 50-61.

(105) Aubrey, B. J.; Kelly, G. L.; Janic, A.; Herold, M. J.; Strasser, A. How does p53 induce apoptosis and how does this relate to p53-mediated tumour suppression? Cell Death & Differentiation 2018, 25, 104-113.

(106) Maréchal, A.; Zou, L. DNA damage sensing by the ATM and ATR kinases. Cold Spring Harbor perspectives in biology 2013, 5, a012716.

(107) Ljungman, M. Dial 9-1-1 for p53: mechanisms of p53 activation by cellular stress. Neoplasia 2000, 2, 208-225.

(108) Sherr, C. J. Divorcing ARF and p53: an unsettled case. Nature Reviews Cancer 2006, 6, 663-673.

(109) Horn, H.; Vousden, K. Coping with stress: multiple ways to activate p53. Oncogene 2007, 26, 1306-1316.

(110) Zhang, L.; Li, J.; Xu, W. A review of the role of Puma, Noxa and Bim in the tumorigenesis, therapy and drug resistance of chronic lymphocytic leukemia. Cancer gene therapy 2013, 20, 1-7.

(111) Hemann, M.; Lowe, S. The p53-BCL-2 connection. Cell death and differentiation 2006, 13, 1256.

(112) Shamas-Din, A.; Brahmbhatt, H.; Leber, B.; Andrews, D. W. BH3-only proteins: Orchestrators of apoptosis. Biochimica et Biophysica Acta (BBA)-Molecular Cell Research 2011, 1813, 508-520.

(113) Gianni, M.; Ponzanelli, I.; Mologni, L.; Reichert, U.; Rambaldi, A.; Terao, M.; Garattini, E. Retinoid-dependent growth inhibition, differentiation and apoptosis in acute promyelocytic leukemia cells. Expression and activation of caspases. Cell Death & Differentiation 2000, 7, 447-460.

(114) Raymond, E.; Faivre, S.; Chaney, S.; Woynarowski, J.; Cvitkovic, E. Cellular and molecular pharmacology of oxaliplatin. Mol Cancer Ther 2002, 1, 227-235.

(115) Shad, P. M.; Karizi, S. Z.; Javan, R. S.; Mirzaie, A.; Noorbazargan, H.; Akbarzadeh, I.; Rezaie, H. Folate conjugated hyaluronic acid coated alginate nanogels encapsulated oxaliplatin enhance antitumor and apoptosis efficacy on colorectal cancer cells (HT29 cell line). Toxicology in Vitro 2020, 65, 104756.

(116) Sanz, G.; Singh, M.; Peuget, S.; Selivanova, G. Inhibition of p53 inhibitors: progress, challenges and perspectives. Journal of molecular cell biology 2019, 11, 586-599.

(117) Vitali, R.; Cesi, V.; Tanno, B.; Ferrari-Amorotti, G.; Dominici, C.; Calabretta, B.; Raschellà, G. Activation of p53-dependent responses in tumor cells treated with a PARC-interacting peptide. Biochemical and biophysical research communications 2008, 368, 350-356.

(118) Khurana, A.; Shafer, D. A. MDM2 antagonists as a novel treatment option for acute myeloid leukemia: perspectives on the therapeutic potential of idasanutlin (RG7388). Onco Targets Ther 2019, 12, 2903-2910.

(119) Wajant, H. The Fas signaling pathway: more than a paradigm. Science 2002, 296, 1635-1636.

(120) Schmidt-Mende, J.; Gogvadze, V.; Hellström-Lindberg, E.; Zhivotovsky, B. Early mitochondrial alterations in ATRA-induced cell death. Cell Death & Differentiation 2006, 13, 119-128.

(121) Ravichandran, R.; Viswanathan, S.; Berlin Grace, V. M.; Bonati, L.; Narayanan, J. Ameliorating effect of lipo-ATRA treatment on the expression of TIG3 and its suppressing effect on PPARγ gene expression in lung cancer animal model. Mol Cell Biochem 2019, 460, 105-112.

(122) Ades, L.; Chevret, S.; De Botton, S.; Thomas, X.; Dombret, H.; Beve, B.; Sanz, M.; Guerci, A.; Miguel, J. S.; Dela Serna, J.; Garo, C.; Stoppa, A. M.; Reman, O.; Stamatoulas, A.; Fey, M.; Cahn, J. Y.; Sotto, J. J.; Bourhis, J. H.; Parry, A.; Chomienne, C.; Degos, L.; Fenaux, P. Outcome of acute promyelocytic leukemia treated with all trans retinoic acid and chemotherapy in elderly patients: the European group experience. Leukemia 2005, 19, 230-233.

(123) Li, S.; Zhang, Y.; Liu, Q.; Zhao, Q.; Xu, L.; Huang, S.; Huang, S.; Wei, X. Oxymatrine inhibits proliferation of human bladder cancer T24 cells by inducing apoptosis and cell cycle arrest. Oncol Lett 2017, 13, 4453-4458.

(124) Wu, C.; Huang, W.; Guo, Y.; Xia, P.; Sun, X.; Pan, X.; Hu, W. Oxymatrine inhibits the proliferation of prostate cancer cells in vitro and in vivo. Mol Med Rep 2015, 11, 4129-4134.

(125) Zhou, G. Z.; Shi, Y. Y.; Cui, L. S.; Li, A. F.; Wang, Q. Q.; Liu, M. Oxymatrine induces A549 human non-small lung cancer cell apoptosis via extrinsic and intrinsic pathways. Mol Med Rep 2018, 17, 1071-1076.

(126) David-Pfeuty, T. The flexible evolutionary anchorage-dependent Pardee's restriction point of mammalian cells. How its deregulation may lead to cancer. Biochimica et Biophysica Acta (BBA)-Reviews on Cancer 2006, 1765, 38-66.

(127) Assoian, R. K.; Yung, Y. A reciprocal relationship between Rb and Skp2: implications for restriction point control, signal transduction to the cell cycle, and cancer. Cell cycle 2008, 7, 24-27.

(128) Asghar, U. S.; Barr, A. R.; Cutts, R.; Beaney, M.; Babina, I.; Sampath, D.; Giltnane, J.; Lacap, J. A.; Crocker, L.; Young, A. Single-cell dynamics determines response to CDK4/6 inhibition in triple-negative breast cancer. Clinical cancer research 2017, 23, 5561-5572.

(129) Asghar, U.; Witkiewicz, A. K.; Turner, N. C.; Knudsen, E. S. The history and future of targeting cyclin-dependent kinases in cancer therapy. Nat Rev Drug Discov 2015, 14, 130-146.

(130) Vitale, I.; Galluzzi, L.; Castedo, M.; Kroemer, G. Mitotic catastrophe: a mechanism for avoiding genomic instability. Nature reviews. Molecular cell biology 2011, 12, 385-392.

(131) Castedo, M.; Perfettini, J.-L.; Roumier, T.; Andreau, K.; Medema, R.; Kroemer, G. Cell death by mitotic catastrophe: a molecular definition. Oncogene 2004, 23, 2825-2837.

(132) Weber, A. M.; Ryan, A. J. ATM and ATR as therapeutic targets in cancer. Pharmacology & therapeutics 2015, 149, 124-138.

(133) Karnitz, L. M.; Zou, L. Molecular Pathways: Targeting ATR in Cancer Therapy. Clinical cancer research : an official journal of the American Association for Cancer Research 2015, 21, 4780-4785.

(134) Mei, L.; Zhang, J.; He, K.; Zhang, J. Ataxia telangiectasia and Rad3-related inhibitors and cancer therapy: where we stand. J Hematol Oncol 2019, 12, 43.

(135) Bøe, C. A.; Håland, T. W.; Boye, E.; Syljuåsen, R. G.; Grallert, B. A novel role for ATR/Rad3 in G1 phase. Scientific reports 2018, 8, 1-12.

(136) Bavetsias, V.; Linardopoulos, S. Aurora Kinase Inhibitors: Current Status and Outlook. Frontiers in oncology 2015, 5, 278-278.

(137) Carvajal, R. D.; Tse, A.; Schwartz, G. K. Aurora kinases: new targets for cancer therapy. Clinical cancer research : an official journal of the American Association for Cancer Research 2006, 12, 6869-6875.

(138) Damodaran, A. P.; Vaufrey, L.; Gavard, O.; Prigent, C. Aurora A kinase is a priority pharmaceutical target for the treatment of cancers. Trends in pharmacological sciences 2017, 38, 687-700.

(139) Dar, A. A.; Goff, L. W.; Majid, S.; Berlin, J.; El-Rifai, W. Aurora Kinase Inhibitors - Rising Stars in Cancer Therapeutics? Molecular Cancer Therapeutics 2010, 9, 268.

(140) D'Assoro, A. B.; Haddad, T.; Galanis, E. Aurora-A Kinase as a Promising Therapeutic Target in Cancer. Frontiers in oncology 2016, 5, 295-295.

(141) Keen, N.; Taylor, S. Aurora-kinase inhibitors as anticancer agents. Nature Reviews Cancer 2004, 4, 927-936.

(142) Gutteridge, R. E.; Ndiaye, M. A.; Liu, X.; Ahmad, N. Plk1 Inhibitors in Cancer Therapy: From Laboratory to Clinics. Mol Cancer Ther 2016, 15, 1427-1435.

(143) Gutteridge, R. E. A.; Ndiaye, M. A.; Liu, X.; Ahmad, N. Plk1 Inhibitors in Cancer Therapy: From Laboratory to Clinics. Molecular cancer therapeutics 2016, 15, 1427-1435.

(144) Plyte, S.; Musacchio, A. PLK1 inhibitors: setting the mitotic death trap. Current Biology 2007, 17, R280-R283.

(145) Ueda, A.; Oikawa, K.; Fujita, K.; Ishikawa, A.; Sato, E.; Ishikawa, T.; Kuroda, M.; Kanekura, K. Therapeutic potential of PLK1 inhibition in triple-negative breast cancer. Laboratory Investigation 2019, 99, 1275-1286.

(146) Talhouet, S. D.; Peron, J.; Vuilleumier, A.; Friedlaender, A.; Viassolo, V.; Ayme, A.; Bodmer, A.; Treilleux, I.; Lang, N.; Tille, J.-C.; Chappuis, P. O.; Buisson, A.; Giraud, S.; Lasset, C.; Bonadona, V.; Trédan, O.; Labidi-Galy, S. I. Clinical outcome of breast cancer in carriers of BRCA1 and BRCA2 mutations according to molecular subtypes. Scientific Reports 2020, 10, 7073.

(147) Tung, N. M.; Garber, J. E. BRCA1/2 testing: therapeutic implications for breast cancer management. British Journal of Cancer 2018, 119, 141-152.

(148) Colombo, R.; Caldarelli, M.; Mennecozzi, M.; Giorgini, M. L.; Sola, F.; Cappella, P.; Perrera, C.; Depaolini, S. R.; Rusconi, L.; Cucchi, U. Targeting the mitotic checkpoint for cancer therapy with NMS-P715, an inhibitor of MPS1 kinase. Cancer research 2010, 70, 10255-10264.

(149) Daniel, J.; Coulter, J.; Woo, J.-H.; Wilsbach, K.; Gabrielson, E. High levels of the Mps1 checkpoint protein are protective of aneuploidy in breast cancer cells. Proceedings of the National Academy of Sciences 2011, 108, 5384-5389.

(150) Janssen, A.; Kops, G. J.; Medema, R. H. Targeting the mitotic checkpoint to kill tumor cells. Hormones and Cancer 2011, 2, 113-116.

(151) Alimova, I.; Ng, J.; Harris, P.; Birks, D.; Donson, A.; Taylor, M. D.; Foreman, N. K.; Venkataraman, S.; Vibhakar, R. MPS1 kinase as a potential therapeutic target in medulloblastoma. Oncology reports 2016, 36, 2633-2640.

(152) van Harten, A. M.; Buijze, M.; van der Mast, R.; Rooimans, M. A.; Martens-de Kemp, S. R.; Bachas, C.; Brink, A.; Stigter-van Walsum, M.; Wolthuis, R. M.; Brakenhoff, R. H. Targeting the cell cycle in head and neck cancer by Chk1 inhibition: a novel concept of bimodal cell death. Oncogenesis 2019, 8, 1-16.

(153) Ma, C. X.; Janetka, J. W.; Piwnica-Worms, H. Death by releasing the breaks: CHK1 inhibitors as cancer therapeutics. Trends in molecular medicine 2011, 17, 88-96.

(154) Qiu, Z.; Oleinick, N. L.; Zhang, J. ATR/CHK1 inhibitors and cancer therapy. Radiotherapy and Oncology 2018, 126, 450-464.

(155) Zhang, Y.; Hunter, T. Roles of Chk1 in cell biology and cancer therapy. International journal of cancer 2014, 134, 1013-1023.

(156) Garimella, S. V.; Rocca, A.; Lipkowitz, S. WEE1 inhibition sensitizes basal breast cancer cells to TRAIL-induced apoptosis. Molecular Cancer Research 2012, 10, 75-85.

(157) Geenen, J. J. J.; Schellens, J. H. M. Molecular Pathways: Targeting the Protein Kinase Wee1 in Cancer. Clinical Cancer Research 2017, 23, 4540.

(158) Lewis, C. W.; Jin, Z.; Macdonald, D.; Wei, W.; Qian, X. J.; Choi, W. S.; He, R.; Sun, X.; Chan, G. Prolonged mitotic arrest induced by Wee1 inhibition sensitizes breast cancer cells to paclitaxel. Oncotarget 2017, 8, 73705-73722.

(159) Matheson, C. J.; Backos, D. S.; Reigan, P. Targeting WEE1 kinase in cancer. Trends in pharmacological sciences 2016, 37, 872-881.

(160) Zheng, H.; Shao, F.; Martin, S.; Xu, X.; Deng, C.-X. WEE1 inhibition targets cell cycle checkpoints for triple negative breast cancers to overcome cisplatin resistance. Scientific Reports 2017, 7, 43517.

(161) Evan, G. I.; Brown, L.; Whyte, M.; Harrington, E. Apoptosis and the cell cycle. Current opinion in cell biology 1995, 7, 825-834.

(162) Wyllie, A.; Kerr, J. R.; Currie, A.: Cell death: the significance of apoptosis. In International review of cytology; Elsevier, 1980; Vol. 68; pp 251-306.

(163) Luoto, K. R.; Meng, A. X.; Wasylishen, A. R.; Zhao, H.; Coackley, C. L.; Penn, L. Z.; Bristow, R. G. Tumor Cell Kill by c-MYC Depletion: Role of MYC-Regulated Genes that Control DNA Double-Strand Break Repair. Cancer Research 2010, 70, 8748.

(164) McMahon, S. B. MYC and the control of apoptosis. Cold Spring Harb Perspect Med 2014, 4, a014407-a014407.

(165) Uribesalgo, I.; Benitah, S. A.; Di Croce, L. From oncogene to tumor suppressor. Cell Cycle 2012, 11, 1757-1764.

(166) Amati, B.; Land, H. Myc—Max—Mad: a transcription factor network controlling cell cycle progression, differentiation and death. Current opinion in genetics & development 1994, 4, 102-108.

(167) Packham, G.; Porter, C. W.; Cleveland, J. L. c-Myc induces apoptosis and cell cycle progression by separable, yet overlapping, pathways. Oncogene 1996, 13, 461.

(168) Pelengaris, S.; Rudolph, B.; Littlewood, T. Action of Myc in vivo—proliferation and apoptosis. Current opinion in genetics & development 2000, 10, 100-105.

(169) Murphy, D. J.; Junttila, M. R.; Pouyet, L.; Karnezis, A.; Shchors, K.; Bui, D. A.; Brown-Swigart, L.; Johnson, L.; Evan, G. I. Distinct thresholds govern Myc's biological output in vivo. Cancer cell 2008, 14, 447-457.

(170) Graeber, T. G.; Osmanian, C.; Jacks, T.; Housman, D. E.; Koch, C. J.; Lowe, S. W.; Giaccia, A. J. Hypoxia-mediated selection of cells with diminished apoptotic potential in solid tumours. nature 1996, 379, 88-91.

(171) Dang, C. V.; Le, A.; Gao, P. MYC-Induced Cancer Cell Energy Metabolism and Therapeutic Opportunities. Clinical Cancer Research 2009, 15, 6479.

(172) Li, T.; Kon, N.; Jiang, L.; Tan, M.; Ludwig, T.; Zhao, Y.; Baer, R.; Gu, W. Tumor suppression in the absence of p53-mediated cell-cycle arrest, apoptosis, and senescence. Cell 2012, 149, 1269-1283.

(173) Zinkel, S.; Gross, A.; Yang, E. BCL2 family in DNA damage and cell cycle control. Cell Death & Differentiation 2006, 13, 1351-1359.

(174) Haapaniemi, E.; Botla, S.; Persson, J.; Schmierer, B.; Taipale, J. CRISPR–Cas9 genome editing induces a p53-mediated DNA damage response. Nature medicine 2018, 24, 927-930.

(175) Speidel, D. The role of DNA damage responses in p53 biology. Archives of toxicology 2015, 89, 501-517.

(176) Helton, E. S.; Chen, X. p53 modulation of the DNA damage response. Journal of cellular biochemistry 2007, 100, 883-896.

(177) Wang, X.; Simpson, E. R.; Brown, K. A. p53: protection against tumor growth beyond effects on cell cycle and apoptosis. Cancer research 2015, 75, 5001-5007.

(178) Hanahan, D.; Weinberg, R. A. Hallmarks of cancer: the next generation. cell 2011, 144, 646-674.

III. TRANSCRIPTIONAL REGULATION ACTIVITY OF A TARGETED ANTIBODY DRUG NANOROD IN BREAST CANCER CELLS

ABSTRACT

Transcriptional activity in cancer cells is a key factor for determining the therapeutic outcome in patients. Therapeutic drugs with diverse mechanisms regulate certain gene expression activity in cancer cells causing enhanced tumor cell death. However, the aberrant gene regulation activity during the tumor evolution process or even following the therapeutic drug treatment significantly causes drug resistance and disease recurrence. Hence, such genomic instability in tumor cell population has to be comprehensively unfolded for better treatment response. In this study, we investigated the transcriptional regulation activity of a Trastuzumab conjugated Paclitaxel drug nanorod system (PTXNR-TTZ) in breast cancer cell lines. We investigated the gene regulation activity of DNA metabolism, cell cycle checkpoint and inflammatory pathways that might determine the therapeutic response or drug resistance in PTXNR-TTZ treatment. Hyperactivity in DNA repair pathways can offset the effect of therapeutic drugs and cause treatment resistance. In HER2-positive breast cancer cells, we found that PTXNR-TTZ did not alter the DNA repair pathways although a significant downregulation in this pathway was observed in individual treatment with Trastuzumab. PTXNR-TTZ also induced significantly high expression of NR4A3 gene. The upregulation of nuclear NR4A3 gene has role in inducing enhanced apoptosis mechanism by activating the pro-apoptotic and inhibiting the anti-apoptotic gene regulation activity.

The pathway enrichment analysis showed a significant upregulation of the Rho GTPase signaling network following PTXNR-TTZ treatment. The effector genes in this pathway are associated with spindle assembly checkpoint (SAC) regulation in mitosis phase and hyperactivation of this pathway is responsible for cell cycle progression and aberrant exit from mitosis phase of the cell cycle potentially causing poor treatment outcome. PTXNR-TTZ also induced oncogenic CDC20 gene expression activity that functions in mitosis phase and promotes the cell cycle progression. In HER2-negative breast cancer cell line, PTXNR-TTZ significantly upregulated a set of tumorigenic chemokine and cytokine encoding genes IL6, CXCL1, CXCL2, CXCL3, CXCL8, IL1A and IL1B suggesting an induction of enhanced survival signaling and aggressive tumorigenic behavior in cancer cells.

1. INTRODUCTION

Chemotherapeutic drugs can be categorized into the cell cycle phase specific or non-specific drugs based on their therapeutic effect window[1-4]. For example, the DNA damaging drugs have almost no therapeutic effect on the cells that are in the resting phase [2]. Rather, the effect is maximum when the cells are actively replicating their genetic contents in the synthesis phase[5-7]. Similarly, the taxanes (*e.g.,* Paclitaxel) depend on the active mitosis cell cycle phase for exerting their therapeutic efficacy [8]. Such variations in treatment outcome are due to the alterations in gene expression in different cell cycle phases [2,4]. In combination chemotherapy, cell cycle mediated drug resistance is minimized by appropriate scheduling of different cell cycle targeted chemotherapeutic

agents [4]. In our recent study, we designed an actively targeted nanoparticle based combination therapeutic system ADN that induced apoptosis in HER2-positive breast cancer cell lines by arresting the cells in the G2/M phase. In this study, we investigated the alterations in gene expressions in breast cancer cells induced by ADN. We hypothesized that the cell cycle plays a critical role in determining the therapeutic efficacy of ADN in HER2-positive breast cancer treatment.

The cell cycle and apoptosis are two complementary mechanisms for tissue homeostasis and normal functioning of the tissues to perform a specific task in a coordinated way [9-15]. Most cells rest at the quiescent phase (G0) and perform tissue specific tasks. At the same time, these cells keep receiving the mitogenic signaling via several growth factors from the cellular environment and enter the cell cycle phase Gap 1(G1) when they commit to divide [16]. In the synthesis (S) phase, the cells start replicating their genetic contents and progress through the Gap 2/Mitosis (G2/M) phase resulting in cell division. During the cell cycle, the cells progress through a subsequent series of regulatory checkpoints[17-20]. These regulatory cell cycle checkpoints make sure that the genetic materials of the dividing cells are kept intact before the distribution to the daughter cells [2]. Failure to maintain the intact nature of the genetic materials causes the initiation of a programmed cell death or apoptosis mechanism to maintain the normal tissue functioning [15]. Mutations and aberrant growth signaling pathways cause the cancer cells to respond more frequently to these external mitogenic signaling and unregulated progression through the cell cycle. Evading the apoptosis mechanism and unregulated division with aberrant genetic contents are the major acquired hallmarks of cancer [21,22]. The cell cycle targeted drugs alter the regulatory machineries of the cells causing forced

apoptosis or halt the cellular growth. The cancer cells also activate a series of molecular machinery *e.g.,* DNA metabolism [23-26], cell cycle checkpoints [27-29], inflammatory pathways[30-32] upon any genotoxic stress on the cells to maintain the aberrant genomic and phenotypic integrity resulting in partial treatment response or therapeutic resistance.

We previously synthesized targeted ADN using rod shaped Paclitaxel nanoparticles (PTXNR) of 500 nm length and 100 nm diameter. We covalently conjugated the nanorods with therapeutic monoclonal antibody (mAb) Trastuzumab (PTXNR-TTZ). The current study extends our investigation in understanding the effects of PTXNR-TTZ on breast cancer cells at the gene expression level. For the investigation, we treated HER2-positive BT-474 and HER2- negative MDA-MB-231 breast cancer cells with PTXNR-TTZ. The cells were also treated by different cell cycle targeted drugs *e.g.,* Trastuzumab and Rapamycin targeting the early G1 phase, 5-Fluorouracil targeting the S phase, and Paclitaxel, Doxorubicin targeting the G2/M phase of the cell cycle. The untreated cells mostly arrested in the G0/G1 phase were used as control. We performed RNAseq analysis following the treatment with different cell cycle targeted drugs. The study aims to investigate the PTXNR-TTZ induced gene regulation activity that might determine the treatment response in breast cancer. We investigated the PTXNR-TTZ induced transcriptional activity in DNA metabolism, cell cycle checkpoint, apoptosis and inflammatory pathways in breast cancer cell lines to determine potential genetic means of cell cycle dependent therapeutic response and drug resistance.

2. METHODS

2.1. RNA EXTRACTION

BT-474 and MDA-MB-231 cells were cultured in hybricare medium and RPMI-1640, respectively supplemented with 10% fetal bovine serum (FBS) and 1% penicillin-streptomycin at 37°C and 5% CO_2. Approximately, 1M cells were seeded in 25 cm^2 cell culture flask for each cell line and treated with IC_{50} doses of 5-Fluorouracil, Doxorubicin, Rapamycin, Paclitaxel, Trastuzumab and Trastuzumab conjugated Paclitaxel drug nanorods (PTXNR-TTZ) (SI Table 1) . After 72 h of incubation, the total RNA was extracted from the samples using TRIzol Plus RNA purification kit (Invitrogen) by following the manufacturerer's protocol. Briefly, 1 ml of TRIzol was used for 1 million cells to lyse. The cell lysates were passed through an 18-21 gauge syringe needle for homogenization. The cell lysates were kept at room temperature (RT) for 5 min for complete dissociation of the nucleoprotein complex. To the lysate mixture 0.2 ml of chloroform was added per 1 ml of TRIzol reagent . The mixture was centrifuged at 12,000×g for 15 minutes at 4°C. The mixture separates into two layers: the bottom red phenol-chloroform layer, an interphase and colorless aquous layer containing the total RNA. The upper phase (~600 µl) was then transferred to a new sterile RNase free tube followed by addition of an equal volume of 70% ethanol. The mixtutre was vortexed well and the total RNA was bound on the membrane provided by the manufacturer. In subsequent steps, the RNA was washed on the membrane and eluted with RNase free water by following the manufacturers protocol. The RNA quality was determined by measuring the RNA integrity number (RIN) using Agilent Bioanalyzer .

2.2. RNAseq ANALYSIS

The extracted RNA samples from BT-474 and MDA-MB-231 human breast cancer cell lines were used for sequencing using the RNAseq technology. Briefly, the mRNA was isolated from the total RNA extract using poly-A enrichment method. The mRNA was fragmented and the fragmentation quality was confirmed using Agilent Bioanalyzer. cDNA was synthesized from the fragmented mRNA and amplified using the polymerase chain reaction (PCR) technique. The mRNA stranded RNAseq library was prepared using TruSeq stranded mRNA library preparation kit (Illumina). The constructed libraries were then sequenced using the NovaSeq 6000 Sequencing System on a single NovaSeq S1 PE-50 flow cell. The samples were sequenced to an average read count of 50 million paired end reads per sample. The library construction and sequencing work was performed with the support of the University of Missouri DNA Core Facility.

2.3. GENOMICS DATA ANALYSIS OF ALTERATIONS IN BC

The Oncoprint analysis was performed in cBioPortal platform to investigate on the DNA copy number alterations, overall survival and genetic co-expressions in HER2-positive breast cancer patients. The clinical data were obtained from the Molecular Taxonomy of Breast Cancer International Consortium (METABRIC) study. The study comprised the genomics data of more than 2,000 primary breast cancer specimens that were obtained from the tumor banks in the UK and Canada. Nearly none of the estrogen receptor positive (ER+) and lymph node-negative (LN-) patients received any form of chemotherapy. In our analysis, we screened 224 HER2-positive breast cancer patients' genomics data from the study according to the PAM50 breast cancer subtype classifier

method. None of the HER2-positive patients had gone through treatment with Trastuzumab.

2.4. DATA NORMALIZATION

The RNAseq gene expression data sets were normalized using the BioJupies RNAseq data analysis platform. For a specific drug treated sample the raw counts of a specific gene expression were divided by the total sum of all gene expression counts and multiplied by a factor of 10^6 and subsequent a log- 10 transform. The resulting normalized unit becomes log10-Counts Per Million (logCPM).

2.5. DIFFERENTIAL GENE EXPRESSION

The differential gene expression table was generated for both BT-474 and MDA-MB-231 breast cancer cell lines using the BioJupies RNAseq data analysis notebook platform. The differential gene expression table was generated by normalizing the gene expression levels of drug-treated samples to the gene expression levels in untreated control samples for each cell line. The platform used the embedded limma R package for generating the differential gene expression table. The heatmaps and hierarchical clustering were generated by python Jupyter notebook (6.0.3) using the seaborn statistical data visualization library. The pathway-specific signature gene sets were derived from the Kegg gene sets database.

2.6. PRINCIPAL COMPONENT ANALYSIS

Principal component analysis (PCA) was performed to identify the similarity and variance across the treatments for a specific gene signature or pathway. The PCA was

generated using the differential G1, S and G2/M cell cycle signature gene expressions obtained from the cell cycle treated drug samples for both BT-474 and MDA-MB-231 cancer cell lines. The analysis was performed using the MATLAB 2018 version. For the analysis we obtained the statistical PC1, PC2 components from the differential cell cycle gene expression signatures across all the drug treatments covering 58.06%, 38.97% of the differentially expressed genes respectively, in BT-474 cells and 62.92%, 20.06%, respectively in MDA-MB-231 cells.

2.7. GENE ONTOLOGY (GO) ENRICHMENT ANALYSIS

The GO enrichment analysis was performed to identify the collective functions of genes or gene sets for a specific biological process. The database contains a large collection of experimentally validated biological functions that correspond to a specific set of genes. The database also contains predicted associations between genes and biological terms. In this study, the GO analysis was generated using the Enrichr. The GO terms were selected for analysis based on the statistical significance (p-value).

2.8. PATHWAY ENRICHMENT ANALYSIS

Pathway enrichment analysis was performed to identify the significant biological or genetic interactions. The analysis aims to understand the intracellular response more clearly following a therapeutic intervention. The Reactome database containing a myriad of such biological or genetic interactions was used for this analysis. The enrichment analysis was generated using Enrichr by leveraging the Reactome database. In this study,

the upregulated or downregulated pathways were selected for analysis based on their statistical significance (p-value).

2.9. GENE REGULATORY NETWORK ANALYSIS

Gene regulatory network analysis was performed to identify the set of genes that are involved in specific intracellular biological functions. The analysis was performed using the NetworkAnalyst platform. The significant differentially upregulated or downregulated gene sets with the log2FC threshold value of 1.5 were used as input for the analysis.

3. RESULTS

3.1. CELL CYCLE GENE SIGNATURES

The PCA was generated using the cell cycle signature (G1-S transition phase, S and early G2 phase, G2/M phase) gene expression values of Rapamycin, 5-Fluorouracil, Trastuzumab, Doxorubicin, Paclitaxel, and PTXNR-TTZ treated BT-474 (Figure 1a) and MDA-MB-231 (Figure 1b) cells normalized to the untreated control cells . In BT-474 cells, the PCA plot showed that Paclitaxel and PTXNR-TTZ, 5-Fluorouracil, and Trastuzumab formed two distinct clusters suggesting lower variance in cell cycle gene expression between the samples in each cluster. Rapamycin and Doxorubicin treated cells formed two distinct clusters suggesting high variance in gene expression between the treatments. In MDA-MB-231 cell line, Paclitaxel and PTXNR-TTZ formed a cluster but with larger variance than in BT-474 cells. This suggests that the alterations in cell cycle gene expression by these drugs slightly vary between BT-474 and MDA-MB-231 cell

lines. Trastuzumab and Rapamycin treated samples were almost invariant in cell cycle gene expression and formed a cluster together. With a slight variance to this cluster, 5-Fluorouracil treated cells formed a distinct cluster. In similar to the BT-474 cells, Doxorubicin treated MDA-MB-231 cells formed a distinctly variant cluster.

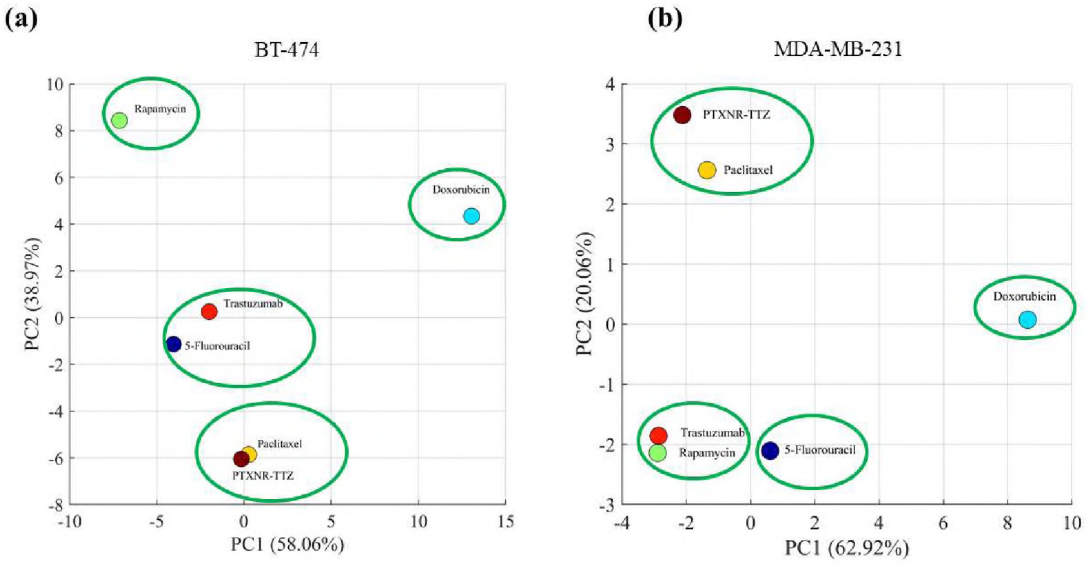

Figure 1. Cell cycle gene signature of cell cycle arresting drugs. PCA plot of cell cycle related gene expression signatures following Rapamycin, 5-Fluorouracil, Doxorubicin, Paclitaxel, Trastuzumab and PTXNR-TTZ drug treatments in (a) BT-474 and (b) MDA-MB-231 cell line

3.2. PTXNR-TTZ DOES NOT ALTER THE DNA METABOLISM PROCESSES IN HER2-POSITIVE BREAST CANCER CELL LINE

Therapeutic drugs that downregulate the DNA metabolism related genes might augment the effect of platinum based therapeutics that induce hyperactivity in DDR pathways causing therapeutic resistance. We investigated the PTXNR-TTZ induced DNA metabolism related gene expressions in HER2-positive breast cancer cells. Paclitaxel or

PTXNR-TTZ did not alter the regulation of DNA metabolism related genes compared to the untreated cancer cells. In contrast, the gene ontology (GO) terms enrichment analysis of the biological process showed that DNA metabolism processes were significantly downregulated by the drugs that target either the G1 or the S phase cell cycle arrest mechanism. In Figure 2a, the colored bubbles represent all the significantly downregulated GO terms for individual treatment with Rapamycin, 5-Fluorouracil and Trastuzumab. The GO terms are represented in a similarity based scatter plots with arbitrary space, called semantic space (with no intrinsic meaning) where the distance depicts the relative similarity between two GO terms. The size of the bubbles represents the percentages of genes annotated with the GO term suggesting a more general GO term (larger bubble) and specific GO term (smaller bubble) . The color bar represents the p-values of individual GO terms. In HER2-positive breast cancer, Rapamycin and Trastuzumab (G1) and 5-Fluorouracil (S) significantly downregulated the DNA replication and DNA repair mechanism in response to therapeutic intervention. Transcriptional signatures of the major DNA repair pathways upon treatment with these drugs were further investigated. Hierarchical clustering was generated for DNA repair pathways with the normalized gene expression values for each treatment compared to the untreated HER2- positive breast cancer cell gene expression. Most of the HR (Figure 2b) and MMR (Figure 2c) pathway related genes were downregulated in response to treatment with Rapamycin, Trastuzumab, and 5-Fluorouracil. Notably, Rapamycin downregulated the HR and MMR pathways by significantly inhibiting the expressions of BRCA2, RAD54B, RAD51, BLM, RAD54L, EMEI, RFC2, RFC3, RFC4, RFC5, MSH2, EXO1, LIG1, and PCNA genes. A significant seven-fold upregulation of NHEJ pathway

associated DNTT gene was overserved upon Doxorubicin treatment while no other treatments showed the DNTT gene expression.

(a)

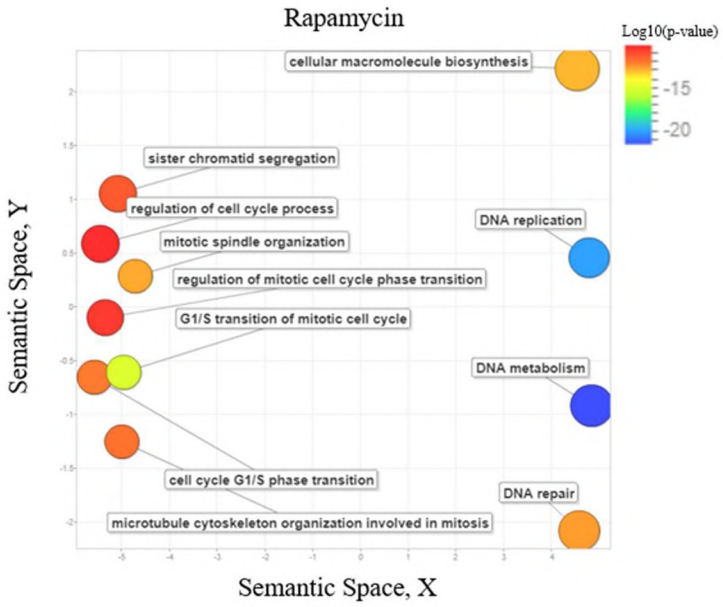

Figure 2. The cell cycle targeted drug induced gene expression analysis in DNA repair pathways. (a) The significantly downregulated GO terms are shown for treatment with Rapamycin, 5-Fluorouracil, and Trastuzumab in BT-474 cell line. The colored bubbles represent a specific GO term that is significantly downregulated in each treatment. The distance between the bubbles represents relative similarity between the respective GO terms. Hierarchical clustering showing alterations in (b) HR and (c) MMR pathways by cell cycle arresting drugs in BT-474 cell line

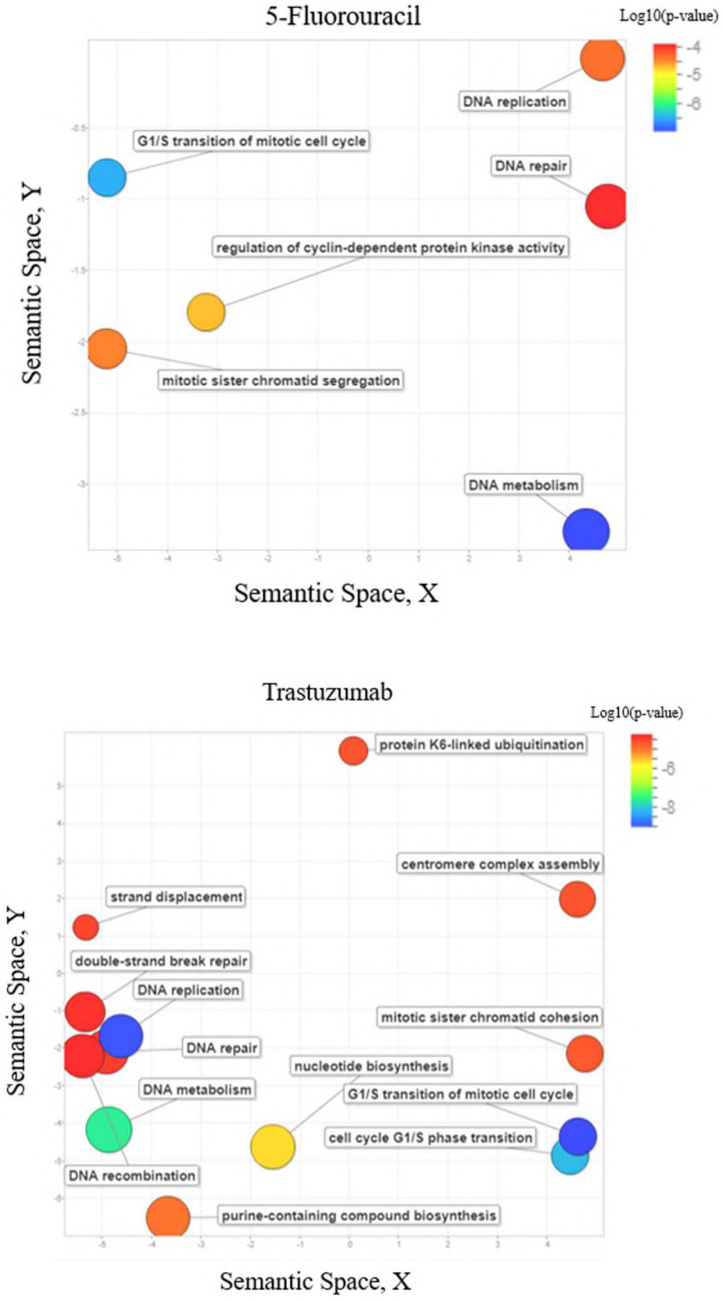

Figure 2. The cell cycle targeted drug induced gene expression analysis in DNA repair pathways.(a) The significantly downregulated GO terms are shown for treatment with Rapamycin, 5-Fluorouracil, and Trastuzumab in BT-474 cell line. The colored bubbles represent a specific GO term that is significantly downregulated in each treatment. The distance between the bubbles represents relative similarity between the respective GO terms. Hierarchical clustering showing alterations in (b) HR and (c) MMR pathways by cell cycle arresting drugs in BT-474 cell line (cont.)

(b)

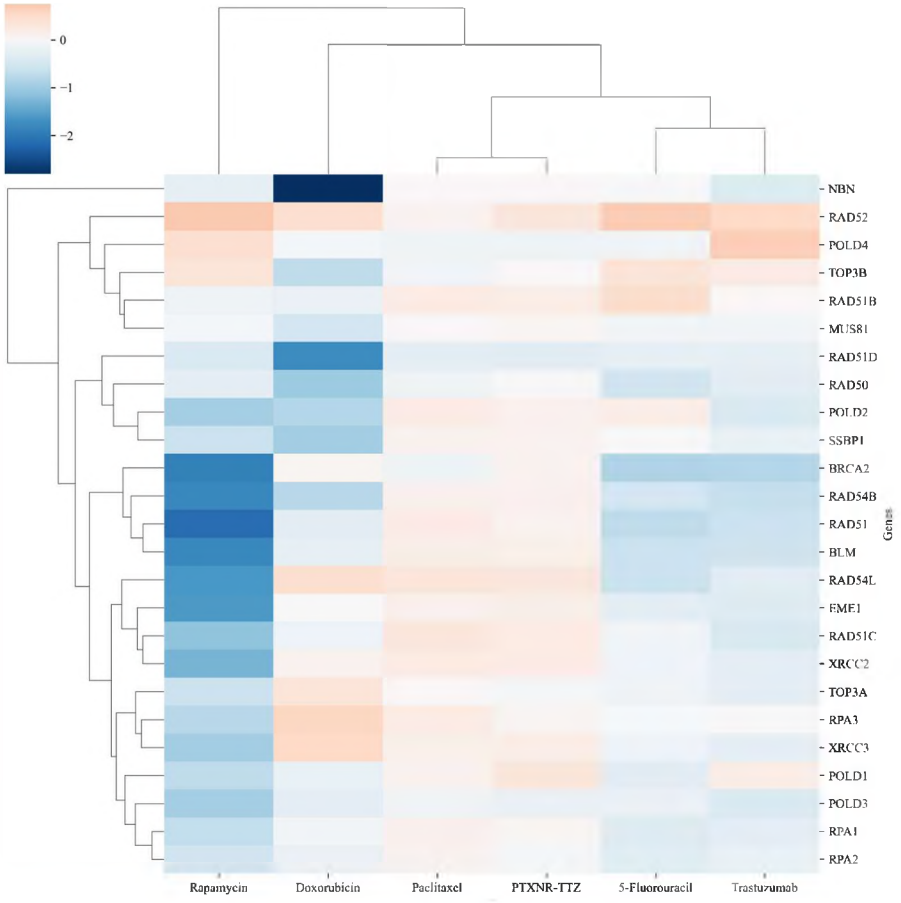

Figure 2. The cell cycle targeted drug induced gene expression analysis in DNA repair pathways.(a) The significantly downregulated GO terms are shown for treatment with Rapamycin, 5-Fluorouracil, and Trastuzumab in BT-474 cell line. The colored bubbles represent a specific GO term that is significantly downregulated in each treatment. The distance between the bubbles represents relative similarity between the respective GO terms. Hierarchical clustering showing alterations in (b) HR and (c) MMR pathways by cell cycle arresting drugs in BT-474 cell line (cont.)

(c)

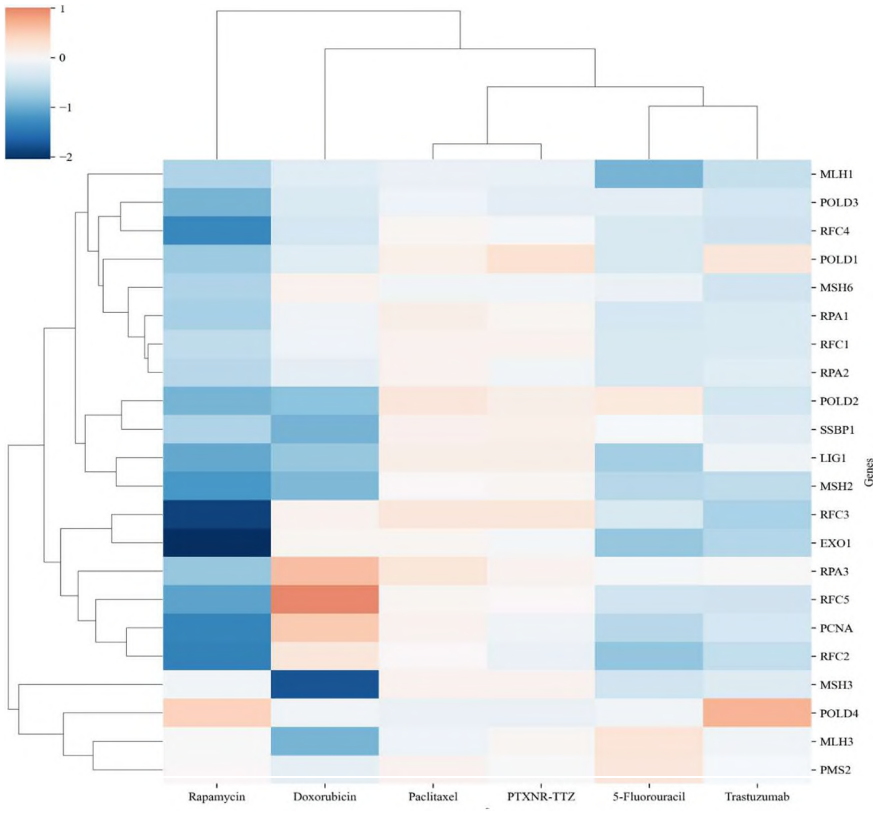

Figure 2. The cell cycle targeted drug induced gene expression analysis in DNA repair pathways.(a) The significantly downregulated GO terms are shown for treatment with Rapamycin, 5-Fluorouracil, and Trastuzumab in BT-474 cell line. The colored bubbles represent a specific GO term that is significantly downregulated in each treatment. The distance between the bubbles represents relative similarity between the respective GO terms. Hierarchical clustering showing alterations in (b) HR and (c) MMR pathways by cell cycle arresting drugs in BT-474 cell line (cont.)

3.3. PTXNR-TTZ MAY INDUCE NR4A3 MEDIATED INTRINSIC APOPTOSIS PATHWAY IN HER2-POSITIVE BREAST CANCER CELL LINE

PTXNR-TTZ induces significant upregulation of PRKG1 and NR4A3 genes in HER2-positive BT-474 cell line (Figure 3).

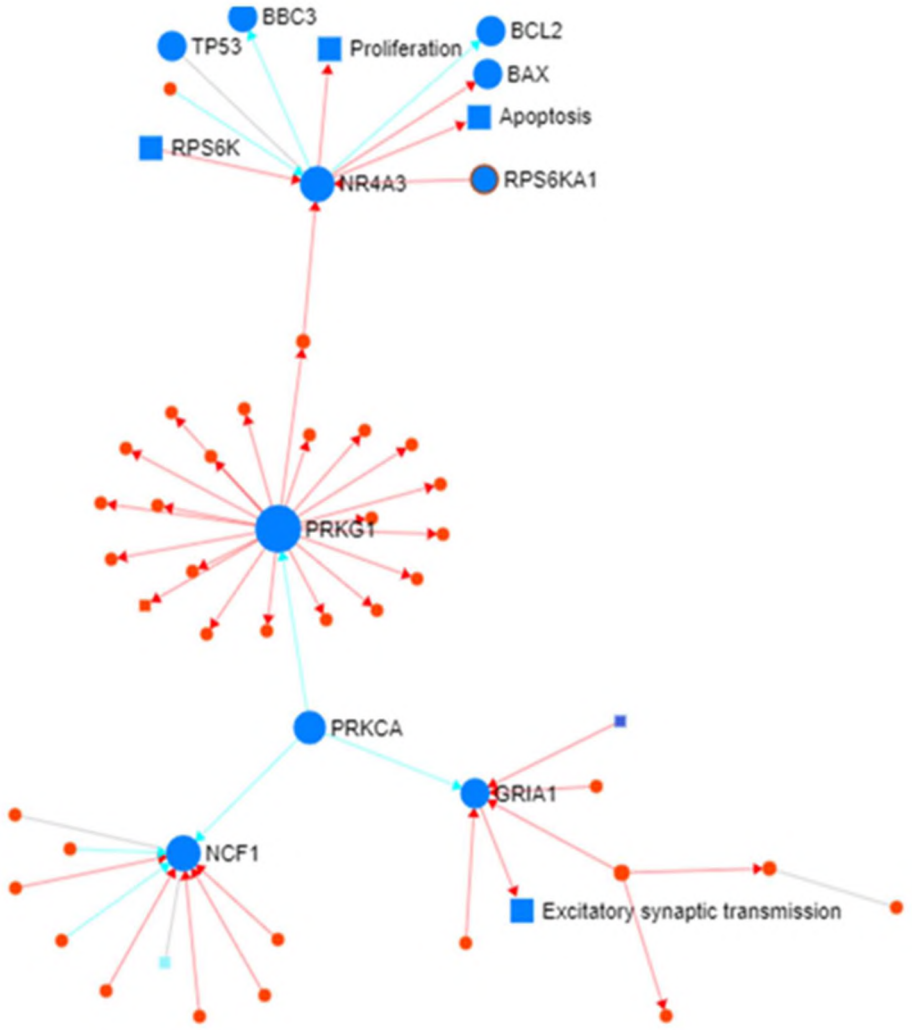

Figure 3. NR4A3 mediated apoptosis induced by PTXNR-TTZ in HER2-positive breast cancer cell line. The gene regulatory network analysis showing the regulation of apoptosis following the activation of PRKG1-NR4A3 axis induced by PTXNR-TTZ in BT-474 cell line

The gene regulatory network showed that upregulation of PRKG1 positively regulates the activation of CREB1, which subsequently regulates the orphan receptor NR4A3 gene. The significantly upregulation of NR4A3 upon PTXNR-TTZ treatment can possibly induce apoptosis in BT-474 cell line. The network showed that the NR4A3 gene

can also be regulated directly by tumor suppressor gene TP53 for apoptosis induction. The NR4A3 function in the gene regulatory network is consistent with the recent finding that showed NR4A3 can induce apoptosis both in p53 dependent and independent manner [33].

3.4. PTXNR-TTZ UPREGULATES DOWNSTREAM EFFECTORS OF Rho-GTPase SIGNALING NETWORK

The Reactome pathway enrichment analysis generated by Enrichr showed significant upregulation of Rho-GTPase signaling pathway (R-HSA-194315) induced by PTXNR-TTZ treatment in BT-474 cell line. In total 37 genes related to this pathway were upregulated with the p value 6.2 e-13, FDR 1.9 e-10 and a Z score of 4.03. A heatmap was generated showing all the 37 upregulated gene expression by PTXNR-TTZ treatment (Figure 4a). The effector proteins of the Rho-GTPase signaling pathway critically regulates the mitosis and cell cycle progression. Cell division cycle protein -20 homologue (encoded by CDC20 gene) is one of the downstream effector proteins in this pathway. The protein binds and activates the anaphase promoting complex APC/C. Together the APC/C^{CDC20} protein complex promotes the exit from mitosis cell cycle phase. The upregulation in CDC20 can promote an aggressive form of breast cancer. A gene regulatory network was generated using all the significantly upregulated genes in the Rho-GTPase signaling pathway. The upregulated genes are shown in red nodes in the network. The network (Figure 4b) shows that CDC20 can be positively regulated by PLK1 gene and subsequently activate the APC/C complex. We found that CDC20 overexpression is correlated with poor overall survival in HER2-positive breast cancer patients. From the METABRIC study, we screened 224 patients with HER2-positive

breast cancer according to PAM-50 plus claudin low subtype breast cancer classifier method. Among 224 patients approximately 4% of the patients (8 patients) had CDC20 DNA copy number alteration. The rest of the 216 patients were considered to be in the unaltered group for the analysis. The overall survival analysis (Figure 4c) showed that the median overall survival for the unaltered group was 107.10 months while the median survival was only 71.63 months in case of the CDC20 altered group (log-rank test p-value 0.296). In the CDC20 altered group, out of 8 patients 6 patients were deceased. Only 4% of the patients showed CDC20 DNA copy number alteration. The mRNA expression shows that two more effector proteins encoding genes of this pathway KIF2C and CDCA8, were also upregulated in most of the HER2-positive breast cancer patients in METABRIC study. In the co expression analysis we observed that KIF2C (Figure 4d) and CDCA8 (Figure 4e) gene expression highly correlated with the CDC20 gene expression. The Spearman correlation factor was 0.86 (p=2.38 e-64) and 0.70 (9.9 e-34) for KIF2C and CDCA8, respectively. We also found that the patients with KIF2C and CDCA8 DNA copy number alterations completely overlapped with the CDC20 altered group in the overall survival analysis. Out of 8 patients with CDC20 alteration, 6 of them also had KIF2C alteration and 2 of them had alterations in CDCA8 DNA copy number. This suggests that KIF2C and CDCA8 might also be a prognostic marker in HER2-positive breast cancer patients along with CDC20. The Oncoprint analysis (Figure 4f) showed that the most of the patients with HER2-positive breast cancer had high CDC20 mRNA expression along with a high expression of KIF2C and CDCA8, suggesting a post transcriptional alteration in patients.

(a)

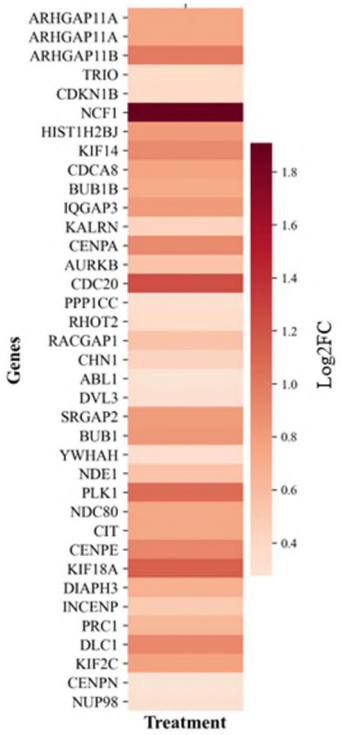

Figure 4. Activation of Rho-GTPase signaling network by PTXNR-TTZ in HER2-positive breast cancer cell line. Heatmap showing the upregulation of downstream effectors in the Rho-GTPase signaling network. (b) Gene regulatory network showing the activation of mitotic progression promoting APC/C complex following overregulation of oncogenic CDC20 gene. (c) Overall survival analysis of HER2-positive breast cancer patients in METABRIC study with CDC20 DNA copy number alterations. The median overall survival of CDC20 altered group (n=8) was 71 months against 110 months in the unaltered group (without CDC20 DNA copy number alteration). Correlation analysis showing mRNA expression data of patients with CDC20 DNA copy number alteration with (d) KIF2C (e) CDCA8 altered patients. The patients with either KIF2C or CDCA8 alterations completely overlapped with the CDC20 altered patients and also showed a high correlation mRNA expression with CDC20 altered patients. The Spearman correlation factor for KIF2C and CDCA8 mRNA expression against CDC20 mRNA expression were 0.86 and 0.71, respectively. (f) The Oncoprint analysis showing the DNA copy number and post transcriptional alterations in CDC20 , KIF2C and CDCA8 genes. The data are shown for individual 224 HER2-positive breast cancer patients in the METABRIC study. The majority of the hER2-positive breast cancer patients showed high mRNA expression for CDC20, KIF2C and CDCA8 though very few patients had transcriptional alterations

(b)

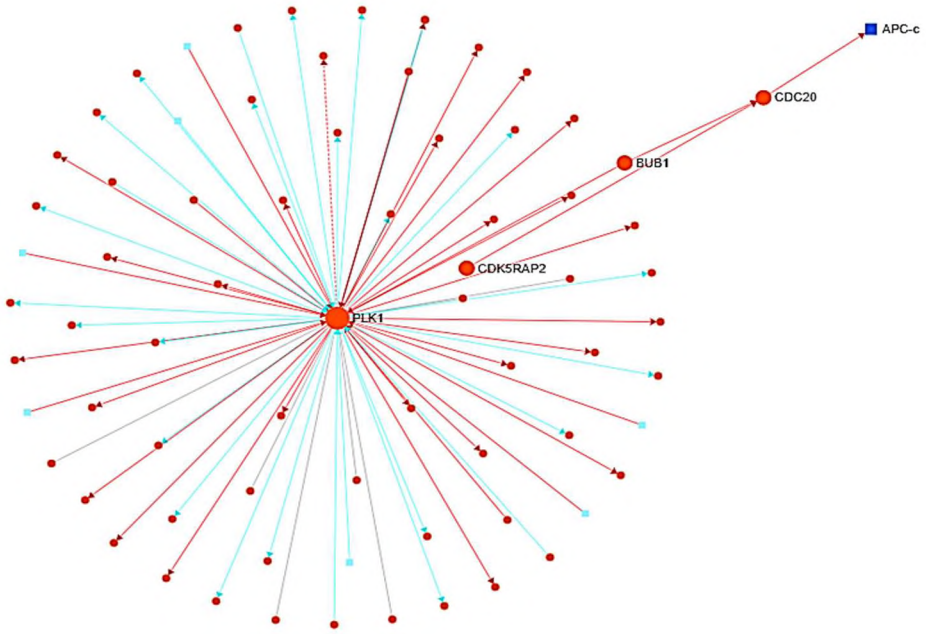

Figure 4. Activation of Rho-GTPase signaling network by PTXNR-TTZ in HER2-positive breast cancer cell line.Heatmap showing the upregulation of downstream effectors in the Rho-GTPase signaling network. (b) Gene regulatory network showing the activation of mitotic progression promoting APC/C complex following overregulation of oncogenic CDC20 gene. (c) Overall survival analysis of HER2-positive breast cancer patients in METABRIC study with CDC20 DNA copy number alterations. The median overall survival of CDC20 altered group (n=8) was 71 months against 110 months in the unaltered group (without CDC20 DNA copy number alteration). Correlation analysis showing mRNA expression data of patients with CDC20 DNA copy number alteration with (d) KIF2C (e) CDCA8 altered patients. The patients with either KIF2C or CDCA8 alterations completely overlapped with the CDC20 altered patients and also showed a high correlation mRNA expression with CDC20 altered patients. The Spearman correlation factor for KIF2C and CDCA8 mRNA expression against CDC20 mRNA expression were 0.86 and 0.71, respectively. (f) The Oncoprint analysis showing the DNA copy number and post transcriptional alterations in CDC20 , KIF2C and CDCA8 genes. The data are shown for individual 224 HER2-positive breast cancer patients in the METABRIC study. The majority of the hER2-positive breast cancer patients showed high mRNA expression for CDC20, KIF2C and CDCA8 though very few patients had transcriptional alterations (cont.)

(c)

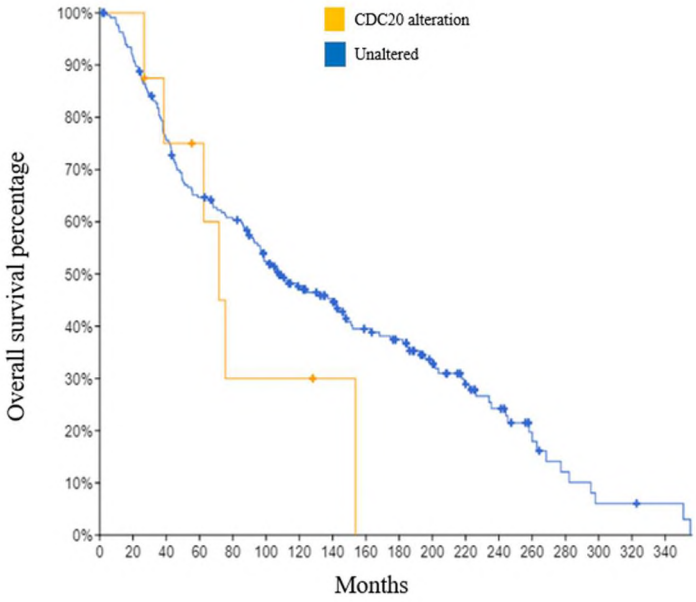

Figure 4. Activation of Rho-GTPase signaling network by PTXNR-TTZ in HER2-positive breast cancer cell line.Heatmap showing the upregulation of downstream effectors in the Rho-GTPase signaling network. (b) Gene regulatory network showing the activation of mitotic progression promoting APC/C complex following overregulation of oncogenic CDC20 gene. (c) Overall survival analysis of HER2-positive breast cancer patients in METABRIC study with CDC20 DNA copy number alterations. The median overall survival of CDC20 altered group (n=8) was 71 months against 110 months in the unaltered group (without CDC20 DNA copy number alteration). Correlation analysis showing mRNA expression data of patients with CDC20 DNA copy number alteration with (d) KIF2C (e) CDCA8 altered patients. The patients with either KIF2C or CDCA8 alterations completely overlapped with the CDC20 altered patients and also showed a high correlation mRNA expression with CDC20 altered patients. The Spearman correlation factor for KIF2C and CDCA8 mRNA expression against CDC20 mRNA expression were 0.86 and 0.71, respectively. (f) The Oncoprint analysis showing the DNA copy number and post transcriptional alterations in CDC20 , KIF2C and CDCA8 genes. The data are shown for individual 224 HER2-positive breast cancer patients in the METABRIC study. The majority of the hER2-positive breast cancer patients showed high mRNA expression for CDC20, KIF2C and CDCA8 though very few patients had transcriptional alterations (cont.)

(d)

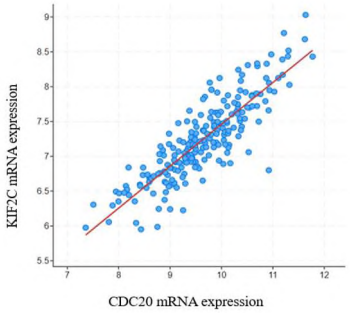

(e)

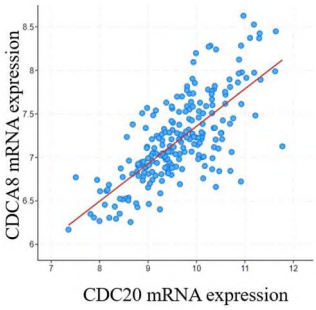

Figure 4. Activation of Rho-GTPase signaling network by PTXNR-TTZ in HER2-positive breast cancer cell line.Heatmap showing the upregulation of downstream effectors in the Rho-GTPase signaling network. (b) Gene regulatory network showing the activation of mitotic progression promoting APC/C complex following overregulation of oncogenic CDC20 gene. (c) Overall survival analysis of HER2-positive breast cancer patients in METABRIC study with CDC20 DNA copy number alterations. The median overall survival of CDC20 altered group (n=8) was 71 months against 110 months in the unaltered group (without CDC20 DNA copy number alteration). Correlation analysis showing mRNA expression data of patients with CDC20 DNA copy number alteration with (d) KIF2C (e) CDCA8 altered patients. The patients with either KIF2C or CDCA8 alterations completely overlapped with the CDC20 altered patients and also showed a high correlation mRNA expression with CDC20 altered patients. The Spearman correlation factor for KIF2C and CDCA8 mRNA expression against CDC20 mRNA expression were 0.86 and 0.71, respectively. (f) The Oncoprint analysis showing the DNA copy number and post transcriptional alterations in CDC20 , KIF2C and CDCA8 genes. The data are shown for individual 224 HER2-positive breast cancer patients in the METABRIC study. The majority of the hER2-positive breast cancer patients showed high mRNA expression for CDC20, KIF2C and CDCA8 though very few patients had transcriptional alterations (cont.)

(f)

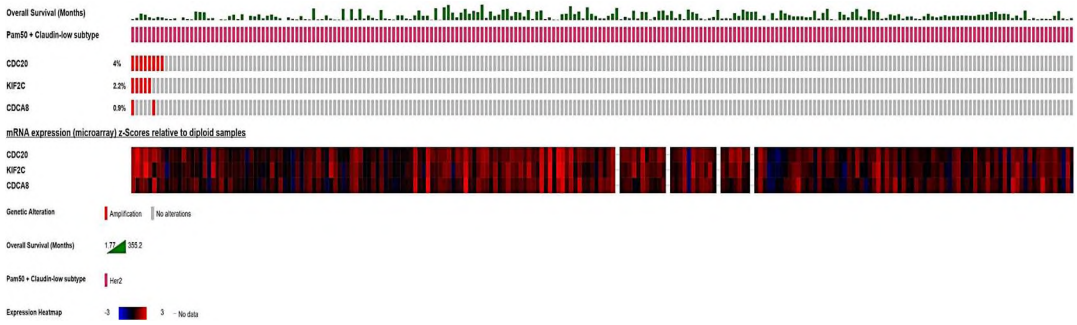

Figure 4. Activation of Rho-GTPase signaling network by PTXNR-TTZ in HER2-positive breast cancer cell line.Heatmap showing the upregulation of downstream effectors in the Rho-GTPase signaling network. (b) Gene regulatory network showing the activation of mitotic progression promoting APC/C complex following overregulation of oncogenic CDC20 gene. (c) Overall survival analysis of HER2-positive breast cancer patients in METABRIC study with CDC20 DNA copy number alterations. The median overall survival of CDC20 altered group (n=8) was 71 months against 110 months in the unaltered group (without CDC20 DNA copy number alteration). Correlation analysis showing mRNA expression data of patients with CDC20 DNA copy number alteration with (d) KIF2C (e) CDCA8 altered patients. The patients with either KIF2C or CDCA8 alterations completely overlapped with the CDC20 altered patients and also showed a high correlation mRNA expression with CDC20 altered patients. The Spearman correlation factor for KIF2C and CDCA8 mRNA expression against CDC20 mRNA expression were 0.86 and 0.71, respectively. (f) The Oncoprint analysis showing the DNA copy number and post transcriptional alterations in CDC20 , KIF2C and CDCA8 genes. The data are shown for individual 224 HER2-positive breast cancer patients in the METABRIC study. The majority of the hER2-positive breast cancer patients showed high mRNA expression for CDC20, KIF2C and CDCA8 though very few patients had transcriptional alterations (cont.)

3.5. PTXNR-TTZ SIGNIFICANTLY INDUCES INFLAMMATORY PATHWAYS IN BREAST CANCER CELL LINES

The Kegg pathway enrichment analysis showed significant upregulation of the TNF signaling pathway (HSA-04668) and NF- kappa B inflammatory signaling pathway (HSA-04064) related genes in the MDA-MB-231 cell line induced by PTZNR-TTZ treatment. In TNF pathway, 18 genes showed overlap in the analysis with p-value 2.6 e-

10, FDR 7.5 e-08 and Z-score of 6.55. The heatmap (Figure 5a) shows the gene expressions of significantly upregulated genes in this pathway. In the NF-kappa B pathway, 12 genes in the analysis showed overlap with this pathway with p-value 3.5 e-06, FDR 0.0002, and Z score of 5.16 and a heatmap was generated showing all the overlapped upregulated genes (Figure 5b). A gene regulatory network was generated using all the significantly upregulated genes in these pathways. All the red nodes in the network represent the upregulated gene expression in our analysis for this particular pathway. The gene regulatory network (Figure 5c) shows that the upregulated genes, in turn, activate the NF-Kappa B p65/p50 signaling complex. The network also suggests that NF-Kappa B p65/p50 signaling complex activation can subsequently induce IL6 expression. Induction of IL6 can positively regulate STAT-3 transcription factor and cause inflammation in triple negative breast cancer cell lines. Such sequential activation of NF-kappa B-IL6-STAT3 inflammatory circuit has been reported to be associated with maintenance of cancer stem cell like population causing therapeutic resistance in breast cancer both *in vitro* and *in vivo*. We further investigated the mRNA expression levels of selected inflammatory genes (CCL20, CXCL1, CXCL2, CXCL3, CXCL8, IL6, IL1A and IL1B) in response to PTXNR-TTZ treatment that has been previously reported to be associated with enhanced inflammation, cancer cell progression or therapeutic resistance. We found that all of these genes were highly upregulated in PTXNR-TTZ treated MDA-MB-231 cell line (Figure 5d). In BT-474 cells, all of the genes except IL1A and CXCL8 were not differentially expressed at all. This suggests that PTXNR-TTZ treatment significantly induced inflammatory pathways in the MDA-MB-231 cell line which might induce therapeutic resistance in treatment.

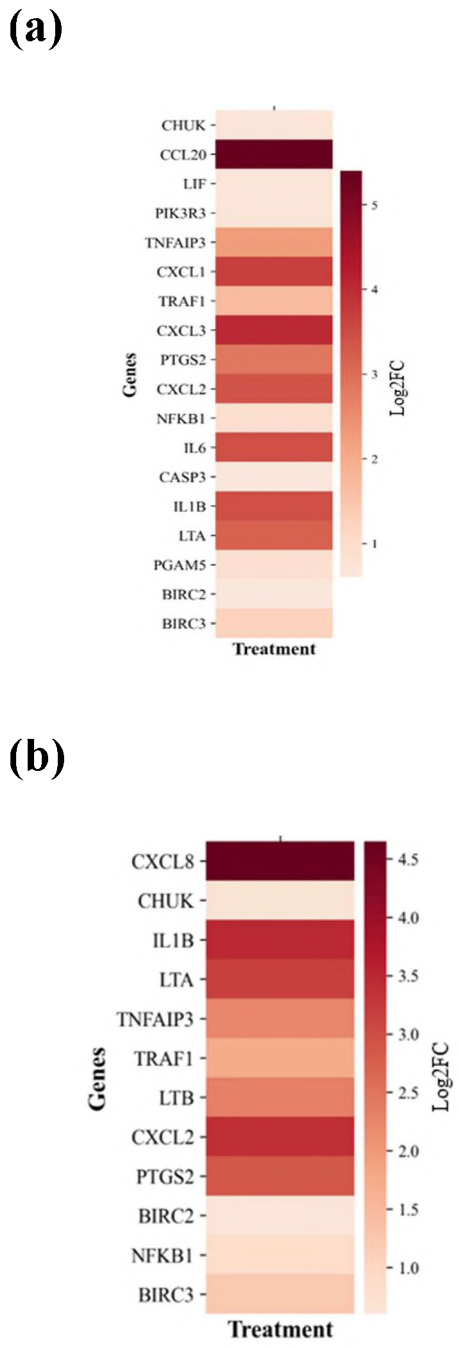

Figure 5. PTXNR-TTZ induces inflammatory gene expressions in triple negative breast cancer cells. The heatmap shows the upregulation of (a) TNF (b) NF-kappa-B pathway genes in MDA-MB-231 cell line induced by PTXNR-TTZ. (c) The gene regulatory network showing the possible activation of the NF-kappa-B p65/p50 signaling complex leading to potential activation of tumorigenic NF-kappa-B –IL6- STAT-3 signaling axis. (d) Gene expression analysis of a set of selected tumorigenesis promoting inflammatory genes in BT-474 and MDA-MB-231 cell line induced by PTXNR-TTZ

(c)

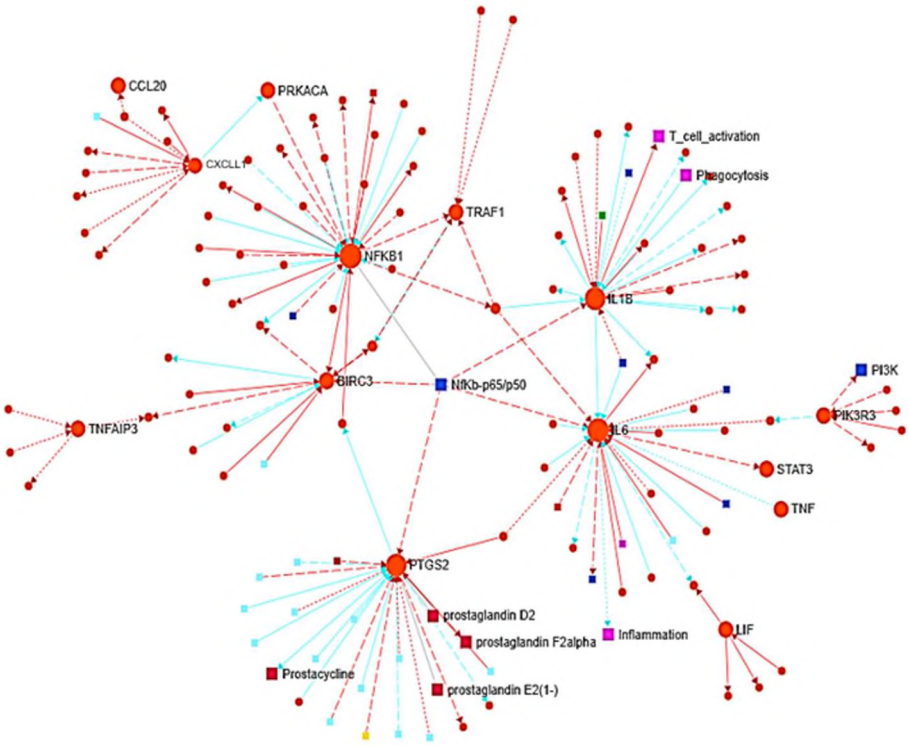

Figure 5. PTXNR-TTZ induces inflammatory gene expressions in triple negative breast cancer cells. The heatmap shows the upregulation of (a) TNF (b) NF-kappa-B pathway genes in MDA-MB-231 cell line induced by PTXNR-TTZ. (c) The gene regulatory network showing the possible activation of the NF-kappa-B p65/p50 signaling complex leading to potential activation of tumorigenic NF-kappa-B –IL6- STAT-3 signaling axis. (d) Gene expression analysis of a set of selected tumorigenesis promoting inflammatory genes in BT-474 and MDA-MB-231 cell line induced by PTXNR-TTZ (cont.)

(d)

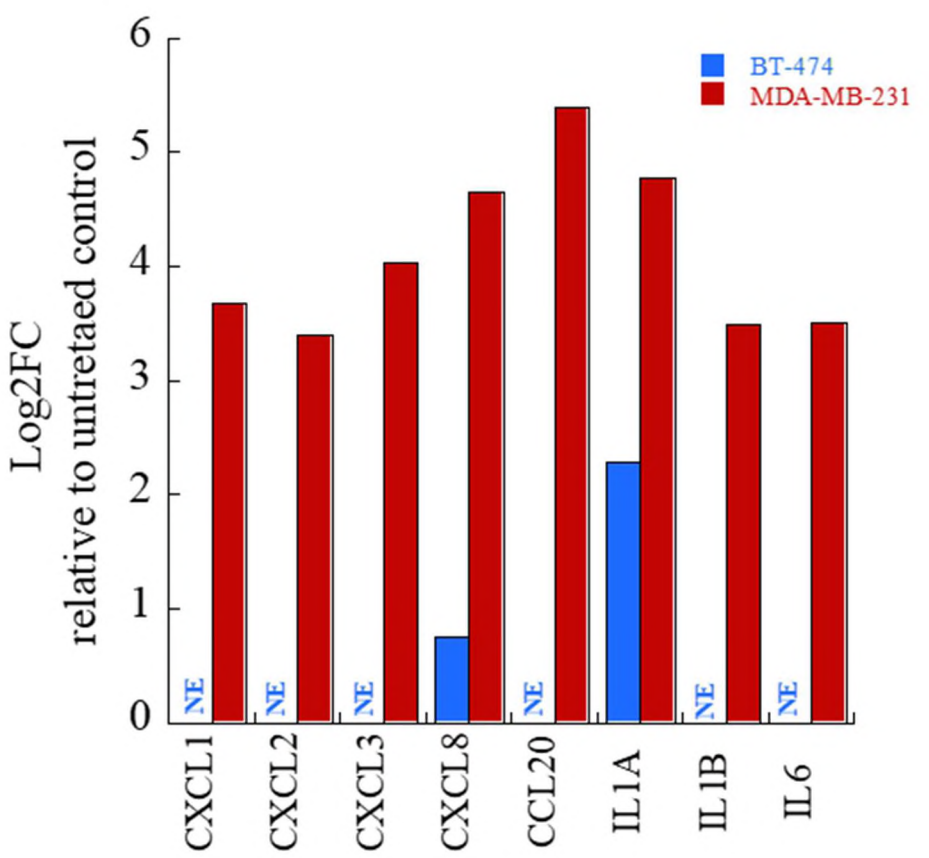

Figure 5. PTXNR-TTZ induces inflammatory gene expressions in triple negative breast cancer cells. The heatmap shows the upregulation of (a) TNF (b) NF-kappa-B pathway genes in MDA-MB-231 cell line induced by PTXNR-TTZ. (c) The gene regulatory network showing the possible activation of the NF-kappa-B p65/p50 signaling complex leading to potential activation of tumorigenic NF-kappa-B –IL6- STAT-3 signaling axis. (d) Gene expression analysis of a set of selected tumorigenesis promoting inflammatory genes in BT-474 and MDA-MB-231 cell line induced by PTXNR-TTZ (cont.)

In our analysis, we observed significantly high expression of IL1A and IL1B in triple negative MDA-MB-231 breast cancer cell line, whereas only IL1A was highly overexpressed in HER2-positive BT-474 cell line upon PTXNR-TTZ treatment. Recently, it has been reported that HER2-overexpression induces the expression of IL1-

alpha (encoded by IL1A), promoting tumorigenesis and chemotherapeutic resistance in HER2-positive breast cancer [34].

4. DISCUSSION

Hyperactive DNA repair and replication mechanisms are the traits of therapeutic drug resistance in cancer cells. Cancer cells activate the several DNA repair pathways in a direct or indirect way in response to the stress caused by the chemo drugs. For example, platinum based drugs inhibit the cancer cells by DNA damage and subsequent DNA damage associated (*e.g.,* p53) apoptosis pathways [35]. In response, hyperactivity of DNA repair pathways such as HR, NER cause the therapeutic resistance to these DNA damaging chemotherapeutic drugs [35]. In particular, mutations or inactivation in HR pathway is influential and one of the major determinants of platinum based therapeutic outcome in high grade serous cancer (HGCC)[36]. A study conducted on HGCC patients who extraordinarily responded to platinum based treatment response showed that overall, 73% of the exceptional responder patients had disruption in HR DNA repair pathway [37]. From the transcriptional analysis, we found that Paclitaxel molecule or PTXNR-TTZ do not alter of affect the DNA metabolism pathways. On the other hand, Rapamycin, 5-Fluorouracil and Trastuzumab downregulate the DNA repair pathways in HER2-positive breast cancer cell line (Figure 2a). The hierarchical heatmap showed that Rapamycin, 5-Fluorouracil, and Trastuzumab specifically altered majority of the gene expression in HR and MMR pathways (Figure 2b, Figure 2c). This suggests that these G1/S cell cycle arresting agents can be used in combination with platinum based chemotherapy for a

possible synergistic outcome by suppressing the hyperactive treatment resistive DNA repair pathways.

We found that PTXNR-TTZ might induce apoptosis in BT-474 cell line via PRKG1- NR4A3 mediated intrinsic apoptosis pathway (Figure 3). Olga et al. recently reported NR4A3 as a novel transcriptional target of p53 transcription factor and mediate apoptosis [33]. The protein p53 directly binds to the promoter region of NR4A3 gene and induces the transcription. NR4A3 interacted with ant-apoptotic protein Bcl-2 for sequestration and induction of apoptosis. Interestingly, the study also showed that the orphan receptor NR4A3 gene also showed tumor suppressive function both in p53 dependent and independent way. In another recent study by Zhao et. al. showed that microRNA miR-665 promoted epithelial-mesenchymal transition (EMT) , cancer cell invasion, and metastasis by inhibiting the NR4A3 gene in MCF-7 and MDA-MB-231 breast cancer cell lines *in vitro* [38].

We found that Rho-GTPase signaling pathway genes were highly overregulated by PTXNR-TTZ treatment in HER2-positive BT-474 breast cancer cell line (Figure 4a). One of the major downstream effectors of this pathway CDC20 gene expression was significantly upregulated in response to PTXNR-TTZ treatment. The gene regulatory network shown in Figure 4b suggests that the overexpression of CDC20 further activates the APC/C complex. The post translational over-regulation of CDC20 gene can potentially cause aberrant mitotic exit and therapeutic resistance. The translated protein Cdc20 is an essential regulator of mitosis and exhibits forced induction of cell cycle progression by partnering with APC/C in subsequent downstream ubiquitination process [39]. Ubiquitination has a critical role in cell cycle control and tumor initiation and

transformation [40]. APC/C binds and gets activated by Cdc20 (cell division cycle 20 homologue) and Cdh1 (Cdc20 homologue-1) forming two distinct multi subunit E3 ubiquitin ligase sub complexes APC/C^{Cdc20} and APC/C^{Cdh1}, respectively to promote cell cycle progression [41,42]. Emerging evidences have suggested two distinct and opposing roles of the closely related cell division cycle proteins Cdc20 and Cdh1 in tumorigenesis. Cdc20 largely functions as an oncogene whereas Cdh1 has tumor suppressive role in the tumorigenesis process [42]. The oncogenic role of Cdc20 has been associated with a wide range of cancer types including breast cancer, pancreatic cancer, prostate cancer, colorectal cancer, lung cancer, glioblastomas and other types [41]. The protein Cdc20 critically regulates the activation of APC/C in the mitosis cell cycle phase. The complex APC/C^{Cdc20} promotes the metaphase to anaphase transition by degrading the cell cycle regulatory proteins [43]. Inhibition of Cdc20 protein has been showed to induce enhanced apoptosis in skin tumor mouse model *in vivo* [44]. The ablation of CDC20 gene in mice caused aberrant mitotic arrest resulting in embryonic lethality suggesting possible role of CDC20 gene in embryonic development [45]. Moreover, inhibition of endogenous Cdc20 resulted in mitotic arrest and subsequent cell death in multiple human cancer cell lines. Zeng et al. showed that inhibition of APC/C^{Cdc20} and APC/C^{Cdh1} by an IR-mimetic inhibitor caused cell death in various cancer cell lines [46]. In the survival analysis of METABRIC data, 224 HER2 positive breast cancer patients showed that the patients who had CDC20 DNA copy number alteration suffered from much worse overall median survival compared to the unaltered group (71.10 vs 107.10 months) (Figure 4c). Altogether, the increasing evidences suggest that CDC20 might be a potential therapeutic in HER2-positive breast cancer treatment to overcome therapeutic resistance and aberrant

mitotic exit upon Paclitaxel based drug treatment. In co-expression analysis, KIF2C and CDCA8 were highly correlated with the CDC20 mRNA expression in METABRIC HER2-positive breast cancer patients (figure 4d, Figure 4e). The patients with KIF2C and CDCA8 DNA copy number alterations completely overlapped with the CDC20 altered patients. Moreover, both KIF2C and CDCA8, along with CDC20, showed high mRNA expression in 224 METABRIC HER2-positive breast cancer patients irrespective of their DNA copy number alterations (Figure 4f). KIF2C and CDCA8 were also upregulated following PTXNR-TTZ treatment. Kinesin family member KIF's are involved in cytoskeleton remodeling and take part in chromosomal segregation and spindle orientation during mitosis[47,48]. Overexpression of kinesin family member 2C or mitotic centromere associated kinesin, KIF2C is associated with detachment of microtubules from the centromere by enhanced microtubule depolymerization. KIF2C has been reported to be positively regulated by aurora-kinase B [49,50] and negative regulation by p53 tumor suppressor protein [51]. KIF2C has been shown to have a role in correcting improper kinetochore-microtubule attachment during mitosis [49,50]. KIF2C overexpression has been shown to induce mammary carcinogenesis, and suppression of KIF2C inhibited the growth of breast cancer cell lines *in vitro*[51]. The cell division cycle associated protein-8, encoded by CDCA8 gene translates a chromosomal passenger complex (CPC) which is an essential regulator of mitosis [52]. The CPC complex functions at the centromere regions ensuring proper chromosomal segregation. The complex is cell cycle regulated and essential for microtubule stabilization and spindle assembly. Overexpression of CDCA8 has also been showed to promote the malignant proliferation of melanoma cell lines *in vitro* and correlated with poor prognosis [53]. Moreover, a recent study leveraging the

weighted gene co-expression network analysis (WCGA) and protein-protein interaction network analysis from the Gene Expression Omnibus (GEO) database showed that both KIF2C and CDCA8 are potential bio marker for metastatic breast cancer [54].

Inflammation is well correlated with poor therapeutic outcomes and increased risk of breast cancer recurrence. The pathway enrichment analysis showed PTXNR-TTZ significantly upregulated the TNF and NF-kappa B inflammatory pathway related genes in MDA-MB-231 cell line (Figure 5a, Figure 5b). We further investigated the induction of these inflammatory pathways using the gene regulatory network generated with the significantly upregulated gene expressions in this pathway. The gene regulatory network showed that the upregulated genes might induce the activation of the NF-kappa B-p65/p50 signaling complex and possible sequential activation of NF-kappa B-IL6-STAT3 signaling axis (Figure 5c). We observed significant upregulation of IL6 in PTXNR-TTZ treated triple negative MDA-MB-231 breast cancer cell line which further suggests the possibility of activation of this signaling circuit. Overregulation of IL6 has been shown to promote stem cell like phenotype in the breast cancer causing tumor progression and therapeutic resistance[55-58]. NF-kappa B activation was shown to be required for the elevated expression of Il6, IL8 and CXCL1 and concurrent inhibition of IL6 and IL8 inhibited the growth of triple negative breast cancer cell growth *in vitro* and *in vivo*[59]. Altogether our transcriptomic analysis suggests that inhibition of IL6 might improve the therapeutic outcome in the taxane based chemotherapeutic treatment of triple negative breast cancer cells. We further investigated the PTXNR-TTZ induced selected inflammatory gene expression signature in MDA-MB-231 cell line and BT-474 cell line. The signature gene set is associated with enhanced inflammation and promotion of cell

proliferation [34]. In MDA-MB-231 cell line we found significantly high expression of the signature genes suggesting a possible role in therapeutic resistance while most of the genes were not expressed at all in BT-474 cell line (Figure 5d). In BT-474 cell line, we also found that IL1A gene is overexpressed upon PTXNR-TTZ treatment. Recently, Liu et. al. showed the role of IL1-alpha (encoded by IL1A gene) on tumorigenesis and therapeutic resistance in HER2-positive breast cancer cell lines [34]. The study showed that HER2 overexpression induced the activation of IL1-alpha and IL6 for maintaining the therapeutically resistant cancer stem cell like phenotype. More importantly, IL1A knockdown depleted the cancer stem cell population, dampened the inflammatory microenvironment and ultimately inhibited the HER2-induced tumorigenesis in HER2-positive breast cancer cells in vivo. The study also showed that pharmacologic blockade of IL1-alpha reduced the therapeutically resistant stem cell population and improved the chemotherapeutic treatment response with Cisplatin and Paclitaxel *in vivo*. Hence, we suggest IL1A might be a crucial therapeutic target to improve therapeutic response in HER2-positive breast cancer.

5. CONCLUSION

The transcriptional regulation of PTXNR-TTZ was investigated in breast cancer cells. PTXNR-TTZ treatment significantly overexpressed PRKG1 and NR4A3 genes in HER2-positive breast cancer cells. It was concluded that the overexpression of the PRKG1-NR4A3 axis might induce an intrinsic apoptosis pathway to inhibit the HER2-positive breast cancer growth. The pathway enrichment analysis showed that the CDC20

was significantly overexpressed by PTXNR-TTZ treatment. CDC20 is a promoter of mitotic exit and might act as an oncogene by activating the anaphase promoting complex APC/C. Two other genes KIF2C and CDCA8 were also upregulated in this pathway which have been reported to have role in cell growth progression. Moreover, KIF2C and CDCA8 genes have recently been proposed as potential metastatic biomarkers in breast cancer. Altogether, it was proposed that targeted inhibition of CDC20, KIF2C and CDCA8 will enhance the therapeutic efficacy in HER2-posiitive breast cancer treatment. PTXNR-TTZ induced high mRNA expression of selected tumorigenic inflammatory genes in MDA-MB-231 cell line which suggests possible causes of drug resistance in triple negative breast cancer cells.

ACKNOWLEDGMENTS

We thank the University of Missouri DNA Core Facility for their technical support with RNAseq analysis. We specially thank Nathan J. Bivens for his tremendous support in this endeavor.

REFERENCES

(1) Jusko, W. J. A pharmacodynamic model for cell-cycle-specific chemotherapeutic agents. Journal of pharmacokinetics and biopharmaceutics 1973, 1, 175-200.

(2) Malhotra, V.; Perry, M. C. Classical chemotherapy: mechanisms, toxicities and the therapeutc window. Cancer biology & therapy 2003, 2, 1-3.

(3) Morgan, G. Chemotherapy and the cell cycle. Cancer Nursing Practice 2003, 2.

(4) Shah, M. A.; Schwartz, G. K. Cell cycle-mediated drug resistance: an emerging concept in cancer therapy. Clinical cancer research 2001, 7, 2168-2181.

(5) Cheung-Ong, K.; Giaever, G.; Nislow, C. DNA-damaging agents in cancer chemotherapy: serendipity and chemical biology. Chemistry & biology 2013, 20, 648-659.

(6) Havelka, A. M.; Berndtsson, M.; Olofsson, M. H.; Shoshan, M. C.; Linder, S. Mechanisms of action of DNA-damaging anticancer drugs in treatment of carcinomas: is acute apoptosis an "off-target" effect? Mini reviews in medicinal chemistry 2007, 7, 1035-1039.

(7) Karran, P. Mechanisms of tolerance to DNA damaging therapeutic drugs. Carcinogenesis 2001, 22, 1931-1937.

(8) Abal, M.; Andreu, J.; Barasoain, I. Taxanes: microtubule and centrosome targets, and cell cycle dependent mechanisms of action. Current cancer drug targets 2003, 3, 193-203.

(9) Evan, G. I.; Brown, L.; Whyte, M.; Harrington, E. Apoptosis and the cell cycle. Current opinion in cell biology 1995, 7, 825-834.

(10) Evan, G. I.; Vousden, K. H. Proliferation, cell cycle and apoptosis in cancer. Nature 2001, 411, 342-348.

(11) King, K. L.; Cidlowski, J. A. Cell cycle and apoptosis: common pathways to life and death. Journal of cellular biochemistry 1995, 58, 175-180.

(12) Maddika, S.; Ande, S. R.; Panigrahi, S.; Paranjothy, T.; Weglarczyk, K.; Zuse, A.; Eshraghi, M.; Manda, K. D.; Wiechec, E.; Los, M. Cell survival, cell death and cell cycle pathways are interconnected: implications for cancer therapy. Drug Resistance Updates 2007, 10, 13-29.

(13) Portt, L.; Norman, G.; Clapp, C.; Greenwood, M.; Greenwood, M. T. Anti-apoptosis and cell survival: a review. Biochimica et Biophysica Acta (BBA)-Molecular Cell Research 2011, 1813, 238-259.

(14) Pucci, B.; Kasten, M.; Giordano, A. Cell cycle and apoptosis. Neoplasia 2000, 2, 291-299.

(15) Vermeulen, K.; Berneman, Z. N.; Van Bockstaele, D. R. Cell cycle and apoptosis. Cell proliferation 2003, 36, 165-175.

(16) Weinberg, R. A.: The biology of cancer; Garland science, 2013.

(17) Besson, A.; Dowdy, S. F.; Roberts, J. M. CDK inhibitors: cell cycle regulators and beyond. Developmental cell 2008, 14, 159-169.

(18) Jacks, T.; Weinberg, R. A. The expanding role of cell cycle regulators. Science 1998, 280, 1035-1036.

(19) Kamb, A. Cell-cycle regulators and cancer. Trends in Genetics 1995, 11, 136-140.

(20) Siegel, R. L.; Miller, K. D.; Jemal, A. Cancer statistics, 2019. CA: a cancer journal for clinicians 2019, 69, 7-34.

(21) Hanahan, D.; Weinberg, R. A. The hallmarks of cancer. cell 2000, 100, 57-70.

(22) Hanahan, D.; Weinberg, R. A. Hallmarks of cancer: the next generation. cell 2011, 144, 646-674.

(23) Davis, J. D.; Lin, S.-Y. DNA damage and breast cancer. World J Clin Oncol 2011, 2, 329.

(24) Harper, J. W.; Elledge, S. J. The DNA damage response: ten years after. Molecular cell 2007, 28, 739-745.

(25) Hosoya, N.; Miyagawa, K. Targeting DNA damage response in cancer therapy. Cancer science 2014, 105, 370-388.

(26) Ljungman, M. Targeting the DNA damage response in cancer. Chemical reviews 2009, 109, 2929-2950.

(27) Collins, I.; Garrett, M. D. Targeting the cell division cycle in cancer: CDK and cell cycle checkpoint kinase inhibitors. Current opinion in pharmacology 2005, 5, 366-373.

(28) Kastan, M. B.; Bartek, J. Cell-cycle checkpoints and cancer. Nature 2004, 432, 316-323.

(29) Weinert, T.; Lydall, D. In Tilte1993.

(30) Aggarwal, B. B.; Vijayalekshmi, R.; Sung, B. Targeting inflammatory pathways for prevention and therapy of cancer: short-term friend, long-term foe. Clinical cancer research 2009, 15, 425-430.

(31) Greten, F. R.; Karin, M. The IKK/NF-κB activation pathway—a target for prevention and treatment of cancer. Cancer letters 2004, 206, 193-199.

(32) Lawrence, T. The nuclear factor NF-κB pathway in inflammation. Cold Spring Harbor perspectives in biology 2009, 1, a001651.

(33) Fedorova, O.; Petukhov, A.; Daks, A.; Shuvalov, O.; Leonova, T.; Vasileva, E.; Aksenov, N.; Melino, G.; Barlev, N. A. Orphan receptor NR4A3 is a novel target of p53 that contributes to apoptosis. Oncogene 2019, 38, 2108-2122.

(34) Liu, S.; Lee, J. S.; Jie, C.; Park, M. H.; Iwakura, Y.; Patel, Y.; Soni, M.; Reisman, D.; Chen, H. HER2 overexpression triggers an IL1α proinflammatory circuit to drive tumorigenesis and promote chemotherapy resistance. Cancer research 2018, 78, 2040-2051.

(35) Wang, D.; Lippard, S. J. Cellular processing of platinum anticancer drugs. Nature reviews Drug discovery 2005, 4, 307-320.

(36) Network, C. G. A. R. Integrated genomic analyses of ovarian carcinoma. Nature 2011, 474, 609.

(37) Garsed, D. W.; Alsop, K.; Fereday, S.; Emmanuel, C.; Kennedy, C. J.; Etemadmoghadam, D.; Gao, B.; Gebski, V.; Garès, V.; Christie, E. L. Homologous recombination DNA repair pathway disruption and retinoblastoma protein loss are associated with exceptional survival in high-grade serous ovarian cancer. Clinical Cancer Research 2018, 24, 569-580.

(38) Zhao, X.-G.; Hu, J.-Y.; Tang, J.; Yi, W.; Zhang, M.-Y.; Deng, R.; Mai, S.-J.; Weng, N.-Q.; Wang, R.-Q.; Liu, J.; Zhang, H.-Z.; He, J.-H.; Wang, H.-Y. miR-665 expression predicts poor survival and promotes tumor metastasis by targeting NR4A3 in breast cancer. Cell Death & Disease 2019, 10, 479.

(39) Kimata, Y.; Baxter, J. E.; Fry, A. M.; Yamano, H. A role for the Fizzy/Cdc20 family of proteins in activation of the APC/C distinct from substrate recruitment. Molecular cell 2008, 32, 576-583.

(40) Penas, C.; Ramachandran, V.; Ayad, N. G. The APC/C ubiquitin ligase: from cell biology to tumorigenesis. Frontiers in oncology 2012, 1, 60.

(41) Wang, L.; Zhang, J.; Wan, L.; Zhou, X.; Wang, Z.; Wei, W. Targeting Cdc20 as a novel cancer therapeutic strategy. Pharmacology & therapeutics 2015, 151, 141-151.

(42) Senft, D.; Qi, J.; Ronai, Z. e. A. Ubiquitin ligases in oncogenic transformation and cancer therapy. Nature Reviews Cancer 2018, 18, 69-88.

(43) Yu, H. Cdc20: a WD40 activator for a cell cycle degradation machine. Molecular cell 2007, 27, 3-16.

(44) Manchado, E.; Guillamot, M.; de Cárcer, G.; Eguren, M.; Trickey, M.; García-Higuera, I.; Moreno, S.; Yamano, H.; Cañamero, M.; Malumbres, M. Targeting mitotic exit leads to tumor regression in vivo: Modulation by Cdk1, Mastl, and the PP2A/B55α, δ phosphatase. Cancer cell 2010, 18, 641-654.

(45) Li, M.; York, J. P.; Zhang, P. Loss of Cdc20 causes a securin-dependent metaphase arrest in two-cell mouse embryos. Molecular and cellular biology 2007, 27, 3481-3488.

(46) Zeng, X.; Sigoillot, F.; Gaur, S.; Choi, S.; Pfaff, K. L.; Oh, D.-C.; Hathaway, N.; Dimova, N.; Cuny, G. D.; King, R. W. Pharmacologic inhibition of the anaphase-promoting complex induces a spindle checkpoint-dependent mitotic arrest in the absence of spindle damage. Cancer cell 2010, 18, 382-395.

(47) Gwon, M.-R.; Cho, J. H.; Kim, J.-R. Mitotic centromere-associated kinase (MCAK/Kif2C) regulates cellular senescence in human primary cells through a p53-dependent pathway. FEBS letters 2012, 586, 4148-4156.

(48) Wang, J.; Ma, S.; Ma, R.; Qu, X.; Liu, W.; Lv, C.; Zhao, S.; Gong, Y. KIF2A silencing inhibits the proliferation and migration of breast cancer cells and correlates with unfavorable prognosis in breast cancer. BMC Cancer 2014, 14, 461.

(49) Andrews, P. D.; Ovechkina, Y.; Morrice, N.; Wagenbach, M.; Duncan, K.; Wordeman, L.; Swedlow, J. R. Aurora B regulates MCAK at the mitotic centromere. Developmental cell 2004, 6, 253-268.

(50) Lan, W.; Zhang, X.; Kline-Smith, S. L.; Rosasco, S. E.; Barrett-Wilt, G. A.; Shabanowitz, J.; Hunt, D. F.; Walczak, C. E.; Stukenberg, P. T. Aurora B phosphorylates centromeric MCAK and regulates its localization and microtubule depolymerization activity. Current Biology 2004, 14, 273-286.

(51) Shimo, A.; Tanikawa, C.; Nishidate, T.; Lin, M. L.; Matsuda, K.; Park, J. H.; Ueki, T.; Ohta, T.; Hirata, K.; Fukuda, M. Involvement of kinesin family member 2C/mitotic centromere-associated kinesin overexpression in mammary carcinogenesis. Cancer science 2008, 99, 62-70.

(52) Higuchi, T.; Uhlmann, F. Passenger acrobatics. Nature 2003, 426, 780-781.

(53) Ci, C.; Tang, B.; Lyu, D.; Liu, W.; Qiang, D.; Ji, X.; Qiu, X.; Chen, L.; Ding, W. Overexpression of CDCA8 promotes the malignant progression of cutaneous melanoma and leads to poor prognosis. International journal of molecular medicine 2019, 43, 404-412.

(54) Cai, Y.; Mei, J.; Xiao, Z.; Xu, B.; Jiang, X.; Zhang, Y.; Zhu, Y. Identification of five hub genes as monitoring biomarkers for breast cancer metastasis in silico. Hereditas 2019, 156, 20.

(55) Iliopoulos, D.; Hirsch, H. A.; Wang, G.; Struhl, K. Inducible formation of breast cancer stem cells and their dynamic equilibrium with non-stem cancer cells via IL6 secretion. Proceedings of the National Academy of Sciences 2011, 108, 1397-1402.

(56) Korkaya, H.; Kim, G.-i.; Davis, A.; Malik, F.; Henry, N. L.; Ithimakin, S.; Quraishi, A. A.; Tawakkol, N.; D'Angelo, R.; Paulson, A. K. Activation of an IL6 inflammatory loop mediates trastuzumab resistance in HER2+ breast cancer by expanding the cancer stem cell population. Molecular cell 2012, 47, 570-584.

(57) Maycotte, P.; Jones, K. L.; Goodall, M. L.; Thorburn, J.; Thorburn, A. Autophagy supports breast cancer stem cell maintenance by regulating IL6 secretion. Molecular cancer research 2015, 13, 651-658.

(58) Ibrahim, S. A.; Hassan, H.; Vilardo, L.; Kumar, S. K.; Kumar, A. V.; Kelsch, R.; Schneider, C.; Kiesel, L.; Eich, H. T.; Zucchi, I. Syndecan-1 (CD138) modulates triple-negative breast cancer stem cell properties via regulation of LRP-6 and IL-6-mediated STAT3 signaling. PloS one 2013, 8, e85737.

(59) Hartman, Z. C.; Poage, G. M.; den Hollander, P.; Tsimelzon, A.; Hill, J.; Panupinthu, N.; Zhang, Y.; Mazumdar, A.; Hilsenbeck, S. G.; Mills, G. B.; Brown, P. H. Growth of Triple-Negative Breast Cancer Cells Relies upon Coordinate Autocrine Expression of the Proinflammatory Cytokines IL-6 and IL-8. Cancer Research 2013, 73, 3470-3480.

IV. POLYMER COATED GOLD-FERRIC OXIDE SUPERPARAMAGNETIC NANOPARTICLES FOR THERANOSTIC APPLICATIONS

ABSTRACT

A multifunctional magnetic nanoparticle (NP) is designed to perform a near-infrared (NIR)-responsive remote control photothermal ablation for the treatment of breast cancer. In contrast to the previously reported studies of gold (Au) magnetic (Fe_3O_4) core-shell nanoparticles (NPs), a Janus-like nanostructure is synthesized with Fe3O4 NPs decorated with Au resulting in an approximate size of 60 nm mean diameter. The surface of trisoctahedral Au–Fe_3O_4 NPs were coated with a positively charged polymer, poly- ι-lysine (PLL) to deliver the NPs inside cells. The PLL coating increased the colloidal stability and robustness of Au–Fe_3O_4 NPs (PLL–Au–Fe_3O_4) in biological media including cell culture medium, phosphate buffered saline (PBS) and PBS with 10% fetal bovine serum. The PLL–Au–Fe_3O_4 NPs were characterized by transmission electron microscopy (TEM), XRD, FT-IR and dynamic light scattering (DLS). The unique properties of both Au surface plasmon resonance and superparamagnetic moment result in a multimodal platform for use as a nanothermal ablator and also as a magnetic resonance imaging (MRI) contrast agent, respectively. Taking advantage of the photothermal therapy, PLL–Au–Fe_3O_4 NPs were incubated with BT-474 and MDA-MB-231 breast cancer cells, investigated for the cytotoxicity and intracellular uptake, and remotely triggered by a NIR laser of ~808 nm (1 W/cm2 for 10 min). It is revealed that no significant (<10%) cytotoxicity was induced by PLL–Au–Fe_3O_4 NPs itself in BT-474

and MDA-MB-231 cells at concentrations up to 100 μg/ml. Brightfield microscopy, fluorescence microscopy and TEM showed significant uptake of PLL–Au–Fe_3O_4 NPs by BT-474 and MDA-MB-231 cells. The cells exhibited 40 and 60% inhibition in BT-474 and MDA-MB-231 cell growth, respectively following the internalized NPs were triggered by a photothermal laser using 100 μg/ml PLL–Au–Fe_3O_4 NPs. The control cells treated with NPs but without laser showed <10% cell death compared to no laser treatment control. Combined together, the results demonstrate a new polymer gold superparamagnetic nanostructure that integrates both diagnostics function and photothermal ablation of tumors into a single multimodal nanoplatform exhibiting a significant cancer cell death.

1. INTRODUCTION

Assembly of the hyperthermia property of superparamagnetic nanoparticles (NPs) with imaging function into a single nanostructure offers a promising way to dynamically monitor the progress of the disease and enhance therapeutic efficacy. Unlike single-component materials, which usually contain only one unique property of the active ingredient, the ingredients of multicomponent materials offer the possibility of multimodal application of these functional components thereby increasing versatility of these materials.[1,2] The development of multicomponent materials as theranostic nanosystems has a potential to establish a new therapeutic mode to combine imaging and hyperthermia, which can greatly increase the therapeutic efficacy with real-time monitoring in tissues. Normal tissues and tumors differ only slightly in relaxation time,

and hence, cannot propagate proper diagnosis signals during magnetic resonance imaging (MRI).[3] The development of new MRI contrast agents based on NPs is a fascinating field of research that focuses on improving MRI techniques for the early detection of disease. Superparamagnetic NPs such as ferric oxide (Fe_3O_4) have been extensively employed as an MRI contrast agent,[4-10] altering the magnetic resonance (MR) signals by reducing the relaxivity through de-phasing of the transverse magnetization.[11,12] A gold (Au) shell coating may be useful in this regard in order to enhance not only the imaging contrasts for MRI but also the photothermal effect *via* the plasmon-derived optical resonances of gold shells in the visible and near-infrared region (NIR).[13] The combination of Au-coated NPs has tremendous potential in improving optical properties, thermal properties, tunable geometry, and imaging contrasts in MRI. As a bifunctional NP, Au–Fe_3O_4 can inherit excellent surface chemistry characteristics, unique optical properties (attributed to Au) and superparamagnetic characteristics attributed to Fe_3O_4. First of all, the NPs offer size controllability, ranging from few to hundreds of nanometers with different and unique size-dependent properties. Second, the NPs can be easily controlled and manipulated from outside with the help of external magnetic field being operated from a distance. Third, the NPs can provide enhanced contrast in medical imaging that can be used to diagnose the situation efficiently. These characteristics would enhance and broaden the application of these nanoparticles for theranostic applications.

While only a few number of Au and magnetic NPs have been approved for clinical and preclinical trials by the U.S. Food and Drug Administration (FDA),[14-17] toxicity of both coated and uncoated magnetic NPs remain a serious concern.[18-21] Both Au and Fe_3O_4 NPs exhibit toxicity to cells *via* numerous mechanisms including the

disruption of cell membrane, DNA damage, induction of oxidative stress, generation of free radicals, impairment of mitochondrial function and alteration in cell signaling among others.[22-24] The toxicity may not be caused by single NP, but rather due to the aggregation of NPs in biological media and serum.[25,26] Given the unstable nature of NP formulation, it is hypothesized that an optimum dose of a cationic polymer coating onto Au–Fe_3O_4 NPs play a role in determining NP configuration on cellular cytotoxicity as well as direct therapy. Coating the surface of Au–Fe_3O_4 NPs with suitable polymers may offer several features: (i) reduced aggregation tendency of the particles; (ii) improved dispersibility; (iii) enhanced colloidal stability; (iv) protected undesirable surface oxidation; (vi) surface conjugation for targeting; (v) decreased cytotoxicity; and (v) increased intracellular uptake by target cells. A charged polymer coating on the NP surface enhances the electrosteric stabilization by attractive and repulsive forces. Poly- ι-lysine (PLL) is a biocompatible polycation that promotes cell adhesion by the presence of amine (–NH_2) groups.[27-29] PLL has been used to increase blood circulation, improve solubility as well as enhance MRI imaging contrasts of gadolinium imaging chelates.[27,29-32] Steric stabilization has proven to be an effective method to improve NP colloidal stability in ionic media.[33] A uniform coating of Fe_3O_4 NPs with polysaccharides leads to a decrease in saturation magnetization as compared to uncoated particles.[34] This drop in saturation magnetization is undesirable due to poor signaling in MRI imaging. Therefore, there is a need for a stable coating on the surface of Au–Fe_3O_4 NPs to prepare colloidal dispersion in biological medium and attain high MRI imaging contrasts.

In this study, multifunctional Au–Fe_3O_4 NPs were designed for medical imaging and hyperthermal treatments of breast cancer cells. To overcome the limitation of

colloidal stability and low dispersity of NPs, a PLL polymeric coating was introduced to the surface of Au–Fe_3O_4 as a physical barrier for preventing NP aggregation as well as enhancing their intracellular uptake by breast cancer cells. Our results showed that the PLL coating on Au–Fe_3O_4 enhanced it stability in biological fluids such as water, phosphate buffered saline (PBS), cell culture medium and PBS containing 10% fetal bovine serum (FBS). PLL coated Au–Fe_3O_4 NPs further enhanced the contrast of MRI imaging signals, exhibited intracellular uptake across the breast cancer cell membrane and decreased the cancer cell viability following photothermal treatment. The novelty of this work is to generate a nanometer-thick PLL layer for the stable dispersion of Au–Fe_3O_4 NPs in biological fluids that results in excellent optical, magnetic and therapeutic properties for the cancer treatment.

2. MATERIALS AND METHODS

2.1. SYNTHESIS OF Au-Fe_3O_4 NPs

The Au–Fe_3O_4 NPs were synthesized by a one-pot synthesis technique based on the method that has been published by Pariti et al.[35] Briefly, the NPs were synthesized by injecting 2.5 mM of $Fe(CO)_5$, 0.25 mM of $HAuCl_4$, 2.5 mM oleic acid, and 2.5 mM of oleylamine into 5 ml of Triton® X-100 at 85 °C. The reaction was conducted for 10 min in a three-neck round bottom flask equipped with a magnetic stir bar and air condenser. The temperature was increased to 300°C. The product was a black precipitate that was isolated from the reaction mixture by magnetic filtration, followed by ultrasonication, centrifugation, and washing to remove excess Triton® X-100 and any unreacted

precursors. The powder collected at the bottom of the centrifuge tube was dried in air. The preparation of Au–Fe_3O_4 NPs was confirmed by XRD analysis using a D/max–2400 diffractometer and CuK radiation (λ = 0.1541 nm).

2.2. POLYMER COATING ON Au-Fe_3O_4 NPs

25 mg of Au-Fe_3O_4 NPs were dispersed in 1 ml of reverse osmosis water. 660 µl of 0.1 % ($\frac{w}{v}$) PLL (Sigma Aldrich, MW: 150000-300000) was added into the NP dispersion and incubated for 24 h at room temperature (~22°C) under continuous shaking. Unbound PLL was removed by centrifuging at 5000×g for 30 min that was repeated twice and measured using the trypan blue assay, spectrophotometry, and a standard curve (SI Figure 1a).[36] The concentration of Au–Fe_3O_4 NPs was determined using a standard curve of the NP absorption at 710 nm peak (SI Figure 1b). The mass ratio of PLL and NPs were calculated. The presence of PLL coating was confirmed by Fourier Transform Infrared (FT-IR) spectroscopy. The FT-IR spectrometer (Perkin-Elmer) was equipped with an Electronic Temperature Control (ETC) EverGlo IR Source and a Deuterated Triglycine Sulfate (DTGS) detector. FT-IR analysis was carried out for uncoated and PLL coated Au–Fe_3O_4 NPs by mixing with potassium bromide (KBr) and a pellet method, after a baseline correction being made with dried KBr, to confirm the compatibility. The pellet was prepared to a pressure of about 5 x 10^6 Pa, in an evacuated chamber, to produce a clear transparent disc of diameter 2 cm and thickness of 0.2 cm. The spectra were recorded at room temperature (~25 °C) from 4000 cm^{-1} to 400 cm^{-1}.

2.3. NANOPARTICLE CHARACTERIZATION

To measure the d_{mean} of Au–Fe_3O_4 and PLL–Au–Fe_3O_4 NPs, transmission electron microscope (TEM) images were obtained using a Tecnai F20 at an accelerating voltage of 120 kV. A drop of 10 µl of each NP sample in water was air-dried on carbon-coated copper grids (Ted Pella). Images were recorded and analyzed using ImageJ (version 1.45S, NIH, USA) to calculate d_{mean} for at least 20 particles. The size distribution of Au–Fe_3O_4 and PLL–Au–Fe_3O_4 NPs was determined by dynamic light scattering (DLS). The zeta potential was measured *via* laser Doppler anemometry using a Zetasizer Nano ZS (Malvern Instruments). Samples were prepared in water, PBS, RPMI 1640 cell culture medium and PBS with 10% FBS. Measurements were performed in triplicates and shown as the mean ± standard deviation (S.D.). The X-ray diffraction (XRD) patterns were performed by a Philips X-Pert X-ray powder diffractometer with CuKa (1.5418 Å) radiation from 5 to 90 degrees. The UV-Vis absorption spectra of Au–Fe_3O_4 and PLL–Au–Fe_3O_4 NPs were measured using a Bio-Tek microplate reader (BioTek Synergy 2) between 400-900 nm. Fourier transform infrared (FT-IR) spectroscopy of Au–Fe_3O_4 and PLL–Au–Fe_3O_4 NPs was carried out using a Perkin Elmer spectrum GX spectrophotometer. Thermal gravimetric analysis (TGA) was performed using a Q50 thermal gravimetric analyzer (TA instruments). The samples were heated from 25°C to 1000°C at a heating rate of 10°C /min under N_2 flow. Results are expressed in weight percent as a function of temperature.

2.4. MRI RELAXOMETRY OF PLL- Au-Fe_3O_4 NPs

To measure the relaxation variables in MRI, Au–Fe_3O_4 NPs coated with PLL (PLL–Au–Fe_3O_4) were prepared in water at 250 μg/ml concentration. All measurements were conducted at room temperature using a Bruker's magnetic relaxometer mq20 (0.47 T) for the spin-spin magnetic relaxation time (T_2) experiments. The specimens were dispersed in PBS and PBS containing 10% FBS at different Au–Fe_3O_4 and PLL–Au–Fe_3O_4 NP concentrations (1, 10 and 100 μg/ml). The proton spin relaxation time, T_2 was measured as a function of the NP concentration.

2.5. CYTOTOXICITY OF PLL- Au-Fe_3O_4 NPs IN BREAST CANCER CELLS

BT-474 and MDA-MB-231 breast cancer cells (ATCC) were cultured at 37°C and 5% CO_2 in Hybri-Care (ATCC) and RPMI 1640 (Life Technologies), respectively supplemented with 10% FBS (Corning) and 1% (100 units/ml) Penicillin-Streptomycin (Gibco). Cells in the exponential growth phase were seeded in a 96-well plate at an initial density of 10,000 cells/ well and incubated overnight. Different concentrations of PLL–Au–Fe_3O_4 NPs (0-500 μg/ml) were added to the cell culture media. After 2 h of incubation, the media was removed, and the cells were washed using PBS followed by re-incubation in cell culture media for additional 72 h. The viable and dead cells were measured using a live–dead (calcein AM; CAM and EthD–1) assay (Invitrogen) and calculated according to the manufacturer's protocol. The cells without any NP treatments were used as the control. The percentage cell death was calculated by the following equation:

$$\% \text{ cell death} = \frac{F_{NPs} - F_{blank}}{F_{control} - F_{blank}} \times 100 \quad (1)$$

Where, F_{NPs} is the Ethd-1 fluorescence of the cells treated with PLL–Au–Fe_3O_4 NPs, F_{blank} is the Ethd-1 fluorescence of the cell culture medium alone, and $F_{control}$ is the Ethd-1 fluorescence of the cells without any NP treatments. The concentration at which cell death was less than 10% was identified as a non-toxic dose.

2.6. INTRACELLULAR UPTAKE OF PLL- Au-Fe_3O_4 NPs

Cellular uptake of PLL–Au–Fe_3O_4 NPs was observed using a Carl Zeiss Axio observer Z1 research microscope system with Apitome.2 optical structuring device. BT-474 and MDA-MB-231cells were seeded in 8-well chambers containing 10,000 cells/well and grown until 70% confluence. PLL–Au–Fe_3O_4 NPs of 100 μg/ml were added to the wells, incubated for 2 h, and washed using PBS for 3 times. Live cells were re-incubated with media and imaged on a Zeiss microscope using a 63x objective (water) through phase contrast. The intracellular uptake of PLL–Au–Fe_3O_4 NPs by BT-474 and MDA-MB-231 cells were further examined by TEM at a voltage of 80 kV. Briefly, cells were seeded in T25 flasks at a density of 1×10^6 cells/ml. After overnight incubation at 37°C and 5% CO_2, the cells were incubated with 100 μg/ml PLL–Au–Fe_3O_4 NPs. After incubation for another 24 h, the medium was carefully removed and cells were washed with PBS for 3 times and fixed at 4°C for 1 h using glutaraldehyde (2.5% in PBS). Then the cells were further subjected to a sequence of treatments to obtain sections that were subsequently mounted onto copper grids before TEM measurements.

2.7. PHOTOTHERMAL TREATMENT OF BREAST CANCER CELLS USING PLL- Au-Fe_3O_4 NPs

A series of specimens with different PLL–Au–Fe_3O_4 NP concentrations (0, 50, 100, 200, 400 and 800 μg/ml) were put into quartz cuvettes and irradiated by an 808 nm laser for 10 min with 1 W/cm^2 power density. An in-situ thermocouple thermometer (Cole-Parmer) was used to record the temperature change. To investigate the *in vitro* photothermal ablation of breast cancer cells, BT-474 and MDA-MB-231 cells were incubated with 100 μg/ml of PLL–Au–Fe_3O_4 NPs in cell culture media for 2 h, washed using PBS (3×) to remove the unbound NPs and re-incubated in the corresponding cell culture media for 72 h. The cells were exposed to NIR light (808 nm pulse laser of 1 W/cm^2 with a diameter of 6 mm for 10 min) to induce photothermal damage. The following control samples were used: cell culture medium, cells without any treatment, and the cells treated with PLL–Au–Fe_3O_4 NPs without any exposure to lasers. After exposure to the NIR light, cells were incubated for an additional 72 h at 37°C. Cell viability was assessed using CAM and EthD-1 (Invitrogen). To further confirm the *in vitro* photothermal ablation of breast cancer cells, cytotoxicity following irradiation was also performed using MTT viability assay (Invitrogen). Briefly, BT-474 and MDA-MB-231 cells were seeded in a 96-well plate at a density of 10,000 cells/well. After overnight incubation at 37°C and 5% CO_2, cells were incubated with PLL–Au–Fe_3O_4 NPs of 0, 50, 100, 200, 400 and 800 μg/ml for 2 h. The medium was replaced with 100 μl of fresh medium. A 10 μl MTT of 5 mg/ml in PBS was added to the medium. Cells were incubated at 37°C for 4 h for labeling cells with MTT. All medium was removed from the well except 25 μl. A 50 μl DMSO was added to each well for dissolving the insoluble

formazan crystals. The absorbance at 540 nm was recorded using a Bio-Tek microplate reader (Synergy 2). Mean and standard deviations of two independent experiments were reported for each sample.

3. STATISTICAL ANALYSIS

Each experiment was carried out with three independent experiments of at least triplicate measurements. The mean differences and standard deviations were evaluated.

4. RESULTS

4.1. SYNTHESIS AND CHARACTERIZATION OF PLL–Au–Fe_3O_4 NPs

TEM images revealed that Au–Fe_3O_4 NPs were uniform and averaged ~55 ± 8.6 nm in diameter (Figure 1a). The thickness of PLL coating on Au–Fe_3O_4 was estimated to be approximately 9 ± 2.5 nm by analyzing the TEM images (Figure 1b and 1c). SI Table 1 shows the amount of PLL coating on Au–Fe_3O_4. The hydrodynamic dimeter of Au–Fe_3O_4 NPs in water as characterized using DLS showed a wide size distribution of Au–Fe_3O_4 dispersions with more than one particle populations and a high polydispersity index (PDI) of 0.856 ± 0.07 (SI Figure 2a). The differences in size between TEM and DLS techniques could be explained by NP agglomeration and the presence of small aggregates. The PLL coating decreased the PDI of Au–Fe_3O_4 NPs from 0.856 to 0.539 ± 0.03 (Table 1). The hydrodynamic diameters of NPs after PLL coating eliminated the large and small particle aggregates in water, PBS, RPMI 1640 cell culture medium and PBS containing 10% FBS indicating a better colloidal stability (SI Figure 2b). The

stability of PLL–Au–Fe_3O_4 NPs was further probed using a time-resolved video (SI Movie File 1). As you can see from this video that Au–Fe_3O_4 NPs without any coating (left hand side tube in the video) precipitate down quickly in water while PLL–Au–Fe_3O_4 NPs (right hand side tube) were stably suspended in black emulsion.

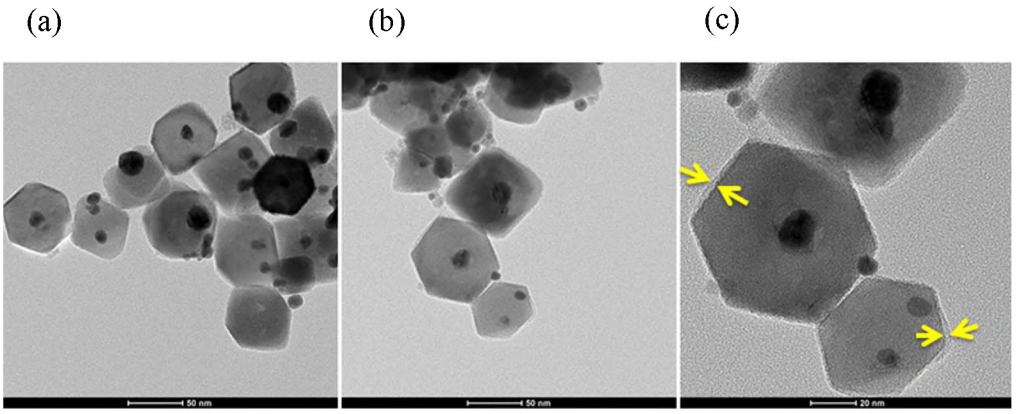

Figure 1. TEM images showing Au–Fe_3O_4 NPs. (a) without, and (b) and (c) with PLL coating. Scale bar = 50 nm in (a) and (b), and 20 nm in (c). The dark black circles indicate Au and the shaded hexagons represent Fe3O4. Arrows in (c) indicate a thin layer of PLL coating

The Au–Fe_3O_4 NPs possess a negative surface charge of -7.9 ± 0.8 mV and -12 ± 7 mV in water and PBS, respectively as determined by zeta potential (Table 1 and Figure 2a). The zeta potentials of Au–Fe_3O_4 NPs increased in cell culture medium and PBS with 10% FBS indicating pronounced differences in the particle surface chemistry caused by different solvent compositions. The PLL coated Au–Fe_3O_4 NPs showed a strong positive charge in water and PBS due to the positive amine groups on the polymer backbone which confirmed the successful grating of PLL polymer on the surface of NPs (Table 1 and Figure 2b). This further confirms that the PLL coating made the NPs disperse better in aqueous solutions and as a result no agglomeration on storage. Particles that are

surface engineered with amine functional groups like PLL has been reported to effective release of encapsulated molecules from endosomal compartments.[37]

Table 1. Characterization of Au–Fe_3O_4 before and after PLL coating

Samples	PDI	ζ-potential (mV) in water	PBS	Cell culture medium	PBS + 10% FBS
Au–Fe_3O_4	0.856 ± 0.07	-7.9 ± 0.8	-12 ± 7	-3.4 ± 5.2	-4.8 ± 2.6
PLL–Au–Fe_3O_4	0.539 ± 0.03	35 ± 10	26 ± 8.5	15.8 ± 9.2	16 ± 6.8

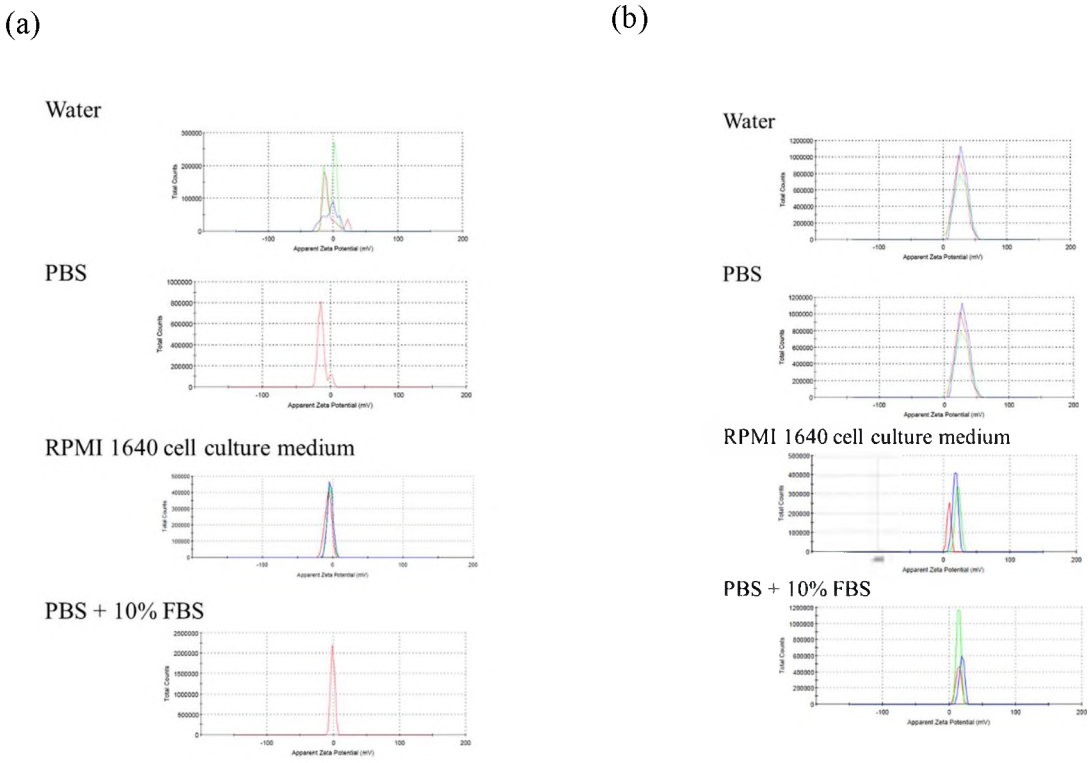

Figure 2. Surface zeta potential. (a) Au–Fe3O4, and (b) PLL–Au–Fe3O4 NPs in water, PBS, RPMI 1640 cell culture medium and PBS containing 10% FBS. Three colored (red, green and blue) lines indicate three replicates from three independent experiments. Multiple peaks in Au–Fe3O4 (a) indicate their aggregation behavior that disappears after PLL coating (b)

The crystal structures of Au–Fe_3O_4 and PLL–Au–Fe_3O_4 NPs were recorded by the X-ray diffraction (XRD), as shown in Figure 3a. The XRD pattern of Fe_3O_4 shows characteristic peaks at (111), (220), (311), (400), (422), (511) and (400) and (111), (220), (220), (311), (222) peaks for Au which is in agreement to the controls of Fe_3O_4–PDF # 65–3107 and Au–PDF # 05–0681, respectively. XRD pattern contains no impurity peak indicating the high purity of Au and Fe_3O_4 samples and perfect phase transformation. The XRD pattern of PLL–Au–Fe_3O_4 NPs has similar diffraction peaks as those of Au–Fe_3O_4 NPs with more peak to noise ratio which could be attributed to PLL polymeric coating.

To confirm the successful synthesis of NPs, UV-Vis absorption and FT-IR spectra were measured. A complete spectra analysis of Au–Fe_3O_4 NPs shows a broad surface plasmon absorption with an absorption maximum at around 710 nm (λ_{max}) (Figure 3b; dotted line).[38] The PLL coating showed an absorption shift to lower wavelengths with an absorption maximum at 640 nm (Figure 3b; solid line). This explains the enhanced dispersion of PLL–Au–Fe_3O_4 NPs in the aqueous phase by redistributing agglomerated Au–Fe_3O_4 NPs.

FT-IR spectra were used to study the transformation of Au–Fe_3O_4 and PLL–Au–Fe_3O_4 NP compositions (Figure 3c). As shown in Figure 3c, the strong absorption peak at about 590 cm^{-1} in the FT-IR of Au–Fe_3O_4 originates from Fe–O stretching of the Fe_3O_4 core. The bare Au- Fe_3O_4 spectrum contains a peak at 1630 cm^{-1} due to water physiosorbed on the iron oxide surface and a broad band around 3400 cm^{-1} due to surface hydroxyl groups (Fe–OH). For PLL–Au–Fe_3O_4 NPs, new and broad absorption bands were observed in the range of 3340 and 3600 cm^{-1}, which were attributed to amine N–H stretching and O–H

stretching, respectively. The peaks at 1647 and 1587 cm^{-1} attributed to to the stretching vibration of C=O from the PLL coating.

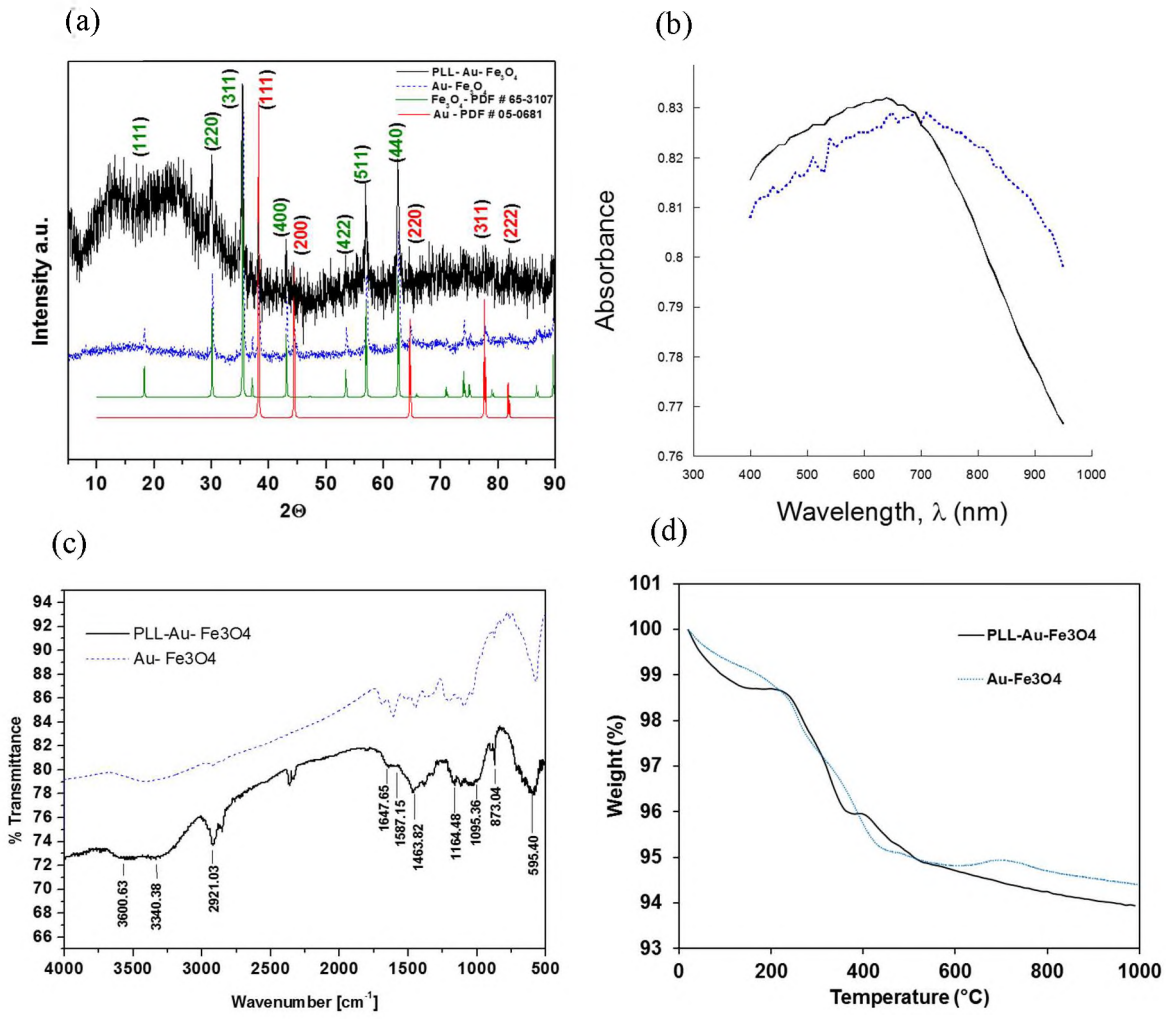

Figure 3.Characterization of PLL–Au–Fe_3O_4 NPs. (a) XRD patterns; (b) Absorption spectra (solid line: PLL–Au–Fe_3O_4 NPs and dotted line: Au–Fe_3O_4 NPs); (c) FT-IR characterization and (d) TGA curves of Au–Fe_3O_4 and PLL–Au–Fe_3O_4 NPs

To quantify the amount of PLL on the surface of PLL–Au–Fe_3O_4 NPs, TGA was performed (Figure 3d). The PLL coating results in a weight loss of 7.4% between 100°C

and 650°C when compared with the uncoated particles (Au–Fe_3O_4). No change in PLL–Au–Fe_3O_4 mass was observed above 850°C. Combinedly, these findings suggest a successful surface functionalization of Au–Fe_3O_4 NPs by PLL polymer coating.

4.2. T_2 MR RELAXIVIITY OF PLL–Au–Fe_3O_4 NPs AS DETERMINED BY MRI

Saturation magnetization value (Ms) and the T_2 relaxation time were analyzed in order to evaluate the magnetic properties of Au–Fe_3O_4 with and without the PLL coating (SI Figure 3). Generally, the spin-spin magnetic relaxation of water protons changes in the presence of magnetic materials in the solution, such as synthesized Au–Fe_3O_4 NPs. This leads to enhance the magnetic property of the solution. Fe_3O_4 NPs are generally used for MR contrast agents because of their capacity to short the T_2 relaxation time of their surrounding protons. As can be clearly seen in SI Figure 3, T_2 was decreased gradually with the increase in NP concentration. The T_2 relaxation time of PLL–Au–Fe_3O_4 NPs was higher than that of Au–Fe_3O_4 NPs due to the fact that the polymer coating displaces the water molecules from the vicinity of the Au–Fe_3O_4 nanocomposite, leading to an increase in the MR values.

4.3. CYTOTOXICITY STUDY BY PLL–Au–Fe_3O_4 NPs AND ITS INTRACELLULAR UPTAKE

Figure 4a shows the cytotoxicity induced by various concentrations of PLL–Au–Fe_3O_4 NPs in BT–474 and MDA–MB–231 cells is dose-dependent. PLL–Au–Fe_3O_4 NPs did not show much cytotoxicity ($\leq$ 20% cell death) at a concentration $\leq$ 100 μg/ml, and hence the concentration was chosen for subsequent studies. To investigate the intracellular uptake of the NPs, phase contrast images were used. It can be seen from

Figure 4b and Figure 4c that the PLL–Au–Fe_3O_4 NPs (black spots as indicated by arrows) entered in the cytoplasm of BT-474 and MDA-MB-231 cells. No black clusters were found in control cells without any NPs indicating the internalization of NPs by the cells. No morphological changes in cellular physiology have been observed when compared to control cells demonstrating negligible cytotoxicity by PLL–Au–Fe_3O_4 NPs. The uptake of PLL–Au–Fe_3O_4 NPs was further evaluated by TEM imaging (SI Figure 4). Clearly, cells treated with NPs show a remarkable distribution inside endoplasmic vesicles of the cells.

(a)

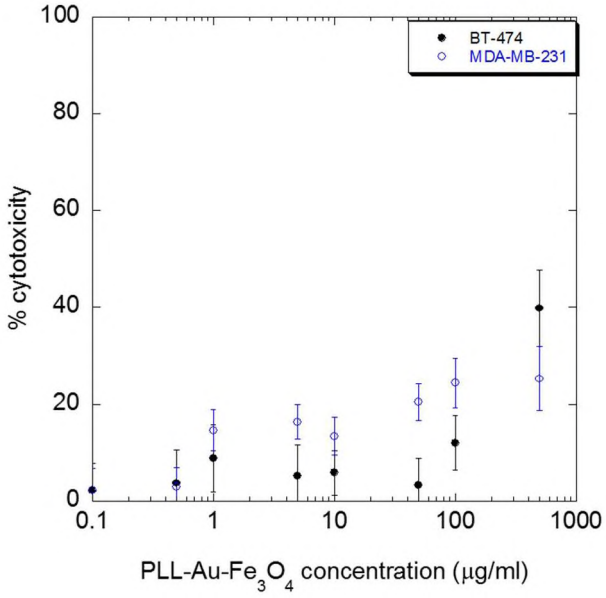

Figure 4.Cytotoxicity and cellular uptake of PLL–Au–Fe_3O_4 NPs. (a) Cytotoxicity of PLL–Au–Fe_3O_4 NPs in BT–474 and MDA–MB–231 cells using live-dead assay at increasing NP concentration; Cellular uptake of PLL–Au–Fe_3O_4 NPs in (b) BT-474 and (c) MDA-MB-231 cells. Arrows indicate the NPs inside cells. Cells without any NP treatment (control) did not show the black NP dots inside cells. Scale bar = 10 µm

(b)

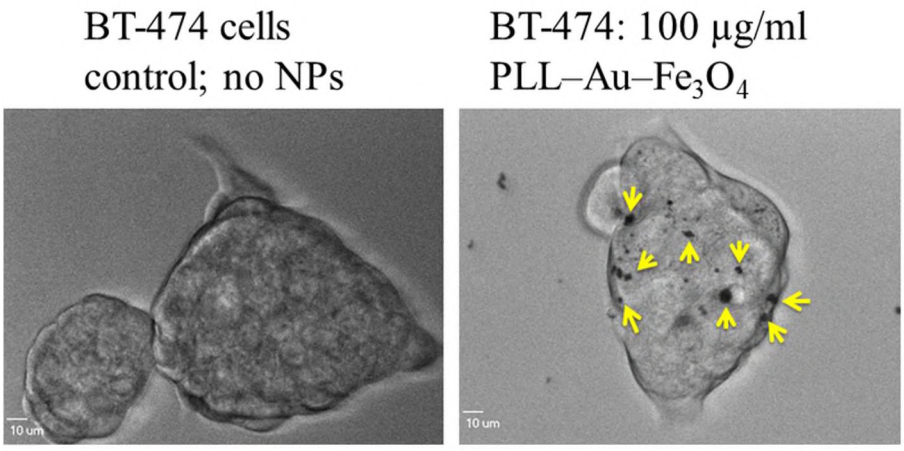

(c)

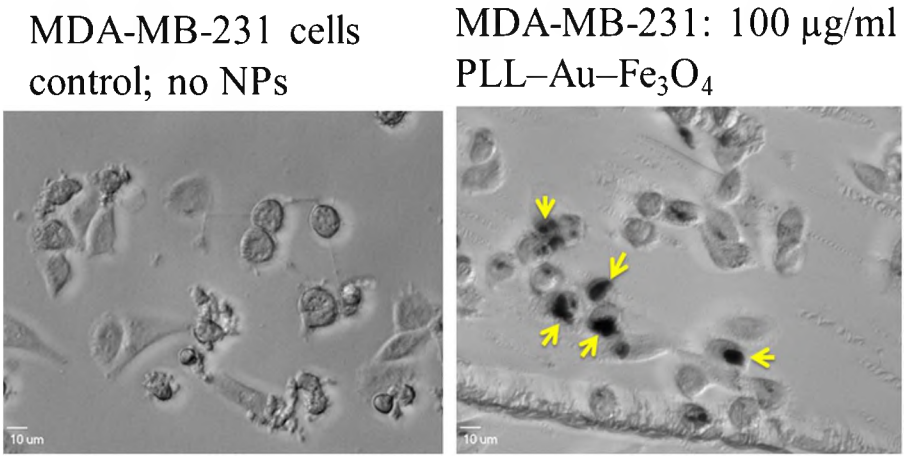

Figure 4.Cytotoxicity and cellular uptake of PLL–Au–Fe_3O_4 NPs.(a) Cytotoxicity of PLL–Au–Fe_3O_4 NPs in BT–474 and MDA–MB–231 cells using live-dead assay at increasing NP concentration; Cellular uptake of PLL–Au–Fe_3O_4 NPs in (b) BT-474 and (c) MDA-MB-231 cells. Arrows indicate the NPs inside cells. Cells without any NP treatment (control) did not show the black NP dots inside cells. Scale bar = 10 µm (cont.)

4.4. PHOTOTHERMAL EFFECTS BY PLL–Au–Fe_3O_4 NPs

In order to investigate, the potential of PLL–Au–Fe_3O_4 as nanothermal ablators, suspensions of the NPs in PBS were irradiated using 808 nm light emitted by a laser. The photothermal behavior of PLL–Au–Fe_3O_4 NPs was investigated by a temperature change

versus the NP concentration (Figure 5). Clearly, the NPs were able to induce a temperature enhancement in a concentration dependent manner.

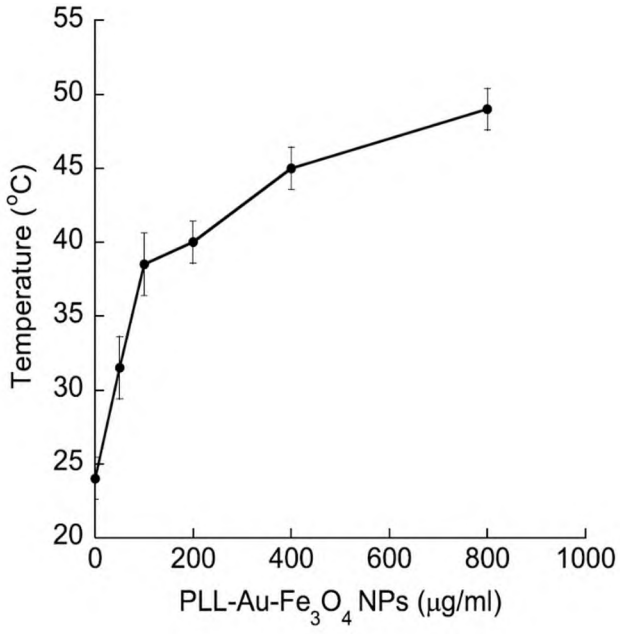

Figure 5. Temperature change of a PBS solution containing PLL–Au–Fe_3O_4 NPs under an 808 nm laser irradiation as a function of different NP concentrations

The temperature of the NP suspension reached 50°C at the PLL–Au–Fe_3O_4 NP concentration of 800 μg/ml. Laser irradiation of PBS negative control without NPs did not show any temperature increase under the same conditions. The results indicate that the synthesized PLL–Au–Fe_3O_4 NPs were able to transform NIR laser into heat under laser irradiation. For laser treatment, BT-474 and MDA-MB-231 cells were first incubated with PLL–Au–Fe_3O_4 NPs for 2 h followed by a wash process to remove un-internalized NPs, laser irradiation for 10 min and then for additional 72 h incubation period. In the control groups (cells + laser irradiation in absence of NPs), no significant

cell death was observed. The cells treated with 100 μg/ml of PLL–Au–Fe_3O_4 NPs but without laser illumination reached 90 ± 4.7% of cell survival rate compared to those treated with PBS control. In contrast, the combination of PLL–Au–Fe_3O_4 NPs and laser treated cells underwent photothermal destruction as shown by both phase contrast and cell viability (green live cells) and dead cell (red stain) staining (Figure 6).

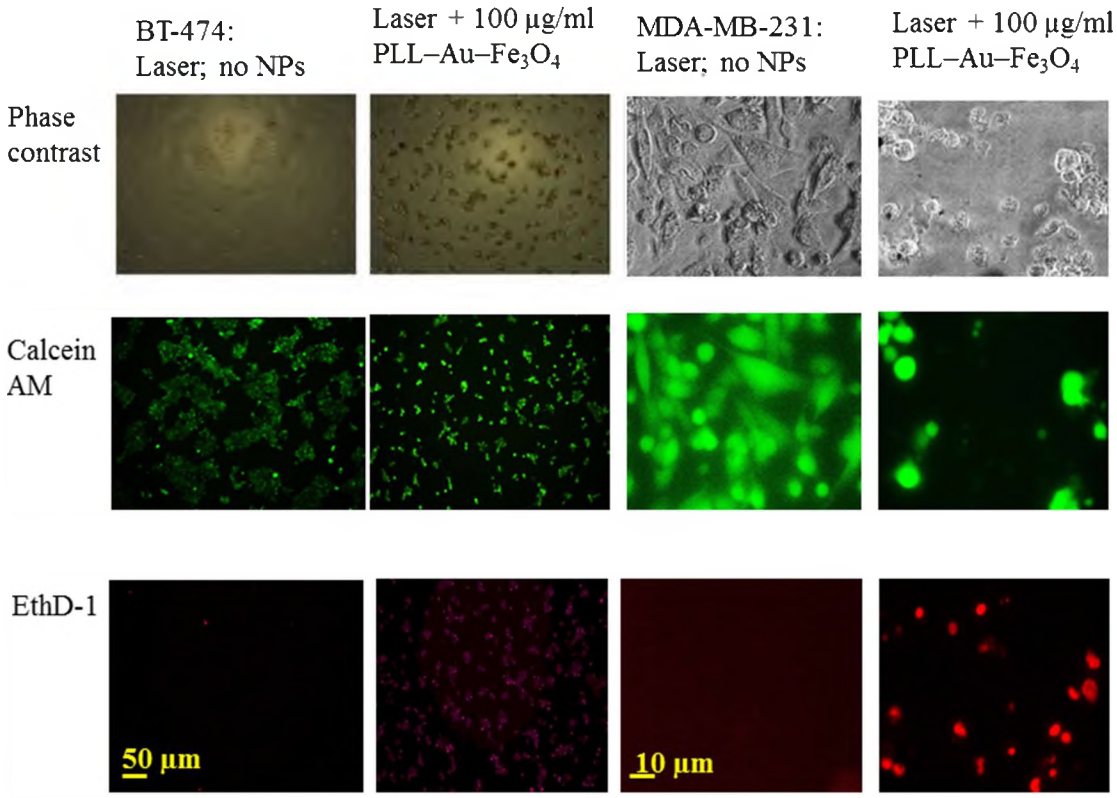

Figure 6. Phase contrast images of PLL–Au–Fe_3O_4 treatment on cancer cells. Phase contrast (row 1) and fluorescence (rows 2 and 3) images of BT-474 and MDA-MB-231 cells treated with 2 h incubation of PLL–Au–Fe_3O_4 followed by 10 min laser irradiation and 72 h of incubation in the medium. Uninternalized NPs were washed with PBS before the imaging. Green fluorescence represents live cells as stained with calcein AM, while the red fluorescence represents dead cells as stained with EthD-1. Scale bars are shown on images

The groups for PLL–Au–Fe_3O_4 NPs + 10 min exposure to laser illumination at 1 W/cm^2 showed the inhibition in cell growth by 49 ± 12% in BT-474 cells (Figure 7; filled circle) and 60 ± 10% in MDA-MB-231 cells (Figure 7; open circle) suggesting significant therapeutic effects following the photothermal treatment. Cells without any treatment, with laser treatment alone and with NP groups showed ≤5% inhibition in cell growth. The cytocompatibility of PLL–Au–Fe_3O_4 NPs was further assessed by MTT cell viability assay (SI Figure 5). The quantitative analysis further reveal that the percentage of cell viability decreased to 63.5 ± 5.5% and 31.6 ± 3.2% in BT-474 and MDA-MB-231 cells, respectively at concentrations ≥10 μg/ml of NPs following laser irradiation.

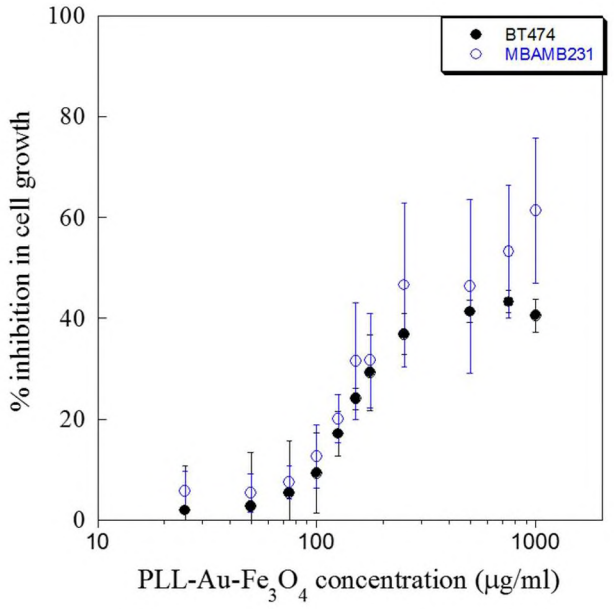

Figure 7. Inhibition of cancer cell growth by PLL–Au–Fe_3O_4 NPs treatment following photothermal therapy. Quantitative assay of BT-474 (solid line; filled circle) and MDA-MB-231 (dotted line; open circle) cell growth inhibition following photothermal therapy in presence of PBS + laser and 100 μg/ml of PLL–Au–Fe_3O_4 NPs. The data represent the average of three independent experiments

5. DISCUSSION

A dumbbell shaped Au–Fe_3O_4 superparamagnetic NPs is synthesized that is similar in morphology to multifaceted Janus particles.[39,40] The structure (Au-decorated Fe_3O_4) is chosen to provide added advantages of both Au and Fe_3O_4 functionalities for the full utilization of their potential. Several Au dots on the Fe_3O_4 host ensures that there is a maximum number of spots for molecular recognition since Au-terminal acts as anchors for targeting agents. Perhaps the most challenging aspect of applying Au–Fe_3O_4 NPs involves the colloidal stability and shelf-life, surface functionalization, cellular internalization, and biocompatibility. Designing a properly grafted surface is therefore of paramount importance. Dextran,[41] PEG,[42] and silica coating[43] have been used extensively, however, each method has its benefits and drawbacks and requires trade-offs and optimizations. For example, although silica coatings can provide colloidal stability, it may also retard R_2 relaxation in MRI imaging, as well dampens the superparamagnetic moment which reduces hyperthermia efficiency. Reduction in the superparamagnetic moment also leads to the necessity for increased dosage of the magnetic NPs. In that regards, the Janus-like particle with larger Fe_3O_4 anchored with several Au dots serves the multifaceted purpose of retaining high superparamagnetic moment over larger size[35] as well as optimizing SPR and photothermal effect of Au. Here, we report a simple and versatile method to adsorb PLL on bare Au–Fe_3O_4 dispersed in aqueous solutions. The polycationic PLL backbone ensures tight coulomb attachment onto anionic surfaces of Au endowing the NP surface with a robust coverage.

This approach can be generalized to many anionic surfaces onto which cationic polymers can adhere tightly, such as glass or silica. The results are comparable with previous studies on Au nanoshells where polymers (*i.e.*, polyethylene imine; PEI) have been used as an intermediate separating layer during the fabrication of Au–Fe_3O_4 where the polymer layer prevents the migration of Au shell into the magnetic core by connecting between the core and shell structure.[44,45] In contrast, we show an outer layer of PLL on the surface of Au–Fe_3O_4 that attribute to the columbic interactions between the Au surface and aliphatic monoamines that is clearly responsible for the observed stability of Au–Fe_3O_4 against aggregation in PBS. The TEM images showed the presence of a layer of PLL of approximately 9 nm thickness. The PLL coating improved the interaction of negatively charged Au–Fe_3O_4 at the cellular level by the resulting surface charge as confirmed by the zeta potential data.

The next step of PLL–Au–Fe_3O_4 involves cell culture experiments that suggest the overall intracellular uptake of the NPs at a non-toxic dose in breast cancer cells. The live/dead assay indicates that PLL–Au–Fe_3O_4 NPs are not cytotoxic in breast cancer cells at concentrations $\leq$100 μg/ml (Figure 5). When compared to other cell viability data of polymer-coated NPs, our results are comparable to the literature data showing 20% reduction in cell viability using similar NP concentrations.[45,46] Furthermore, the results from the phase contrast imaging microscopy demonstrated the effective internalization of the NPs presumably due to the combination of electrostatic interaction with the negatively charged glycocalyx on the cell membrane[47,48] and the receptor-mediated endocytosis *via* EGCG.[49-53] The results are in agreement with the previous finding where Au NPs functionalized with methoxy-PEG-thiol were internalized by MDA-MB-231

cells *via* endocytosis.[54,55] Importantly, the observed uptake of PLL–Au–Fe_3O_4 NPs in breast cancer cells associated with low toxicity suggest a potential theranostic use of these Au NPs. It is worth noting that PLL–Au–Fe_3O_4 had higher levels of uptake in MDA-MB-231 cells than BT-474 cells. The differences in cell surface protein expressions and proteoglycans may attribute to the differential uptake of NPs inside the cells.[56-58] Importantly, the higher observed uptake of PLL–Au–Fe_3O_4 in MDA-MB-231 than BT-474 cells was associated with pronounced toxicity (Figure 5 and 6) suggesting a potential theranostic use of these gold nanoparticles.

Multiple studies have demonstrated the heating effect of Au shell NPs. Thermal ablation using PEG-coated Au nanoshells with silica cores have been reported to induce photothermal morbidity in SK-BR-3 breast cancer cells.[59] The treated cells revealed lost in cell membrane integrity and cell death that was not observed in the controls with laser irradiation or gold nanoshells alone.[59] Photothermal destruction was effective in reducing colon tumors in mice with a mean survival life of 90 days after the treatment.[60] We found that at 100 μg/ml of PLL–Au–Fe_3O_4 and 10 min laser exposure, a ΔT of 15±7.6°C was achieved. The current study reveals the effectiveness of using PLL–Au–Fe_3O_4 as a potent MRI-visible photosensitizer during the laser irradiation of cancer cells.[61-63] The noticeable combination of properties of PLL–Au–Fe_3O_4 with the local application of NIR laser irradiation offers a promising approach for the photothermal ablation therapy of breast cancer cells following internalization inside cells.

6. CONCLUSIONS

A multifunctional NP was constructed using the PLL polymer coating on Au–Fe_3O_4 with a mean diameter of ~60 nm that are less prone to aggregation and thus suitable for a wide range of biological applications. PLL–Au–Fe_3O_4 NPs showed good colloidal stability, NIR light absorption property, magnetic relaxivity and cytocompatibility. Upon exposure to a NIR light, the SPR of Au increased their temperature inside the cells. The PLL–Au–Fe_3O_4 NPs were also demonstrated the importance of having a surface of the polymer layer that enhanced MRI contrast. As an integrated all-in-one NP platform, the polymeric theranostic agent was shown for intracellular uptake and hyperthermal treatments of breast cancer cells for further translational therapeutic applications.

6.1. FUNDING

This research was funded by S.B.'s start-up and ACS PRF 56629-UNI7 to S.S.

ACKNOWLEDGMENTS

For this work, we would like to acknowledge the Environmental Research Center (ERC) and Materials Research Center (MRC) at Missouri S&T for TEM and Zetasizer use. The authors would like to thank Dr. Hai-Lung Tsai of the Department of Mechanical Engineering at Missouri S&T to allow us using their laser facility.

REFERENCES

(1) Key, J.; Park, K. Multicomponent, Tumor-Homing Chitosan Nanoparticles for Cancer Imaging and Therapy. International Journal of Molecular Sciences 2017, 18.

(2) Ma, Y.; Liang, X. L.; Tong, S.; Bao, G.; Ren, Q. S.; Dai, Z. F. Gold Nanoshell Nanomicelles for Potential Magnetic Resonance Imaging, Light-Triggered Drug Release, and Photothermal Therapy. Advanced Functional Materials 2013, 23, 815-822.

(3) Bammer, R.; Skare, S.; Newbould, R.; Liu, C.; Thijs, V.; Ropele, S.; Clayton, D. B.; Krueger, G.; Moseley, M. E.; Glover, G. H. Foundations of Advanced Magnetic Resonance Imaging. NeuroRx 2005, 2, 167-196.

(4) Belyanina, I.; Kolovskaya, O.; Zamay, S.; Gargaun, A.; Zamay, T.; Kichkailo, A. Targeted Magnetic Nanotheranostics of Cancer. Molecules 2017, 22.

(5) Chen, C. W.; Syu, W. J.; Huang, T. C.; Lee, Y. C.; Hsiao, J. K.; Huang, K. Y.; Yu, H. P.; Liao, M. Y.; Lai, P. S. Encapsulation of Au/Fe3O4 nanoparticles into a polymer nanoarchitecture with combined near infrared-triggered chemo-photothermal therapy based on intracellular secondary protein understanding. Journal of Materials Chemistry B 2017, 5, 5774-5782.

(6) Hu, J.; Dehsorkhi, A.; Al-Jamal, W. T.; Zhang, Y.; Chen, S. Y.; Yang, C. Y.; Tan, D.; Zhao, Q.; Yang, C.; Wang, Y. L. Studies on the Photothermal Effect of PEGylated Fe3O4 Nanoparticles. Nanoscience and Nanotechnology Letters 2017, 9, 556-561.

(7) Tang, J. L.; Zhou, H. G.; Liu, J. M.; Liu, J.; Li, W. Q.; Wang, Y. Q.; Hu, F.; Huo, Q.; Li, J. Y.; Liu, Y.; Chen, C. Y. Dual-Mode Imaging-Guided Synergistic Chemo- and Magnetohyperthermia Therapy in a Versatile Nanoplatform To Eliminate Cancer Stem Cells. Acs Applied Materials & Interfaces 2017, 9, 23497-23507.

(8) Wang, Y. X. J.; Idee, J. M. A comprehensive literatures update of clinical researches of superparamagnetic resonance iron oxide nanoparticles for magnetic resonance imaging. Quantitative Imaging in Medicine and Surgery 2017, 7, 88-122.

(9) Yang, H. Y.; Jang, M. S.; Li, Y.; Lee, J. H.; Lee, D. S. Multifunctional and Redox-Responsive Self-Assembled Magnetic Nanovectors for Protein Delivery and Dual-Modal Imaging. Acs Applied Materials & Interfaces 2017, 9, 19184-19192.

(10) Yang, R. M.; Fu, C. P.; Fang, J. Z.; Xu, X. D.; Wei, X. H.; Tang, W. J.; Jiang, X. Q.; Zhang, L. M. Hyaluronan-modified superparamagnetic iron oxide nanoparticles for bimodal breast cancer imaging and photothermal therapy. International Journal of Nanomedicine 2017, 12, 197-206.

(11) Hemery, G.; Garanger, E.; Lecommandoux, S.; Wong, A. D.; Gillies, E. R.; Pedrono, B.; Bayle, T.; Jacob, D.; Sandre, O. Thermosensitive polymer-grafted iron oxide nanoparticles studied by in situ dynamic light backscattering under magnetic hyperthermia. Journal of Physics D-Applied Physics 2015, 48.

(12) Kale, S. S.; Burga, R. A.; Sweeney, E. E.; Zun, Z. H.; Sze, R. W.; Tuesca, A.; Subramony, J. A.; Fernandes, R. Composite iron oxide-Prussian blue nanoparticles for magnetically guided T-1-weighted magnetic resonance imaging and photothermal therapy of tumors. International Journal of Nanomedicine 2017, 12, 6413-6424.

(13) Narayanan, S.; Sathy, B. N.; Mony, U.; Koyakutty, M.; Nair, S. V.; Menon, D. Biocompatible Magnetite/Gold Nanohybrid Contrast Agents via Green Chemistry for MRI and CT Bioimaging. Acs Applied Materials & Interfaces 2012, 4, 251-260.

(14) Salah, E. D. T. A.; Bakr, M. M.; Kamel, H. M.; Abdel, K. M.: Magnetite nanoparticles as a single dose treatment for iron deficiency anemia. Google Patents, 2010.

(15) Thiesen, B.; Jordan, A. Clinical applications of magnetic nanoparticles for hyperthermia. International Journal of Hyperthermia 2008, 24, 467-474.

(16) Bashir, M. R.; Bhatti, L.; Marin, D.; Nelson, R. C. Emerging applications for ferumoxytol as a contrast agent in MRI. Journal of Magnetic Resonance Imaging 2015, 41, 884-898.

(17) Kharlamov, A. N.; Gabinsky, J. L. Plasmonic Photothermic and Stem Cell Therapy of Atherosclerotic Plaque As a Novel Nanotool for Angioplasty and Artery Remodeling. Rejuvenation Research 2012, 15, 222-230.

(18) Pisanic, T. R.; Blackwell, J. D.; Shubayev, V. I.; Fiñones, R. R.; Jin, S. Nanotoxicity of iron oxide nanoparticle internalization in growing neurons. Biomaterials 2007, 28, 2572-2581.

(19) Hanini, A.; Schmitt, A.; Kacem, K.; Chau, F.; Ammar, S.; Gavard, J. Evaluation of iron oxide nanoparticle biocompatibility. International Journal of Nanomedicine 2011, 6, 787-794.

(20) Zhang, X.-D.; Wu, D.; Shen, X.; Liu, P.-X.; Fan, F.-Y.; Fan, S.-J. In vivo renal clearance, biodistribution, toxicity of gold nanoclusters. Biomaterials 2012, 33, 4628-4638.

(21) Siddiqi, N. J.; Abdelhalim, M. A. K.; El-Ansary, A. K.; Alhomida, A. S.; Ong, W. Y. Identification of potential biomarkers of gold nanoparticle toxicity in rat brains. Journal of Neuroinflammation 2012, 9, 123-123.

(22) Joris, F.; Valdeperez, D.; Pelaz, B.; Soenen, S. J.; Manshian, B. B.; Parak, W. J.; De Smedt, S. C.; Raemdonck, K. The impact of species and cell type on the nanosafety profile of iron oxide nanoparticles in neural cells. Journal of Nanobiotechnology 2016, 14.

(23) Lewinski, N.; Colvin, V.; Drezek, R. Cytotoxicity of nanoparticles. Small 2008, 4, 26-49.

(24) Escamilla-Rivera, V.; Uribe-Ramirez, M.; Gonzalez-Pozos, S.; Lozano, O.; Lucas, S.; De Vizcaya-Ruiz, A. Protein corona acts as a protective shield against Fe3O4-PEG inflammation and ROS-induced toxicity in human macrophages. Toxicology Letters 2016, 240, 172-184.

(25) Soenen, S. J.; Rivera-Gil, P.; Montenegro, J.-M.; Parak, W. J.; De Smedt, S. C.; Braeckmans, K. Cellular toxicity of inorganic nanoparticles: Common aspects and guidelines for improved nanotoxicity evaluation. Nano Today 2011, 6, 446-465.

(26) Smith, B. M.; Pike, D. J.; Kelly, M. O.; Nason, J. A. Quantification of Heteroaggregation between Citrate-Stabilized Gold Nanoparticles and Hematite Colloids. Environmental Science & Technology 2015, 49, 12789-12797.

(27) Shiraishi, K.; Kawano, K.; Maitani, Y.; Yokoyama, M. Polyion complex micelle MRI contrast agents from poly(ethylene glycol)-b-poly(l-lysine) block copolymers having Gd-DOTA; preparations and their control of T1-relaxivities and blood circulation characteristics. Journal of Controlled Release 2010, 148, 160-167.

(28) Al-Jamal, K. T.; Al-Jamal, W. T.; Akerman, S.; Podesta, J. E.; Yilmazer, A.; Turton, J. A.; Bianco, A.; Vargesson, N.; Kanthou, C.; Florence, A. T.; Tozer, G. M.; Kostarelos, K. Systemic antiangiogenic activity of cationic poly-L-lysine dendrimer delays tumor growth. Proceedings of the National Academy of Sciences of the United States of America 2010, 107, 3966-3971.

(29) Tunyaboon, L.; Hannah, H. K.; Kelly, D.; Caitlin, B.; Dipak, B.; Daniel, F.; Yue-Wern, H.; Sutapa, B. Bioresponsive polymer coated drug nanorods for breast cancer treatment. Nanotechnology 2017, 28, 045601.

(30) Alconcel, S. N. S.; Baas, A. S.; Maynard, H. D. FDA-approved poly(ethylene glycol)-protein conjugate drugs. Polymer Chemistry 2011, 2, 1442-1448.

(31) Vexler, V. S.; Clément, O.; Schmitt-Willich, H.; Brasch, R. C. Effect of varying the molecular weight of the MR contrast agent Gd-DTPA-polylysine on blood pharmacokinetics and enhancement patterns. Journal of Magnetic Resonance Imaging 1994, 4, 381-388.

(32) Bogdanov, A.; Wright, S. C.; Marecos, E. M.; Bogdanova, A.; Martin, C.; Petherick, P.; Weissleder, R. A long-circulating co-polymer in "passive targeting" to solid tumors. Journal of Drug Targeting 1997, 4, 321-&.

(33) Gref, R.; Lück, M.; Quellec, P.; Marchand, M.; Dellacherie, E.; Harnisch, S.; Blunk, T.; Müller, R. H. 'Stealth' corona-core nanoparticles surface modified by polyethylene glycol (PEG): influences of the corona (PEG chain length and surface density) and of the core composition on phagocytic uptake and plasma protein adsorption. Colloids and Surfaces B: Biointerfaces 2000, 18, 301-313.

(34) Amstad, E.; Zurcher, S.; Mashaghi, A.; Wong, J. Y.; Textor, M.; Reimhult, E. Surface Functionalization of Single Superparamagnetic Iron Oxide Nanoparticles for Targeted Magnetic Resonance Imaging. Small 2009, 5, 1334-1342.

(35) Pariti, A.; Desai, P.; Maddirala, S. K. Y.; Ercal, N.; Katti, K. V.; Liang, X.; Nath, M. Superparamagnetic Au-Fe3O4 nanoparticles: one-pot synthesis, biofunctionalization and toxicity evaluation. Materials Research Express 2014, 1.

(36) Grotzky, A.; Manaka, Y.; Fornera, S.; Willeke, M.; Walde, P. Quantification of [small alpha]-polylysine: a comparison of four UV/Vis spectrophotometric methods. Analytical Methods 2010, 2, 1448-1455.

(37) Luo, R.; Mutukumaraswamy, S.; Venkatraman, S. S.; Neu, B. Engineering of erythrocyte-based drug carriers: control of protein release and bioactivity. Journal of Materials Science: Materials in Medicine 2012, 23, 63-71.

(38) Lou, L.; Yu, K.; Zhang, Z.; Huang, R.; Wang, Y.; Zhu, Z. Facile methods for synthesis of core–shell structured and heterostructured Fe3O4@Au nanocomposites. Applied Surface Science 2012, 258, 8521-8526.

(39) Lattuada, M.; Hatton, T. A. Synthesis, properties and applications of Janus nanoparticles. Nano Today 2011, 6, 286-308.

(40) Perro, A.; Reculusa, S.; Ravaine, S.; Bourgeat-Lami, E.; Duguet, E. Design and synthesis of Janus micro- and nanoparticles. Journal of Materials Chemistry 2005, 15, 3745-3760.

(41) Li, W.; Tutton, S.; Vu, A. T.; Pierchala, L.; Li, B. S. Y.; Lewis, J. M.; Prasad, P. V.; Edelman, R. R. First-pass contrast-enhanced magnetic resonance angiography in humans using ferumoxytol, a novel ultrasmall superparamagnetic iron oxide (USPIO)-based blood pool agent. Journal of Magnetic Resonance Imaging 2005, 21, 46-52.

(42) Shen, J. W.; Li, K. Y.; Cheng, L.; Liu, Z.; Lee, S. T.; Liu, J. Specific Detection and Simultaneously Localized Photothermal Treatment of Cancer Cells Using Layer-by-Layer Assembled Multifunctional Nanoparticles. Acs Applied Materials & Interfaces 2014, 6, 6443-6452.

(43) Pinho, S. L. C.; Pereira, G. A.; Voisin, P.; Kassem, J.; Bouchaud, V.; Etienne, L.; Peters, J. A.; Carlos, L.; Mornet, S.; Geraldes, C. F. G. C.; Rocha, J.; Delville, M.-H. Fine Tuning of the Relaxometry of γ-Fe2O3@SiO2 Nanoparticles by Tweaking the Silica Coating Thickness. ACS Nano 2010, 4, 5339-5349.

(44) Goon, I. Y.; Lai, L. M. H.; Lim, M.; Munroe, P.; Gooding, J. J.; Amal, R. Fabrication and Dispersion of Gold-Shell-Protected Magnetite Nanoparticles: Systematic Control Using Polyethyleneimine. Chemistry of Materials 2009, 21, 673-681.

(45) Hoskins, C.; Min, Y.; Gueorguieva, M.; McDougall, C.; Volovick, A.; Prentice, P.; Wang, Z.; Melzer, A.; Cuschieri, A.; Wang, L. Hybrid gold-iron oxide nanoparticles as a multifunctional platform for biomedical application. Journal of Nanobiotechnology 2012, 10, 27.

(46) Hoskins, C.; Cuschieri, A.; Wang, L. The cytotoxicity of polycationic iron oxide nanoparticles: Common endpoint assays and alternative approaches for improved understanding of cellular response mechanism. Journal of Nanobiotechnology 2012, 10, 15.

(47) Schweiger, C.; Hartmann, R.; Zhang, F.; Parak, W. J.; Kissel, T. H.; Rivera_Gil, P. Quantification of the internalization patterns of superparamagnetic iron oxide nanoparticles with opposite charge. Journal of Nanobiotechnology 2012, 10, 28.

(48) Ojea-Jiménez, I.; García-Fernández, L.; Lorenzo, J.; Puntes, V. F. Facile preparation of cationic gold nanoparticle-bioconjugates for cell penetration and nuclear targeting. ACS Nano 2012, 6, 7692-7702.

(49) Ahmad, N.; Feyes, D. K.; Agarwal, R.; Mukhtar, H.; Nieminen, A.-L. Green Tea Constituent Epigallocatechin-3-Gallate and Induction of Apoptosis and Cell Cycle Arrest in Human Carcinoma Cells. JNCI: Journal of the National Cancer Institute 1997, 89, 1881-1886.

(50) Liang, Y.-C.; Lin-shiau, S.-Y.; Chen, C.-F.; Lin, J.-K. Suppression of extracellular signals and cell proliferation through EGF receptor binding by (−)-epigallocatechin gallate in human A431 epidermoid carcinoma cells. Journal of Cellular Biochemistry 1997, 67, 55-65.

(51) Pianetti, S.; Guo, S.; Kavanagh, K. T.; Sonenshein, G. E. Green Tea Polyphenol Epigallocatechin-3 Gallate Inhibits Her-2/Neu Signaling, Proliferation, and Transformed Phenotype of Breast Cancer Cells. Cancer Research 2002, 62, 652-655.

(52) Tachibana, H.; Koga, K.; Fujimura, Y.; Yamada, K. A receptor for green tea polyphenol EGCG. Nature Structural &Amp; Molecular Biology 2004, 11, 380.

(53) Shukla, R.; Chanda, N.; Zambre, A.; Upendran, A.; Katti, K.; Kulkarni, R. R.; Nune, S. K.; Casteel, S. W.; Smith, C. J.; Vimal, J.; Boote, E.; Robertson, J. D.; Kan, P.; Engelbrecht, H.; Watkinson, L. D.; Carmack, T. L.; Lever, J. R.; Cutler, C. S.; Caldwell, C.; Kannan, R.; Katti, K. V. Laminin receptor specific therapeutic gold nanoparticles (198AuNP-EGCg) show efficacy in treating prostate cancer. Proceedings of the National Academy of Sciences 2012, 109, 12426-12431.

(54) Shukla, R.; Bansal, V.; Chaudhary, M.; Basu, A.; Bhonde, R. R.; Sastry, M. Biocompatibility of Gold Nanoparticles and Their Endocytotic Fate Inside the Cellular Compartment: A Microscopic Overview. Langmuir 2005, 21, 10644-10654.

(55) Shenoy, D.; Fu, W.; Li, J.; Crasto, C.; Jones, G.; DiMarzio, C.; Sridhar, S.; Amiji, M. Surface functionalization of gold nanoparticles using hetero-bifunctional poly(ethylene glycol) spacer for intracellular tracking and delivery. International Journal of Nanomedicine 2006, 1, 51-57.

(56) Holliday, D. L.; Speirs, V. Choosing the right cell line for breast cancer research. Breast Cancer Research 2011, 13, 215.

(57) Sheridan, C.; Kishimoto, H.; Fuchs, R. K.; Mehrotra, S.; Bhat-Nakshatri, P.; Turner, C. H.; Goulet, R.; Badve, S.; Nakshatri, H. CD44+/CD24-breast cancer cells exhibit enhanced invasive properties: an early step necessary for metastasis. Breast Cancer Research 2006, 8, R59.

(58) Lacroix, M.; Leclercq, G. Relevance of Breast Cancer Cell Lines as Models for Breast Tumours: An Update. Breast Cancer Research and Treatment 2004, 83, 249-289.

(59) Hirsch, L. R.; Stafford, R. J.; Bankson, J. A.; Sershen, S. R.; Rivera, B.; Price, R. E.; Hazle, J. D.; Halas, N. J.; West, J. L. Nanoshell-mediated near-infrared thermal therapy of tumors under magnetic resonance guidance. Proceedings of the National Academy of Sciences 2003, 100, 13549-13554.

(60) Hirsch, L. R.; Gobin, A. M.; Lowery, A. R.; Tam, F.; Drezek, R. A.; Halas, N. J.; West, J. L. Metal Nanoshells. Annals of Biomedical Engineering 2006, 34, 15-22.

(61) Sciortino, F.; Casterou, G.; Eliat, P. A.; Troadec, M. B.; Gaillard, C.; Chevance, S.; Kahn, M. L.; Gauffre, F. Simple Engineering of Polymer-Nanoparticle Hybrid Nanocapsules. Chemnanomat 2016, 2, 796-799.

(62) Ma, Y.; Huang, W.; Liu, C.; Li, Y.; Xia, Y.; Yang, X.; Sun, W.; Bai, H.; Li, Q.; Peng, Z. Immunization against TGF-beta1 reduces collagen deposition but increases sustained inflammation in a murine asthma model. Human vaccines & immunotherapeutics 2016, 12, 1876-1885.

(63) Hoskins, C.; Min, Y.; Gueorguieva, M.; McDougall, C.; Volovick, A.; Prentice, P.; Wang, Z. G.; Melzer, A.; Cuschieri, A.; Wang, L. J. Hybrid gold-iron oxide nanoparticles as a multifunctional platform for biomedical application. Journal of Nanobiotechnology 2012, 10.

V. ISOLATION AND PURIFICATION OF GLYCOGLYCEROLIPIDS TO INDUCE APOPTOSIS IN BREAST CANCER CELLS

ABSTRACT

Monogalactosyldiacylglycerol (MGDG) is the most abundant type of glycoglycerolipid found in the plant cell membrane and mostly in the chloroplast thylakoid membrane. The amphiphilic nature of MGDG is attractive in pharmaceutical fields for interaction with other biological molecules and hence exerting therapeutic anti-cancer, anti-viral, and anti-inflammatory activities. In this study, we investigated the therapeutic efficacy of cyanobacteria derived MGDG to inhibit breast cancer cell growth. MGDG was extracted from a cyanobacteria *Synechocystis* sp. PCC 6803 followed by a subsequent fractionation by column chromatographic technique. The purity and molecular structure of MGDG were analyzed by nuclear magnetic resonance (NMR) spectroscopy analysis. The presence of MGDG in the extracted fraction was further confirmed and quantified by high-performance liquid chromatography (HPLC). The anti-proliferation activity of the extracted MGDG molecule was tested against BT-474 and MDA-MB-231 breast cancer cell lines. The in vitro study showed that MGDG extracted from *Synechocystis* sp. PCC 6803 induced apoptosis in (70 ± 8) % of BT-474 ($p<0.001$) and (58 ± 5) % of MDA-MB-231 cells ($p <0.001$) using ~60 and 200 ng/ml of concentrations, respectively. The half-maximal inhibitory concentration, IC50 of MGDG extracted from *Synechocystis* sp. PCC 6803 were (27.2 ± 7.6) and (150 ± 70) ng/ml in BT-474 and MDA-MB-231 cell lines, respectively. Quantification of caspase-3/7 activity

showed 2.3 and 2.1-fold ($p<0.01$) higher protein expressions in the MGDG treated BT-474 and MDA-MB-231 cells, respectively than untreated controls conferring to the caspase-dependent apoptosis. The MGDG did not show any significant cytotoxic side effects in human dermal fibroblasts cells. A commercially available MGDG control did not induce any apoptotic cell death in cancer cells substantiating the potential of the MGDG extracted from *Synechocystis* sp. PCC 6803 for the treatment of breast cancer cells through the apoptosis-mediated pathway.

1. INTRODUCTION

Glycoglycerolipids (GGLs) are natural products abundantly found in the cell membrane of marine algae,[1,2] cyanobacteria,[3,4] and higher plants,[5-9] with one or two carbohydrate units, glycerol, and diversified acyl lipid groups.[9,10] GGLs are conserved in both gram-negative and gram-positive bacteria, *i.e.*, *Bacillus pumilus*,[11] *Lactobacillus plantarum*,[12] *Microbacterium* sp.,[13] *Micrococcus luteus*,[14] and *Phormidium tenue*[15] with highly conserved structures. The amphiphilic nature of GGLs is attractive in pharmaceutical fields for interaction with other biological molecules and hence exerting therapeutic anti-cancer,[16-18] anti-viral,[19,20] and anti-inflammatory activities.[21,22] GGLs potently inhibit angiogenesis,[23] cancer cells,[16] and solid tumor[18,24,25] growth by selectively inhibiting the replicative DNA polymerase activity both *in vitro* and *in vivo*.[17,18,25] Monogalactosyl diacylglycerol (MGDG), a GGL isolated from spinach, combined with gemcitabine anti-cancer drug revealed synergistic effects of inhibitive proliferation on human pancreatic cancer cell lines BxPC-3, MiaPaCa2, and PANC-1

through the inhibition of DNA replicative pols alpha and gamma activities, compared with MGDG or gemcitabine alone.[26] The fractions of GGLs *e.g.,* MGDG, digalactosyl diacylglycerol (DGDG), and sulfoquinovosyl diacylglycerol (SQDG) in spinach potently affect *in vitro* colon cancer cells, angiogenesis, and solid tumor growth *via* their inhibitory activities of DNA polymerase.[18,23-25] Naturally occurring sulfoquinovosylglycerolipids show promising anti-proliferative activity toward human cancer cells not only by targeting DNA polymerases,[27] but also inhibiting the mitotic centromere-associated kinesin (MCAK).[17] Another interesting feature of these compounds is their involvement in cell recognition and signaling which make them promising agents in drug delivery systems.[28] Several GGLs have been related to the activation of natural killer T cells, which is a central event in a variety of immune responses including the development of autoimmunity, tolerance, and maintenance in defense responses to tumors and infectious agents.[29] A series of sulfonic acid-containing GGLs isolated from cultured cyanobacteria (blue-green algae) have been discovered as a new class of compounds to inhibit the cytopathic effects of the human immunodeficiency virus (HIV-1).[20] The high potential of GGL therapy strategy has attracted great interest in recent years and thus is explored to evaluate its therapeutic efficiency for the treatment of breast cancer cells.

We investigated the anti-proliferative efficacy of marine cyanobacterium *Synechocystis* sp. derived MGDG molecule on human epidermal growth factor receptor-2 (HER2)-positive BT-474, MDA-MB-231 triple-negative breast cancer cells, and human dermal fibroblasts. MGDG molecule is more abundantly and predominantly present in cyanobacterial cell chloroplast membrane than in plant sources. MGDG constitutes

nearly 60% of the chloroplast lipid in *Synechocystis* sp. cyanobacterial cells. *Synechocystis* sp. PCC 6803 was chosen because monogalactosyldiacylglycerol (MGDG) from this strain contains 18:3 fatty acid residues making it a more lipophilic molecule than other polar MGDG molecules with 16:0 carbon fatty acid residues.[30] This characteristic of glycoglycerolipids from *Synechocystis* sp. PCC 6803 would catalyze the intracellular uptake and high biological activation to induce apoptosis in breast cancer cells. Polyunsaturated fatty acids containing 18:3 γ- linolenic acid (GLA) showed higher apoptosis in various cancer cells (cervical, gastric, and prostate cancers) than normal cells both *in vitro* and *in vivo* by generating reactive oxygen species, suppressing angiogenesis *via* Akt cell signaling pathway and inducing apoptosis.[31-34] . The plant-derived MGDG molecule abundantly contains 18:3 α- linolenic acid (n-3 ALA) on average at the sn-1 fatty acid chain. The plant extract MGDG or n-3 ALA, a member of ω-3 fatty acids, and its active metabolites have known anti-cancer activity. However, the treatment efficacy is limited by the higher dosage requirement for inducing apoptosis and cell death posing off-target toxicity to the healthier cells. In contrast, the marine cyanobacteria *Synechocystis* sp. derived MGDG molecule predominantly contains 18:3 n-6 GLA at the sn-1 fatty acid chain. The n-6 GLA molecule, a member of the ω-6 fatty acids selectively inhibits breast tumor cells without affecting the healthy cells[35,36]. Moreover, the n-6 GLA molecule has been shown to sensitize breast cancer cells to antimitotic and endocrine therapeutic drugs *in vitro*. Hence, the cyanobacteria derived MGDG molecule is of great interest in the current study. We separated MGDG with high purity from the total lipid extract of *Synechocystis* sp. PCC 6803 cyanobacterial cells. In this study, we comparatively investigated the anti-proliferative and apoptosis induction efficacy of the

cyanobacterial extract MGDG with high n-6 GLA content and plant extract n-3 ALA-rich pure MGDG in BT-474 and MDA-MB-231 breast cancer cells.

2. MATERIALS AND METHODS

2.1. GROWTH KINETICS OF *Synechocystis* sp. PCC 6803

Synechocystis sp. PCC 6803 was a kind donation from Dr. Himadri Pakrasi's laboratory at Washington University in St. Louis.[9,37-40] The *Synechocystis* sp. was cultured in batch cultures of 10 ml solid and 250 ml liquid BG11 media at 30°C and 300 rpm in a rotary shaker under 30 μmol/m^2/s (~2200 Lux) fluorescent lamps [41]. Fluorescence microscopic images of PCC 6803 and the corresponding spectra analysis were captured using a scanning laser inverted confocal microscope (Ti-Eclipse; Nikon). For the growth curve analysis, the species was inoculated in a 5 ml liquid BG11 media. 150 μl aliquots of liquid samples were transferred to a 96 well plate (Corning) at different times to measure the growth kinetics of PCC 6803 after adjusting the initial absorbance at 680 nm, $A_{680,0}$= 0.05 at 24 h. BG11 media alone without any inoculum was used as a negative control. The maximum absorbance at the wavelength of 680 nm was measured using a microplate reader (BioTek). The specific growth rate, α was computed using Equation (3).

$$\frac{dA_{680}}{dt} = \alpha N \tag{1}$$

Where A_{680} is the absorbance of cells at time, t. By integrating Equation (1) from $t = 0$ to $t = t$,

$$ln\frac{A_{680_t}}{A_{680_0}} = \alpha(t - t_0) \quad (2)$$

$$\alpha = \frac{ln\frac{A_{680_t}}{A_{680_0}}}{(t - t_0)} \quad (3)$$

The doubling time, t_d is calculated using Equation (4):

$$t_d = \frac{0.693}{\alpha} \quad (4)$$

2.2. TOTAL LIPID EXTRACTION FROM *Synechocystis* Sp. PCC 6803

The total lipid was extracted from the *Synechocystis* sp. using the Bligh and Dyer Method [42]. Cell pellets from 250 ml of culture were collected at $A_{680,t}$= 3.0 after 120 h, centrifuged at 15,000 g for 15 min and suspended in deionized water for two times to remove residual medium. One ml of cell suspension was mixed with 3.75 ml of chloroform: methanol (1:2, v/v) solution for 15 min using a vortex mixer. After thorough mixing, 1.25 ml of chloroform was added and vortexed for 1 min. Two distinctive layers were obtained after adding 1.25 ml of water to the mixture. The chloroform layer (lower phase) contained all the lipids, and the aqueous methanol layer (upper phase) contained the non-lipid fractions. The upper phase was discarded carefully, and the lower phase was collected. Chloroform was then evaporated completely under vacuum in a fume hood to obtain the total lipid. Total lipid was reconstituted in 1 ml of chloroform and stored in -20° C.

2.3. SEPARATION OF MGDG USING COLUMN CHROMATOGRAPHY

Total lipid was fractionated using the normal phase column chromatography technique. A handmade column was used for the separation process (SI Figure 1 (a)). Silica gel (particle size 10-40 micron) particles were used as a stationary phase. Chloroform and acetone were used as mobile phases. A gradient elution method was applied for the fractionation (SI Table 1). Samples (A-K) were collected for each combination of the eluent and labeled for further detection, structural analysis, and quantification (SI Figure 1 (b)).

2.4. IDENTIFICATION OF MGDG USING NMR ANALYSIS

The presence of the MGDG molecule in the eluted fractions was investigated using ^{1}H NMR analysis. Each of the eluted fractions was analyzed to investigate the presence of MGDG molecule. The plant extract standard MGDG molecule was used as a reference. MGDG (> 99% purity, MW: 752.369) was purchased from Avanti Polar Lipids Inc. Chloroform-d ($CDCl_3$) was chosen both as the reference and the solvent for NMR analysis. The NMR peaks have been interpreted from the lipid handbook NMR database [43] and the previous studies on structural analysis of plant-derived GGLs [44,45].

2.5. QUANTITATIVE ANALYSIS OF MGDG USING HPLC-UV

The extracted MGDG molecule was both detected and quantified using a HPLC-UV system. The following instruments and solvents were used for chromatographic analysis. Column: LiChrospher 100 Diol (particle size: 5 µm, column size: 250 ×4 mm) (Millipore Sigma), guard column: LiChroCart 4-4, mobile phase: chloroform (solvent A),

methanol-water (95:5) (solvent B), detector: UV, injection volume: 20-25 µL, flow rate: 1 ml/min. The MGDG molecule was detected by the UV detector at 240 nm. The gradient elution method used in HPLC is shown in SI Table 2 and SI Table 3 [46]. A calibration curve was developed correlating the peak areas against the increasing concentrations of plant extract standard MGDG. The peak areas corresponding to the known concentrations of standard MGDG are shown in SI Table 4.

2.6. *IN VITRO* THERAPEUTIC EFFICACY

BT-474, MDA-MB-231, and human dermal fibroblast cells (ATCC) were cultured in Hybri-care ATCC 46-X medium, RPMI 1640, and fibroblast growth factor supplemented basal medium (ATCC), respectively, supplemented with 10% fetal bovine serum (FBS) and 1% penicillin-streptomycin at 37°C and 5% CO_2. Approximately, 10,000 cells per well were plated in 96-well plates and treated with 0-200 ng/ml doses of standard MGDG and extracted MGDG from *Synechocystis* sp. by column chromatography technique. To examine the cytotoxicity effects on human dermal fibroblasts, the cells were treated with 100 ng/ml of MGDG extracted from *Synechocystis* sp. and MGDG standard. After 72 h of incubation, cell viability was assessed using MTT (3-(4, 5-dimethylthiazol-2-yl)-2, 5-diphenyltetrazolium bromide, MW 414) assay. MTT reagent was added to each well to convert into an insoluble formazan from water-soluble MTT. After 4 h, sodium dodecyl sulfate (SDS) solution prepared in 0.01 N HCl was added to each well to solubilize the formazan. The percentage of live cells proportional to the absorbance value of solubilized formazan solution was quantified by measuring the absorbance at 570 nm (BioTek Synergy 2). The absorbance value was adjusted by

subtracting the mean absorbance level of wells containing medium only. Cell viability was calculated as a means of six wells containing BT-474, MDA-MB-231, and dermal fibroblast cells. The cells treated with PBS were used as live control that was placed in every alternative column in the well plate adjacent to corresponding dosage or treatments to remove the variability in the number of seeded cells in adjacent wells. The live controls were replicated at least six times for each dosage. For dead control, we treated the cells with saponin in at least six replicates. The % cell viability was calculated as follows Equation (5):

$$\%\ cell\ viability = \frac{A_{570\ of\ sample} - A_{570\ of\ medium}}{A_{570\ of\ live\ cells} - A_{570\ of\ medium}} \times 100 \quad (5)$$

2.7. APOPTOSIS ASSAY

The BT-474 and MDA-MB-231 cells were investigated for the caspase-dependent apoptosis mechanism by staining for the cleaved or active form of caspase-3/7 marker fluorescence dye. The cells at a density of 10,000 cells/ml were seeded in 96 well plates in replicates of at least n=3. The cells were treated with MGDG extracted from *Synechocystis* sp. PCC 6803 and MGDG standard and were incubated for 48 and 72 h. The cells treated with PBS were used as live control with at least three replicates. After incubation, cells were stained with green fluorescent active caspase-3/7 marker (Invitrogen). The cells were imaged in the phase contrast field along with green fluorescent signals using a Zeiss Apotome 2.0 microscope equipped with a 10X objective, 470/40 excitation filter, and 525/50 nm emission filter. To quantify the caspase-3/7 protein expression, 50,000 each of BT-474 and MDA-MB-231 cells were treated with 100 ng/ml of MGDG. After 48 and 72 h of incubation, cells were washed

twice using 100 µl of PBS and stained with 5 µM of caspase-3/7 green fluorescence apoptosis marker in 100 µl of the respective medium. The cells were incubated for 30-45 minutes at 37°C. The fluorescence data was detected for 20,000 events/sample and acquired using a flow cytometer (BD Accuri C6 plus). The bandpass filters used in the flow cytometry were 530/30 and 585/40, respectively. The laser excitation wavelength was 488 nm.

2.8. STATISTICAL ANALYSIS

Each experiment was carried out in independent repetitions to have at least triplicates valid measurements. The results were reported as mean ± standard deviation and analyzed using the Student's t-tests with two-tailed hypotheses and using the JMP statistical software (version 15, SAS Institute). For toxicity analysis, $P<0.001$ was considered as statistically significant and was denoted by ***. For quantification of apoptosis assay in flow cytometry, $p<0.01$ was considered statistically significant and was denoted by ***.

3. RESULTS

3.1. *Synechocystis* sp. GROWTH CURVE KINETICS AND MOLECULAR STRUCTURE OF MGDG

Figure 1 demonstrates the confocal fluorescence images and fluorescence emission spectra analysis of *Synechocystis* sp. PCC 6803, indicating that the microorganism grew properly with the highest absorbance spectrum at 680 nm [47,48].

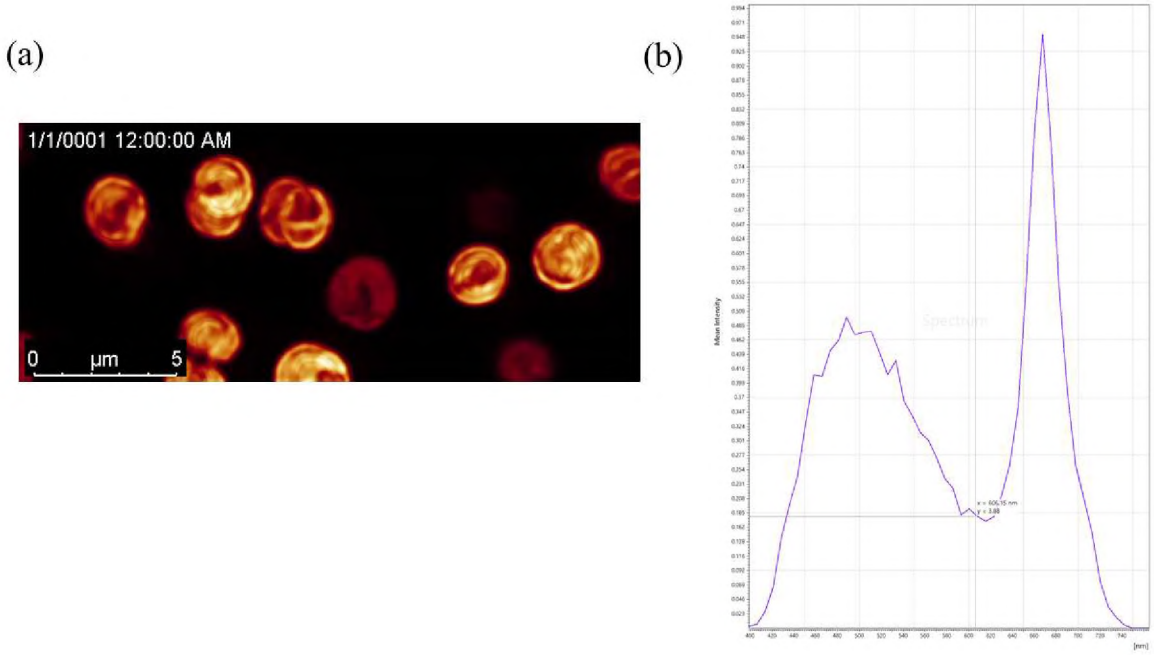

Figure 1. (a) Time-lapse video microscopic images of *Synechocystis* sp. PCC 6803, and (b) its fluorescence emission spectra analysis. Red color indicates the abundance of photosynthetic pigments

The growth kinetics of *Synechocystis* sp. PCC 6803 was studied to obtain the maximum total lipid yield. The growth curve shows that the lag phase extended for almost 30 h (Figure 2a). It took the species for six days to reach the stationary phase. The specific growth rate, α was calculated as 0.04 h^{-1}. The doubling time (t_d) was calculated as 18.3 h. We extracted the MGDG molecule from the cells at the beginning of the stationary phase for maximum yield. Structurally, the MGDG molecule is constructed on a glycerol backbone (Figure 2b). The galactose residue is bound to the sn-3 position of the glycerol backbone *via* a β-anomeric linkage. This head group remains conserved across the average molecular structures found in plant and cyanobacterial sources. The molecule has two long fatty acid chains in the sn-1 and sn-2 position of the backbone.

The long fatty acid chains show variability in length, double bond position, and degree of unsaturation across and within the sources [7,9]. Typically, 18:1 or 18:3 /16:3 or 16:0 (sn-1/sn-2) average fatty acid composition is common in plant extract MGDG [45,49]. In contrast, the fatty acid composition can vary from long-chain composition of 18/16 (sn-1/sn-2) to a very long chain composition of 34 configurations in *Synechocystis* sp. extract MGDG [7,50]. Mostly, the *Synechocystis* sp. PCC 6803 contains the 18:3 GLA polyunsaturated fatty acid chain at the sn-1 position and 16:0 palmitic acid saturated fatty acid chain at the sn-2 position [7,51,52].

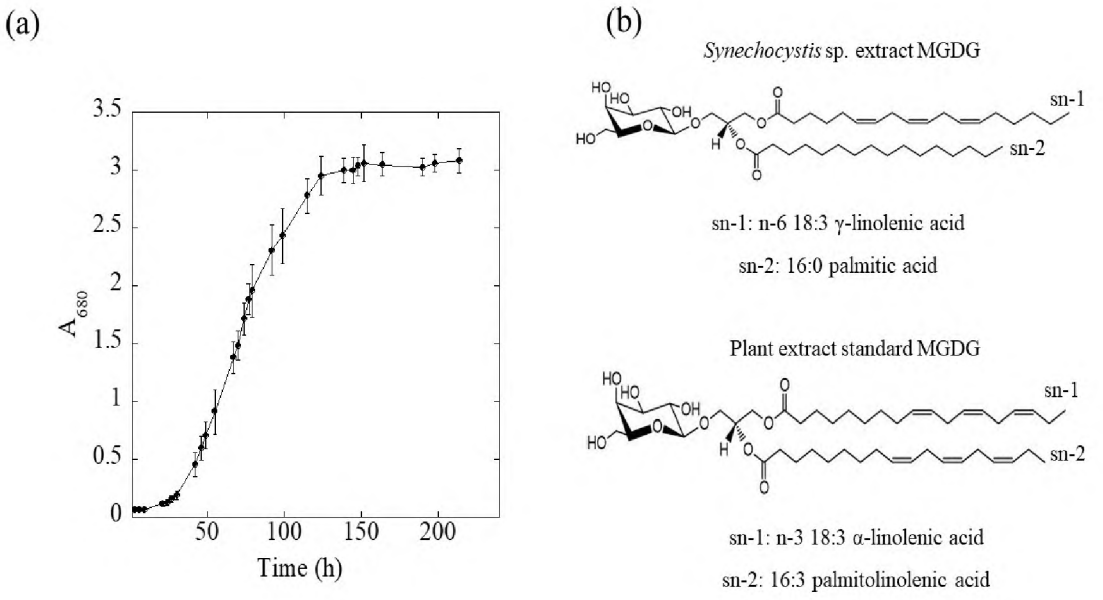

Figure 2. The growth kinetics of *Synechocystis* sp. and structure of MGDG. (a) Growth curve of *Synechocystis* sp. PCC 6803 wild type strain. The growth was measured in terms of absorbance value obtained at 680 nm. (b) Structure of MGDG extracted from *Synechocystis* sp. PCC 6803 containing n-6 18:3 γ-linolenic acid (n-6 GLA) and 16:0 palmitic acid at sn-1 and sn-2 fatty acid chains, respectively (upper panel); the most abundant structure of plant extracted MGDG standard containing n-3 18:3 α-linolenic acid (n-3 ALA) and 16:3 palmitolinolenic acid at sn-1 and sn-2 fatty acid chains, respectively (lower panel)

3.2. NMR ANALYSIS CONFIRMS THE SEPARATION OF MGDG FROM TOTAL LIPID EXTRACT

MGDG molecule was separated from the total lipid extract of *Synechocystis* sp. PCC 6803 using column chromatography. The fractions with each eluent were collected separately and analyzed individually by NMR analysis. The MGDG molecule was separated with an eluent combination of 40% chloroform and 60% acetone. The fractions (H, I, J) were collected with the same eluent combination. The NMR analysis confirms the presence of MGDG molecule in fraction I (Figure 3).

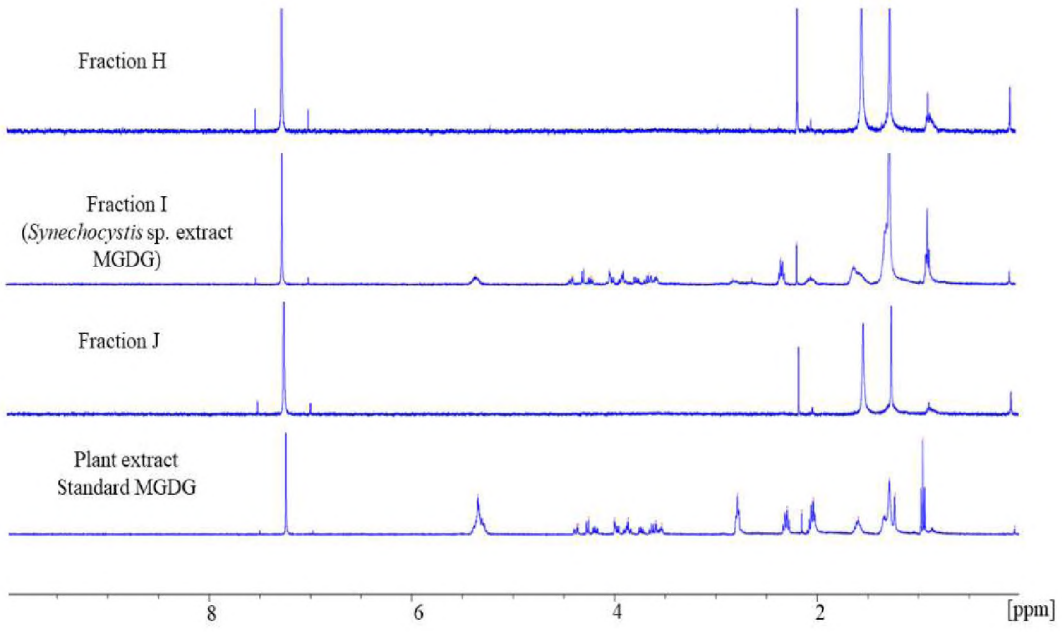

Figure 3. Confirmation of the presence of MGDG extracted from *Synechocystis* sp. PCC 6803 in fraction I. ^{1}H NMR analysis of *Synechocystis* sp. extracted fractions H, I, and J with 40% chloroform and 60% acetone eluent combination. The NMR spectra of the MGDG standard are shown in the lowest panel. The NMR analysis confirms the presence of MGDG molecule in fraction I

The set of NMR peaks of fraction I were completely identical to the standard MGDG molecule suggesting the separation of MGDG molecule with high purity. The structure of MGDG in fraction I was analyzed from the peaks obtained in the NMR analysis (Figure 4).

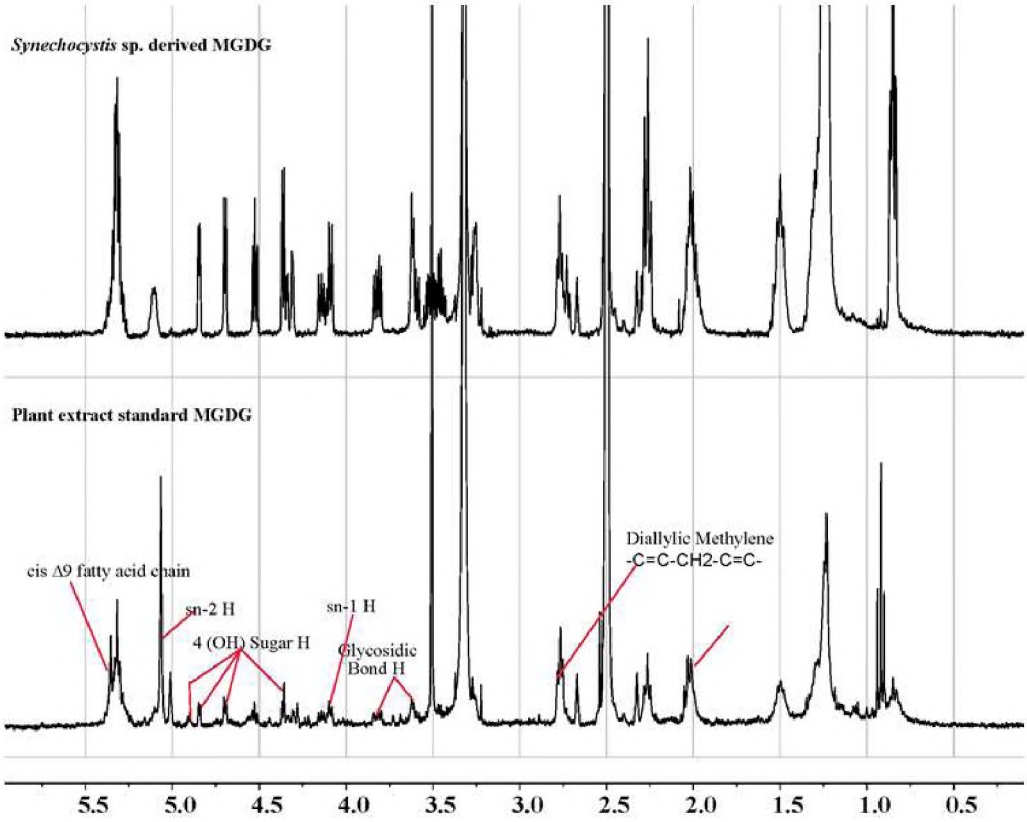

Figure 4. Structural identification of MGDG extracted from *Synechocystis* sp. PCC 6803. 1H NMR analysis of MGDG extracted from the *Synechocystis* sp. shows that the fraction molecule (upper panel) contains all the major structural H components δ 2.8 (diallylic methylene), δ 3.6 and 3.8 (Glycosidic H moiety), δ 4.18 (sn-1 H), δ 5.15 (sn-2 H), δ 5.25 cis Δ9 moieties present in the standard MGDG molecule (lower panel). The cyanobacterial NMR spectra are identical to the NMR spectra of the MGDG standard confirming the purity of the extracted MGDG molecule

The chemical shift values at δ 4.18, 5.15 represent the sn-1 and sn-2 H atom, respectively. The peaks at δ 4.29, 4.55, 4.70, and 4.85 confirm four H atoms of the OH group in the carbohydrate sugar present in MGDG. Glycosidic bond in MGDG is represented by the chemical shift δ 3.6 and 3.8. A very broad and sharp peak at chemical shift δ 5.25 might represent the unsaturated cis Δ9 fatty acid attached to the sn-1 or sn-2 position [43]. The presence of the unsaturated fatty acids can be confirmed by the diallylic methylene functional group at chemical shift δ 2.8. The results are consistent with the NMR data of MGDG reported earlier by Marcolongo *et. al.* and Maeda *et. al.* [44,45].

3.3. DETECTION AND QUANTIFICATION OF MGDG USING HPLC-UV SYSTEM

The *Synechocystis* sp. extracted MGDG molecule was detected and quantified using the HPLC coupled with a UV detector. The correlation of area under the peak with known concentrations of standard MGDG was observed in HPLC analysis (Figure 5). The R^2 value of the fitted curve was 0.99. After the separation of MGDG from total lipid extract in chromatographic fraction I, the fraction was run through the HPLC column for quantification. The peak obtained at 6.24 min confirmed the presence of the MGDG molecule (Figure 6). The amount of detected MGDG in fraction I was quantified using the concentration correlation plot obtained in Figure 5.

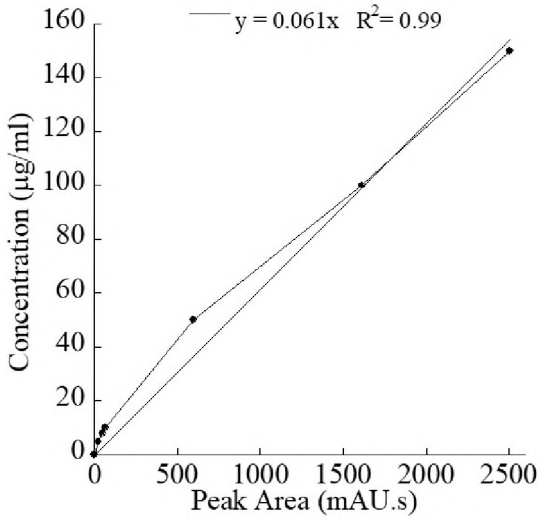

Figure 5. Calibration curve for quantification of MGDG extracted from *Synechocystis* sp. PCC 6803. A standard calibration curve was prepared using known concentrations of plant extract MGDG molecule and the corresponding peak areas in terms of milli-absorbance unit × seconds (mAu.s) in HPLC-UV analysis. The equation obtained for the unknown concentration of the MGDG molecule for any known peak area is y= 0.061x with the R2 value of 0.99

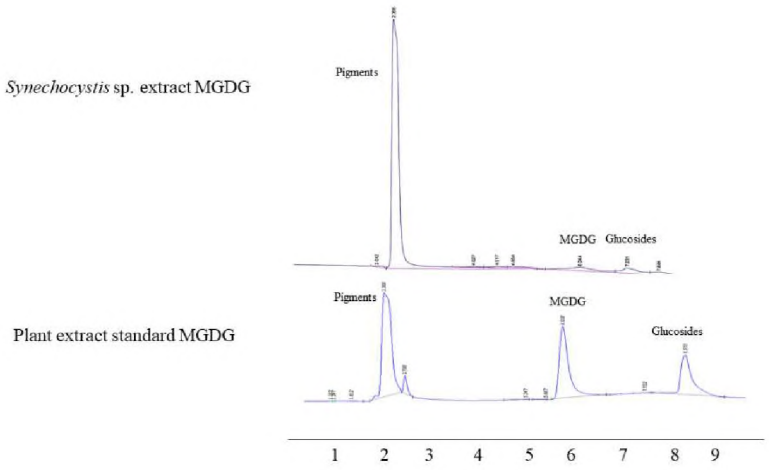

Figure 6. HPLC-UV analysis of MGDG extracted from *Synechocystis* sp. PCC 6803. (upper panel) and MGDG standard (lower panel). The MGDG peak was obtained at ~6 minutes for the MGDG molecule from both of the sources. The peaks obtained at ~2 and ~7-8 minutes represent the pigments and glucosides peaks eluted with the methanol/ water solvents

3.4. *IN VITRO* ANTI-PROLIFERATION EFFICACY

To determine the anti-proliferation efficacy in vitro, the dose-response cytotoxicity of MGDG extracted *Synechocystis* sp. and MGDG standard was evaluated. The anti-proliferation activity of extracted MGDG was compared against the MGDG standard in HER2-positive BT-474 (Figure 7a) and MDA-MB-231 triple-negative breast cancer cells (Figure 7b). In BT-474 cells, MGDG extracted from *Synechocystis* sp. inhibited up to 70% cell proliferation over the concentration range of 0-200 ng/ml (•, Figure 7a). The maximum inhibition in BT-474 cells was (70 ± 8) % at 60 ng/ml ($p < 0.001$). At higher concentrations (>60 ng/ml), a decrease in % cell death was observed in BT-474 cells indicating cell-dependent drug resistance to MGDG extracted from *Synechocystis* sp.[53,54] In MDA-MB-231 cell line, for the concentration range of 0-200 ng/ml, MGDG extracted from *Synechocystis* sp. showed significant cell growth inhibition from 0-60% in a dose-dependent manner (•, Figure 7b). The extracted MGDG inhibited (58 ± 5) % of MDA-MB-231 breast cancer cells at the concentration of 200 ng/ml ($p < 0.001$). The half-maximal inhibitory concentration, IC50 values of MGDG extracted from *Synechocystis* sp. are (27.2 ± 7.6) and (150 ± 70) ng/ml in BT-474 and MDA-MB-231 cells, respectively. In contrast, in both BT-474 and MDA-MB-231 cell lines, standard MGDG did not show any statistically significant anti-proliferation activity (<10% cell death) compared to untreated positive control within the concentration range of 0-200 ng/ml (o, Figures 7a and 7b).

(a)

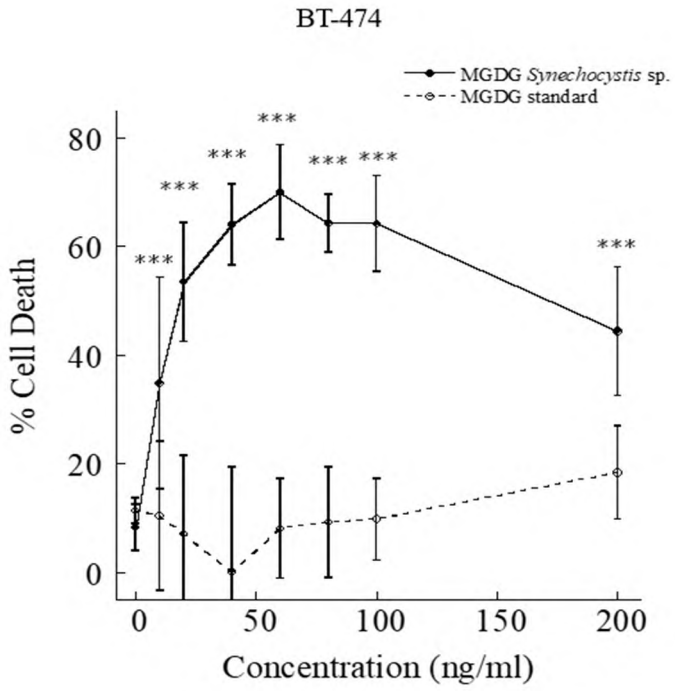

Figure 7. *In vitro* anti-cell proliferation analysis. MGDG extracted from Synechocystis sp. PCC 6803 (solid line) and MGDG standard (dotted line) in (a) BT-474 and (b) MDA-MB-231 cell lines. Mean percentage values are presented from six replicates (n=6) for each drug dosage. The MGDG from the Synechocystis sp. inhibits up to 70% ($p<0.001$) and 60% ($P<0.001$) of BT-474 and MDA-MB-231 cancer cells, respectively where MGDG standard does not show any toxicity within the concentration range of 0-200 ng/ml. *** indicates the p-value < 0.001 showing a statistical significant difference between % cell death in MGDG extracted from the Synechocystis sp. and MGDG standard. (c) MGDG extracted from the Synechocystis sp. does not show any cytotoxic side effects in human dermal fibroblasts normal cell line control

(b)

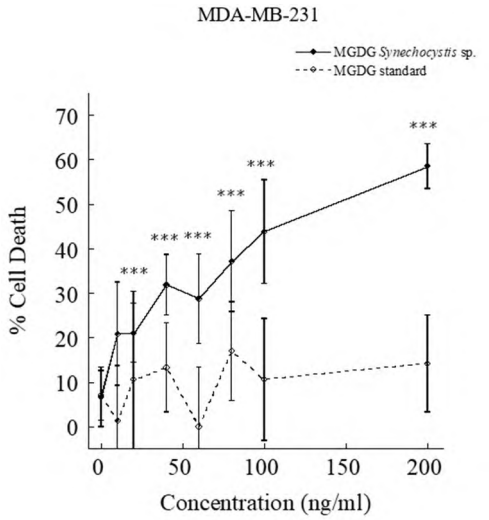

(c)

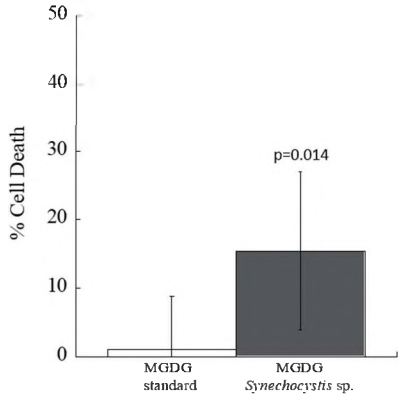

Figure 7. *In vitro* anti-cell proliferation analysis. MGDG extracted from *Synechocystis* sp. PCC 6803(solid line) and MGDG standard (dotted line) in (a) BT-474 and (b) MDA-MB-231 cell lines. Mean percentage values are presented from six replicates (n=6) for each drug dosage. The MGDG from the *Synechocystis* sp. inhibits up to 70% ($p<0.001$) and 60% ($P<0.001$) of BT-474 and MDA-MB-231 cancer cells, respectively where MGDG standard does not show any toxicity within the concentration range of 0-200 ng/ml. *** indicates the p-value < 0.001 showing a statistical significant difference between % cell death in MGDG extracted from the *Synechocystis* sp. and MGDG standard. (c) MGDG extracted from the *Synechocystis* sp. does not show any cytotoxic side effects in human dermal fibroblasts normal cell line control (cont.)

Although MGDG from *Synechocystis* sp. induced the % cell death of breast cancer cells in a concentration-dependent manner, the cytotoxicity of fibroblast cells (normal cell control) was less (<15%) than breast cancer cells after exposure to 100 ng/ml of MGDG for 72 h (Figure 7c), indicating that breast cancer cells were more sensitive to the MGDG derived from *Synechocystis* sp. than normal cells. Taken together, the results revealed that MGDG extracted from *Synechocystis* sp. induced selective apoptotic cell death in BT-474 and MDA-MB-231 breast cancer cells with different potency after 72 h of incubation, while causing less toxicity in normal fibroblasts.

3.5. *Synechocystis* sp. EXTRACTED MGDG INDUCES CASPASE-DEPENDENT APOPTOSIS

To investigate the late phase apoptosis, BT-474 and MDA-MB-231 cells were treated with 100 ng/ml of MGDG extracted from *Synechocystis* sp. and MGDG standard and stained with green fluorescently labeled caspase-3/7, a well-known apoptotic marker. The assay utilizes a nucleic acid binding dye conjugated with a four amino acid peptide, DEVD (Asp-Glu-Val-Asp motifs) that is recognized by caspase-3/7 and cleaved, enabling the dye to bind with DNA and fluoresce at ~530 nm [55-57]. The conjugated dye is non-fluorescent until the DEVD peptide is cleaved by active caspase-3/7. After 48 h and 72 h of treatment, cells treated with MGDG extracted from *Synechocystis* sp. showed green fluorescently stained DNA indicating the activation of caspase-3/7 in BT-474 (Figure 8a) and MDA-MB-231 cells (Figure 8b). The combined phase and fluorescent signal images show the overlap of caspase-3/7 positive cells and the unhealthy shrinking cells suggesting the initiation of apoptosis. The induction of apoptosis was assessed by Western blot technique (SI Figure 3). The Western blot analysis showed that the full-

length caspase-3 (MW: 32 KDa) expression was reduced in BT-474 and MDA-MB-231 cells treated with MGDG from *Synechocystis* sp., while the protein expression did not change in cells treated with MGDG standard relative to untreated cell controls. The reduced expression of full-length caspase-3 suggests the cleavage of the protein into an active form of low molecular weight (17 kDa) active cleaved caspase-3. The cleaved caspase-3/7 expression was quantified using flow cytometry. The fold enhancement of caspase-3/7 was quantified using flow cytometry analysis (Figures 8c and 8d). We observed a statistically significant increase of 1.7±0.04 fold ($p<0.01$) in caspase-3/7 concentrations after 48 h and a statistically significant 2.34±0.44 fold ($p<0.01$) increase after 72 h in BT-474 cells treated with MGDG extracted from *Synechocystis* sp. compared to untreated cell controls (filled column, Figure 8c). After 72 h, the number of apoptotic cells in the extracted MGDG treated cells significantly increased 2.1±0.03 fold ($p<0.01$) in MDA-MB-231 cells (filled column, Figure 8d). MGDG standard did not show any significant changes in cleaved caspase-3/7 expressions compared to untreated control cells. The obtained scatter plots and histogram data from flow cytometry are shown for each treatment in SI Figure 5. These results are in good agreement with fluorescent microscopic images indicating the cells being shrunk and round shaped with a complete halt in growth of cancer cells. In contrast, after 48 and 72 h of treatment, there was no sign of apoptosis in the standard MGDG treated compared to untreated cell controls (open column, Figures 8c, and 8d). The untreated cells and the cells treated with standard MGDG were compact multilayered colonized and elongated in shape in the case of BT-474 and MDA-MB-231 cell lines, respectively, and were observed healthy suggesting continuous growth capability.

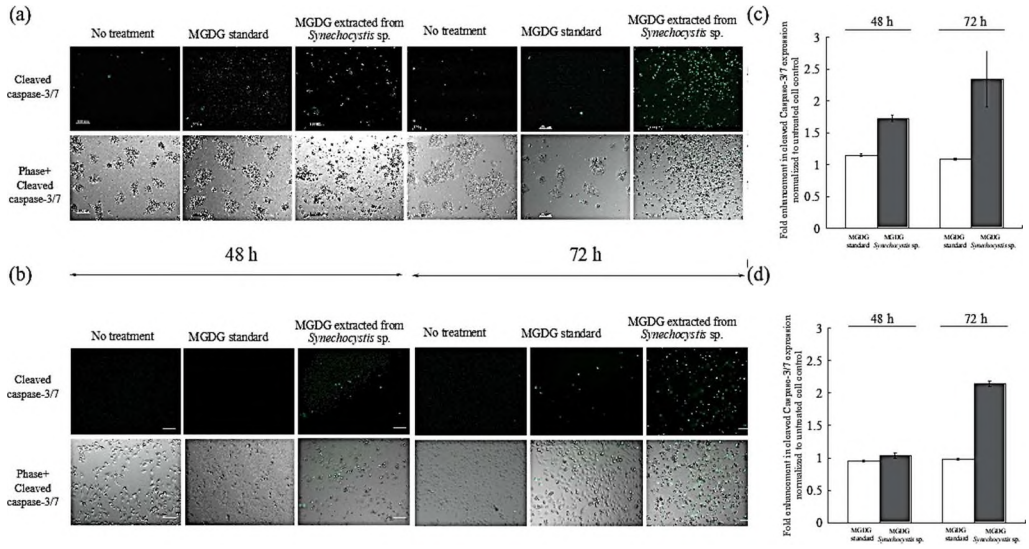

Figure 8. *In vitro* apoptosis induction. MGDG extracted from the Synechocystis sp. and MGDG standard after 48 and 72 h treatments in (a) BT-474, and (b) MDA-MB-231 cells. The green fluorescence of apoptotic caspase-3/7 proteins increases in both BT-474 and MDA-MB-231 cells treated with MGDG extracted from the Synechocystis sp. The combined phase contrast and the fluorescence images show that the cyanobacterial extracted MGDG enhances the intensity and density of green fluorescence cells indicative of caspase-dependent apoptosis in both cell lines. In contrast, cells treated with MGDG standard molecule did not show any sign of apoptosis in either cell line even after 72 h of treatment. The scale bars represent 100 μm. Quantification of the active caspase-3/7 expression in (c) BT-474, and (d) MDA-MB-231 cells treated with MGDG extracted from the Synechocystis sp. and MGDG standard after 48 h and 72 h of treatments. In BT-474 cells, the active caspase-3/7 expression was increased by 1.7 ($p<0.01$) and 2.3 ($p<0.01$) fold after 48 h and 72 h treatments, respectively compared to untreated control. The increase in caspase-3/7 expression was 2.1 ($p<0.01$) fold after 72 h treatment in MDA-MB-231 cells compared to the untreated control. Mean ± standard deviation from two independent experiments in at least three replicates (n=6) are presented. *** indicates the p-value < 0.01, showing a statistically significant difference compared to untreated control cells

4. DISCUSSION

MGDG contains fatty acyl groups derived from two fatty acid molecules at sn-1 and sn-2 position and a polar head at sn-3 position in a 3-carbon glycerol scaffold (Figure 2b). Fatty acid molecules such as n-6 GLA may exert anti-proliferative effect by

regulating genes and proteins involved in cell cycle and apoptosis, altering the cellular composition of fatty acids, and by producing downstream anti-proliferative metabolites such as 1-series prostaglandins and free radical molecules from cyclooxygenase (COX) catalyzed lipid peroxidation. The potent anti-proliferative activity of the MGDG is mostly attributed to the fatty acyl components of the MGDG molecular structure.[58,59] The structure of the MGDG molecule and the fatty acid content of MGDG derived from *Synechocystis* sp. PCC 6803 is well studied. The molecule is rich in 18:3 n-6 GLA fatty acids. The fast atom bombardment tandem mass spectrometry (FAB-MS) analysis of glycolipids derived from *Synechocystis* sp. PCC 6803 showed 18:3 n-6 GLA, 18:2, and 18:1 combination of fatty acid chains with a relative abundance of 100, 47 and 41, respectively at the sn-1 position[7]. Yuzawa *et. al.* showed the relative abundance of n-6 GLA, 18:2, and 18:1 fatty acid content in wild type *Synechocystis* sp. derived MGDG as 30%, 10%, and 5% respectively[52]. However, the larger fatty acid chains at the sn-1 position have also been reported recently. The time of flight mass spectrometry (TOF-MS) analysis of the same cyanobacterial strain showed the predominance of 34:2 or 34:3 fatty acid chain at the sn-1 position [50]. Wada et. al. showed that the most abundant n-6 GLA moiety in *Synechocystis* sp. derived MGDG is subject to desaturation when the growth temperature was shifted from 38°C to 22°C [51]. In contrast to the variable sn-1 fatty acid content, the sn-2 position was shown to be conserved mostly with 16: 0 (palmitic acid) fatty acid chain in *Synechocystis* sp. derived MGDG and was not affected with the shifts in temperature [7,51,52].

The MGDG lipid molecule was separated in a normal phase column using chloroform and acetone gradient eluent combinations. The column length to diameter

ratio was ~10. Multiple samples were collected with each eluent combination for better purification. We confirmed the presence of MGDG molecule in fraction I using ^{1}H NMR analysis (Figure 3). Though fraction H, I, and J were eluted with the same mobile phase combination of 40% chloroform and 60% acetone, only fraction I contained the MGDG molecule. The peaks obtained for a fraction I identical with >99% pure standard MGDG molecule suggests the high purity of MGDG molecule in that fraction. The diallylic methylene moiety obtained at δ 2.8 in the NMR analysis shown in Figure 4 confirmed the polyunsaturation in the long fatty acid chain at the sn-1 position. The extracted MGDG molecule in fraction I was quantified using the HPLC-UV system. We prepared a calibration curve (Figure 5) with known >99% pure standard MGDG molecule to quantify the MGDG in each extracted fraction. The peak obtained at retention time 6.24 min shown in Figure 6, upper panel corresponds to the MGDG molecule in the fraction [46]. The large peak obtained at retention time 2.36 min is the lipid pigments eluted initially by the chloroform. The peak at 7.23 min might be due to the presence of steryl glucosides present as a contaminant in the fraction[46]. Glucosides do not have any known effects on the HER2-positive and triple-negative breast cancer cells. The peaks for pigments and glucosides were also observed in the standard >99% pure standard MGDG chromatogram (Figure 6, lower panel). So, the contaminant should not have any effect in this study during the drug formulation used for cytotoxicity analysis. However, the GGL molecules are detected with high quality and precision using the evaporative light scattering detectors (ELSD) providing with sharp and clear peaks in the chromatogram.[46,60,61]

We investigated the *in vitro* anti-proliferation efficacy of cyanobacteria derived MGDG molecule in comparison with MGDG molecule from plant source on the HER2-positive and triple-negative breast cancer cell lines. We observed significant differences in the % of cancer cell death using MGDG extracted from *Synechocystis* sp. *versus* a commercially available MGDG standard. MGDG extracted from *Synechocystis* sp. induced apoptosis in (70 ± 8) % of BT-474 and (58 ± 5) % of MDA-MB-231 cells at 60 and 200 ng/ml, respectively, while <15% cell death was observed in fibroblasts at 100 ng/ml. While the precise mechanism by which each molecule works about their cell-killing effect is unknown, it is possible that the presence of polyunsaturated γ-linolenic acid in the sn-1 position and palmitic acid in the sn-2 position of MGDG from *Synechocystis* sp. resulted in the mitochondrial depolarization, cytochrome c release, DNA fragmentation and generation of free radicals causing specific cell death response in breast cancer cells compared to normal cells.[62-66] γ-linolenic acid has been shown to exhibit anti-proliferative activities specifically in a variety of cancer cell lines both *in vitro* and *in vivo*. γ-linolenic acid inhibited the cell growth of four human neuroblastoma cell lines (GOTO, SK-N-DZ, NKP, and NCG) *in vitro*,[67] three human glioma cell lines (MOG, U87, U373) and a rodent glioma cell line (C6) *in vitro* and a rat C6 glioma model *in vivo*.[68] Glioma regression and apoptosis had been reported using both C18 and C20 fatty acids of the n-6 and n-3 series γ-linolenic acid along with the preservation of normal neural tissue and vasculature in adjacent brain.[68] γ-linolenic acid at a concentration of 150 μM inhibited Walker 256 cancer cell growth both *in vitro* and *in vivo* causing decrease in mitochondrial membrane potential, and increase in cytochrome c release, caspase activation, and DNA fragmentation.[63] The

mitochondrial apoptosis pathway was likely induced by an increase in reactive oxygen species (ROS), lipid peroxide production, ATP generation and the deposition of large amounts of triacylglycerol in the form of lipid droplets.[63,65] A diet containing 5.5% γ-linolenic acid caused 45% decrease in Walker 256 tumor growth *in vivo* by reducing mitochondrial metabolic activity.[62] More interestingly, *in vitro*, *in vivo* and clinical study data showed that γ-linolenic acid has selective anti-proliferative actions in cancer cells with little or no side effects on normal cell growth. Polyunsaturated fatty acids including γ-linolenic acid incubated with human breast, lung, and prostate cancer cells suppressed the cancer cell growth exhibiting no adverse effects on normal human fibroblasts or normal animal cell lines.[69] Intraarterial injection of a lithium salt derivative of γ-linolenic acid demonstrated its ability to selectively suppress angiogenesis.[64] These reports, together with our data increases lead to the conclusion that MGDG from *Synechocystis* sp. is a promising cancer therapeutic agent with high selectivity of cancer cell growth inhibition leading to apoptosis and a decrease in cancer development. Also, saturated fatty acid, palmitic acid at the sn-2 position of MGDG from *Synechocystis* sp. plays a significant role in the elevation of calcium flux, endoplasmic reticulum stress, caspase-3, and caspase-9 activity, and thus inducing apoptosis which is in good agreement with previous reports.[70-72] Treatment of mouse 3T3-L1 and rat primary preadipocytes with palmitic acid induced multiple cell signaling pathways, endoplasmic reticulum stress responses, and cell cycle arrest leading to apoptosis.[70] Palmitic acid induced oxidative stress and DNA damage in rodent-derived insulin-secreting cell line RINm5F and primary human fibroblasts.[72] Spinach MGDG molecule in combination with gemcitabine *in vitro* [59]and radiation *in vivo* [73] showed enhanced suppression of

MIAPaCa-2, PANC-1, and BxPC-3 pancreatic cancer cell lines compared to MGDG treatment alone. With the *in vitro* spinach MGDG treatment alone the IC_{50} values for the mentioned pancreatic cell lines ranged from 18-25 μM [73,74]. MGDG molecule extracted from the spinach has been shown to inhibit human replicative and repair DNA polymerase enzymes with the IC_{50} values ranging from 10-200 μM.[59] These results illustrate the specificity of the MGDG extracted from *Synechocystis* sp. PCC 6803 to breast cancer cells by caspase-dependent apoptotic pathway.

5. CONCLUSION

Fatty acids are of great interest as natural anti-proliferative factors because of their selective inhibition of cancer cells. The structure and efficacy of fatty acid molecules are variable within and across the sources. We investigated the cancer cell inhibition efficacy of plant and cyanobacterial derived MGDG molecule. The marine cyanobacteria Synechocystis sp. derived MGDG molecule predominantly rich in n-6 GLA was separated from the total lipid extract in this study. The molecule was separated in a handmade low-cost normal phase silica column with the gradient elution method using chloroform and acetone as the mobile phase. We confirmed the presence of MGDG molecule in the fraction eluted with 40% chloroform and 60% acetone eluent combination. The NMR analysis confirmed the high purity of the separated MGDG molecule from the cyanobacterial total lipid extract. The separated MGDG molecule was quantified by the HPLC-UV system. The anti-proliferative activity of the cyanobacterial MGDG was tested against the MDA-MB-231 breast cancer cell line. The in vitro

cytotoxicity study showed that MGDG extracted from Synechocystis sp. PCC 6803 potently inhibited (70 ± 8)% and (58 ± 5)% of BT-474 and MDA-MB-231 cells, respectively using 60 and 200 ng/ml of the MGDG. The IC50s of MGDG extracted from Synechocystis sp. are (27.2 ± 7.6) and (150 ± 70) ng/ml in BT-474 and MDA-MB-231 cells, respectively. In contrast, plant extract n-3 ALA-rich MGDG did not have any cytotoxic effect in the concentration range of 0-200 ng/ml. It did not show any cytotoxic effects in human dermal fibroblasts normal cell controls. Our results support these findings showing that the cyanobacteria derived MGDG induces caspase-dependent apoptosis pathway to inhibit the HER2-positive BT-474 and triple-negative MDA-MB-231 breast cancer cell growth. Further studies involving additional mechansisms of actions, intracellular uptake, and robust screening of additional cancer cell lines will confirm the potential novel therapeutic efficacy of cyanobacteria derived MGDG molecule for a low dosage selective treatment of cancer cells.

ACKNOWLEDGMENTS

The authors would like to thank Dr. Michelle Liberton and Dr. Himadri Pakrasi of the Department of Biology at Washington University in St. Louis for the kind donation of Synechocystis sp. PCC 6803. The authors are also thankful to Dr. Wenyan Liu of the Department of Chemistry at Missouri University of Science and Technology for kind help with HPLC analysis. This work was supported by the Center for Biomedical Research (CBR) at Missouri S&T.

REFERENCES

(1) Illijas, M. I.; Indy, J. R.; Yasui, H.; Itabashi, Y. Lipid Class and Fatty Acid Composition of a Little-known and Rarely Collected Alga Exophyllum wentii Weber-van Bosse from Bali Island, Indonesia. Journal of Oleo Science 2009, 58, 103-110.

(2) Al-Fadhli, A.; Wahidulla, S.; D'Souza, L. Glycolipids from the red alga Chondria armata (Kutz.) Okamura. Glycobiology 2006, 16, 902-915.

(3) Kim, Y. H.; Choi, J. S.; Hong, J.; Yoo, J. S.; Kim, M. S. Identification of acylated glycoglycerolipids from a cyanobacterium, Synechocystis sp., by tandem mass spectrometry. Lipids 1999, 34, 847-853.

(4) Marcolongo, G.; De Appolonia, F.; Venzo, A.; Berrie, C. P.; Carofiglio, T.; Berrini, C. C. Diacylglycerolipids isolated from a thermophile cyanobacterium from the Euganean hot springs. Natural Product Research 2006, 20, 766-774.

(5) Kim, Y. H.; Kim, E.-H.; Lee, C.; Kim, M.-H.; Rho, J.-R. Two New Monogalactosyl Diacylglycerols from Brown Alga Sargassum thunbergii. Lipids 2007, 42, 395-399.

(6) Kim, Y. H.; Choi, J.-S.; Hong, J.; Yoo, J. S.; Kim, M. S. Identification of acylated glycoglycerolipids from a cyanobacterium, Synechocystis sp., by tandem mass spectrometry. Lipids 1999, 34, 847-853.

(7) Kim, Y. H.; Choi, J.-S.; Yoo, J. S.; Park, Y.-M.; Kim, M. S. Structural Identification of Glycerolipid Molecular Species Isolated from CyanobacteriumSynechocystissp. PCC 6803 Using Fast Atom Bombardment Tandem Mass Spectrometry. Analytical Biochemistry 1999, 267, 260-270.

(8) Marcolongo, G. A., F.D.; Venzo, A.; Berrie, C.P.; Carofiglio, T.; and Berrini, C.C. Diacylglycerolipids isolated from a thermophile cyanobacterium from the Euganean hot springs. Natural Product Research 2006, 20, 766-774.

(9) Hölzl, G.; Dörmann, P. Structure and function of glycoglycerolipids in plants and bacteria. Progress in lipid research 2007, 46, 225-243.

(10) Benning, C. A role for lipid trafficking in chloroplast biogenesis. Progress in Lipid Research 2008, 47, 381-389.

(11) Ramm, W.; Schatton, W.; Wagner-Döbler, I.; Wray, V.; Nimtz, M.; Tokuda, H.; Enjyo, F.; Nishino, H.; Beil, W.; Heckmann, R.; Lurtz, V.; Lang, S. Diglucosyl-glycerolipids from the marine sponge-associated Bacillus pumilus strain AAS3: Their production, enzymatic modification and properties. Applied Microbiology and Biotechnology 2004, 64, 497-504.

(12) Rakhuba, D.; Novik, G.; Dey, E. S. Application of supercritical carbon dioxide (scCO2) for the extraction of glycolipids from Lactobacillus plantarum B-01. Journal of Supercritical Fluids 2009, 49, 45-51.

(13) Wicke, C.; Hüners, M.; Wray, V.; Nimtz, M.; Bilitewski, U.; Lang, S. Production and structure elucidation of glycoglycerolipids from a marine sponge-associated Microbacterium species. Journal of Natural Products 2000, 63, 621-626.

(14) Bultel-Poncé, V.; Debitus, C.; Blond, A.; Cerceau, C.; Guyot, M. Lutoside: An acyl-1-(Acyl-6'-mannobiosyl)-3-glycerol isolated from the Sponge-associated bacterium Micrococcus luteus. Tetrahedron Letters 1997, 38, 5805-5808.

(15) Shirahashi, H.; Murakami, N.; Watanabe, M.; Nagatsu, A.; Sakakibara, J.; Tokuda, H.; Nishino, H.; Iwashima, A. Isolation and Identification of Anti-tumor-Promoting Principles from the Fresh-Water Cyanobacterium Phormidium tenue. Chemical & Pharmaceutical Bulletin 1993, 41, 1664-1666.

(16) Morimoto, T.; Nagatsu, A.; Murakami, N.; Sakakibara, J.; Tokuda, H.; Nishino, H.; Iwashima, A. Anti-tumour-promoting glyceroglycolipids from the green alga, Chlorella vulgaris. Phytochemistry 1995, 40, 1433-1437.

(17) Hou, C.-C.; Chen, Y.-P.; Wu, J.-H.; Huang, C.-C.; Wang, S.-Y.; Yang, N.-S.; Shyur, L.-F. A Galactolipid Possesses Novel Cancer Chemopreventive Effects by Suppressing Inflammatory Mediators and Mouse B16 Melanoma. Cancer Research 2007, 67, 6907-6915.

(18) Maeda, N.; Kokai, Y.; Ohtani, S.; Hada, T.; Yoshida, H.; Mizushina, Y. Inhibitory effects of preventive and curative orally administered spinach glycoglycerolipid fraction on the tumor growth of sarcoma and colon in mouse graft models. Food Chemistry 2009, 112, 205-210.

(19) Loya, S.; Reshef, V.; Mizrachi, E.; Silberstein, C.; Rachamim, Y.; Carmeli, S.; Hizi, A. The Inhibition of the Reverse Transcriptase of HIV-1 by the Natural Sulfoglycolipids from Cyanobacteria: Contribution of Different Moieties to Their High Potency. Journal of Natural Products 1998, 61, 891-895.

(20) Gustafson, K. R. Mining the extensive chemical diversity of the NCl natural products repository for new agents that can target HIV. Planta Medica 2015, 81, 858-858.

(21) Bergé, J. P.; Debiton, E.; Dumay, J.; Durand, P.; Barthomeuf, C. In Vitro Anti-inflammatory and Anti-proliferative Activity of Sulfolipids from the Red Alga Porphyridium cruentum. Journal of Agricultural and Food Chemistry 2002, 50, 6227-6232.

(22) Zhang, H.; Oh, J.; Jang, T.-S.; Min, B. S.; Na, M. Glycolipids from the aerial parts of Orostachys japonicus with fatty acid synthase inhibitory and cytotoxic activities. Food chemistry 2012, 131, 1097-1103.

(23) Maeda, N.; Matsubara, K.; Yoshida, H.; Mizushina, Y. Anti-cancer Effect of Spinach Glycoglycerolipids as Angiogenesis Inhibitors Based on the Selective Inhibition of DNA Polymerase Activity. Mini-Reviews in Medicinal Chemistry 2011, 11, 32-38.

(24) Maeda, N. K., Y.; Ohtani, S.; Sahara, H.; Hada, T.; Ishimaru, C.; Kuriyama, I.; Yonezawa, Y.; Iijima, H.; Yoshida, H.; Sato, N.; and Mizushina, Y. Anti-Tumor Effects of the Glycolipids Fraction from Spinach which Inhibited DNA Polymerase Activity. Nutrition and Cancer 2007, 57, 216-223.

(25) Naoki, M.; Takahiko, H.; Hiromi, Y.; Yoshiyuki, M. Inhibitory Effect on Replicative DNA Polymerases, Human Cancer Cell Proliferation, and In Vivo Anti-Tumor Activity by Glycolipids from Spinach. Current Medicinal Chemistry 2007, 14, 955-967.

(26) Akasaka, H.; Sasaki, R.; Yoshida, K.; Takayama, I.; Yamaguchi, T.; Yoshida, H.; Mizushina, Y. Monogalactosyl diacylglycerol, a replicative DNA polymerase inhibitor, from spinach enhances the anti-cell proliferation effect of gemcitabine in human pancreatic cancer cells. Biochimica et Biophysica Acta (BBA) - General Subjects 2013, 1830, 2517-2525.

(27) Ohta, K.; Hanashima, S.; Mizushina, Y.; Yamazaki, T.; Saneyoshi, M.; Sugawara, F.; Sakaguchi, K. Studies on a novel DNA polymerase inhibitor group, synthetic sulfoquinovosylacylglycerols: inhibitory action on cell proliferation. Mutation Research - Genetic Toxicology and Environmental Mutagenesis 2000, 467, 139-152.

(28) Faivre, V.; Rosilio, V. Interest of glycolipids in drug delivery: From physicochemical properties to drug targeting. Expert Opinion on Drug Delivery 2010, 7, 1031-1048.

(29) Kinjo, Y.; Tupin, E.; Wu, D.; Fujio, M.; Garcia-Navarro, R.; Benhnia, M. R. E. I.; Zajonc, D. M.; Ben-Menachem, G.; Ainge, G. D.; Painter, G. F.; Khurana, A.; Hoebe, K.; Behar, S. M.; Beutler, B.; Wilson, I. A.; Tsuji, M.; Sellati, T. J.; Wong, C. H.; Kronenberg, M. Natural killer T cells recognize diacylglycerol antigens from pathogenic bacteria. Nature Immunology 2006, 7, 978-986.

(30) Grzyb, J.; Gieczewska, K.; Łabuz, J.; Sztatelman, O. Detailed characterization of Synechocystis PCC 6803 ferredoxin:NADP+ oxidoreductase interaction with model membranes. Biochimica et Biophysica Acta (BBA) - Biomembranes 2018, 1860, 281-291.

(31) Dai, J.; Shen, J.; Pan, W.; Shen, S.; Das, U. N. Effects of polyunsaturated fatty acids on the growth of gastric cancer cells in vitro. Lipids Health Dis 2013, 12, 71-71.

(32) Madhavi, N.; Das, U. N. Effect of n-6 and n-3 fatty acids on the survival of vincristine sensitive and resistant human cervical carcinoma cells in vitro. Cancer letters 1994, 84, 31-41.

(33) Berquin, I. M.; Edwards, I. J.; Kridel, S. J.; Chen, Y. Q. Polyunsaturated fatty acid metabolism in prostate cancer. Cancer and Metastasis Reviews 2011, 30, 295-309.

(34) Lu, X.; Yu, H.; Ma, Q.; Shen, S.; Das, U. N. Linoleic acid suppresses colorectal cancer cell growth by inducing oxidant stress and mitochondrial dysfunction. Lipids Health Dis 2010, 9, 106-106.

(35) Bégin, M. E.; Ells, G.; Das, U. N.; Horrobin, D. F. Differential killing of human carcinoma cells supplemented with n-3 and n-6 polyunsaturated fatty acids. Journal of the National Cancer Institute 1986, 77, 1053-1062.

(36) Menendez, J. A.; Vellon, L.; Colomer, R.; Lupu, R. Effect of γ-Linolenic Acid on the Transcriptional Activity of the Her-2/neu (erbB-2) Oncogene. Journal of the National Cancer Institute 2005, 97, 1611-1615.

(37) Hori, K.; Nobusawa, T.; Watanabe, T.; Madoka, Y.; Suzuki, H.; Shibata, D.; Shimojima, M.; Ohta, H. Tangled evolutionary processes with commonality and diversity in plastidial glycolipid synthesis in photosynthetic organisms. Biochimica Et Biophysica Acta-Molecular and Cell Biology of Lipids 2016, 1861, 1294-1308.

(38) Ungerer, J.; Pakrasi, H. B. Cpf1 Is A Versatile Tool for CRISPR Genome Editing Across Diverse Species of Cyanobacteria. Scientific Reports 2016, 6, 39681.

(39) Berla, B. M.; Saha, R.; Maranas, C. D.; Pakrasi, H. B. Cyanobacterial Alkanes Modulate Photosynthetic Cyclic Electron Flow to Assist Growth under Cold Stress. Scientific Reports 2015, 5, 14894.

(40) Wada, H.; Murata, N. Synechocystis PCC6803 mutants defective in desaturation of fatty acids. Plant and Cell Physiology 1989, 30, 971-978.

(41) Rippka, R.; Deruelles, J.; Waterbury, J. B.; Herdman, M.; Stanier, R. Y. Generic Assignments, Strain Histories and Properties of Pure Cultures of Cyanobacteria. Microbiology 1979, 111, 1-61.

(42) Bligh, E. G.; Dyer, W. J. A rapid method of total lipid extraction and purification. Canadian journal of biochemistry and physiology 1959, 37, 911-917.

(43) Gunstone, F. D.; Harwood, J. L.; Dijkstra, A. J.: The lipid handbook with CD-ROM; CRC press, 2007.

(44) Marcolongo, G.; De Appolonia, F.; Venzo, A.; Berrie, C. P.; Carofiglio, T.; Ceschi Berrini, C. Diacylglycerolipids isolated from a thermophile cyanobacterium from the Euganean hot springs. Natural product research 2006, 20, 766-774.

(45) Maeda, N.; Hada, T.; Yoshida, H.; Mizushina, Y. Inhibitory effect on replicative DNA polymerases, human cancer cell proliferation, and in vivo anti-tumor activity by glycolipids from spinach. Current medicinal chemistry 2007, 14, 955-967.

(46) Sugawara, T.; Miyazawa, T. Separation and determination of glycolipids from edible plant sources by high-performance liquid chromatography and evaporative light-scattering detection. Lipids 1999, 34, 1231.

(47) Krumova, S. B.; Laptenok, S. P.; Borst, J. W.; Ughy, B.; Gombos, Z.; Ajlani, G.; van Amerongen, H. Monitoring photosynthesis in individual cells of Synechocystis sp. PCC 6803 on a picosecond timescale. Biophys J 2010, 99, 2006-2015.

(48) Murton, J.; Nagarajan, A.; Nguyen, A. Y.; Liberton, M.; Hancock, H. A.; Pakrasi, H. B.; Timlin, J. A. Population-level coordination of pigment response in individual cyanobacterial cells under altered nitrogen levels. Photosynth Res 2017, 134, 165-174.

(49) Murakami, C.; Kumagai, T.; Hada, T.; Kanekazu, U.; Nakazawa, S.; Kamisuki, S.; Maeda, N.; Xu, X.; Yoshida, H.; Sugawara, F. Effects of glycolipids from spinach on mammalian DNA polymerases. Biochemical pharmacology 2003, 65, 259-267.

(50) Sato, N. Is monoglucosyldiacylglycerol a precursor to monogalactosyldiacylglycerol in all cyanobacteria? Plant and Cell Physiology 2015, 56, 1890-1899.

(51) Wada, H.; Murata, N. Temperature-induced changes in the fatty acid composition of the cyanobacterium, Synechocystis PCC6803. Plant Physiology 1990, 92, 1062-1069.

(52) Yuzawa, Y.; Shimojima, M.; Sato, R.; Mizusawa, N.; Ikeda, K.; Suzuki, M.; Iwai, M.; Hori, K.; Wada, H.; Masuda, S. Cyanobacterial monogalactosyldiacylglycerol-synthesis pathway is involved in normal unsaturation of galactolipids and low-temperature adaptation of Synechocystis sp. PCC 6803. Biochimica et Biophysica Acta (BBA)-Molecular and Cell Biology of Lipids 2014, 1841, 475-483.

(53) Balaji, S. A.; Udupa, N.; Chamallamudi, M. R.; Gupta, V.; Rangarajan, A. Role of the Drug Transporter ABCC3 in Breast Cancer Chemoresistance. PLOS ONE 2016, 11, e0155013.

(54) Hultsch, S.; Kankainen, M.; Paavolainen, L.; Kovanen, R.-M.; Ikonen, E.; Kangaspeska, S.; Pietiäinen, V.; Kallioniemi, O. Association of tamoxifen resistance and lipid reprogramming in breast cancer. BMC Cancer 2018, 18, 850.

(55) Khalili, J. S.; Yu, X.; Wang, J.; Hayes, B. C.; Davies, M. A.; Lizee, G.; Esmaeli, B.; Woodman, S. E. Combination Small Molecule MEK and PI3K Inhibition Enhances Uveal Melanoma Cell Death in a Mutant GNAQ- and GNA11-Dependent Manner. Clinical Cancer Research 2012, 18, 4345-4355.

(56) Miyata, M.; Kambe, M.; Tajima, O.; Moriya, S.; Sawaki, H.; Hotta, H.; Kondo, Y.; Narimatsu, H.; Miyagi, T.; Furukawa, K.; Furukawa, K. Membrane sialidase NEU3 is highly expressed in human melanoma cells promoting cell growth with minimal changes in the composition of gangliosides. Cancer Science 2011, 102, 2139-2149.

(57) Huang, T.-C.; Lee, J.-F.; Chen, J.-Y. Pardaxin, an antimicrobial peptide, triggers caspase-dependent and ROS-mediated apoptosis in HT-1080 cells. Mar Drugs 2011, 9, 1995-2009.

(58) Xu, Y.; Qian, S. Y. Anti-cancer activities of ω-6 polyunsaturated fatty acids. Biomed J 2014, 37, 112-119.

(59) Akasaka, H.; Sasaki, R.; Yoshida, K.; Takayama, I.; Yamaguchi, T.; Yoshida, H.; Mizushina, Y. Monogalactosyl diacylglycerol, a replicative DNA polymerase inhibitor, from spinach enhances the anti-cell proliferation effect of gemcitabine in human pancreatic cancer cells. Biochimica et Biophysica Acta (BBA)-General Subjects 2013, 1830, 2517-2525.

(60) Kobayashi, N.; Noel, E. A.; Barnes, A.; Rosenberg, J.; DiRusso, C.; Black, P.; Oyler, G. A. Rapid detection and quantification of triacylglycerol by HPLC-ELSD in Chlamydomonas reinhardtii and Chlorella strains. Lipids 2013, 48, 1035-1049.

(61) Picchioni, G.; Watada, A.; Whitaker, B. Quantitative high-performance liquid chromatography analysis of plant phospholipids and glycolipids using light-scattering detection. Lipids 1996, 31, 217-221.

(62) Colquhoun, A. Gamma-linolenic acid alters the composition of mitochondrial membrane subfractions, decreases outer mitochondrial membrane binding of hexokinase and alters carnitine palmitoyltransferase I properties in the Walker 256 rat tumour. Biochimica et Biophysica Acta (BBA) - Molecular and Cell Biology of Lipids 2002, 1583, 74-84.

(63) Colquhoun, A.; Schumacher, R. I. γ-Linolenic acid and eicosapentaenoic acid induce modifications in mitochondrial metabolism, reactive oxygen species generation, lipid peroxidation and apoptosis in Walker 256 rat carcinosarcoma cells. Biochimica et Biophysica Acta (BBA) - Molecular and Cell Biology of Lipids 2001, 1533, 207-219.

(64) Das, U. N. Tumoricidal and anti-angiogenic actions of gamma-linolenic acid and its derivatives. Current pharmaceutical biotechnology 2006, 7, 457-466.

(65) Das, U. N. Tumoricidal action of cis-unsaturated fatty acids and their relationship to free radicals and lipid peroxidation. Cancer letters 1991, 56, 235-243.

(66) Sagar, P. S.; Das, U. N. Cytotoxic action of cis-unsaturated fatty acids on human cervical carcinoma (HeLa) cells in vitro. Prostaglandins Leukot Essent Fatty Acids 1995, 53, 287-299.

(67) Fujiwara, F.; Todo, S.; Imashuku, S. Antitumor effect of gamma-linolenic acid on cultured human neuroblastoma cells. Prostaglandins, leukotrienes, and medicine 1986, 23, 311-320.

(68) Leaver, H.; Bell, H.; Rizzo, M. T.; Ironside, J.; Gregor, A.; Wharton, S.; Whittle, I. Antitumour and pro-apoptotic actions of highly unsaturated fatty acids in glioma. Prostaglandins, leukotrienes, and essential fatty acids 2002, 66 1, 19-29.

(69) Bégin, M. E.; Das, U. N.; Ells, G.; Horrobin, D. F. Selective killing of human cancer cells by polyunsaturated fatty acids. Prostaglandins, leukotrienes, and medicine 1985, 19, 177-186.

(70) Guo, W.; Wong, S.; Xie, W.; Lei, T.; Luo, Z. Palmitate modulates intracellular signaling, induces endoplasmic reticulum stress, and causes apoptosis in mouse 3T3-L1 and rat primary preadipocytes. American journal of physiology. Endocrinology and metabolism 2007, 293, E576-586.

(71) Katsoulieris, E.; Mabley, J. G.; Samai, M.; Green, I. C.; Chatterjee, P. K. alpha-Linolenic acid protects renal cells against palmitic acid lipotoxicity via inhibition of endoplasmic reticulum stress. Eur J Pharmacol 2009, 623, 107-112.

(72) Beeharry, N.; Lowe, J. E.; Hernandez, A. R.; Chambers, J. A.; Fucassi, F.; Cragg, P. J.; Green, M. H. L.; Green, I. C. Linoleic acid and antioxidants protect against DNA damage and apoptosis induced by palmitic acid. Mutation Research/Fundamental and Molecular Mechanisms of Mutagenesis 2003, 530, 27-33.

(73) Akasaka, H.; Mizushina, Y.; Yoshida, K.; Ejima, Y.; Mukumoto, N.; Wang, T.; Inubushi, S.; Nakayama, M.; Wakahara, Y.; Sasaki, R. MGDG extracted from spinach enhances the cytotoxicity of radiation in pancreatic cancer cells. Radiation oncology 2016, 11, 153.

(74) Maeda, N.; Matsubara, K.; Yoshida, H.; Mizushina, Y. Anti-cancer effect of spinach glycoglycerolipids as angiogenesis inhibitors based on the selective inhibition of DNA polymerase activity. Mini reviews in medicinal chemistry 2011, 11, 32-38.

SECTION

2. CONCLUSION

The synthesis and therapeutic efficacy of PTXNR-TTZ ADNs *in vitro* were presented which arrested the HER2-positive breast cancer cells in G2/M phase of the cell cycle and induced caspase mediated apoptosis. The synthesized ~95 nm in diameter and 500 nm in length PTXNR particles showed significantly high stability in aqueous phase compared to the PTX, suggesting removal of the compromising need for organic carrier solvent for intravenous delivery. The *in vitro* toxicity analysis showed that the engineered drug PTXNR-TTZ was more efficacious than the individual drug treatments with PTX or TTZ alone, inhibiting >80% of HER2-positive cell line growth suggesting a synergistic effect on the cancer cells. The IC_{50} of PTXNR-TTZ on HER2-positive BT-474 breast cancer cell line was 106 nM, facilitating lower dose and reduced side effects than the individual treatment with PTX and TTZ alone. The Western blot analysis showed that PTXNR-TTZ significantly downregulated the anti-apoptotic protein XIAP and induced caspase dependent apoptosis pathway in HER2-positive breast cancer cell line. Altogether, the investigation might facilitate rational remodeling of conventional combination therapy in cancer through ADN that integrates high therapeutic index and active targeting capability.

The present work showed that PTXNR-TTZ induced apoptosis in HER2-positive breast cancer cell lines following the G2/M cell cycle arrest. The cell cycle is critical for normal tissue functioning and also an important regulator of ungoverned cancer cell

progression. Hence, a comprehensive knowledge of cell cycle regulation and its regulators is a prior need for better understanding of cancer. The review article presented in the dissertation has discussed some of the critical intracellular cell cycle regulating signaling pathways such as MAPK/Ras/Raf/ERK, PI3K/Akt. Jak-STAT. The intrinsic and extrinsic apoptosis pathways were also discussed. The article showed the molecular interplay between the cell proliferation and cell death pathways.

Transcriptional regulation and genetic alterations induced by PTXNR-TTZ was investigated in breast cancer cell lines. The objective of the study was to investigate the potential role of cell cycle arresting mechanism on the therapeutic efficacy of the PTXNR-TTZ treatment in breast cancer cells. PTXNR-TTZ significantly overexpressed PRKG1 and NR4A3 genes in HER2-positive cell line. The gene regulatory network showed that PTXNR-TTZ might potentially induce intrinsic apoptosis pathway through positive regulation of PRKG1- NR4A3 gene expression. PTXNR-TTZ treatment upregulated the CDC20 gene expression which plays an oncogenic role in cancer progression. The study concluded that hyperactivity of CDC20 and subsequent activation of its substrates *e.g.,* APC/C might cause therapeutic inefficacy of PTXNR-TTZ treatment in HER2-positive breast cancer cells. Hence, we proposed CDC20 as a potential therapeutic target to enhance the treatment response of PTXNR-TTZ. PTXNR-TTZ also significantly upregulated a set of tumor promoting inflammatory genes in a non-specific triple negative MDA-MB-231 cell line. Taken together, the study investigated cell cycle dependent gene regulatory pathways induced by PTXNR-TTZ that can be addressed for possible therapeutic response or treatment resistance in breast cancer cells.

Additionally, in this work, multifunctional efficacy of a polymer coated superparamagnetic nanoparticle therapeutic system was investigated in cancer treatment. The work showed the significant enhancement of the metal nanoparticle stability by using a biocompatible polymer coating and utilization as a potential nanomedicine platform. The application of the therapeutic platform integrated both diagnostics and therapeutics capability in a single system.

Finally, *in vitro* anti-proliferation efficacy of a natural glycoglycerolipid molecule MGDG, was investigated for breast cancer treatment. The MGDG molecule rich in ω-6 γ-linolenic fatty acid content was extracted from a cyanobacterial species *Synechocystis* sp. A simple low cost technique was shown in the study to efficiently extract the MGDG molecule with high purity. The molecule had better therapeutic efficacy than the commercial plant extract molecule and did not show any significant toxicity in normal human cell line. Altogether, the study presented a cost effective extraction method and anti-proliferation efficacy of a natural source potential anti-cancer molecule.

3. FUTURE WORKS

3.1. INVESTIGATION OF THERAPEUTIC EFFICACY OF PTXNR-TTZ IN *IN VIVO* SETTINGS

We have shown the formulation of a combination therapeutic system PTXNR-TTZ for targeted HER2-positive breast cancer cell growth inhibition. We thoroughly investigated the therapeutic efficacy of PTXNR-TTZ in *in vitro* settings. The *in vitro* results showed synergistic cell growth inhibition in HER2-positive breast cancer cell line by PTXNR-TTZ treatment. In future, we propose to investigate the therapeutic efficacy of PTXNR-TTZ in an *in vivo* HER2-positive breast cancer model.

- ***In vivo* tumor cell growth inhibition:** A cell derived xenografts (CDX) model with the HER2-positive breast cancer phenotype will be chosen for the *in vivo* study. For example, an established BT-474 cancer cell line transplanted (subcutaneously) nude mice model representing the luminal B/HER2-positive subtype of breast cancer is available and can be used for investigating the *in vivo* tumor growth inhibition upon intraperitoneal injection (i.p.) of PTXNR-TTZ drug. The controls for the investigation will include 1) no treatment, 2) PTXNR treatment, 3) TTZ treatment and 4) combination treatment of PTXNR+TTZ. The tumor growth can be monitored in every 3 days and normalized to the initial tumor volume at the starting point of the treatment.
- ***In vivo* biodistribution study:** The PTXNR-TTZ particles will be functionalized with a metal binding chelator molecule p-SCN-Bn-DOTA (SBnD) by utilizing the solvent accessible the ε-lysine amino group of TTZ. The immunoconjugate (TTZ-SBnD) will then be radiolabeled with ^{64}Cu isotope to produce a radioactive PTXNR-TTZ-SBnD-^{64}Cu

complex. For biodistribution analysis, the PTXNR-TTZ-SBnD-^{64}Cu complex will be intravenously administered in a subcutaneously engrafted BT-474 tumor bearing mice model. The mice will be sacrificed at 2, 6, 12, 24, 48 and 72 h following administration of the radioactive complex. The organs will be separated and weighed followed by the measurement of the radioactivity. The time dependent measurements for each organ will be expressed as a percentage of injected dose per gram (%ID/gram).

3.2. INVESTIGATION OF GENE REGULATION ACTIVITY OF PTXNR-TTZ IN *IN VITRO* AND *IN VIVO* PLATFORM

We found that PTXNR-TTZ significantly induced the high mRNA expression of NR4A3 and PRKG1 genes in HER2-positive breast cancer cells by analyzing the transcriptional data obtained from RNAseq analysis. In subsequent gene regulatory network analysis, we showed that the overregulation of NR4A3-PRKG1 axis can potentially mediate the intrinsic apoptosis pathway. We have also showed the activation of downstream Rho-GTPase signaling pathway in HER2-positive breast cancer cells by PTXNR-TTZ treatment. Notably, we found that PTXNR-TTZ significantly upregulates the CDC20 gene expression which exerts an oncogenic activity in tumor progression by activating APC/C^{CDC20} complex. We predicted that the targeted inhibition of CDC20 will enhance the therapeutic efficacy of PTXNR-TTZ. In future, we propose to verify our predictions from RNA sequencing data analysis experimentally in both *in vitro* and *in vivo* settings. The gene expression of NR4A3 and PRKG1 and induction of possible apoptosis pathway in HER2-positive breast cancer will be investigated in HER2-positive cell lines *in vitro* and in mouse xenograft model *in vivo*. Similarly, *in vitro* and *in vivo*

therapeutic efficacy of PTXNR-TTZ will be evaluated upon targeted inhibition of CDC20 gene expression. We have outlined our plans in the following points.

- **Investigation of PTXNR-TTZ induced NR4A3 mediated apoptosis:** The HER2-positive cell lines BT-474 and SK-BR-3 will be treated with PTXNR-TTZ *in vitro*. The controls will include 1) no treatment 2) PTXNR treatment 3) TTZ treatment 4) PTXNR+TTZ treatment. The gene expression of NR4A3 and PRKG1 will be investigated using reverse transcriptase quantitative polymerase chain reaction (RT-qPCR) analysis. For RT-qPCR analysis, the cells will be lysed followed by the synthesis of cDNA from the cell lysates. The synthesized cDNA will then be incorporated with the primers of NR4A3 and PRKG1 genes along with the DNA polymerase enzymes for subsequent RT-PCR amplification reactions. Appropriate commercial kits and manufacturer's protocols will be used for cDNA synthesis and RT-qPCR reactions. For *in vitro* apoptosis response study, the total protein will be extracted from the HER2-positive breast cancer cell lines. The PTXNR-TTZ treated HER2-negative cell line extracted total protein will be used as a control sample. The protein expression of NR4A3, PRKG1 and other downstream proteins associated with intrinsic apoptosis pathway will be investigated using the Western blot analysis. For *in vivo* analysis, the PTXNR-TTZ drug along with the other appropriate controls will be injected in a transplanted xenograft mice model with established HER2-positive breast tumor. For selective gene expression analysis, a patient derived xenografts (PDX) immune-deficient mice model with established HER2-positive breast cancer is more preferable than CDX model due to high similarity and maintenance in the genomic signature of the tumor tissue representing the original primary tumor in patient. The tumor volume will be monitored and tumor tissue sample will be collected upon significant

volume remission with PTXNR-TTZ treatment. The total protein will be extracted from the tumor tissue for subsequent protein expression analysis using Western blot technique.

- **Efficacy of PTXNR-TTZ upon targeted inhibition of CDC20 gene expression:** The PTXNR-TTZ induced gene expression of CDC20 in HER2-positive breast cancer cell lines will be verified by RT-qPCR analysis. To investigate the possible role of CDC20 gene overexpression on cell growth CDC20 will be inhibited by a CDC20 antagonist drug. The CDC20 gene may be knocked down using an appropriate silencing RNA (siRNA) molecule as well. The cell viability assays will be conducted following the PTXNR-TTZ treatment with the cells 1) before, and 2) after the targeted inhibition of CDC20 gene expression. The control treatments will include 1) no treatment, and 2) PTXNR+TTZ treatment. The investigation can also be conducted in an immune-deficient nude mice PDX model with established HER2-positive breast cancer phenotype. The mice will be treated with i.p. injection of CDC20 inhibitor for CDC20 gene inhibition. The mice treated with i.p. injection of PTXNR-TTZ along with other mentioned appropriate controls before and after the CDC20 inhibition will be monitored every three days and normalized to tumor volume at treatment start point.

APPENDIX A.

SUPPLEMENTARY INFORMATION: PAPER I

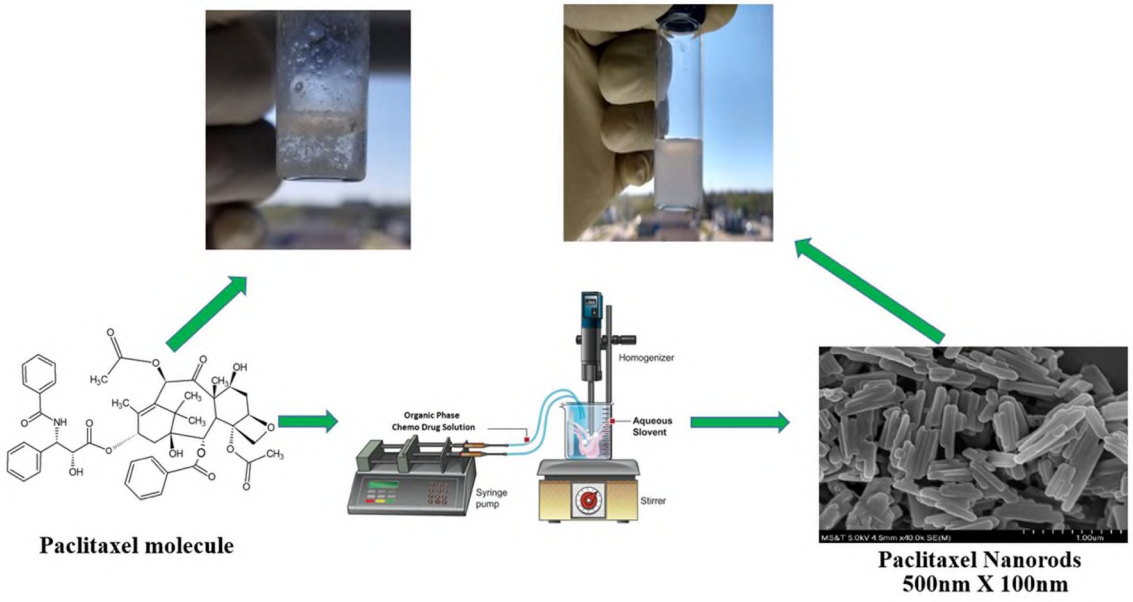

Figure 1. Synthesis process of PTXNRs. PTXNRs were synthesized using the nanoprecipitation method. The figure shows the stability of the paclitaxel molecule and PTXNR in aqueous media before and after the synthesis process

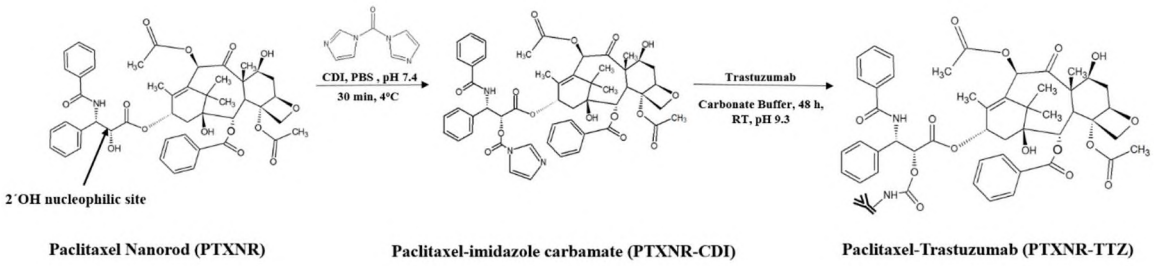

Figure 2. Schematic diagram of reactions involved for PTXNR functionalization and TTZ conjugation on the surface of PTXNRs

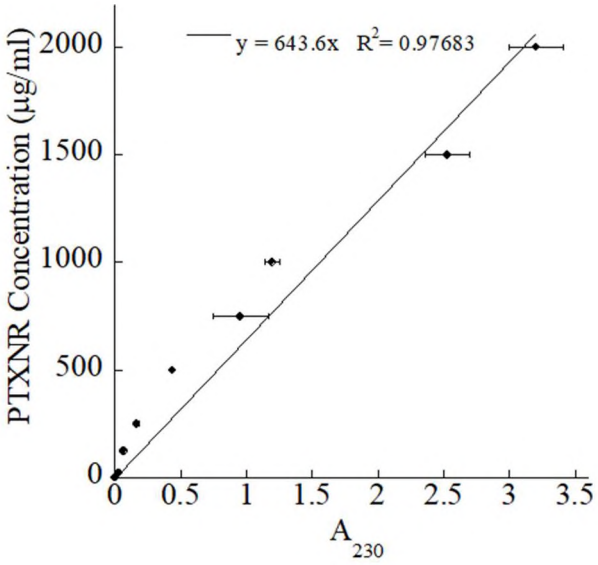

Figure 3. Calibration curve of PTX for quantification of the amount of PTXNRs in PTXNR-TTZ particles after conjugation with TTZ. The calibration curve was obtained using PTXNRs in PBS at 230 nm absorbance values

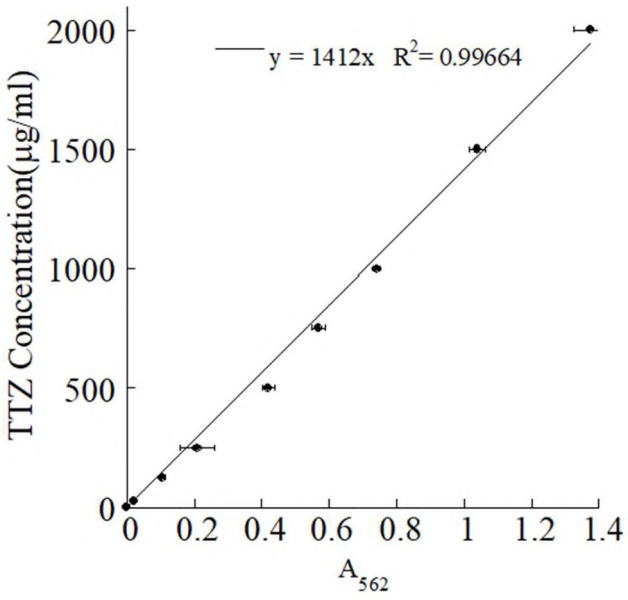

Figure 4. Calibration curve of Trastuzumab (TTZ) monoclonal antibody for quantification of unconjugated TTZ after conjugation with Paclitaxel nanorods (PTXNRs). The calibration curve was obtained using a BCA protein quantification assay at 562 nm absorbance values

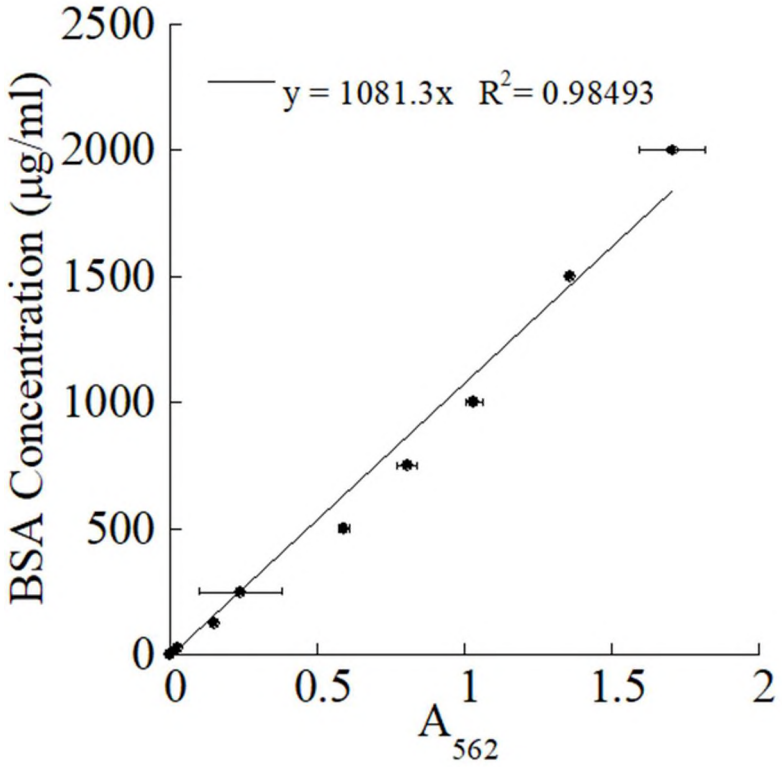

Figure 5. Calibration curve of BSA protein for quantification of protein in cell lysates for Western blot experiments. The calibration curve was obtained using a BCA protein quantification assay at 562 nm absorbance values

Table 1. Stability analysis of PTXNR and PTXNR-TTZ as a measure of zeta potential value, ζ (mV)

	Zeta potential, ζ (mV)	
Sample	**DI water**	**PBS**
PTXNR	-32.6± 4.82	-13.4± 2.81
PTXNR-TTZ	-17.1±3.83	-9.5± 0.02

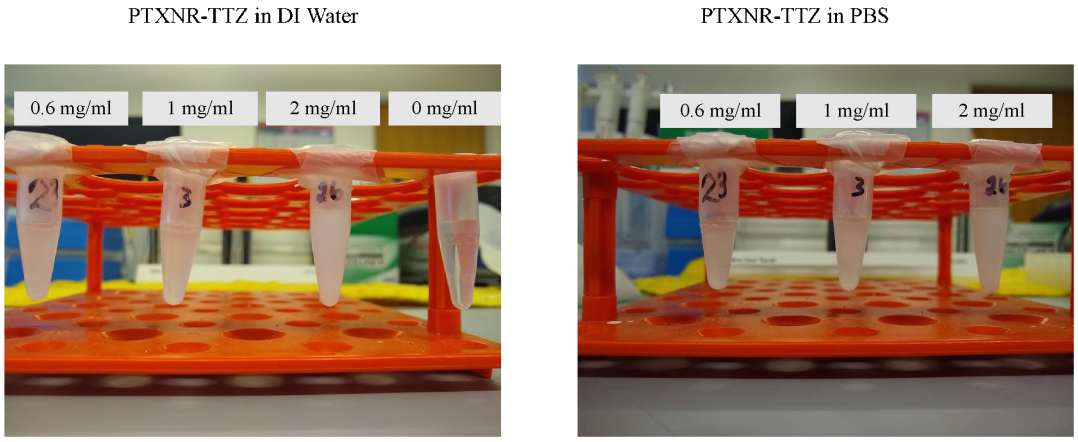

Figure 6. Colloidal suspensions of PTXNR-TTZ in DI water and PBS at 0.6, 1, and 2 mg/ml concentrations

Table 2. Analysis of TTZ conjugation on the surface of PTXNRs

Initial PTX amount (mg)	**% NR formation**	**Initial PTXNR-CDI amount (mg)**	**Initial TTZ amount (mg)**	**% TTZ conjugation efficiency**	**Amount of PTXNR in 1 mg of PTXNR-TTZ (mg)**	**Amount of TTZ in 1 mg of PTXNR-TTZ (mg)**	**PTXNR : TTZ (w/w)**
30	64.98±2.37	1.0	0.10	95.24±1.40	0.8±0.02	0.2±0.02	4.0±0.53

(a) Untreated

(b) PTXNR

(c) TTZ

(d) PTXNR-TTZ

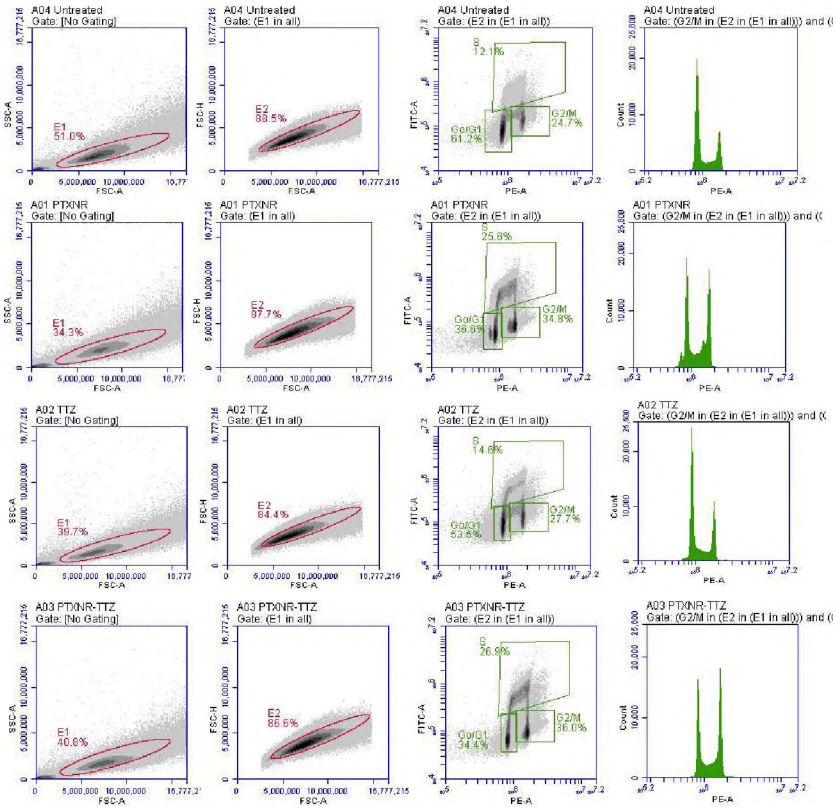

Figure 7. Flow cytometry data for cell cycle analysis of (a) untreated, (b) PTXNR, (c) TTZ, and (d) PTXNR-TTZ treated BT-474 cells after 24 h. The side scatter (SSC-A) *versus* forward scatter (FSC-A) gating is used to identify BT-474 cells as gated by E1. The forward scatter height (FSC-H) *versus* forward scatter area (FSC-A) density plots exclude doublet cells for accurate counting as shown by E2 gating. The plots showing FITC-A and PE-A represent live cells and their stained DNA, respectively, and gated for DNA analysis using Count *versus* PE-A plots. The Count *versus* PE-A plots were analyzed using the flow cytometry software to calculate the percentage arrests in G0/G1 (first sharp peak), S (flattened areas), and G2/M (second sharp peak) phases

(a) Untreated

(b) PTXNR

(c) TTZ

(d) PTXNR-TTZ

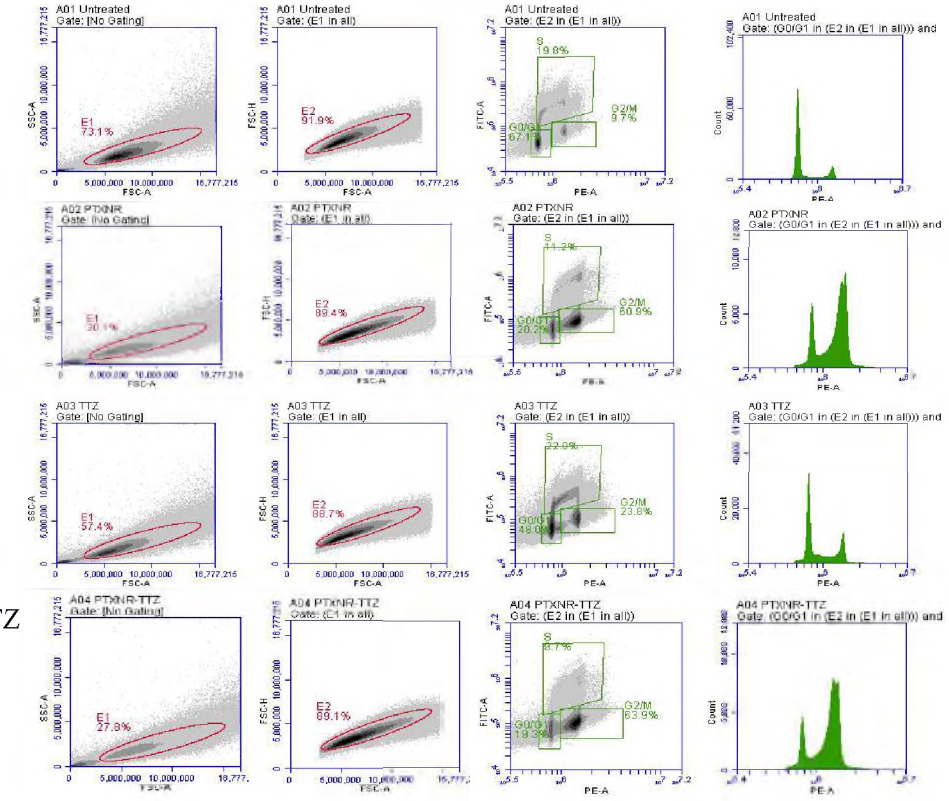

Figure 8. Flow cytometry data for cell cycle analysis of (a) untreated, (b) PTXNR, (c) TTZ, and (d) PTXNR-TTZ treated BT-474 cells after 48 h. The histogram of relative DNA content in Count *versus* PE-A plots shows a shift in peaks from G0/G1 to G2/M cells in PTXNR and PTXNR-TTZ treated cells compared to untreated and TTZ treated cells

(a) Untreated

(b) PTXNR

(c) TTZ

(d) PTXNR-TTZ

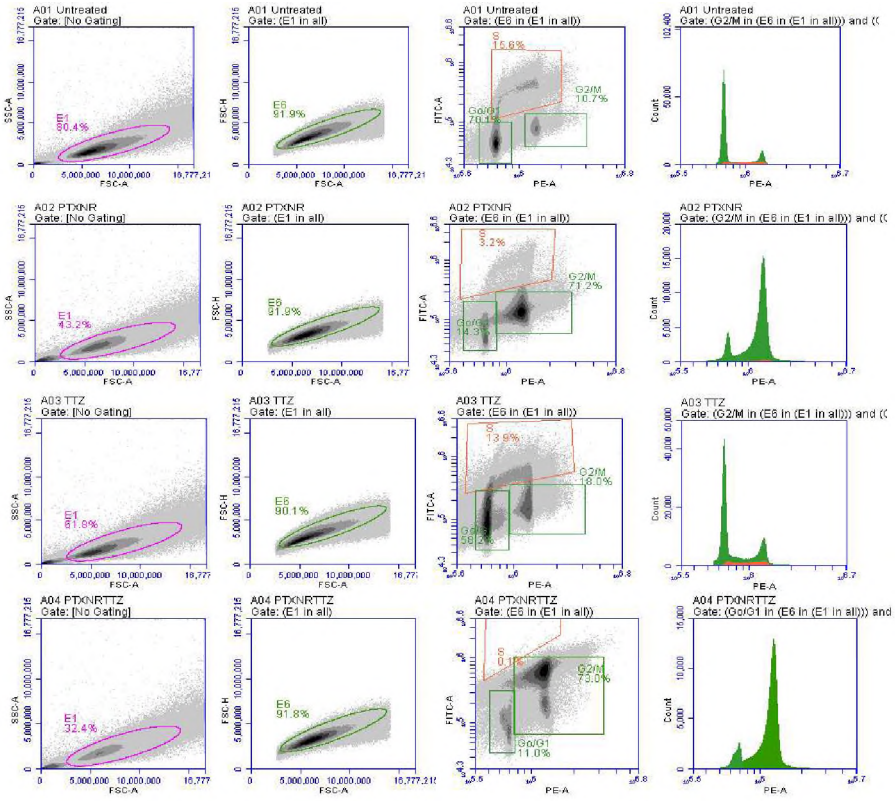

Figure 9. Flow cytometry data for cell cycle analysis of (a) untreated, (b) PTXNR, (c) TTZ, and (d) PTXNR-TTZ treated BT-474 cells after 72h. By the end of the incubation periods, >80% of cells were arrested in G2/M phases after PTXNR and PTXNR-TTZ treatments, while untreated and TTZ treated cells showed most cells in G0/G1

APPENDIX B.

SUPPLEMENTARY INFORMATION: PAPER IV

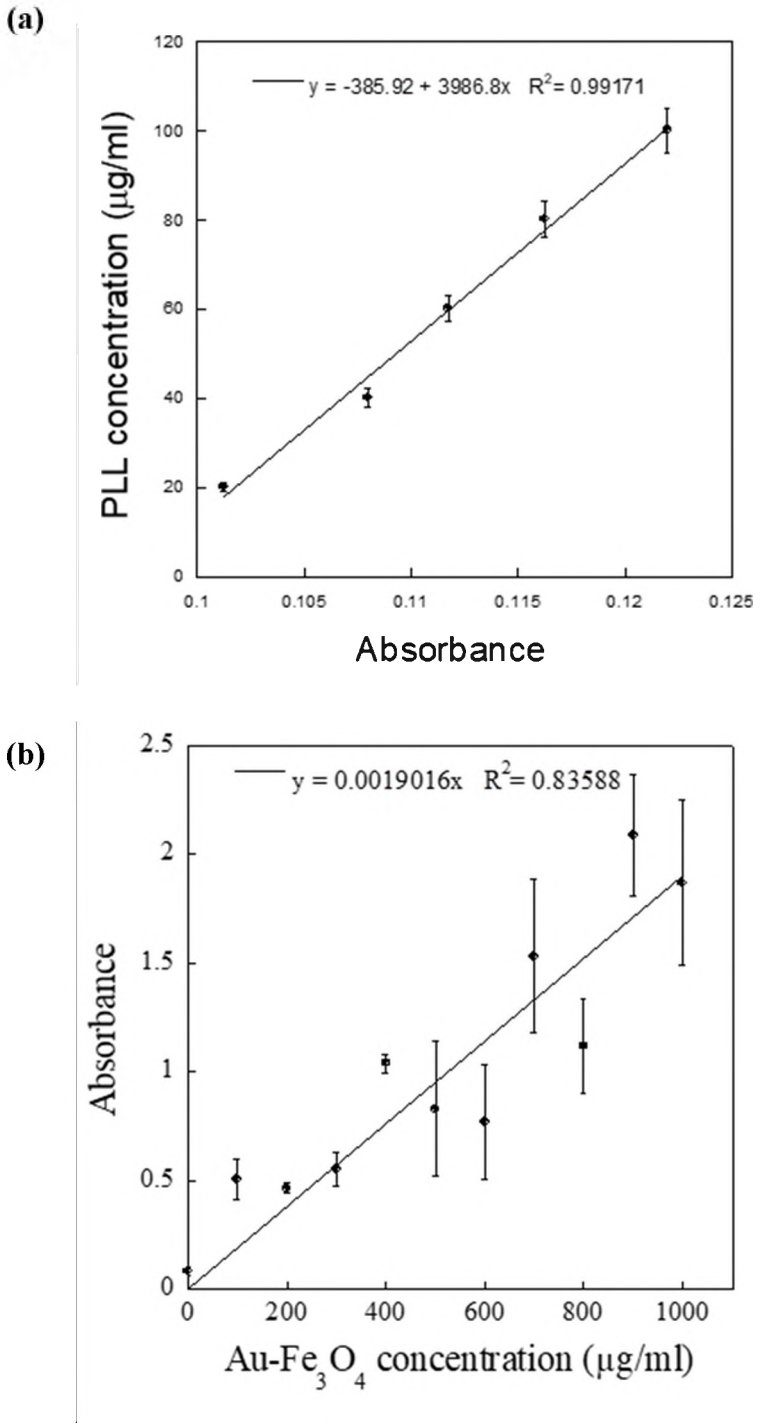

Figure 1. (a): PLL trypan blue standard curve; and (b) Au–Fe_3O_4 concentration measurement standard line

(a)

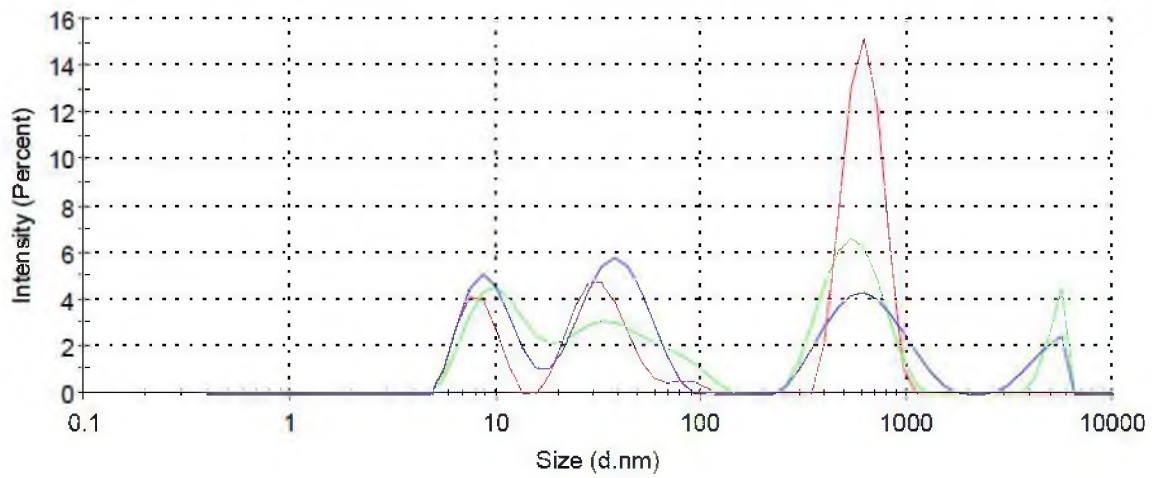

(b)

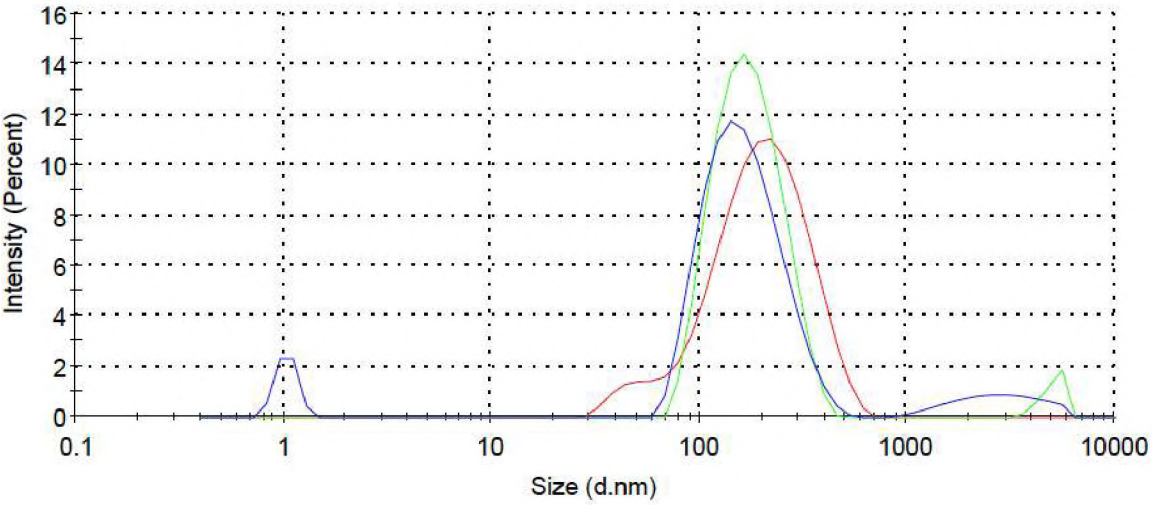

Figure 2. Hydrodynamic diameters of (a) Au–Fe_3O_4 NPs and (b) PLL coated Au–Fe_3O_4 NPs in water as measured by dynamic light scattering (DLS). Three color codes indicate three independent DLS measurements

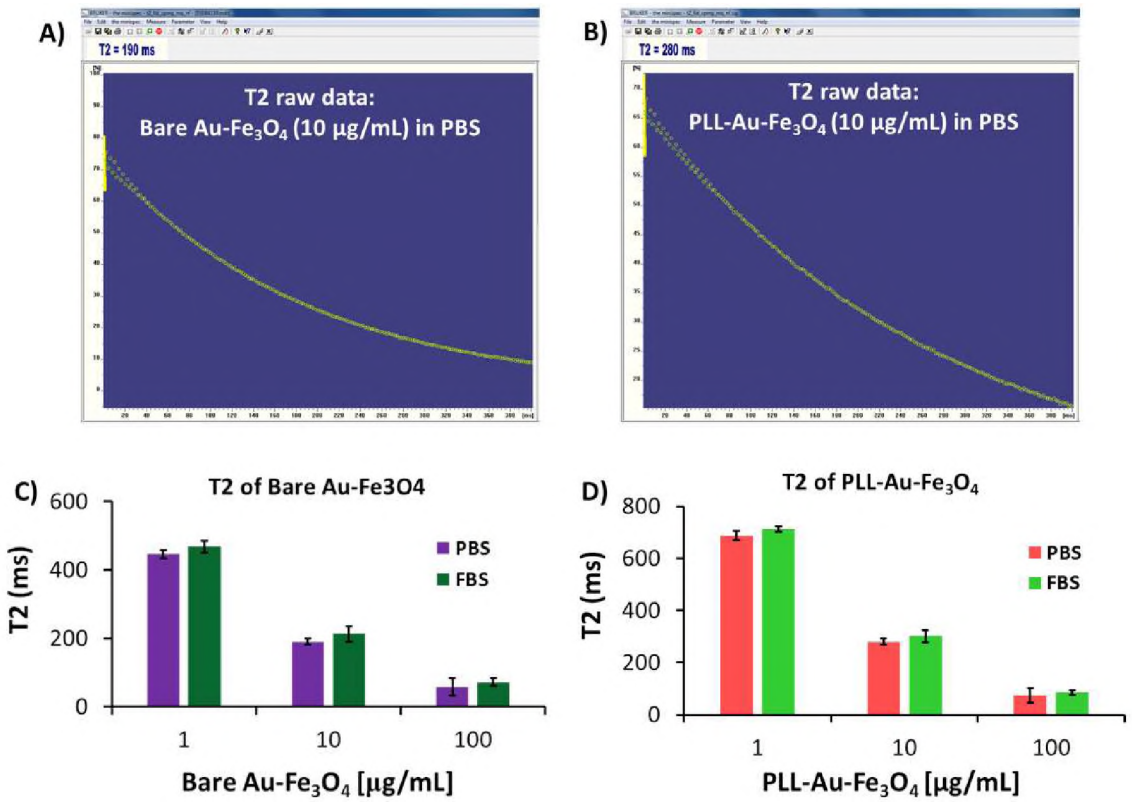

Figure 3. Magnetic relaxation (MR) characterization of (A and C) Au–Fe_3O_4 and (B and D) PLL–Au–Fe_3O_4 NPs. A) Spin-spin MR (T_2 ms) of bare Au–Fe_3O_4 NPs was found to be 190 ms, whereas, it was B) 280 ms for PLL–Au–Fe_3O_4 NPs at a given concentration of 10 µg/mL. This change in T_2 MR value is the indicative of effective PLL coatings. Concentration dependent (1-100 µg/mL) T_2 values were obtained in PBS (pH 7.2) and in 10% FBS for C) Au–Fe_3O_4 and D) PLL–Au–Fe_3O_4 NPs. These results indicated that with increase in concentration, the MR properties of these NPs increase and were found to be stable in physiological pH and in sera

(a)

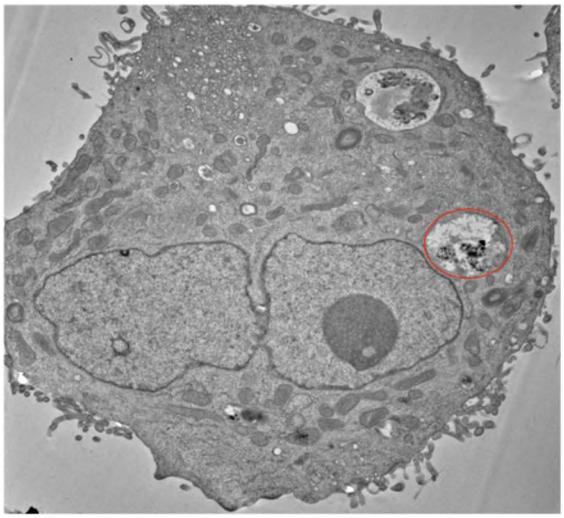

(b)

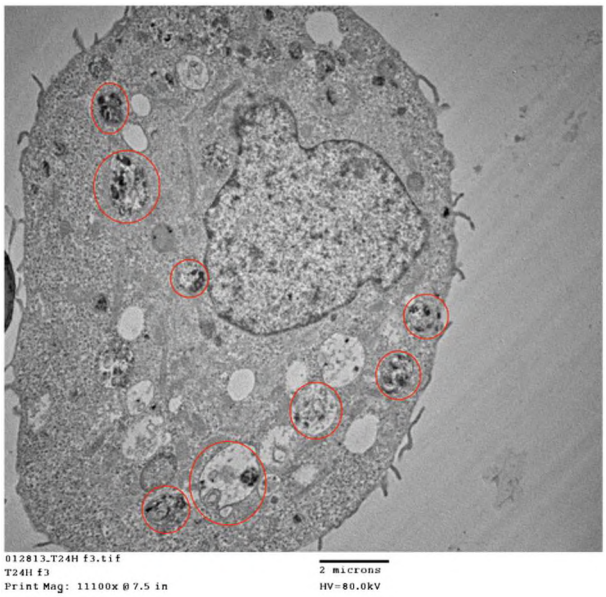

Figure 4. The PLL–Au–Fe_3O_4 NPs uptake by (a) BT-474 and (b) MDA-MB-231 cells after 24 h incubation. Red circles indicate the endosomal vesicles that clearly retain the NPs as appeared in dark black spots

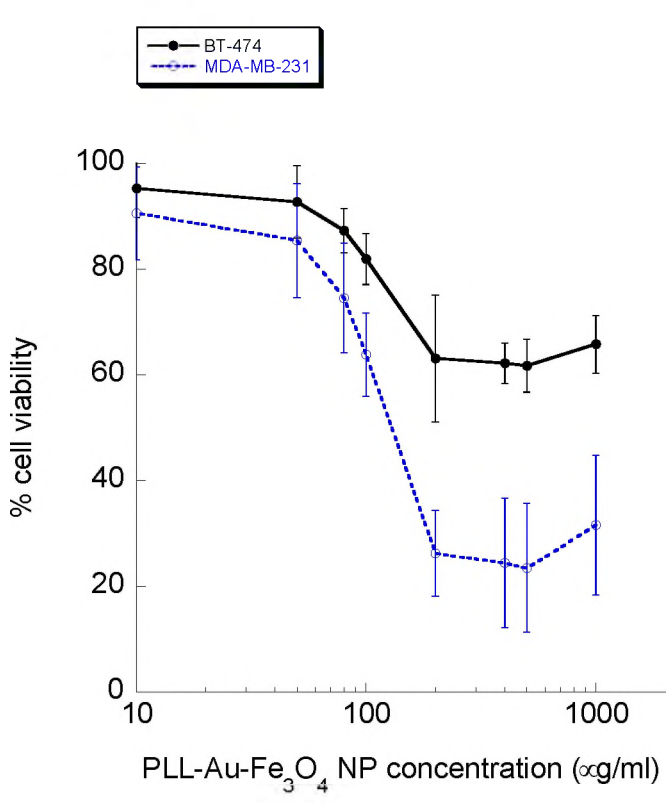

Figure 5. MTT cell viability assay of BT-474 (filled circle, solid line) and MDA-MB-231 (open circle, dotted line) cell viability after treatment with PLL–Au–Fe_3O_4 NPs under a 650 nm laser irradiation for 10 min

Table 1. The percentage encapsulation efficiency of PLL on Au–Fe_3O_4 NPs

mg Au–Fe_3O_4	**mg of PLL in PLL–Au–Fe_3O_4**	**% PLL encapsulation efficiency**
25	0.47 ± 0.03	73 ± 3

APPENDIX C.

SUPPLEMENTARY INFORMATION: PAPER V

(a)

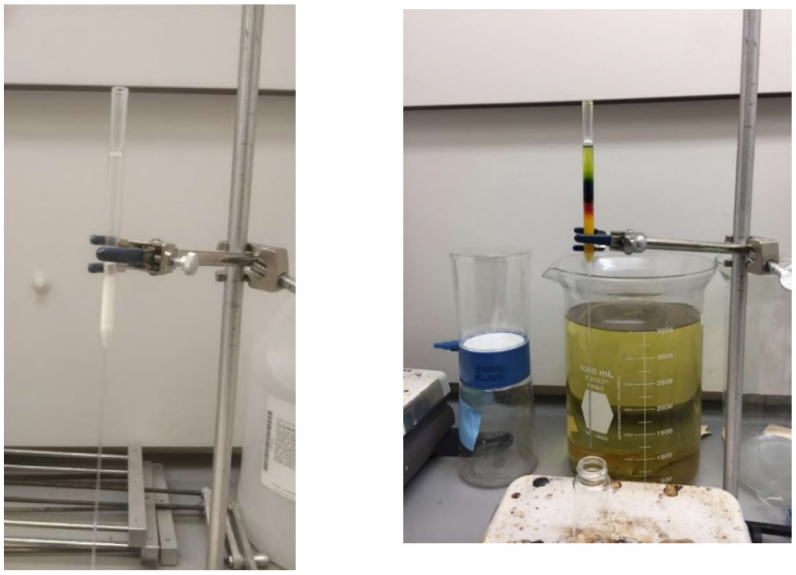

(b)

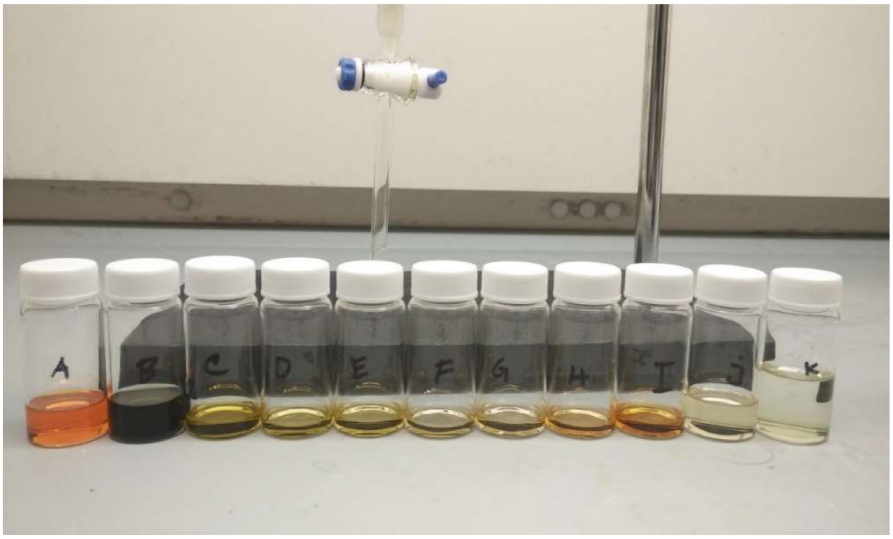

Figure 1. Fractionation of total lipid using column chromatography technique.
(a) Fractionation of total lipid in a handmade column. Silica gel (10-40 μm) was used as a stationary phase. Chloroform and acetone were used as the mobile phase.
(b) The fractionated samples were collected separately by observing the color difference of individual lipid class. Eluent 1: fraction A, eluent 2: fraction B, eluent 3: fraction C, D, E, F, G, eluent 4: fraction H, I, J, eluent 5: fraction K

Table 1. Chromatographic fractionation method of total lipid, A-Chloroform; B-Acetone

Eluent	**A (%)**	**B (%)**	**Volume (ml)**
1	100	0	10
2	90	10	10
3	75	25	10
4	40	60	10
5	0	100	10

Table 2. HPLC column preparation and conditions for detection and quantification of MGDG

Column	LiChrospher 100 Diol 25-4, 5 µm (Normal Phase Column)
Detector	UV (240 nm)
Mobile phase	Solution A: Chloroform, Solution B: Methanol/water (95:5 v/v)
Flow rate	1 ml/min
Injection volume	25 µl
Column temperature	RT

Table 3. HPLC elution method for detection and quantification of MGDG

Time (min)	A (%)	B (%)
0	99	1
15	75	25
20	10	90
25	10	90
30	99	1

Table 4. Corresponding peak areas of increasing concentration of standard MGDG

Concentration (µg/ml)	Peak Area (mAU.s)
0	0
5	24.57
8	47.26
10	66.28
50	596.63
100	1610.78
150	2505.67

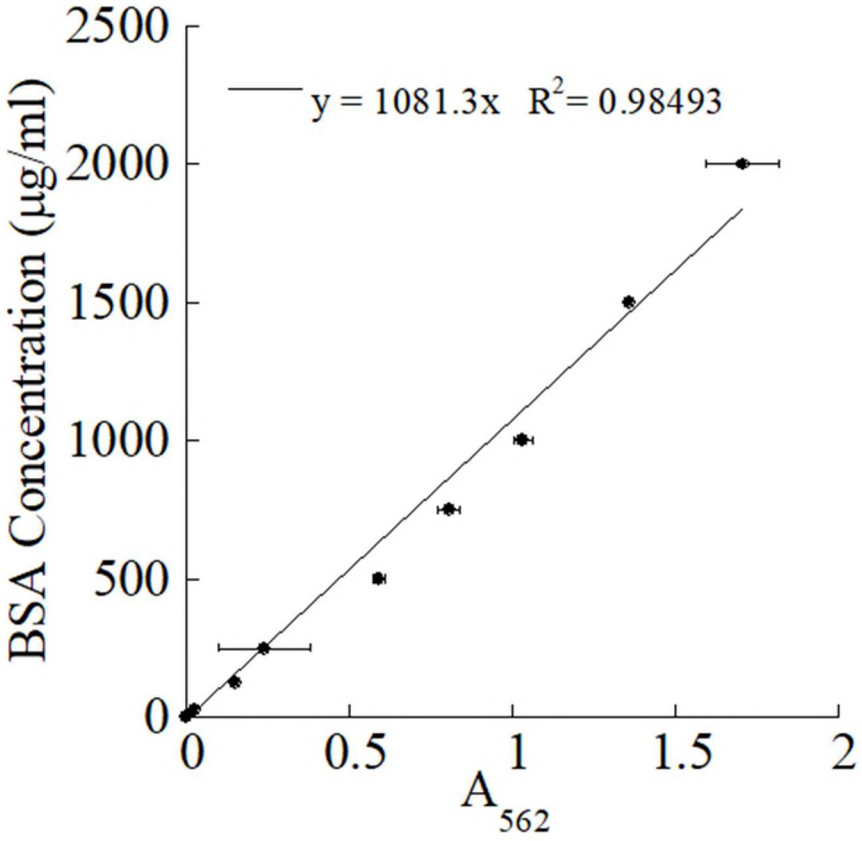

Figure 2. Calibration curve of BSA protein for quantification of protein in cell lysates for Western blot experiments. The calibration curve was obtained using a BCA protein quantification assay at 562 nm absorbance values

1. WESTERN BLOT ANALYSIS

Western blot analysis was performed to verify the active caspase-3 expression of the standard and *Synechocystis* sp. extracted MGDG treated BT-474 and MDA-MB-231 cells. Approximately, 10^6 cells were seeded in 25 cm^2 cell culture flasks and treated with 100 ng/ml standard MGDG and *Synechocystis* sp. extracted MGDG. After 72 h of incubation, the cells were trypsinized for total protein extraction using the radioimmunoprecipitation assay (RIPA) lysis buffer. The total protein was quantified using the BCA calibration curve (SI Figure 2). For SDS-PAGE, the samples were prepared in 2X Laemmli loading buffer. The samples were denatured at 86°C for 2-3 min and loaded on the 16% Novex Tris-Glycine gels (Invitrogen). The gel was run in tris-glycine-SDS running buffer at constant 200 V for 30-40 min. The separated protein bands on the gel were transferred to the nitrocellulose membrane using the Power Blotter (Invitrogen). The membrane blot was rinsed briefly with tris buffered saline including 1% tween-20 (TBST) for 2-3 min and was blocked with 3% bovine serum albumin (BSA) protein (Fisher Scientific) at room temperature for 5 h. After blocking, the membrane was incubated overnight in the primary antibody caspase-3 (ThermoFisher, Cat. 43-7800) and actin (ThermoFisher Cat. MA5-11869) at 4°C with the dilution factor of 1:500 and 1:3000, respectively. The membrane was washed 3-5 times with TBST buffer for 5 min each followed by the incubation with anti-mouse horseradish peroxidase (HRP) conjugated secondary antibody (ThermoFisher Cat. A27025). The membrane blot was incubated in secondary the antibody for 1 h with the dilution factor of 1:10,000 followed by washing with TBST buffer. Finally, the blot was incubated in electro-

chemiluminescent reagent (Super Signal West Dura, ThermoFisher, and Cat. 34075) for 5 min and was imaged using a Bio-Rad gel imaging system.

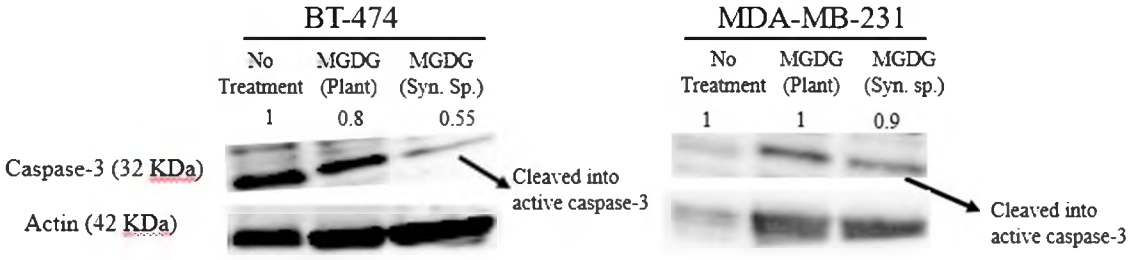

Figure 3. The Western blot assay confirming the reduced full-length caspase-3 protein expressions in BT-474 (left panel) and MDA-MB-231 (right panel) cell lines treated with MGDG extracted from *Synechocystis* sp. compared to untreated and MGDG standard treated samples. Caspase-3 (32 kDa) is cleaved into lower molecular weight (17kDa) active caspase-3/7 that is shown by fluorescence microscopic images and flow cytometry quantification in Figure 8 of the main texts

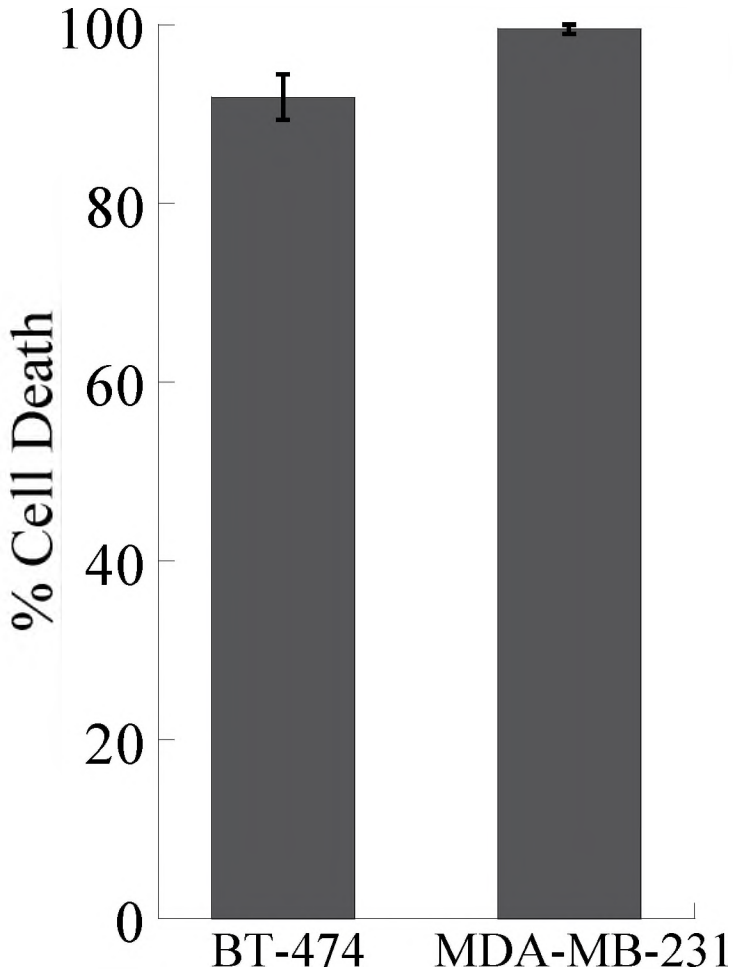

Figure 4. Dead control cells induced by saponin was used in MTT assay

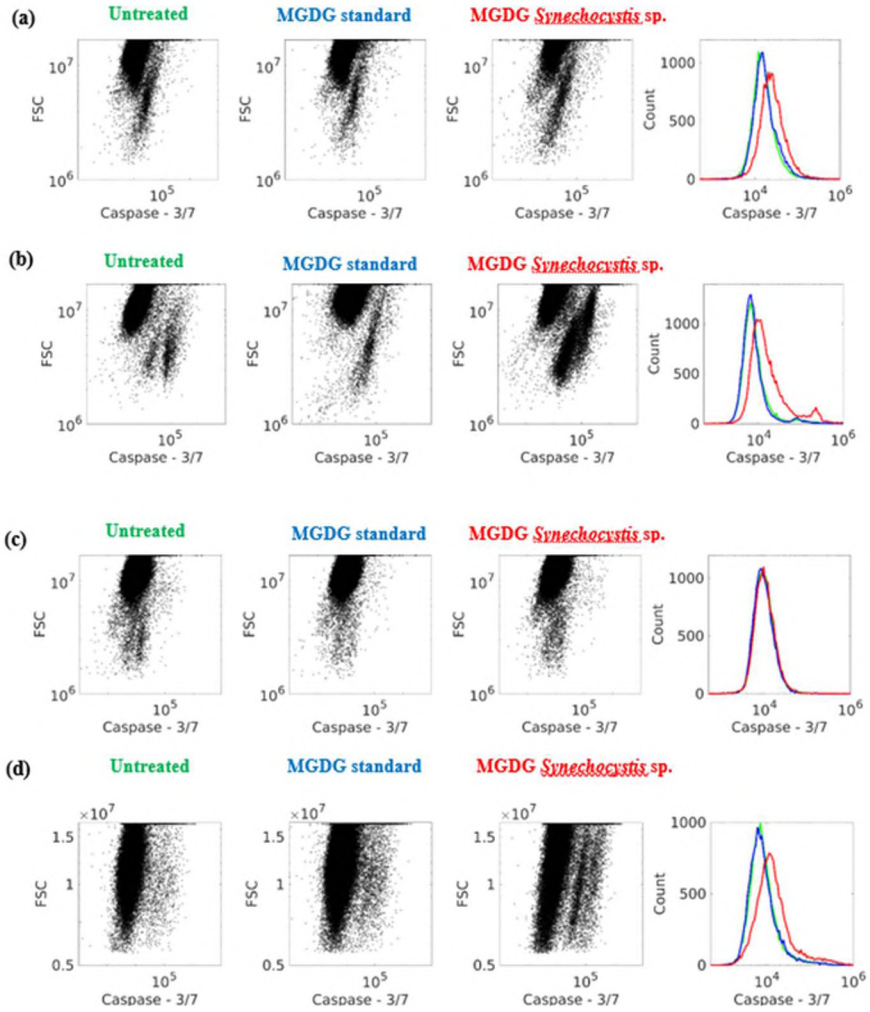

Figure 5. Quantification of apoptosis assay. For quantification of apoptosis induction the BT-474 and MDA-MB-231 cells were treated with standard plant extract MGDG and *Synechocystis* sp. extracted MGDG with 100 ng/ml dose. The cleaved caspase-3/7 fluorescence intensity data were collected using flow cytometry. The scatter plots were generated for each treatment showing cleaved caspase-3/7 fluorescence data in x-axis and forward scattering (FSC) values in y-axis. A combined histogram was also generated for each treatment showing cleaved caspase-3//7 fluorescence intensity distribution in cell population. The green, blue and red lines represent the histogram data for untreated, MGDG standard treated and *Synechocystis* sp. extracted MGDG treated samples. The scatter plots and combined histograms were generated for treatments in BT-474 cell line after (a) 48 h and (b) 72 h and in MDA-MB-231 cell line after (c) 48 h and (d) 72 h. In BT-474 cell line, the mean cleaved caspase-3/7 fluorescence intensity was shifted by 1.7±0.04 ($p<0.01$) and 2.34±0.44 ($p<0.01$) fold in *Synechocystis* sp. extracted MGDG treated cells compared to untreated control cells after 48 h and 72 h of treatment, respectively. In MDA-MB-231 cell line, the shift in mean fluorescence intensity was 0.95±0.01 and 2.1±0.03 fold ($p<0.01$) in *Synechocystis* sp. treated cells after 48 h and 72 h, respectively compared to untreated control cells

BIBLIOGRAPHY

(1) Siegel, R. L.; Miller, K. D.; Jemal, A. Cancer statistics, 2019. CA: a cancer journal for clinicians 2019, 69, 7-34.

(2) Shi, J.; Kantoff, P. W.; Wooster, R.; Farokhzad, O. C. Cancer nanomedicine: progress, challenges and opportunities. Nature Reviews Cancer 2017, 17, 20.

(3) Specification, P. A.: Terminology for nanomaterials. British Standards Institute London, 2007.

(4) Kim, B. Y.; Rutka, J. T.; Chan, W. C. Nanomedicine. New England Journal of Medicine 2010, 363, 2434-2443.

(5) Kim, B. Y. S.; Rutka, J. T.; Chan, W. C. W. Nanomedicine. New England Journal of Medicine 2010, 363, 2434-2443.

(6) Peer, D.; Karp, J. M.; Hong, S.; Farokhzad, O. C.; Margalit, R.; Langer, R. Nanocarriers as an emerging platform for cancer therapy. Nature nanotechnology 2007, 2, 751-760.

(7) Xia, Y.; Xiong, Y.; Lim, B.; Skrabalak, S. E. Shape-controlled synthesis of metal nanocrystals: simple chemistry meets complex physics? Angewandte Chemie International Edition 2009, 48, 60-103.

(8) Doll, T. A.; Raman, S.; Dey, R.; Burkhard, P. Nanoscale assemblies and their biomedical applications. Journal of The Royal Society Interface 2013, 10, 20120740.

(9) Wang, A. Z.; Tepper, J. E. Nanotechnology in radiation oncology. Journal of clinical oncology : official journal of the American Society of Clinical Oncology 2014, 32, 2879-2885.

(10) Fisher, B. Biological Research in the Evolution of Cancer Surgery: A Personal Perspective. Cancer Research 2008, 68, 10007-10020.

(11) Fisher, B. Cancer surgery: A commentary. Cancer Treat Rep 1984, 68, 31-41.

(12) Baskar, R.; Dai, J.; Wenlong, N.; Yeo, R.; Yeoh, K.-W. Biological response of cancer cells to radiation treatment. Frontiers in molecular biosciences 2014, 1, 24.

(13) Kannan, R.; Zambre, A.; Chanda, N.; Kulkarni, R.; Shukla, R.; Katti, K.; Upendran, A.; Cutler, C.; Boote, E.; Katti, K. V. Functionalized radioactive gold nanoparticles in tumor therapy. Wiley Interdisciplinary Reviews: Nanomedicine and Nanobiotechnology 2012, 4, 42-51.

(14) Van den Heuvel, F.; Locquet, J.-P.; Nuyts, S. Beam energy considerations for gold nano-particle enhanced radiation treatment. Physics in Medicine & Biology 2010, 55, 4509.

(15) Wunderlich, G.: Radioactive Microspheres. In Clinical Nuclear Medicine; Springer, 2020; pp 951-959.

(16) Abshire, D.; Lang, M. K. In Tilte2018; Elsevier.

(17) Baskar, R.; Lee, K. A.; Yeo, R.; Yeoh, K.-W. Cancer and radiation therapy: current advances and future directions. Int J Med Sci 2012, 9, 193-199.

(18) Jackson, S. P.; Bartek, J. The DNA-damage response in human biology and disease. Nature 2009, 461, 1071-1078.

(19) Chen, H. H.; Kuo, M. T. Improving radiotherapy in cancer treatment: promises and challenges. Oncotarget 2017, 8, 62742.

(20) Wang, W.; Zhang, F.; Hu, K.; Hou, X. Image-guided, intensity-modulated radiation therapy in definitive radiotherapy for 1433 patients with cervical cancer. Gynecologic Oncology 2018, 151, 444-448.

(21) Gupta, T.; Narayan, C. A. Image-guided radiation therapy: Physician's perspectives. Journal of medical physics/Association of Medical Physicists of India 2012, 37, 174.

(22) Ma, L.; Wang, L.; Tseng, C. L.; Sahgal, A. Emerging technologies in stereotactic body radiotherapy. Chinese clinical oncology 2017, 6, S12.

(23) Czernin, J.; Allen-Auerbach, M.; Schelbert, H. R. Improvements in cancer staging with PET/CT: literature-based evidence as of September 2006. Journal of Nuclear Medicine 2007, 48, 78S.

(24) Bar-Shalom, R.; Yefremov, N.; Guralnik, L.; Gaitini, D.; Frenkel, A.; Kuten, A.; Altman, H.; Keidar, Z.; Israel, O. Clinical performance of PET/CT in evaluation of cancer: additional value for diagnostic imaging and patient management. Journal of nuclear medicine 2003, 44, 1200-1209.

(25) Chandarana, H.; Wang, H.; Tijssen, R. H. N.; Das, I. J. Emerging role of MRI in radiation therapy. Journal of magnetic resonance imaging : JMRI 2018, 48, 1468-1478.

(26) Das, I. J.; McGee, K. P.; Tyagi, N.; Wang, H. Role and future of MRI in radiation oncology. The British journal of radiology 2019, 92, 20180505.

(27) Abshire, D.; Lang, M. K. The Evolution of Radiation Therapy in Treating Cancer. Seminars in oncology nursing 2018, 34, 151-157.

(28) Chidambaram, M.; Manavalan, R.; Kathiresan, K. Nanotherapeutics to overcome conventional cancer chemotherapy limitations. Journal of pharmacy & pharmaceutical sciences 2011, 14, 67-77.

(29) Bianchini, G.; Balko, J. M.; Mayer, I. A.; Sanders, M. E.; Gianni, L. Triple-negative breast cancer: challenges and opportunities of a heterogeneous disease. Nature reviews Clinical oncology 2016, 13, 674.

(30) Kondo, N.; Takahashi, A.; Ono, K.; Ohnishi, T. DNA damage induced by alkylating agents and repair pathways. Journal of nucleic acids 2010, 2010.

(31) Malhotra, V.; Perry, M. C. Classical chemotherapy: mechanisms, toxicities and the therapeutc window. Cancer biology & therapy 2003, 2, 1-3.

(32) Fu, D.; Calvo, J. A.; Samson, L. D. Balancing repair and tolerance of DNA damage caused by alkylating agents. Nature Reviews Cancer 2012, 12, 104-120.

(33) Longley, D. B.; Harkin, D. P.; Johnston, P. G. 5-fluorouracil: mechanisms of action and clinical strategies. Nature reviews cancer 2003, 3, 330-338.

(34) Burger, R. M.; Peisach, J.; Horwitz, S. B. Mechanism of bleomycin action: in vitro studies. Life sciences 1981, 28, 715-727.

(35) Dorr, R. T. In Tilte1992.

(36) Zunino, F.; Capranico, G. DNA topoisomerase II as the primary target of anti-tumor anthracyclines. Anti-cancer drug design 1990, 5, 307.

(37) Chow, K.-C.; Macdonald, T. L.; Ross, W. E. DNA binding by epipodophyllotoxins and N-acyl anthracyclines: implications for mechanism of topoisomerase II inhibition. Molecular Pharmacology 1988, 34, 467-473.

(38) Jordan, M. A.; Thrower, D.; Wilson, L. Mechanism of inhibition of cell proliferation by Vinca alkaloids. Cancer research 1991, 51, 2212-2222.

(39) Yang, C.-P. H.; Horwitz, S. B. Taxol®: the first microtubule stabilizing agent. International journal of molecular sciences 2017, 18, 1733.

(40) Weaver, B. A. How Taxol/paclitaxel kills cancer cells. Molecular biology of the cell 2014, 25, 2677-2681.

(41) Rahier, N. J.; Thomas, C. J.; Hecht, S. M. Camptothecin and its analogs. Anticancer agents from natural products 2005, 5, 22.

(42) Crow, R. T.; Crothers, D. M. Structural modifications of camptothecin and effects on topoisomerase I inhibition. Journal of medicinal chemistry 1992, 35, 4160-4164.

(43) Couzin-Frankel, J.: Cancer immunotherapy. American Association for the Advancement of Science, 2013.

(44) Postow, M. A.; Callahan, M. K.; Wolchok, J. D. Immune checkpoint blockade in cancer therapy. Journal of clinical oncology 2015, 33, 1974.

(45) Ribas, A.; Wolchok, J. D. Cancer immunotherapy using checkpoint blockade. Science 2018, 359, 1350-1355.

(46) Seidel, J. A.; Otsuka, A.; Kabashima, K. Anti-PD-1 and anti-CTLA-4 therapies in cancer: mechanisms of action, efficacy, and limitations. Frontiers in oncology 2018, 8, 86.

(47) Wei, S. C.; Duffy, C. R.; Allison, J. P. Fundamental mechanisms of immune checkpoint blockade therapy. Cancer discovery 2018, 8, 1069-1086.

(48) Stoiber, S.; Cadilha, B. L.; Benmebarek, M.-R.; Lesch, S.; Endres, S.; Kobold, S. Limitations in the design of chimeric antigen receptors for cancer therapy. Cells 2019, 8, 472.

(49) Hudis, C. A. Trastuzumab—mechanism of action and use in clinical practice. New England Journal of Medicine 2007, 357, 39-51.

(50) Shashidharamurthy, R.; Bozeman, E. N.; Patel, J.; Kaur, R.; Meganathan, J.; Selvaraj, P. Immunotherapeutic strategies for cancer treatment: a novel protein transfer approach for cancer vaccine development. Medicinal research reviews 2012, 32, 1197-1219.

(51) Peer, D. Harnessing RNAi nanomedicine for precision therapy. Molecular and cellular therapies 2014, 2, 5.

(52) de Lázaro, I.; Mooney, D. J. A nanoparticle's pathway into tumours. Nature Materials 2020, 19, 486-487.

(53) Rosenblum, D.; Joshi, N.; Tao, W.; Karp, J. M.; Peer, D. Progress and challenges towards targeted delivery of cancer therapeutics. Nature communications 2018, 9, 1-12.

(54) Barenholz, Y. C. Doxil®—the first FDA-approved nano-drug: lessons learned. Journal of controlled release 2012, 160, 117-134.

(55) Gradishar, W. J.; Tjulandin, S.; Davidson, N.; Shaw, H.; Desai, N.; Bhar, P.; Hawkins, M.; O'Shaughnessy, J. Phase III trial of nanoparticle albumin-bound paclitaxel compared with polyethylated castor oil–based paclitaxel in women with breast cancer. Journal of clinical oncology 2005, 23, 7794-7803.

(56) Miele, E.; Spinelli, G. P.; Miele, E.; Tomao, F.; Tomao, S. Albumin-bound formulation of paclitaxel (Abraxane® ABI-007) in the treatment of breast cancer. International journal of nanomedicine 2009, 4, 99.

(57) Silverman, J. A.; Deitcher, S. R. Marqibo®(vincristine sulfate liposome injection) improves the pharmacokinetics and pharmacodynamics of vincristine. Cancer chemotherapy and pharmacology 2013, 71, 555-564.

(58) Rosenthal, E.; Poizot-Martin, I.; Saint-Marc, T.; Spano, J.-P.; Cacoub, P.; Group, D. S. Phase IV study of liposomal daunorubicin (DaunoXome) in AIDS-related Kaposi sarcoma. American journal of clinical oncology 2002, 25, 57-59.

(59) Zhang, H. Onivyde for the therapy of multiple solid tumors. Onco Targets Ther 2016, 9, 3001.

(60) Lamb, Y. N.; Scott, L. J. Liposomal irinotecan: a review in metastatic pancreatic adenocarcinoma. Drugs 2017, 77, 785-792.

(61) Lancet, J. E.; Uy, G. L.; Cortes, J. E.; Newell, L. F.; Lin, T. L.; Ritchie, E. K.; Stuart, R. K.; Strickland, S. A.; Hogge, D.; Solomon, S. R.: Final results of a phase III randomized trial of CPX-351 versus 7+ 3 in older patients with newly diagnosed high risk (secondary) AML. American Society of Clinical Oncology, 2016.

(62) Swenson, C.; Perkins, W.; Roberts, P.; Janoff, A. Liposome technology and the development of Myocet™(liposomal doxorubicin citrate). The Breast 2001, 10, 1-7.

(63) Leonard, R.; Williams, S.; Tulpule, A.; Levine, A.; Oliveros, S. Improving the therapeutic index of anthracycline chemotherapy: focus on liposomal doxorubicin (Myocet™). The Breast 2009, 18, 218-224.

(64) Meyers, P. A. Muramyl tripeptide (mifamurtide) for the treatment of osteosarcoma. Expert review of anticancer therapy 2009, 9, 1035-1049.

(65) Frampton, J. E. Mifamurtide. Pediatric Drugs 2010, 12, 141-153.

(66) Kim, T.-Y.; Kim, D.-W.; Chung, J.-Y.; Shin, S. G.; Kim, S.-C.; Heo, D. S.; Kim, N. K.; Bang, Y.-J. Phase I and pharmacokinetic study of Genexol-PM, a cremophor-free, polymeric micelle-formulated paclitaxel, in patients with advanced malignancies. Clinical cancer research 2004, 10, 3708-3716.

(67) Maeda, H. SMANCS and polymer-conjugated macromolecular drugs: advantages in cancer chemotherapy. Advanced drug delivery reviews 2001, 46, 169-185.

(68) Maeda, H. Macromolecular therapeutics in cancer treatment: the EPR effect and beyond. Journal of Controlled Release 2012, 164, 138-144.

(69) Chauhan, V. P.; Jain, R. K. Strategies for advancing cancer nanomedicine. Nature materials 2013, 12, 958-962.

(70) Byrne, J. D.; Betancourt, T.; Brannon-Peppas, L. Active targeting schemes for nanoparticle systems in cancer therapeutics. Advanced drug delivery reviews 2008, 60, 1615-1626.

(71) Bertrand, N.; Wu, J.; Xu, X.; Kamaly, N.; Farokhzad, O. C. Cancer nanotechnology: the impact of passive and active targeting in the era of modern cancer biology. Advanced drug delivery reviews 2014, 66, 2-25.

(72) Shi, J.; Xiao, Z.; Kamaly, N.; Farokhzad, O. C. Self-assembled targeted nanoparticles: evolution of technologies and bench to bedside translation. Accounts of chemical research 2011, 44, 1123-1134.

(73) Maruyama, K. PEG-immunoliposome. Bioscience reports 2002, 22, 251-266.

(74) Karmali, P. P.; Kotamraju, V. R.; Kastantin, M.; Black, M.; Missirlis, D.; Tirrell, M.; Ruoslahti, E. Targeting of albumin-embedded paclitaxel nanoparticles to tumors. Nanomedicine: Nanotechnology, Biology and Medicine 2009, 5, 73-82.

(75) Davis, M. E.; Zuckerman, J. E.; Choi, C. H. J.; Seligson, D.; Tolcher, A.; Alabi, C. A.; Yen, Y.; Heidel, J. D.; Ribas, A. Evidence of RNAi in humans from systemically administered siRNA via targeted nanoparticles. Nature 2010, 464, 1067-1070.

(76) Pederzoli, F.; Tosi, G.; Vandelli, M. A.; Belletti, D.; Forni, F.; Ruozi, B. Protein corona and nanoparticles: how can we investigate on? Wiley Interdisciplinary Reviews: Nanomedicine and Nanobiotechnology 2017, 9, e1467.

(77) Xiao, W.; Gao, H. The impact of protein corona on the behavior and targeting capability of nanoparticle-based delivery system. International Journal of Pharmaceutics 2018, 552, 328-339.

(78) Caracciolo, G.; Farokhzad, O. C.; Mahmoudi, M. Biological identity of nanoparticles in vivo: clinical implications of the protein corona. Trends in biotechnology 2017, 35, 257-264.

(79) Hadjidemetriou, M.; Kostarelos, K. Evolution of the nanoparticle corona. Nature nanotechnology 2017, 12, 288-290.

(80) Cheng, X.; Tian, X.; Wu, A.; Li, J.; Tian, J.; Chong, Y.; Chai, Z.; Zhao, Y.; Chen, C.; Ge, C. Protein corona influences cellular uptake of gold nanoparticles by phagocytic and nonphagocytic cells in a size-dependent manner. ACS applied materials & interfaces 2015, 7, 20568-20575.

(81) Schmidt, M. M.; Wittrup, K. D. A modeling analysis of the effects of molecular size and binding affinity on tumor targeting. Molecular cancer therapeutics 2009, 8, 2861-2871.

(82) Sahay, G.; Alakhova, D. Y.; Kabanov, A. V. Endocytosis of nanomedicines. Journal of controlled release 2010, 145, 182-195.

(83) Vermeulen, L. M.; De Smedt, S. C.; Remaut, K.; Braeckmans, K. The proton sponge hypothesis: Fable or fact? European Journal of Pharmaceutics and Biopharmaceutics 2018, 129, 184-190.

(84) Sahay, G.; Querbes, W.; Alabi, C.; Eltoukhy, A.; Sarkar, S.; Zurenko, C.; Karagiannis, E.; Love, K.; Chen, D.; Zoncu, R. Efficiency of siRNA delivery by lipid nanoparticles is limited by endocytic recycling. Nature biotechnology 2013, 31, 653-658.

(85) Stuchbery, R.; J Kurganovs, N.; J McCoy, P.; C Nelson, C.; M Hayes, V.; M Corcoran, N.; M Hovens, C. Target acquired: progress and promise of targeted therapeutics in the treatment of prostate cancer. Current cancer drug targets 2015, 15, 394-405.

(86) Pearce, A. K.; O'Reilly, R. K. Insights into active targeting of nanoparticles in drug delivery: advances in clinical studies and design considerations for cancer nanomedicine. Bioconjugate chemistry 2019, 30, 2300-2311.

(87) Hamaguchi, T.; Matsumura, Y.; Nakanishi, Y.; Muro, K.; Yamada, Y.; Shimada, Y.; Shirao, K.; Niki, H.; Hosokawa, S.; Tagawa, T. Antitumor effect of MCC-465, pegylated liposomal doxorubicin tagged with newly developed monoclonal antibody GAH, in colorectal cancer xenografts. Cancer science 2004, 95, 608-613.

(88) Camp, E.; Wang, C.; Little, E.; Watson, P.; Pirollo, K.; Rait, A.; Cole, D.; Chang, E.; Watson, D. Transferrin receptor targeting nanomedicine delivering wild-type p53 gene sensitizes pancreatic cancer to gemcitabine therapy. Cancer gene therapy 2013, 20, 222-228.

(89) Senzer, N.; Nemunaitis, J.; Nemunaitis, D.; Bedell, C.; Edelman, G.; Barve, M.; Nunan, R.; Pirollo, K. F.; Rait, A.; Chang, E. H. Phase I study of a systemically delivered p53 nanoparticle in advanced solid tumors. Molecular Therapy 2013, 21, 1096-1103.

(90) Adams, G. P.; Weiner, L. M. Monoclonal antibody therapy of cancer. Nature biotechnology 2005, 23, 1147-1157.

(91) Romond, E. H.; Perez, E. A.; Bryant, J.; Suman, V. J.; Geyer Jr, C. E.; Davidson, N. E.; Tan-Chiu, E.; Martino, S.; Paik, S.; Kaufman, P. A. Trastuzumab plus adjuvant chemotherapy for operable HER2-positive breast cancer. New England Journal of Medicine 2005, 353, 1673-1684.

(92) Lane, D. Designer combination therapy for cancer. Nature Biotechnology 2006, 24, 163-164.

(93) Brasó-Maristany, F.; Griguolo, G.; Pascual, T.; Paré, L.; Nuciforo, P.; Llombart-Cussac, A.; Bermejo, B.; Oliveira, M.; Morales, S.; Martínez, N.; Vidal, M.; Adamo, B.; Martínez, O.; Pernas, S.; López, R.; Muñoz, M.; Chic, N.; Galván, P.; Garau, I.; Manso, L.; Alarcón, J.; Martínez, E.; Gregorio, S.; Gomis, R. R.; Villagrasa, P.; Cortés, J.; Ciruelos, E.; Prat, A. Phenotypic changes of HER2-positive breast cancer during and after dual HER2 blockade. Nature communications 2020, 11, 385.

(94) Marty, M.; Cognetti, F.; Maraninchi, D.; Snyder, R.; Mauriac, L.; Tubiana-Hulin, M.; Chan, S.; Grimes, D.; Antón, A.; Lluch, A. Randomized phase II trial of the efficacy and safety of trastuzumab combined with docetaxel in patients with human epidermal growth factor receptor 2–positive metastatic breast cancer administered as first-line treatment: the M77001 study group. Journal of clinical oncology 2005, 23, 4265-4274.

(95) Von Minckwitz, G.; Procter, M.; De Azambuja, E.; Zardavas, D.; Benyunes, M.; Viale, G.; Suter, T.; Arahmani, A.; Rouchet, N.; Clark, E. Adjuvant pertuzumab and trastuzumab in early HER2-positive breast cancer. New England Journal of Medicine 2017, 377, 122-131.

(96) Goldhirsch, A.; Gelber, R. D.; Piccart-Gebhart, M. J.; De Azambuja, E.; Procter, M.; Suter, T. M.; Jackisch, C.; Cameron, D.; Weber, H. A.; Heinzmann, D. 2 years versus 1 year of adjuvant trastuzumab for HER2-positive breast cancer (HERA): an open-label, randomised controlled trial. The Lancet 2013, 382, 1021-1028.

(97) Piccart-Gebhart, M. J.; Procter, M.; Leyland-Jones, B.; Goldhirsch, A.; Untch, M.; Smith, I.; Gianni, L.; Baselga, J.; Bell, R.; Jackisch, C. Trastuzumab after adjuvant chemotherapy in HER2-positive breast cancer. New England Journal of Medicine 2005, 353, 1659-1672.

(98) Slamon, D.; Eiermann, W.; Robert, N.; Pienkowski, T.; Martin, M.; Press, M.; Mackey, J.; Glaspy, J.; Chan, A.; Pawlicki, M. Adjuvant trastuzumab in HER2-positive breast cancer. New England Journal of Medicine 2011, 365, 1273-1283.

(99) Perez, E.; Romond, E.; Suman, V. Trastuzumab plus adjuvant chemotherapy for HER2-positive breast cancer: Final planned joint analysis of overall survival (OS) from NSABP B-31 and NCCTG N9831. Journal of clinical oncology : official journal of the American Society of Clinical Oncology 2014, 32, 3744-3752.

(100) Baselga, J.; Norton, L.; Albanell, J.; Kim, Y. M.; Mendelsohn, J. Recombinant humanized anti-HER2 antibody (Herceptin) enhances the antitumor activity of paclitaxel and doxorubicin against HER2/neu overexpressing human breast cancer xenografts. Cancer Res 1998, 58, 2825-2831.

(101) Topham, C. H.; Taylor, S. S. Mitosis and apoptosis: how is the balance set? Current opinion in cell biology 2013, 25, 780-785.

(102) Vegran, F.; Boidot, R.; Coudert, B.; Fumoleau, P.; Arnould, L.; Garnier, J.; Causeret, S.; Fraise, J.; Dembele, D.; Lizard-Nacol, S. Gene expression profile and response to trastuzumab-docetaxel-based treatment in breast carcinoma. Br J Cancer 2009, 101, 1357-1364.

(103) Tolaney, S. M.; Barry, W. T.; Dang, C. T.; Yardley, D. A.; Moy, B.; Marcom, P. K.; Albain, K. S.; Rugo, H. S.; Ellis, M.; Shapira, I.; Wolff, A. C.; Carey, L. A.; Overmoyer, B. A.; Partridge, A. H.; Guo, H.; Hudis, C. A.; Krop, I. E.; Burstein, H. J.; Winer, E. P. Adjuvant Paclitaxel and Trastuzumab for Node-Negative, HER2-Positive Breast Cancer. New England Journal of Medicine 2015, 372, 134-141.

(104) Tolaney, S. M.; Guo, H.; Pernas, S.; Barry, W. T.; Dillon, D. A.; Ritterhouse, L.; Schneider, B. P.; Shen, F.; Fuhrman, K.; Baltay, M.; Dang, C. T.; Yardley, D. A.; Moy, B.; Marcom, P. K.; Albain, K. S.; Rugo, H. S.; Ellis, M. J.; Shapira, I.; Wolff, A. C.; Carey, L. A.; Overmoyer, B.; Partridge, A. H.; Hudis, C. A.; Krop, I. E.; Burstein, H. J.; Winer, E. P. Seven-Year Follow-Up Analysis of Adjuvant Paclitaxel and Trastuzumab Trial for Node-Negative, Human Epidermal Growth Factor Receptor 2-Positive Breast Cancer. Journal of clinical oncology : official journal of the American Society of Clinical Oncology 2019, 37, 1868-1875.

(105) Chalouni, C.; Doll, S. Fate of Antibody-Drug Conjugates in Cancer Cells. J Exp Clin Cancer Res 2018, 37, 20-20.

(106) Chalouni, C.; Doll, S. Fate of antibody-drug conjugates in cancer cells. Journal of Experimental & Clinical Cancer Research 2018, 37, 20.

(107) Kalim, M.; Chen, J.; Wang, S.; Lin, C.; Ullah, S.; Liang, K.; Ding, Q.; Chen, S.; Zhan, J. Intracellular trafficking of new anticancer therapeutics: antibody–drug conjugates. Drug design, development and therapy 2017, 11, 2265.

(108) Kovtun, Y. V.; Audette, C. A.; Ye, Y.; Xie, H.; Ruberti, M. F.; Phinney, S. J.; Leece, B. A.; Chittenden, T.; Blättler, W. A.; Goldmacher, V. S. Antibody-drug conjugates designed to eradicate tumors with homogeneous and heterogeneous expression of the target antigen. Cancer research 2006, 66, 3214-3221.

(109) Parslow, A. C.; Parakh, S.; Lee, F.-T.; Gan, H. K.; Scott, A. M. Antibody–drug conjugates for cancer therapy. Biomedicines 2016, 4, 14.

(110) Schrama, D.; Reisfeld, R. A.; Becker, J. C. Antibody targeted drugs as cancer therapeutics. Nature reviews Drug discovery 2006, 5, 147-159.

(111) Sievers, E. L.; Senter, P. D. Antibody-drug conjugates in cancer therapy. Annual review of medicine 2013, 64.

(112) Wagner-Rousset, E.; Janin-Bussat, M.-C.; Colas, O.; Excoffier, M.; Ayoub, D.; Haeuw, J.-F.; Rilatt, I.; Perez, M.; Corvaïa, N.; Beck, A. In Tilte2014; Taylor & Francis.

(113) Beck, A.; Goetsch, L.; Dumontet, C.; Corvaïa, N. Strategies and challenges for the next generation of antibody–drug conjugates. Nature reviews Drug discovery 2017, 16, 315-337.

(114) Casi, G.; Neri, D. Antibody–Drug Conjugates and Small Molecule–Drug Conjugates: Opportunities and Challenges for the Development of Selective Anticancer Cytotoxic Agents: Miniperspective. Journal of medicinal chemistry 2015, 58, 8751-8761.

(115) Gordon, M. R.; Canakci, M.; Li, L.; Zhuang, J.; Osborne, B.; Thayumanavan, S. Field guide to challenges and opportunities in antibody–drug conjugates for chemists. Bioconjugate chemistry 2015, 26, 2198-2215.

(116) Kamath, A. V.; Iyer, S. Challenges and advances in the assessment of the disposition of antibody-drug conjugates. Biopharmaceutics & drug disposition 2016, 37, 66-74.

(117) Nejadmoghaddam, M.-R.; Minai-Tehrani, A.; Ghahremanzadeh, R.; Mahmoudi, M.; Dinarvand, R.; Zarnani, A.-H. Antibody-drug conjugates: possibilities and challenges. Avicenna J Med Biotechnol 2019, 11, 3.

(118) Sau, S.; Alsaab, H. O.; Kashaw, S. K.; Tatiparti, K.; Iyer, A. K. Advances in antibody–drug conjugates: a new era of targeted cancer therapy. Drug discovery today 2017, 22, 1547-1556.

(119) Beck, A.; Goetsch, L.; Dumontet, C.; Corvaïa, N. Strategies and challenges for the next generation of antibody-drug conjugates. Nat Rev Drug Discov 2017, 16, 315-337.

(120) Benderra, Z.; Faussat, A. M.; Sayada, L.; Perrot, J.-Y.; Tang, R.; Chaoui, D.; Morjani, H.; Marzac, C.; Marie, J.-P.; Legrand, O. MRP3, BCRP, and P-glycoprotein activities are prognostic factors in adult acute myeloid leukemia. Clinical cancer research 2005, 11, 7764-7772.

(121) Naito, K.; Takeshita, A.; Shigeno, K.; Nakamura, S.; Fujisawa, S.; Shinjo, K.; Yoshida, H.; Ohnishi, K.; Mori, M.; Terakawa, S. Calicheamicin-conjugated humanized anti-CD33 monoclonal antibody (gemtuzumab zogamicin, CMA-676) shows cytocidal effect on CD33-positive leukemia cell lines, but is inactive on P-glycoprotein-expressing sublines. Leukemia 2000, 14, 1436-1443.

(122) Tang, R.; Cohen, S.; Perrot, J.-Y.; Faussat, A.-M.; Zuany-Amorim, C.; Marjanovic, Z.; Morjani, H.; Fava, F.; Corre, E.; Legrand, O. P-gp activity is a critical resistance factor against AVE9633 and DM4 cytotoxicity in leukaemia cell lines, but not a major mechanism of chemoresistance in cells from acute myeloid leukaemia patients. BMC cancer 2009, 9, 1-10.

(123) Strop, P.; Liu, S.-H.; Dorywalska, M.; Delaria, K.; Dushin, R. G.; Tran, T.-T.; Ho, W.-H.; Farias, S.; Casas, M. G.; Abdiche, Y. Location matters: site of conjugation modulates stability and pharmacokinetics of antibody drug conjugates. Chemistry & biology 2013, 20, 161-167.

(124) Junutula, J. R.; Raab, H.; Clark, S.; Bhakta, S.; Leipold, D. D.; Weir, S.; Chen, Y.; Simpson, M.; Tsai, S. P.; Dennis, M. S. Site-specific conjugation of a cytotoxic drug to an antibody improves the therapeutic index. Nature biotechnology 2008, 26, 925.

(125) Hamblett, K. J.; Senter, P. D.; Chace, D. F.; Sun, M. M.; Lenox, J.; Cerveny, C. G.; Kissler, K. M.; Bernhardt, S. X.; Kopcha, A. K.; Zabinski, R. F. Effects of drug loading on the antitumor activity of a monoclonal antibody drug conjugate. Clinical cancer research 2004, 10, 7063-7070.

(126) Strop, P.; Delaria, K.; Foletti, D.; Witt, J. M.; Hasa-Moreno, A.; Poulsen, K.; Casas, M. G.; Dorywalska, M.; Farias, S.; Pios, A. Site-specific conjugation improves therapeutic index of antibody drug conjugates with high drug loading. Nature biotechnology 2015, 33, 694-696.

(127) Jaracz, S.; Chen, J.; Kuznetsova, L. V.; Ojima, I. Recent advances in tumor-targeting anticancer drug conjugates. Bioorganic & medicinal chemistry 2005, 13, 5043-5054.

(128) Chari, R. V.; Miller, M. L.; Widdison, W. C. Antibody–drug conjugates: an emerging concept in cancer therapy. Angewandte Chemie International Edition 2014, 53, 3796-3827.

(129) Abdollahpour-Alitappeh, M.; Lotfinia, M.; Gharibi, T.; Mardaneh, J.; Farhadihosseinabadi, B.; Larki, P.; Faghfourian, B.; Sepehr, K. S.; Abbaszadeh-Goudarzi, K.; Abbaszadeh-Goudarzi, G. Antibody–drug conjugates (ADCs) for cancer therapy: Strategies, challenges, and successes. Journal of Cellular Physiology 2019, 234, 5628-5642.

(130) Singh, A. P.; Sharma, S.; Shah, D. K. Quantitative characterization of in vitro bystander effect of antibody-drug conjugates. Journal of pharmacokinetics and pharmacodynamics 2016, 43, 567-582.

(131) Masuda, S.; Miyagawa, S.; Sougawa, N.; Sawa, Y. CD30-targeting immunoconjugates and bystander effects. Nature reviews Clinical oncology 2015, 12, 245.

(132) Scott, L. J. Brentuximab vedotin: a review in CD30-positive Hodgkin lymphoma. Drugs 2017, 77, 435-445.

(133) Schönberger, S.; van Beekum, C.; Götz, B.; Nettersheim, D.; Schorle, H.; Schneider, D. T.; Casati, A.; Craveiro, R. B.; Calaminus, G.; Dilloo, D. Brentuximab vedotin exerts profound antiproliferative and pro-apoptotic efficacy in CD30-positive as well as cocultured CD30-negative germ cell tumour cell lines. Journal of Cellular and Molecular Medicine 2018, 22, 568-575.

(134) Katz, J.; Janik, J. E.; Younes, A. Brentuximab vedotin (SGN-35). Clinical Cancer Research 2011, 17, 6428-6436.

(135) van der Lee, M. M.; Groothuis, P. G.; Ubink, R.; van der Vleuten, M. A.; van Achterberg, T. A.; Loosveld, E. M.; Damming, D.; Jacobs, D. C.; Rouwette, M.; Egging, D. F. The preclinical profile of the duocarmycin-based HER2-targeting ADC SYD985 predicts for clinical benefit in low HER2-expressing breast cancers. Molecular cancer therapeutics 2015, 14, 692-703.

(136) Hong, E. E.; Erickson, H.; Lutz, R. J.; Whiteman, K. R.; Jones, G.; Kovtun, Y.; Blanc, V.; Lambert, J. M. Design of coltuximab ravtansine, a CD19-targeting antibody–drug conjugate (ADC) for the treatment of B-cell malignancies: structure–activity relationships and preclinical evaluation. Molecular pharmaceutics 2015, 12, 1703-1716.

(137) Golfier, S.; Kopitz, C.; Kahnert, A.; Heisler, I.; Schatz, C. A.; Stelte-Ludwig, B.; Mayer-Bartschmid, A.; Unterschemmann, K.; Bruder, S.; Linden, L. Anetumab ravtansine: a novel mesothelin-targeting antibody–drug conjugate cures tumors with heterogeneous target expression favored by bystander effect. Molecular cancer therapeutics 2014, 13, 1537-1548.

(138) Thomas, A.; Teicher, B. A.; Hassan, R. Antibody–drug conjugates for cancer therapy. The Lancet Oncology 2016, 17, e254-e262.

(139) Alley, S. C.; Okeley, N. M.; Senter, P. D. Antibody–drug conjugates: targeted drug delivery for cancer. Current opinion in chemical biology 2010, 14, 529-537.

VITA

Muhammad Raisul Abedin grew up in a remote town in Chandpur, Bangladesh. He pursued his Bachelor's degree in Chemical Engineering from Bangladesh University of Engineering and Technology (BUET), Dhaka, Bangladesh (2017). He worked on the development of a low cost and mammalian cell friendly antibacterial paper towel and filter at the International Centre for Diarrheal Disease Research, Bangladesh (ICDDR, B). In January 2018, he joined "Biomaterials and Tissue Engineering Lab" at the Department of Chemical and Biochemical Engineering in Missouri S&T as a graduate Ph.D. student. His primary research goal was engineering a synergistic drug delivery system that combines targeted nanoscale drug nanoparticles and combination therapeutic approach for breast cancer treatment. Since January 2018, he authored in seven scientific articles that include publications in *Journal of Nanobiotechnology (2018)*, *ACS Applied Bio Materials (2019)* and *Scientific Reports (2020)*. He published in the prestigious high impact journals including *Nature* and *ACS*. He also presented five conference talks and three research posters in the AIChE Annual Meetings (2018, 2019) and the OBI Symposium (2019) at Missouri S&T. He was the semifinalist at 3MT thesis presentation competition organized by Missouri S&T. His research on personalized medicine was highlighted by the University of Missouri System addressing the precision medicine initiative project (2018). His research expertise lied in designing nanoparticle based targeted therapeutic platforms for cancer treatment and mechanistic analysis of cancer therapeutic response at cellular, molecular and genetic levels. In December 2020, he received his Ph.D. in Chemical Engineering from Missouri S&T.